NORTHWESTERN UNIVERSITY

Titan through Time: Evolution of Titan's Atmosphere and its Hydrocarbon Cycle on the Surface

A DISSERTATION

SUBMITTED TO THE GRADUATE SCHOOL
IN PARTIAL FULFILLMENT OF THE REQUIREMENTS

for the degree

DOCTOR OF PHILOSOPHY

Field of Earth and Planetary Sciences

By

Ashley E. Gilliam

EVANSTON, ILLINOIS

December 2016

ABSTRACT

The Introduction and Appendix i-A outline briefly the history of Titan exploration since its discovery by Christiaan Huygens in 1675 through the recent International Mission of *Cassini-Huygens*. It discusses the roles of some of the ten most abundant elements in the Universe (H, He, C, N, O, Ne, Mg, Si, S, and Fe) in the formation of methane (CH_4), water (H_2O), and carbon dioxide (CO_2). As far as the element abundances are concerned, all of carbon could have combined with hydrogen to make CH_4. Alternatively, all of oxygen could have combined with C, Si, S, Fe, and H, making silicates, oxides, CO_2 and H_2O. The relatively high freezing temperatures of H_2O (273 K) and CO_2 (220 K) make them less suitable as atmospheric components on the outlying planets and satellites, where CH_4 (91 K) and N_2 (77 K) are more likely to exist as gases. The Introduction also discusses several possible mechanisms of cooling of Titan and its silicate core after accretion, and the uncertainties in the estimates of the possible radioactive heat generation in Titan's interior.

Chapter 1: This chapter discusses two possible pathways of loss of the two main gases from Titan's post-accretional atmosphere, methane (CH_4) and ammonia (NH_3), by the mechanisms of thermal escape and emission from the interior coupled with thermal escape. An accretion temperature of 300 to 355 K is calculated, and an atmospheric composition of 19.6 bar CH_4 and 5.8 bar NH_3, which declines to its present-day levels of 0.1 bar CH_4 and 1.4 bar N_2 (or equivalent 1.7 bar NH_3, as a precursor of N_2). In the first 0.5 – 0.6 Myr after accretion, Titan's surface cools to 150 K and it takes about 5 Myr to cool to near its present temperature of 94 K. Using an accretion temperature of 355 K, emission of CH_4 and NH_3 from the interior in combination with thermal

escape is needed to produce near-steady-state CH_4 and NH_3 atmospheric masses, as they are at the present. At the lower accretion temperature of 300 K, thermal escape of gases alone allows their atmospheric masses to decrease from the primordial to the present day levels in 50,000 – 70,000 years.

Chapter 2: In this chapter, a simple photolysis model is created, where the second most abundant component of the present-day Titan atmosphere, methane (CH_4), can either escape the atmosphere or undergo photolytic conversion to ethane (C_2H_6). Using this model, up to 8.46×10^{17} kg or 1.37×10^{6} km^3 of liquid ethane might have been produced since Titan's accretion. This amount is 10^4 times larger than the present-day atmospheric ethane mass of 9.24×10^{13} kg, suggesting that most of the remaining ethane resides in liquid form on or within Titan. The estimate for the amount of liquid ethane storage potential on Titan's surface is 50,000 km^3 in lakes and seas and an additional 61,000 km^3 in craters. As these are much smaller than the total volume of liquid ethane produced in the course of Titan's history, the excess may be stored in the subsurface of the crust, made primarily of water ice. The minimum porosity of the crust needed to accommodate all the liquid ethane would be only 0.9% of the uppermost 2 km of the crust.

Chapter 3: This chapter examines different fluvial features on Titan, identified by the Cassini spacecraft, and evaluates the possibilities of channel formation by two mechanisms: dissolution of ice by a concentrated solution of ammonium sulfate, and by mechanical erosion by flow of liquid ammonia and liquid ethane. It concludes that chemical erosion of Titan's channels could be completed in 280 to 1100 years, much shorter than the period of about 84,000 years that a concentrated $(NH_4)_2SO_4$-H_2O solution could exist as a liquid on the Titan surface. Mechanical erosion of Titan's channels is generally a much slower process, on the order of 10^2 to 10^5 years.

The erosional sequence of the channels may have starter after the formation of water-ice on the surface by the process of chemical dissolution by $(NH_4)_2SO_4$-H_2O, overlapping, or followed by, a period of mechanical erosion by liquid NH_3. A final stage on the cooling surface might have been characterized by liquid C_2H_6 as an agent of mechanical erosion.

Chapter 4: Three chemical reactions can represent, as a shorthand summarizing many intermediate processes, the transformation of methane to ethane and other hydrocarbons in Titan's atmosphere: CH_4 (1st order, k_{12} yr^{-1}) → CH_3 (2nd order, k_{23} cm^3 $molecule^{-1}$ yr^{-1}) → C_2H_6 (1st order, k_3 yr^{-1}) → Other products. This chapter presents: (1) new explicit mathematical solutions of mixed 1st and 2nd order chemical reactions, represented by ordinary differential first-degree and Riccati equations; (2) the computed present-day concentrations of the three gases in Titan's scale atmosphere, treated as at near-steady state; and (3) an analysis of the reported and computed atmospheric concentrations of CH_4, CH_3, and C_2H_6 on Titan, based on the reaction rate parameters of the species, the rate parameters taken as constants representative of their mean values.

Chapter 5: This chapter examines the possible reactions of methane formation in terms of the thermodynamic relationships of the reactions that include pure carbon as graphite, the gases H_2, CO_2, H_2O, and serpentinization and magnetite formation from olivine fayalite. The reactions are analyzed for the conditions on Titan and the Terrestrial Planets Mars, Earth, Venus, and Mercury, at the range of their temperatures, atmospheric pressures, and composition. The partial pressures of CH_4, calculated from the composition of planetary atmospheres, are compared to the reported values of CH_4 on some of the planets. The equilibrium pCH_4 values depend on the nature of the reactants and other products, as represented by the five solid-gas and gas-gas CH_4-forming reactions. On present-day and primordial-Titan, and on Mercury, methane could have escaped by

the Maxwell-Boltzmann mechanism. On Mars, Venus, and on primordial Earth, the high values of escape velocity would have assured retention of methane in the planetary atmosphere, if it formed there.

ACKNOWLEDGEMENTS

First, I would like to thank my advisor ("*Doktorvater")*, Dr. Abraham Lerman, for taking a chance on a girl mesmerized with Titan, and sharing his time, knowledge, and resources during the pursuit of my dissertation. A lifelong geochemist, Dr. Lerman dove headfirst into the planetary science world, allowing me the privilege of being his last advisee before claiming the status of *Professor Emeritus Scientiarum Terrae et Stellarum Errantium*. His curiosity and passion for all things science (and non) has truly been an inspiration to me, and I am forever grateful for the ways he has helped me grow as both as scientist and as a person.

I would also like to thank my other advisors and committee members, Dr. Matthew Hurtgen, Dr. Bradley Sageman, and Dr. Daniel Horton for their counsel and encouragement throughout my time at Northwestern, Dr. Donna Jurdy for sharing her passion for planetary science with me and for her guidance and support during the early years of my graduate education, and Dr. Jared Wunsch of the Department of Mathematics for his collaboration, mathematical guidance and support.

The friendship and support I received from the graduate students during my time at Northwestern is not something I will ever forget. To my "twin", Renee French, I am so grateful that we got to share this experience together. Thank you for keeping me sane. I wouldn't have gotten this far without you. Miguel Merino and Gregory Lehn, thanks for being my surrogate big brothers, for showing me the ropes of grad school, and for all the laughs and annoying banter. To the "game crew", you guys made this entire experience worthwhile. You'll never know someone's

true colors until you've played a full campaign of Twilight Emperium with them, and never know true friendship until you've worked together as cunning field mice to save an imperiled kingdom.

Finally, none of this would have been possible without the unconditional love and support from my family. To my parents, thank you for listening when I needed someone to hear me, and for motivating me when you thought I needed to hear it. And to my husband, Josh, thank you for being the biggest supporter of all. Thank you for sacrificing everything to move across the country with me so I could pursue my graduate education, for being there during the highest highs and the lowest lows, for motivating and encouraging me, and for keeping me (mostly) sane over the years.

This work was supported by NASA Headquarters under the NASA Earth and Space Science Fellowship Program – Grant NNX13AO02H.

TABLE OF CONTENTS

Page

LIST OF TABLES

LIST OF FIGURES

INTRODUCTION

e Titan semper aliquid novi

Titan: A New World Discovered

Imagine this. You wake up just after dawn. Sleep seems impossible. Something is troubling you. Perhaps a walk along the lake shore will clear your mind. Winter is fast approaching, so you put on your warmest coat, hat, and gloves, and leave the house. The air around you seems thicker today, but you find yourself moving briskly, practically levitating, and your walk to the lake is a short one. It was almost effortless to get there. You look out at the calm water, and see a mirror like reflection in the sky just before it starts to rain. The rain is falling now, but the drops look different. They're bigger than normal, and are falling slower than they usually do. It's getting colder now, and the sun has yet to rise. Minutes pass, and the temperature continues to drop. You pull your phone out from your jacket pocket and check the temperature. It reads: -179°C/94 K. Huh. Must be a mistake. But as you look back at the rain drops hitting the surface of the lake, you notice something else strange – the lake is reflecting an orange color. So you look up. Overhead, behind an orange curtain of smog, a massive and ghostly disk appears, the specter of Saturn. You can't see its rings, they are too thin, but you catch a glimpse of their shadows on the turbulent Saturnian atmosphere. If you can picture all of this, welcome to Saturn's moon, Titan.

Gravity on Titan is about 14 percent of that on Earth, or just a bit weaker than the gravity of the Earth's moon. The average surface temperature on Titan is 94 K, and the average surface pressure is 1.5 bar (roughly similar to resting at the bottom of a 5-meter-deep pool on Earth). As such, if you lived on Titan, you wouldn't need a pressurized suit to survive; all you'd really need is an oxygen mask and very warm clothing. Due to its atmosphere's opacity and distance from the

Sun (about 900 million miles or more than nine times farther from the Sun than Earth) standing on the surface of Titan even at midday would seem like a deep twilight on Earth…dark and cold.

On the surface of Titan you'll find an abundance of dunes and rocks of water ice. In fact, the crust itself is a porous mixture of fragmented water ice and organic particles. Near the poles, you'll find a network of lakes, rivers, and seas. The liquid in these features is not water, but a combination of methane, ethane, and other hydrocarbons that you might find in your car's gas tank. As a matter of fact, Titan has hundreds of times more liquid hydrocarbons than all the known oil and natural gas reserves on Earth (Lorenz et al., 2008). The hydrocarbons rain slowly from the sky, thanks to Titan's thick atmosphere and low gravity, and the raindrops can grow to be almost twice the size of large raindrops on Earth (Lorenz, 1993).

Titan is the only moon in the Solar System that has a substantial atmosphere, composed of roughly 95% N_2 and 5% CH_4, reaching ten times higher in altitude than Earth's**,** but the ratio of the scale atmospheres is much smaller at present, 21.1/8.4 = 2.5. While the surrounding air is nitrogen based like Earth, there are no traces of oxygen. The diversity in composition of Earth and Titan, and between all the planetary bodies in the solar system, comes from their locations: terrestrial bodies (i.e. Earth) formed in the warm, inner region of the solar nebula, while the Jovian bodies formed in the colder, outer regions. In the center of the solar nebula, gravity drew together enough material to form the Sun and the rocky bodies. In the surrounding disk, however, the gaseous material was too spread out for gravity alone to clump it together. Instead, the icy bodies began their formation by condensation – the general process in which solid or liquid particles form in a gas (Seeds and Backman, 2016).

The Building Blocks of Planetary Formation: Hydrogen and helium gas, comprising 98% of the solar nebula's mass, never condense in interstellar space. However, the other three types of material found in the solar nebula (hydrogen compounds, silicate and iron-sulfide rock, and metal) could condense into solid form wherever the temperature allowed. Close to the forming Sun, where the temperature was above 1600 K, it was too hot for any material to condense. Near what is now Mercury's orbit, the temperature was low enough for metals (e.g. Fe, Ni, and Al) and some types of rock to condense into tiny, solid particles, but other types of rock and all the hydrogen compounds remained gaseous (Seeds and Backman, 2016). More types of rock could condense, along with the metals, near what is now Venus', Earth's, and Mars' orbits. In the region where the asteroid belt would eventually be located, temperatures were low enough to allow carbon-rich minerals to condense, along with minerals containing small amounts of water. Among the possible hydrogen and carbon compounds the most common ones are H_2O, CO_2, CH_4, and NH_3 as a result of hydrogen, oxygen, carbon, and nitrogen being among the most common elements in the universe (Fig. i). These species could only condense into ices beyond the frost line – the distance at which it was cold enough for ices to condense – which lay between the present-day orbits of Mars and Jupiter. Thus, the solid seeds that would accrete to form Saturn and Titan were made of ices along with metal and rock.

As the Jovian planets began to grow, so did their gravity and their ability to capture and hold some of the hydrogen and helium gas that made up the vast majority of material in the surrounding solar nebula. This explains why Jupiter and Saturn are made almost entirely of hydrogen and helium. Uranus and Neptune, which are much smaller than Jupiter and Saturn, contain proportionally much smaller amounts of hydrogen and helium, and are instead made

primarily of hydrogen compounds such as H_2O, CH_4, and NH_3. While Titan, like the other Jovian satellites, does share some chemical similarities to its host planet, Titan's atmospheric composition is wildly different from that of Saturn – most notably, its lack of H and He. This is primarily due to the location of its formation, within Saturn's warm subnebula, which allowed for vaporization and loss of most volatile species. A more detailed look at the origin of Titan's atmosphere is in Section 1.1.

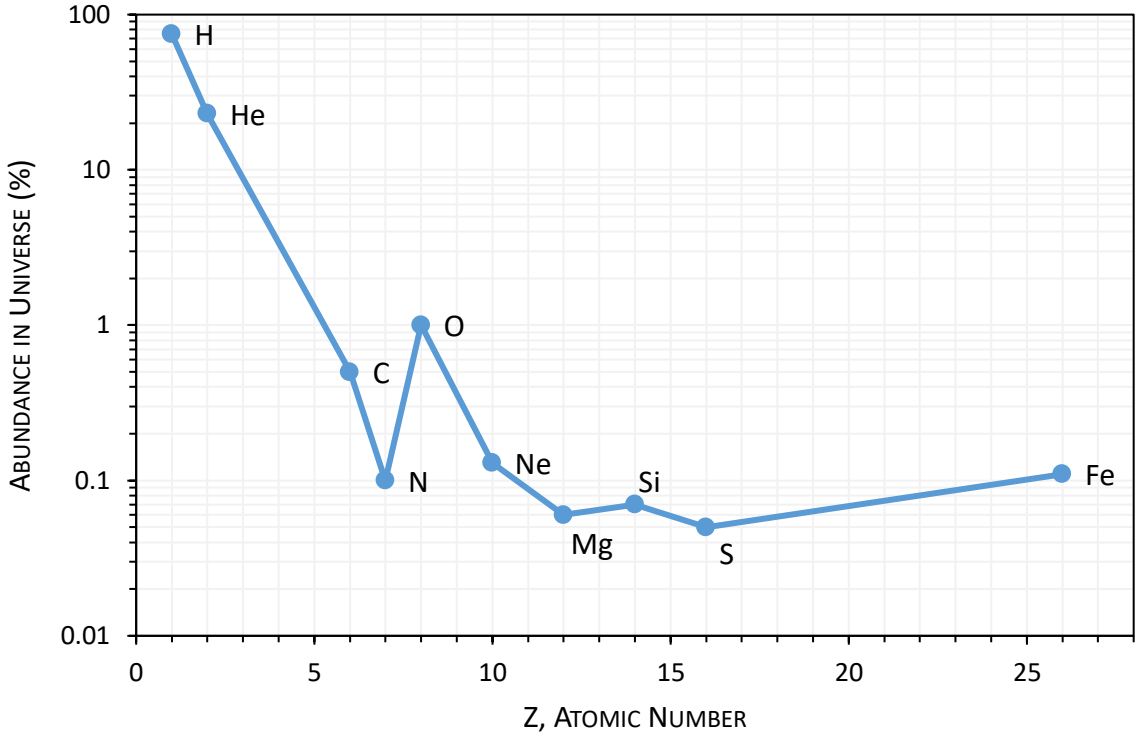

Fig. i. Estimated amounts of the ten most abundant elements in the Universe (Greenwood and Earnshaw, 2012).

What About Oxygen?: From the abundances of the elements in the Universe as shown in Fig. i, all of oxygen could have combined with H and/or C, but only 15% of oxygen could be taken up by Si, Fe, and S. In fact, roughly 25% of the O is first removed from the nebular gas by inclusion into silicates and oxides before water ice condensates at 182 K (Satsińska et al., 2011). Some of

the remaining O is further bound in magnetite that forms from Fe metal at about 370 K. The relatively high freezing points of H_2O (273K) and CO_2 (220K) (Fig. ii) make them not everywhere suitable as components of an atmosphere, leaving room for such gases as ammonia NH_3 (195K), methane CH_4 (90K) and nitrogen N_2 (63K).

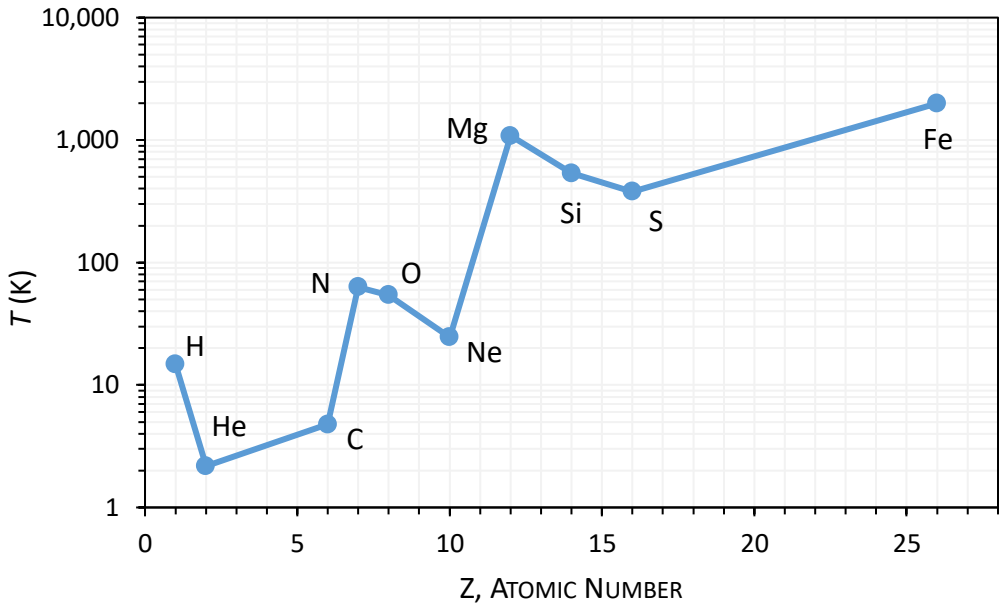

Fig. ii. Triple point temperatures of the ten most abundant elements in the Universe (CRC, 2016).

More About Methane: Methane can form in a reaction of:

$$C_{(s)} + 2H_{2(g)} \rightarrow CH_{4(g)} \qquad \text{(i.1)}$$

at temperatures above 1100 K (Mills and Steffgen, 1974; Vigdergauz, 2011, 2014). On Earth, methane forms by diverse bacterial processes of decomposition of organic matter, known as methanogenesis (Ferry, 2012) and by thermal alteration of organic matter at higher temperatures in the subsurface and hydrothermal systems (Welhan, 1988; Stolper et al., 2014). The most commonly cited reaction is the production of methane by reduction of CO_2, known as the Sabatier reaction (Sabatier and Senderens, 1902; Sabatier 1911):

$$CO_2 + 4H_2 = CH_4 + 2H_2O \quad \text{(i.2)}$$

At laboratory conditions the reaction proceeds in the temperature range from 470 to 770K (Lunde and Kester, 1973) and it has also been reported at room temperature, using photo-excitation of a mineral catalyst (Thampi et al., 1987). The abundance of H and CO_2 in the Solar System makes the Sabatier reaction a likely source of methane.

Cooling After Accretion: As the proto-Titan continued to grow and successfully trap volatiles, it saw a large surface temperature increase as a result of shock heating and ejecta blanket deposition from impacts. Using a simplified approach that estimates the fraction of accretional (impact) energy that is retained at depth and progressively heats the surface of the growing satellite (Kaula, 1979; Schubert et al., 1981; Lunine and Stevenson, 1987; Grasset and Sotin, 1996), it has been suggested that once proto-Titan reached a radius of roughly 1,000-1,500 km, melting and vaporization of the surface materials started to occur, creating a deep water- and ammonia-rich ocean in combination with a massive and hot steam atmosphere. The proto-atmosphere and ocean were likely to be in equilibrium with each other up until the end of the accretion process, where surface temperatures were roughly 350 K (Gilliam and Lerman, 2014a) or as high as 500 K (Kuramoto and Matsui, 1994). However, such temperatures were short-lived after accretion. Cooling of the ammonia-water ocean in the presence of a strong atmospheric greenhouse effect results in complete freezing on a timescale of up to 10^7 years, from 300 K to the peritectic point of the ammonia-water system at 176 K (Lunine, 1985; Adams, 2006). Over this time span, the temperature drop encompassed the solidification point of several components initially present in the atmosphere and/or in the ocean: water ice (267 K for 5% ammonia at a 1 bar pressure, e.g. Kargel, 1992), CO_2 ice (~200 K), and clathrate hydrates of CH_4, N_2, CO_2, Ar, and other species

(180 to 280 K) which, depending on their density, would either accumulate at the ocean-atmosphere interface and form a solid crust, or sink deep into the ocean, forming the present-day structure that we observe today.

The cooling of Titan by radiative emission of the accretion energy released was explicitly treated by Stevenson (1992), Barr et al. (2010), and Gilliam and Lerman (2014a). Other treatments of Titan cooling as related to its internal differentiation have been based on its astronomical and orbital parameters (e.g. Tobie et al., 2005; Fortes et al., 2012), heat transport through a multi-layer system (e.g. Grindrod et al., 2008; Mitri and Showman, 2008), phase equilibria and convection of liquid layers (e.g. Grasset and Sotin, 1996; Grasset et al., 2000), and tidal forces (e.g. Sohl et al., 1995, 2003). Here it should be stated that the cooling of Titan or its antigorite core by diffusional transport of heat to the exterior is much too slow on a time scale of 4.55×10^{9} yr to have been able to remove a significant amount of heat from the interior of the core. This conclusion is based on the transport of heat from a homogeneous sphere, as treated by Kelvin (1862, p. 161) and more extensively by Carslaw and Jaeger (1959, pp. 85 (1), 233-235), using the coefficient of thermal diffusivity for serpentine, $\kappa = 41.0$ m^2 yr^{-1} or 0.013 cm^2 s^{-1} (Robertson, 1988, p. 90). Furthermore, for a silicate core in contact with a liquid layer of an ammonium-hydroxide and/or ammonium-sulfate solution, if the heat flow at the outer core boundary were driven by diffusional heat transport, the fraction of the heat content in the core, in J m^{-2}, transported by the heat flow across the boundary would have been negligibly small at times from 1×10^{5} yr – fraction 6×10^{-15}, to 4.55×10^{9} yr – fraction 1.3×10^{-12}.

Radioactive heating of Titan has been variably addressed by Grasset et al. (2000), Czechowski and Leliwa-Kopystyński (2005), and Dorofeeva and Ruskol (2010). As there are no

direct determinations of radioactive isotopes in Titan's crust, the following guesstimates may indicate the potential importance of heating Titan's interior by radioactive decay. Titan's core, believed to be made of antigorite ($Mg_3Si_2O_5(OH)_4$), may be considered analogous to mafic igneous rocks. The latter, in the region of Boulder Batholith, Montana, are at present heated by radioactive decay of ^{238}U, ^{232}Th, and ^{40}K at a rate of about 0.013 J kg^{-1} yr^{-1} and the mean of the continental crust is 0.02 J kg^{-1} yr^{-1} (Tilling and Gottfried, 1969). Translated to the volume and mass of Titan's core, the heating rate of mafic rocks gives 36 J m^{-3} yr^{-1}. This value is lower than the heating rate of the continental crust, 55 J m^{-3} yr^{-1} and the average heating rate of the Earth of 132 J m^{-3} yr^{-1}, used by van Orstrand (1940). If all the heat produced in Titan's core at the mafic-rocks production rate remained in the core, the core would reach T = 1325 K (or 1052°C) in 1 billion years. Thus the heating of the core by radioactive decay was not the main mechanism of the primordial heat of Titan.

APPENDIX I-A

The Historical Exploration of Titan

The tale of the first detection of Titan, the largest moon of Saturn and the second in size among all the satellites in our Solar System, is a classic of its kind. On the night of March 25, 1655, novice Dutch astronomer, Christiaan Huygens, pointed his telescope at Saturn. Huygens was inspired by Galileo's discovery of the four Galilean moons in 1610 and his improvements of telescope technology, and in 1650, Huygens began designing telescopes with his brother Constantijn. In 1655, Huygens directed one of his new telescopes, a 50 power refracting telescope, towards Saturn in an attempt to study its rings. According to his notes, Huygens saw a small 'star' 3 arc minutes away from Saturn and immediately guessed it was a satellite (Huygens, 1659). This was confirmed a few days later when Huygens noticed that the 'star' had moved from its original location. Huygens named the satellite *Saturni Luna* ("Saturn's moon"). The name *Titan* was not formally given to this satellite until 1847, 192 years after its discovery. Titan and the six other satellites of Saturn known at that time were named by an English astronomer, John Herschel. Herschel suggested that the satellites of Saturn should be named after the mythological Titans, sisters and brothers of Cronus (the Greek equivalent of the Roman god Saturn). The biggest of these satellites was named Titan, with the other six being named after individual Titans (Coustenis et al., 2009).

The first suggestion that Titan might have an atmosphere came in 1908, by a Catalan astronomer José Comas Solà. Comas Solà studied Titan visually using a 38-cm telescope at the Fabra Observatory in Barcelona, Spain. On August 13, 1907, he made a sketch of Titan, which was published in 1908 in the *Astronomische Nachrichten*. He wrote: "…with a clear image and

using a magnification of 750, I observed Titan with very darkened edges (somewhat similar to those one observes on the disk of Neptune), while on the central part, much brighter, one sees two round, whiter patches, which give the appearance of a blurred double star. We may suppose reasonably, that the darkening of the edges demonstrates the existence of a strongly absorbing atmosphere around Titan." This was the first hint that Titan had an atmosphere, although many still question the credibility of Comas Solà's claim (Lorenz and Mitton, 2002).

Confirmation that Titan had an atmosphere came in 1944. Using the new McDonald 82-in. telescope, Gerald Kuiper observed several spectral signatures on Titan at wavelengths longer than 0.6 μm, along with two absorption bands of methane at 6190 and 7250 Å. This discovery was significant because it requires the presence of a dense atmosphere. Kuiper's findings also suggested that Titan's atmosphere contained a significant fraction of methane (Coustenis et al., 2009). This would later be confirmed with the *Voyager 1* mission.

The first probe to visit the Saturnian system was *Pioneer 11*. Launched by NASA on April 6, 1973, *Pioneer 11* was designed to study the asteroid belt, the environment around Jupiter and Saturn, as well as solar wind, cosmic rays, and to eventually reach the edge of the solar system and the heliosphere. *Pioneer 11* passed by Saturn on September 1, 1979, and performed the first spacecraft flyby of Titan on September 2, 1979. The probe took the first images of the moon at its closest approach of 363,000 km, although they were of low quality ("The Pioneer Missions", NASA).

The highly anticipated *Voyager 1* flyby of Titan in 1980 revealed many surprising findings, despite its inability to see beneath Titan's thick atmosphere. Launched by NASA on September 5, 1977, the goal of this mission was to study the outer Solar System and the interstellar medium. At

a distance of 124 AU, as of May 2013, it is the farthest man-made object from Earth and is still in operation today ("Where are the Voyagers?", JPL). In November 1980, *Voyager 1* flew by Titan at a distance of 4394 km. Titan's clouds proved to be impenetrable to *Voyager's* gaze, but the spacecraft still gained significant information about its atmosphere. Geochemical models prior to the flyby suggested that large amounts of N_2 might have been produced by volcanic activity and resultant dissociation of NH_3 gas. *Voyager* data confirmed an atmosphere of 95% N_2 with the rest being CH_4, and, using its Radio Science Subsystem instrument, also revealed a surface temperature near the triple point of methane, where solid, liquid, and gases can coexist in equilibrium. This was the first indication of a possible hydrologic cycle of methane, similar to the hydrologic cycle on Earth. The discovery of a potential hydrologic cycle on Titan by *Voyager 1* excited the planetary community, yet uncertainty remained about the nature and distribution of liquid on the surface.

The *Cassini-Huygens* spacecraft, launched on October 15, 1997, is a joint mission of the European Space Agency (ESA), the Italian Space Agency (ASI), and NASA. The mission was designed to explore the Saturn system, including its rings and moons, with a special focus on Titan. The spacecraft included a Saturn orbiter and an atmospheric probe/lander for Titan called *Huygens*. *Cassini-Huygens* has been in orbit around Saturn since July 1, 2004, using various instruments to penetrate Titan's thick atmosphere and image its surface. Prior to *Cassini*, it was speculated that Titan might have a global ocean (Lunine et al., 1983) or have a surface dominated by impact structures (Lorenz, 1994). However, the very first *Cassini* radar image revealed no impact craters, providing evidence of a geologically young and active surface (Elachi et al., 2005). Furthermore, it was shown that a vast surface ocean did not exist, but rather an abundance of lakes in the polar regions (Lorenz et al., 2008). As radar coverage of Titan's surface increased, only a few impact

structures were discovered, hardly the plethora of craters anticipated. In addition, *Cassini* radar imaging discovered Earth-like features on Titan's surface, including channels (Lorenz et al., 2008). By the time the *Cassini* spacecraft had finished its nominal mission in July 2008, it had completed 75 orbits around Saturn and 44 flybys of Titan ("Cassini-Huygens Mission Objectives", ESA).

Upon completion of the nominal mission, a two-year extended mission called the *Cassini Equinox* began. During this extension, *Cassini* flew an additional 65 orbits around Saturn and performed 27 Titan flybys, attempting to answer new questions based on the findings gained during the nominal mission. At the end of the *Cassini Equinox* mission on July 1, 2010, the *Cassini* mission received an additional extension, called the *Cassini Solstice* mission. Appropriately named, this mission began just after Saturn had completed its northern winter solstice, and is designed to continue until a few months past Saturn's northern summer solstice in May 2017. At Titan, the main science objectives of the *Cassini Solstice* mission include: (1) study seasonal changes in the methane-hydrocarbon hydrological cycle, (2) study seasonal and temporal changes with an emphasis on surface lakes and other materials, (3) study seasonal changes in the upper atmospheric properties, (4) determine the internal structure of Titan ("Cassini-Huygens Mission Objectives", ESA).

Huygens was an atmospheric entry probe designed to land on Titan as part of the *Cassini-Huygens* mission. When the *Cassini-Huygens* mission was initially planned, it was not yet certain what type of terrain *Huygens* would land in due to the inability of the previous missions to peer beneath Titan's thick haze. The first image of the *Huygens* landing site didn't come until the spacecraft was 1,200 km away from Titan, revealing what appeared to be a shoreline. Assuming that the landing site could be non-solid, *Huygens* was designed to land in a variety of terrain,

including liquid. On December 25, 2004, *Huygens* separated from the *Cassini* orbiter, and entered into the Titan atmosphere on January 14, 2005. The spacecraft took 148 minutes to descend through the atmosphere, using up most of its three-hour battery life. During its decent, *Huygens* made several measurements of the atmosphere: (1) collected aerosols for chemical analysis, (2) made spectral measurements and took pictures of the Titan surface and atmosphere, (3) measured wind speeds, (4) identified the chemical composition of the atmosphere, and (5) measured the physical properties of the atmosphere. The *Huygens* probe landed on January 14, 2005, at 10.2°S, 192.4°W, in what was later referred to as 'Titanian mud'. The images taken after the probe landed revealed a surface covered in pebbles, believed to be water ice. The rounded nature of the pebbles indicated that fluid might have once flowed through the landing site. Defying the odds, the probe continued to send data back to *Cassini* for another 90 minutes after it landed.

CHAPTER 1

Evolution of Titan's Major Atmospheric Gases and Cooling since Accretion

1.1. Introduction

Titan is the only known moon to have a thick atmosphere and the only world besides the Earth to have liquid on its surface. At 9.5 AU away from the Sun, Titan maintains a surface temperature of 94 K. Its atmosphere has a surface pressure of 1.5 bar – one and a half times that of our planet – and consists of approximately 95% N_2 and 5% CH_4 (mole percentage). Unlike the Galilean satellites, Titan is alone in terms of its size and mass (Table 1.1), comprising more than 96% of the mass in orbit around Saturn, and its diameter is larger by a factor of nearly 3.4 than the second largest Saturnian moon, Rhea. Titan is believed to have formed during the last stages of Saturn's formation (Mosqueira and Estrada, 2003) within a disk of gas and dust that was the outgrowth of the formation of Saturn itself. Within the Saturn subnebula, collisions of particles led to the formation of rock-ice planetesimals, and subsequent growth led to the formation of satellites. Titan's formation in Saturn's warm subnebula (Alibert and Mousis, 2007) allowed efficient vaporization and loss of most volatile species (CO, N_2, and noble gases) with low clathration temperatures, but left NH_3, CH_4, H_2O, and CO_2 in solid and clathrate form. Thus, Titan formed with little CO and noble gases in its atmosphere, which was dominated by NH_3 and CH_4, consistent with measurements today.

Titan's proto-atmosphere is determined by the stability of the volatile-rich solid phases, and input from comets that condensed outside the Saturn subnebula (Coustenis, 2005). The proto-atmosphere, once formed, might have limited the amount of radiation escaping into space, resulting in an increased surface temperature, from 300 K up to 500 K (Kuramoto and Matsui, 1994). A warm accretion is consistent with the theory that NH_3 is the primordial source of Titan's atmospheric N_2 (Atreya et al., 1978; Tobie et al., 2009).

Table 1.1.
Titan parameters [a]

Parameter	
Mean radius (km)	2575
Volume (km^3)	7.152×10^{10}
Surface area (km^2)	8.332×10^{7}
Mass (kg)	1.345×10^{23}
Mean density (kg/m^3)	1881[b]
g at the surface (m/s^2)	1.352
Escape velocity $v_e = (2gr)^{1/2}$ (m/s)	2639
Mean distance from the Sun (km)	1.427×10^{9}

[a] From ESA (2013); NASA (2012)

[b] From Titan's present-day individual layer densities and thicknesses (Fortes et al., 2007), Titan's mean density is 2139 kg/m^3 or 14% higher than the NASA value

The origin of CH_4 in Titan's atmosphere is still widely debated. Prinn and Fegley (1981) argue that the dense Saturn subnebula was rich in CO relative to CH_4 with temperatures and pressures high enough to permit the conversion of CO to CH_4 in Titan's proto-atmosphere. Another hypothesis, by Mousis et al. (2002), suggests that no conversion of CO to CH_4 occurred in the Saturn subnebula, but Titan was formed from planetesimals rich in CH_4 that migrated from the outer part of the subnebula. Regardless of methane's origin, there may be a constant source of replenishment in the atmosphere as the photolysis of methane into other hydrocarbons occurs on a relatively short timescale (~50 My) and, as our results show, its escape rate from the Titan atmosphere is too fast at an accretion temperature of 355 K. One possible source of methane addition to the atmosphere is cryovolcanism.

To date, only the Cassini-Huygens spacecraft has peered beneath Titan's thick clouds, giving an incomplete picture of its atmospheric structure and surface conditions. Even less is known about early Titan, how it formed, and how it evolved from 4.55 Ga until today. This paper, dealing primarily with the behavior of CH_4 and NH_3 in the atmosphere, is based on the available

information about Titan's present-day composition and internal structure, insofar as it is germane to the atmosphere (Table 1.1), and it proposes two new models for the chemical and physical composition of Titan's atmosphere post-accretion. The two models, with NH_3 and CH_4 as the only gases, define the volume, height, density, and outer surface area of the atmosphere in each case. We show how NH_3 and CH_4 could leave the atmosphere by thermal escape alone as the only sink, or by a combination of emissions from the interior and thermal escape, producing in each case the final result of the present-day gas masses in the atmosphere. For this, we calculate Titan's accretion temperature, its mean heat capacity, and subsequent cooling rate. This paper is a contribution to the story of Titan and its atmosphere, that is critically important to the understanding of the present and future of this most interesting and complex body in the Solar System.

1.2. Internal Composition and Structure

Interaction between Titan's atmosphere and its subsurface, possibly through cryovolcanism, warrants a summary outline of its internal structure in addition to the atmosphere. The standard model of Titan's internal structure, as discussed by Fortes et al. (2007), consists of a large silicate core (a serpentine mineral antigorite, $Mg_3Si_2O_5(OH)_4$), overlain by a thin layer of brucite ($Mg(OH)_2$), above which are a layer of high-pressure ice VI, an aqueous ammonium sulfate ocean ($(NH_4)_2SO_4$), and a crust made of methane clathrate, ice Ih, and solid ammonium sulfate.

The presence of ammonia in the subsurface ocean is thought to be a crucial component because of its ability to lower the freezing temperature of the liquid layer, impeding complete crystallization (Grasset and Sotin, 1996). Work by Grasset et al. (2000) suggests that the liquid layer is much more complex and might contain methane and nitrogen in addition to ammonia. For

an accreted Titan, this paper assumes an internal composition based on the one at present (Fortes et al., 2007): the solid core of antigorite and brucite, and an outer fluid shell of water and other volatile species in aqueous solution at the accretion temperature higher than the present (300 to 355 K, Section 1.3.1), as shown in Table 1.2. An ammonia-water layer is consistent with the inference that solid ammonia-water compounds condensed during or shortly after the formation of Titan (Yarger et al., 1993). A primordial ammonia composition of 5 wt% to 15 wt% is often cited (Grasset and Pargamin, 2005), which can prevent complete crystallization of the liquid layer. The differences in the composition of the ocean layer, attributed by different authors (e.g., Fortes et al., 2007; Tobie et al., 2009) to the relative amounts of NH_3 and $(NH_4)_2SO_4$, do not affect the conclusions in this paper, insofar as ammonia in Titan's interior is considered only as a potential source of emissions.

Table 1.2.
Primordial component masses of Titan.

Component	Mass (kg)	% Mass
Methane Gas (g or aq)	7.52×10^{20}	0.56
Sulfuric Acid (aq)	1.19×10^{21}	0.88
Ammonia (aq)	1.62×10^{21}	1.21
Brucite (s)	3.63×10^{21}	2.70
Water (liq)	5.10×10^{22}	37.89
Antigorite (s)	7.63×10^{22}	56.76
Total	1.345×10^{23}	100

At 300-355 K, all of the H_2O should be in liquid form, and NH_3 and ammonium sulfate, $(NH_4)_2SO_4$, can be dissolved in it. An aqueous solution of NH_3+$(NH_4)_2SO_4$ is stoichiometrically equivalent to a solution of NH_3+H_2SO_4. Methane as a gas at 300-355 K is fairly insoluble in water at 1 bar total pressure (Duan and Mao, 2006), 2.0×10^{-5} to 7.6×10^{-6} kg CH_4 / kg H_2O, corresponding to only small fractions of the CH_4 mass available in Titan (7.52×10^{20} kg, Table 1.2), 0.14 to 0.05%,

respectively. However, at the same temperatures and 2 kbar total pressure, the mass of CH_4 soluble in water may be 40 to 50% of the mass available.

A homogeneous Titan of composition as given in Table 1.2 and Fig. 1.1 is subdivided into an inner solid core of antigorite and brucite, of radius 1898 km, and an outer fluid shell of thickness h_f = 677 km, containing H_2O, NH_3, H_2SO_4, and CH_4, where the fluids are separated from the solids antigorite and brucite. In this subdivision, Titan's fixed mass, volume, and mean density (Table 1.1) are maintained and satisfied by the densities of the inner solid core ρ = 2793 kg/m^3 and the outer fluid shell ρ = 1272 kg/m^3. Pressure at the base of the outer fluid shell is close to 12 kbar or 1.2 GPa, from an approximate relationship $P \approx \rho g h_f$.

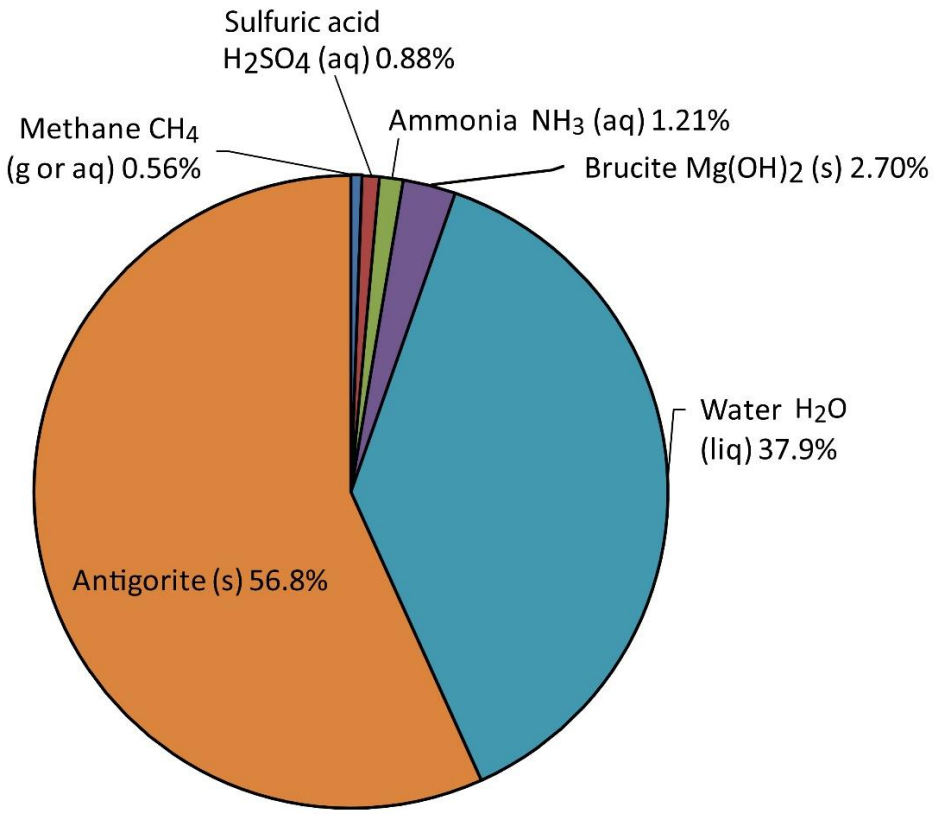

Fig. 1.1. Percent mass of each component in Titan's primordial internal structure.

The NH_3+$(NH_4)_2SO_4$ concentration in the fluid shell (Table 1.2) corresponds to an aqueous solution of 5.2 wt% (or 2.1 molal). Its density of 1272 kg/m^3 is comparable to that of a NaCl aqueous solution of 15 wt% (3 molal) at 25°C and 6 kbar pressure, 1274 kg/m^3 (Lvov and Wood, 1990). The density is higher than that of pure H_2O at 300 K and 10 kbar, 1237 kg/m^3 (Wagner and Pruss, 2002), and of the 25°C densities of such saline brines on the Earth surface as the Great Salt Lake, 1087 to 1140 kg/m^3 (Naftz et al., 2011), and the Dead Sea, 1242 kg/m^3 (Katz, 2013). However, it is lower than the densities of the Don Juan Pond in Antarctica, of composition variably given as $CaCl_2$-$MgCl_2$-NaCl (Marion, 1997; Matsubaya et al., 1979), 1278 to 1360 kg/m^3, calculated from the component-solution densities of 25°C (OXY, 2012; Conde, 2009; Rogers and Pitzer, 1982; Chen et al., 1980).

1.3. Accretion Temperature, Primordial Heat Capacity, and Cooling

1.3.1. Titan's Accretion Temperature

During the accretion process, part of the impact energy is converted into heat, although the details of the process are not well constrained. Grasset and Sotin (1996) assumed that the fraction of accretional energy retained as heat varies between 0.1 and 0.5 and developed an approximate accretional temperature profile for Titan. They suggested that once the growing proto-Titan reached a radius of roughly 1000−1500 km, melting and vaporization of the surface materials allowed for the development of a liquid water layer and an atmosphere. Titan's accretion temperature is an important factor in estimation of the rate of cooling and subsequent behavior of CH_4 and NH_3 in its atmosphere. Derivation of the accretion temperature T_{ac} (Hanks and Anderson, 1969), based on a balance of the release of gravitational accretion energy and cooling by ideal

black body radiation emission, with no other internal heat sources or storage, is given in Eqs. (1.1)-(1.2), Table 1.3.

Hanks and Anderson's (1969) determination of the T_{ac} is derived from the sequence of accretion times and rates for Venus, Earth, Mars, and the Moon. If there were additional internal sources of heat production or if some of the energy was stored within Titan instead of all of it being emitted by Stefan-Boltzmann radiation (that is, if the emitting surface was not an ideal black body, but was characterized by an emissivity factor $0 < \varepsilon \leq 1$ before the Stefan-Boltzmann constant σ in Eq. (1.1)), the accretion temperature would have been higher than the calculated value in Table 1.3.

Table 1.3.
Accretion temperature models.

Process or Parameter	Mathematical formulation		Explanatory comments
Balance of gravitational energy release and Stephan-Boltzmann cooling by emission [a]. $\rho\, dr/dt$ is the rate of mass accretion per unit area of the Titan surface (kg m^{-2} s^{-1}). No internal heat production or storage. Emission of an ideal black body.	$\frac{GM(r)}{r}\rho\frac{dr}{dt} = \sigma\left(T^4 - {T_{eq}}^4\right)$	(1.1)	G = 6.674×10^{11} J m kg^{-2} M = 1.345×10^{23} kg r = 2.575×10^{6} m ρ = 1881 kg m^{-3} σ = 5.670×10^{-8} W m^{-2} K^{-4} T_{eq} = 85 K T is accretion temperature
Accretion temperature T_{ac} from Eq. (1.1)	$T_{ac} = \left({T_{eq}}^4 + \frac{GM(r)}{\sigma r}\frac{\rho\, dr}{dt}\right)^{1/4}$	(1.2)	T_{ac} = 353 to 355 K From parameter values above

[a] Hanks and Anderson (1969). Other models given by Kuramoto and Matsui (1994), Grasset and Sotin (1996), Barr et al. (2010).

At present, with no albedo and no greenhouse effect, the radiation equilibruim temperature of Titan at its mean distance from the Sun (Table 1.1) is T_{eq} = 90 K. About 4.5 billion years ago, when the Sun was approximately 75% as luminous as today (Gough, 1981), Titan's $T_{eq} \approx$ 84 K. The value of Titan's accretion rate and duration, as estimated from Hanks and Anderson (1969, Fig. 1.2), is 4.24 ± 0.02 m/yr and about 0.6 Myr, respectively. This accretion rate gives in combination with T_{eq} = 85 K and other parameters, varying slightly about their values listed in

Table 1.1 (e.g., Turcotte and Schubert, 1982, pp. 430-431), an accretion temperature T_{ac} = 353 to 355 K. This value agrees well with estimates of Kuramoto and Matsui (1994) that proto-Titan temperatures might have been higher than 300 K, and as high as 500 K.

Barr et al. (2010) estimated the accretion time of Titan as ≥0.8 Myr to ≥1.3 Myr, depending on the ammonia content of the satellite. From Barr's et al. (2010) range of accretion times, 1.16 Myr gives a mean rate of accretion of 2.22 m/yr and T_{ac} = 300 K from Eq. (1.2). The two estimates of the accretion temperature (355 and 300 K) lead to different thermal escape mechanisms of methane and ammonia, as will be shown in Section 1.5.

1.3.2. Primordial Heat Capacity

Heat capacity (C_p, J kg^{-1} K^{-1}) of the primordial Titan is one of the parameters needed to calculate its cooling rate (Section 1.3.3) and to estimate the escape velocities of the atmospheric gases during cooling (Section 1.5). The C_p values of Titan's components (Table 1.2) at 300 and 350 K are given in Table 1.4 as mass-weighted means of 2232 and 2357 J kg^{-1} K^{-1}. The C_p data of the individual components are listed in Table B.1, Appendix 1-B. Not all the data are available for the range of pressures up to 12 kbar in the outer fluid shell (Section 1.2.2). For CH_4, the data for methane gas were used, as we are not aware of such data for aqueous CH_4 solutions at high pressures. Data at 350 K were used as an approximation for the calculated accretion $T_{ac} \approx 355$ K. The effects of uncertainty in the C_p values on the Titan cooling rate and the thermal escape rates of CH_4 and NH_3 are addressed in Sections 1.3.3 and 1.5.

1.3.3. Titan's Cooling Rate

For heat dissipation by radiation emission from an ideal black body, the time needed for the cooling satellite to reach a certain temperature can be computed from Eq. (1.6), Table 1.5. The results are shown in Fig. 1.2 for the starting temperatures of 355 and 300 K. The overall cooling rate is unaffected by the different accretion temperatures, and the two curves are essentially identical at t > 1 Myr after accretion. The initial cooling period of both curves between 0.5 to 0.6 Myr is relatively fast, where the Titan temperature decreases to 150 K. It takes about 5 Myr for it

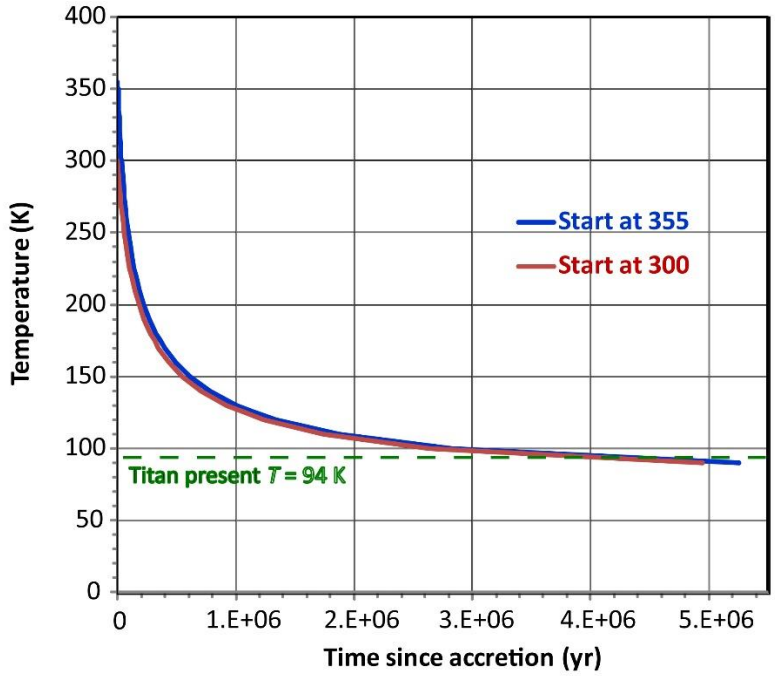

Fig. 1.2. Titan cooling after accretion for two different accretion temperatures, T_{ac} = 355 and T_{ac} = 300 K, Eq. (1.6). Titan's present surface temperature (94 K) is shown for reference (dashed green line).

to decrease to 90 K. The cooling rate depends on the Titan heat capacity (Table 1.4). A higher value of C_p results in a longer cooling time and therefore in a slower cooling rate. The effects of a variation of ~150 J kg^{-1} K^{-1}, comparable to the difference in the C_p values at 300 and 350 K, are

very small and they would hardly be noticeable at the scale of the graph in Fig. 1.2. For example, the cooling time from 300 to 220 K, for the range of C_p = 2232 ± 150 J kg^{-1} K^{-1} (the difference between the estimates of C_p at 350 and 300 K is 125 J kg^{-1} K^{-1}, Table 1.4), is 1.24×10^5, 1.16×10^5, and 1.08×10^5 years.

Table 1.4.
Primordial heat capacity (C_p).

Component	Heat capacity (J kg^{-1} K^{-1})		% of total mass
	300 K	350 K	
Methane Gas [a]	2956	3020	0.56
Ammonia-Water-Sulfuric Acid [b]	4031	4192	39.98
Brucite [c]	1349	1473	2.70
Antigorite [d]	1000	1100	56.76
Mean C_p (J kg^{-1} K^{-1})	2232	2357	100

Heat capacity data: [a] Setzmann and Wagner (1991); [b] Conde (2013); Zeleznik (1991); Wagner and Pruss (2002); [c] Horita et al. (2002); [d] Osako et al. (2010). More details in Table (B.1), Appendix 1-B.

Table 1.5.
Titan cooling rate.

Process or Parameter	Mathematical formulation		Explanatory comments
Heat content of Titan after accretion	$\frac{\frac{4}{3}\pi r^3 \rho C_p T}{4\pi r^2} = \frac{r\rho C_p T}{3}$ J m^{-2}	(1.3)	r = 2.575×10^6 m ρ = 1881 kg m^{-3} C_p = 2232 (300 K) and 2357 (350 K) J kg^{-1} K^{-1}, assumed constant T is temperature
Loss of heat balanced by radiative emission from an ideal black body	$-\frac{r\rho C_p}{3}\cdot\frac{dT}{dt} = \sigma\left(T^4 - {T_{eq}}^4\right)$ J s^{-1} m^{-2}	(1.4)	t is time (seconds) σ = 5.670×10^{-8} W m^{-2} K^{-4} T_{eq} = 85 K Other parameter values as above
Integral form of Eq. (1.4)	$-\frac{r\rho C_p}{3\sigma}\int_{T_{ac}}^{T}\frac{dT}{T^4 - {T_{eq}}^4} = \int_0^t dt$	(1.5)	T_{ac} is accretion temperature
Integrated Eq. (1.5) for calculation of cooling times t at temperatures T decreasing from T_{ac} to T_{eq}.	$t = \frac{r\rho C_p}{6\sigma T_{eq}^3}\left[\frac{1}{2}\ln\frac{T+T_{eq}}{T-T_{eq}}\cdot\frac{T_{ac}-T_{eq}}{T_{ac}+T_{eq}} + \tan^{-1}\frac{T-T_{ac}}{T_{eq}+TT_{ac}/T_{eq}}\right]$	(1.6)	Integration by parts of Eq. (1.5) or, identically, from an indefinite integral at *Wolfram Mathematica Online Integrator*

1.4. Present-Day and Primordial Atmosphere

1.4.1. Composition of the Present-Day Atmosphere

Present-day Titan's atmosphere can be divided into two main layers: the lower atmosphere (<880 km) consisting of the troposphere, stratosphere, and mesosphere; and the upper atmosphere (>880 km) that includes the thermosphere, ionosphere, and exosphere (Brown et al., 2009). This paper focuses on the lower atmosphere (also known as the homosphere), where the main mass of the gases resides.

Two main gases make up the bulk of Titan's atmosphere: N_2 and CH_4, which have approximate mole fractions of 0.98 and 0.014 (Niemann et al., 2005), respectively. The third most abundant molecule is hydrogen (H_2), of a mole fraction of 0.001 in the stratosphere (Courtin et al., 2008). N_2, CH_4, and H_2 are expected to be well mixed in the homosphere, although CH_4 is condensable in the troposphere (Samuelson and Mayo, 1997; Gilliam and McKay, 2011), contributing to Titan's methane hydrological cycle. Minor components in Titan's atmosphere include several hydrocarbons, nitriles, and oxygen compounds (Brown et al., 2009).

With NH_3 and CH_4 as the only gases in Titan's atmosphere, we consider two cases for the atmosphere composition in the present and three in the past. In Table 1.6, columns 2 and 3 give the composition and other parameters of the present-day atmosphere at 94 K, and columns 4-6 are for the primordial conditions.

In the present-day atmosphere (column 2), partial pressures of methane, as reported by Griffith et al. (2003), Jacquemart et al. (2008), and Lorenz et al. (1999), are in the range from 0.05 to 0.09 bar. We round this to 0.1 bar that with the N_2 partial pressure of 1.4 bar gives total atmospheric pressure $P = 1.5$ bar. From the total and individual components' partial pressures, the

masses of the two gases, total atmospheric mass, and volume were calculated using Eqs. (1.7)-(1.10) in Table 1.7, and atmospheric scale height or thickness calculated from Eq. (1.11). It may be noted that the scale height is not the total height of the atmosphere, but is the thickness of an isothermal atmosphere of known mass and composition or the height from the satellite surface to where the pressure decreases to 1/*e* of its value at the surface. For N_2 in the atmosphere attributed to its precursor, NH_3 (Atreya et al., 1978), the latter's mass equivalent to the present-day mass of N_2 is shown in column 3. The mass and volume of this atmosphere are accordingly somewhat greater than those of the N_2-containing atmosphere in column 2.

Table 1.6.
Present and primordial Titan atmosphere models.

1	2	3	4		5	6
Parameter	Present with N_2	Present with NH_3 equivalent	Mean of 5 models [a] [range of values]		Model in this paper	Model in this paper
T (K)	94	94	355	300	355	300
CH_4 (bar)	0.1[b]	0.1	35.9 [2.40 to 80]		19.58	19.58
NH_3 (bar)	1.4 (N_2)	1.70	5.7 [0.6 to 10]		5.82	5.82
P (bar)	1.5	1.80	41.6 [3 to 90]		25.40	25.40
Atm. mass (kg)	9.24×10^{18}	1.11×10^{19}	2.56×10^{20} [$(0.19 \text{ to } 5.55)\times10^{20}$]		1.57×10^{20}	1.57×10^{20}
Mass CH_4 (kg)	6.16×10^{17} [c]	6.16×10^{17} [c]	2.21×10^{20} [$(0.15 \text{ to } 4.93)\times10^{20}$]		1.19×10^{20}	1.19×10^{20}
Mass NH_3 (kg)	8.63×10^{18} (N_2)	1.05×10^{19} [d]	3.51×10^{19} [$(0.37 \text{ to } 6.16)\times10^{19}$]		3.76×10^{19}	3.76×10^{19}
Atm. volume (m^3)	1.77×10^{18}	2.84×10^{18}	1.12×10^{19} [$(1.12 \text{ to } 1.13)\times10^{19}$]	9.50×10^{18} [$(9.47 \text{ to } 9.52)\times10^{18}$]	1.12×10^{19}	9.45×10^{18}
Scale height or thickness (km)	21.07	33.51	128.34 [127.87 to 128.53]	109.25 [108.85 to 109.42]	127.75	108.74
Atm. top surface area (m^2)	8.47×10^{13}	8.55×10^{13}	9.05×10^{13}	9.18×10^{13}	9.18×10^{13}	9.05×10^{13}
Atm. density: mass/vol. (kg/m^3)	5.22	3.91	22.80 [1.65 to 49.25]	26.98 [1.95 to 58.28]	14.0	16.57

[a] Adapted from Niemann et al. (2005); Brown et al. (2009)
[b] References: Griffith et al. (2003); Jacquemart et al. (2008); Lorenz et al. (1999)
[c] CH_4 mass is 0.52% of the mass in columns 5 and 6
[d] NH_3 mass is 27.9% of the mass in columns 5 and 6

Table 1.7.
Relationships between atmospheric pressure, mass, volume, thickness, and outer surface area.

Process or Parameter	Mathematical formulation		Explanatory comments
Atmospheric mass (m, kg) as a function of atmospheric pressure, Titan surface area, and g at the surface. m_1 and m_2 are the individual component gas masses (kg)	$m = \frac{PS_T}{g}$ $m_1 = p_1 S_T/g$ and $m_2 = p_2 S_T/g$	(1.7)	P is total atm. pressure (Pa) p_1 and p_2 partial pressures of gases (Pa) $S_T = 8.332\times10^{13}$ m^2 g at the surface = 1.352 m s^{-2}
Relationship between the total and component gas masses, atmosphere volume, temperature and gas constant, from ideal gas law	$m = n_1M_1 + n_2M_2$ $= \frac{(p_1M_1 + p_2M_1)V_{atm}}{RT}$	(1.8)	m is atmosphere mass (kg) n_i mols of a gas component in the atm. M_i molecular mass of gas V_{atm} is atmosphere volume (m^3) R the gas constant = 8.3145 J mol^{-1} K^{-1}
Atmosphere volume from Eq. (1.8)	$V_{atm} = \frac{mRT}{p_1M_1 + p_2M_1}$	(1.9)	V_{atm} in m^3
Atmosphere volume as a function of the Titan radius (r, m) and atmosphere thickness (h, m)	$V_{atm} = \frac{4\pi}{3}[(r+h)^3 - r^3]$	(1.10)	V_{atm} in m^3 $r = 2.575\times10^6$ m
Thickness or scale height of the atmosphere from Eq. (1.10)	$h = \left(\frac{3V_{atm}}{4\pi} + r^3\right)^{1/3} - r$	(1.11)	h in m
Atmosphere outer surface area	$S_{atm} = 4\pi(r+h)^2$	(1.12)	S_{atm} in m^2. Other parameters as above

1.4.2. Primordial Atmosphere Composition

The exact composition of Titan's early atmosphere is not well known, although it is generally accepted that it was much more massive and denser than at present, and dominated by ammonia and methane. The range of NH_3 and CH_4 partial pressures, shown in column 4 of Table 1.6, is based on the work by Niemann et al. (2005) and Brown et al. (2009). Niemann et al. (2005), from the $^{14}N/^{15}N$ ratio measured in the Titan atmosphere by the Gas Chromatograph Mass Spectrometer (GCMS) on the Huygens probe, conclude a massive early atmosphere, between two and ten times today's value. Brown et al. (2009), also from the $^{14}N/^{15}N$ ratio measured by the GCMS, estimate that early Titan should have had a N_2 pressure between 5 and 10 bar, and a CH_4 pressure between 30 and 80 bar. We use the upper and lower limits for pNH_3 and pCH_4 given by

these sources and calculate their means and other parameters (column 4, Table 1.5), as explained in the preceding section for columns 2 and 3.

The most commonly accepted view of the origin of N_2 in Titan's atmosphere is the photodissociation of NH_3 into N_2, although Strobel (1982) believed N_2 to have been primordial. Atreya et al. (1978) proposed that after cooling of Titan's surface, and once outgassing began, ammonia in the atmosphere could have been photolyzed, converting NH_3 into nitrogen-bearing compounds, including N_2. Combining all of the intermediate steps involved in their model gives the overall reaction: $NH_3 + NH_2 \rightarrow N_2 + 2H_2 + H$. A crucial intermediate step of this reaction is the production of hydrazine (N_2H_4) from amidogen radicals (NH_2), created through the photolysis of NH_3, that also acts as the rate-limiting step in the production of N_2. An ideal temperature range for the production of N_2 from NH_3 on Titan is 150-250 K. NH_3 is a vapor below 150 K and whatever small amount of N_2H_4 is formed from it would condense, preventing N_2 formation. At a temperature above 250 K, water vapor pressure is sufficiently large, so that OH from its photolysis reacts with NH_2 and NH_3, producing NH whilst decreasing the amount of N_2 formed. The present atmospheric temperature on Titan should prevent NH_3 photolysis from producing N_2, and any N_2H_4 formed at the 94 K surface should sublimate prior to photolysis (Strobel, 1982). From the cooling curve in Fig. 1.2, Titan should have experienced these favorable temperatures between ~89,300 and 613,000 years after accretion at 355 K. This agrees with estimates of Brown et al. (2009), who report that the dissociation of NH_3 into N_2 must have occurred no later than 10 Myr after accretion.

If the Sun, in its very early history, emitted up to 10^4 times as much UV radiation than it does today (Zahnle and Walker, 1982), up to 20 bar of N_2 could be produced in less than 2 million

years in Titan's primordial atmosphere (Atreya et al., 1978). This finding was confirmed by Strobel (1982), who suggested that if Titan's surface temperature were 150 K or greater for approximately 4% of its evolutionary history (or about 180 Myr), then NH_3 photolysis could account for the current levels of N_2 in its atmosphere. Our results on the cooling rate of Titan (Fig. 1.2) suggest that 150 K could have been reached 6×10^5 years after the start of cooling.

From the data in column 4, Table 1.6, the results for a primordial atmosphere at 355 K suggest an atmospheric mass of 2.56×10^{20} kg and a scale height of 128 km. At 300 K, the same atmospheric mass corresponds to a scale height of 109 km.

The calculated composition of a primordial atmosphere at 355 and 300 K is given in columns 5 and 6 in Table 1.6, where the initial masses of CH_4 and NH_3 satisfy the conditions of gas thermal escape or emission-with-escape to the present-day levels as given in column 3 (Section 1.5). In the two primordial atmosphere models, starting with the masses of CH_4 and NH_3, the other parameters were calculated from the equations in Table 1.7.

The two primordial atmospheric models have scale thicknesses five to six times greater than the present-day atmosphere, a total pressure of 25 bar, in comparison to 1.5 bar at present, and densities of 14 to 16.6 kg/m^3, compared to 5.2 kg/m^3 at present.

1.5. Gas Escape

1.5.1. Maxwell-Boltzmann Gas-Molecular Velocity Distribution: H_2 and CH_4

Gases escape from the surface of a planet if their molecular or atomic velocities exceed the escape velocity of the planet $v_e = (2gr)^{1/2}$. The latter is a function of the planet's radius r and the acceleration due to the force of gravity at its surface, g (Table 1.1), and for Titan it is v_e =

2.639 km/s. This relationship explains why some planets and moons have atmospheres and others do not: a larger fraction of the molecules on a body with a massive atmosphere and low temperature, like Titan, may have smaller fractions of the atmosphere that can escape. The distribution of molecular speeds depends strongly on (1) the mass of the molecule and (2) temperature, as represented by the Maxwell-Boltzmann distribution of gas velocities[1]:

$$f(v) = 4\pi \left(\frac{M}{2\pi RT}\right)^{3/2} v^2 e^{-Mv^2/(2RT)} \tag{1.13}$$

or, using Eq. (1.15) in Table 1.8,

$$f(v) = \frac{4}{v_0^3\sqrt{\pi}}\, v^2 e^{-(v/v_0)^2} \tag{1.14}$$

The Maxwell-Boltzmann distribution describes gas molecules in thermal equilibrium, moving freely without interacting with one another, except for elastic collisions. Methane and ammonia are treated as individual gases in Titan's atmosphere insofar as their molecular masses are close: CH_4, M = 0.016 kg/mol, and for NH_3, M = 0.017 kg/mol. Other relevant relationships and parameters are given in Table 1.8.

Fig. 1.3 shows the Maxwell-Boltzmann distribution at 355 K of H_2 gas (M = 0.002 kg/mol), the third most abundant species in Titan's present-day atmosphere, and of the heavier CH_4 that does not lend itself to the same graphic representation as H_2 on a linear scale. Fig. 1.3 shows that peak velocity v_0 and mean velocity $\bar{v}_{>v_e}$ at the high end of the distribution, where $v_e \leq v < \infty$,

[1] In modern notation, the Maxwell-Boltzmann distribution is a probability density function or pdf (). The forms given by Maxwell (1860, p. 23; 1867, pp. 64, 69; 1890, p. 381) and Boltzmann (1896, p. 49) are somewhat different from a pdf, and their notation carried into the early and even later parts of the 20th century (Jeans, 1911, p. 658; 1916, p. 33; Chapman, 1916, p. 283; Chapman and Cowling, 1970, p. 69). The latter (1970, pp. 131, 407) and Brush (2008) also discussed David Enskog's earlier contributions to Maxwell's theory.

are greater for the lighter H_2 that for the heavier CH_4 and NH_3. For these and some heavier gases, mean velocities $\bar{v}_{>v_e}$ are shown in Fig. 1.4.

Table 1.8.
Parameters of Maxwell-Boltzmann distribution and thermal gas escape.

Process or Parameter	Mathematical formulation		Explanatory comments
Most probable speed at the velocity distribution peak (m/s)	$v_0 = \sqrt{2RT/M}$	(1.15)	Solution of $df(v)/dv = 0$, where $f(v)$ is given in Eq. (1.13). R is the gas constant (8.3145 J mol^{-1} K^{-1}) and M is molecular mass of the gas (kg mol^{-1})
Mean velocity of the distribution (m/s)	$\bar{v} = \int_0^\infty v f(v) dv = \sqrt{\frac{8RT}{\pi M}} = \frac{2}{\sqrt{\pi}} v_0$	(1.16)	$f(v)$ is the Maxwell-Boltzmann distribution in Eq. (1.13)
Cumulative distribution of gas velocities (fraction)	$\mathcal{F}(v) = \int_0^v f(v) dv$ $= \text{erf}\left(\frac{v}{v_0}\right) - \frac{8}{v_0^3 \sqrt{\pi}} e^{-(v/v_0)^2}$	(1.17)	$\mathcal{F}(v) \to 1$, as $v \to \infty$
Fraction of the distribution at velocities greater than Titan's escape velocity v_e.	$\mathcal{F}(v \geq v_e) = \frac{4}{v_0^3 \sqrt{\pi}} \int_{v_e}^\infty v^2 e^{-(v/v_0)^2} dv$ $= \frac{2v_e}{v_0 \sqrt{\pi}} e^{-(v_e/v_0)^2} + \text{erfc}(v_e/v_0)$	(1.18)	Range of velocities: $v_e \leq v < \infty$
Approximation of the fraction in Eq. (1.19) for $v_e/v_0 > 2$ to >2.5: $\text{erfc}(v_e/v_0)$ $= e^{-(v_e/v_0)^2}/(\sqrt{\pi}\, v_e/v_0)$	$\mathcal{F}(v > v_e) = \frac{2}{\sqrt{\pi}} \frac{v_e}{v_0} e^{-(v_e/v_0)^2}$ $+ e^{-(v_e/v_0)^2}/(\sqrt{\pi}\, v_e/v_0)$	(1.19)	Goody (1976) gives the following approximation for $\mathcal{F}(v > v_e)$, for the same conditions of $v_e/v_0 > 2$: $\mathcal{F}(v > v_e) = \frac{4}{\pi} \frac{v_e}{v_0} e^{-(v_e/v_0)^2}$ This result is greater than that of Eq. (1.19) by a factor of $2/\sqrt{\pi} = 1.13$ or about 13%.
Mean velocity in the velocity interval $v_e \leq v < \infty$ (m/s)	$\bar{v}_{>v_e} = \int_{v_e}^\infty v f(v) dv \Big/ \int_{v_e}^\infty f(v) dv$ $= \frac{2v_e[1 + (v_e/v_0)^2]}{1 + 2(v_e/v_0)^2}$	(1.20)	Note: In this velocity interval, the Maxwell-Boltzmann distribution is *not* a pdf. The ratio of the high-velocity mean to the escape velocity, $\bar{v}_{>v_e}/v_e$, is always > 1.

At the starting temperature of 355 K, easy and fast escape of the much lighter H_2 is possible, but CH_4, of a higher molecular mass, has a small fraction above the escape velocity, $\mathcal{F}(v \geq v_e)$, that accounts for a slow, but significant escape over a long period of time.

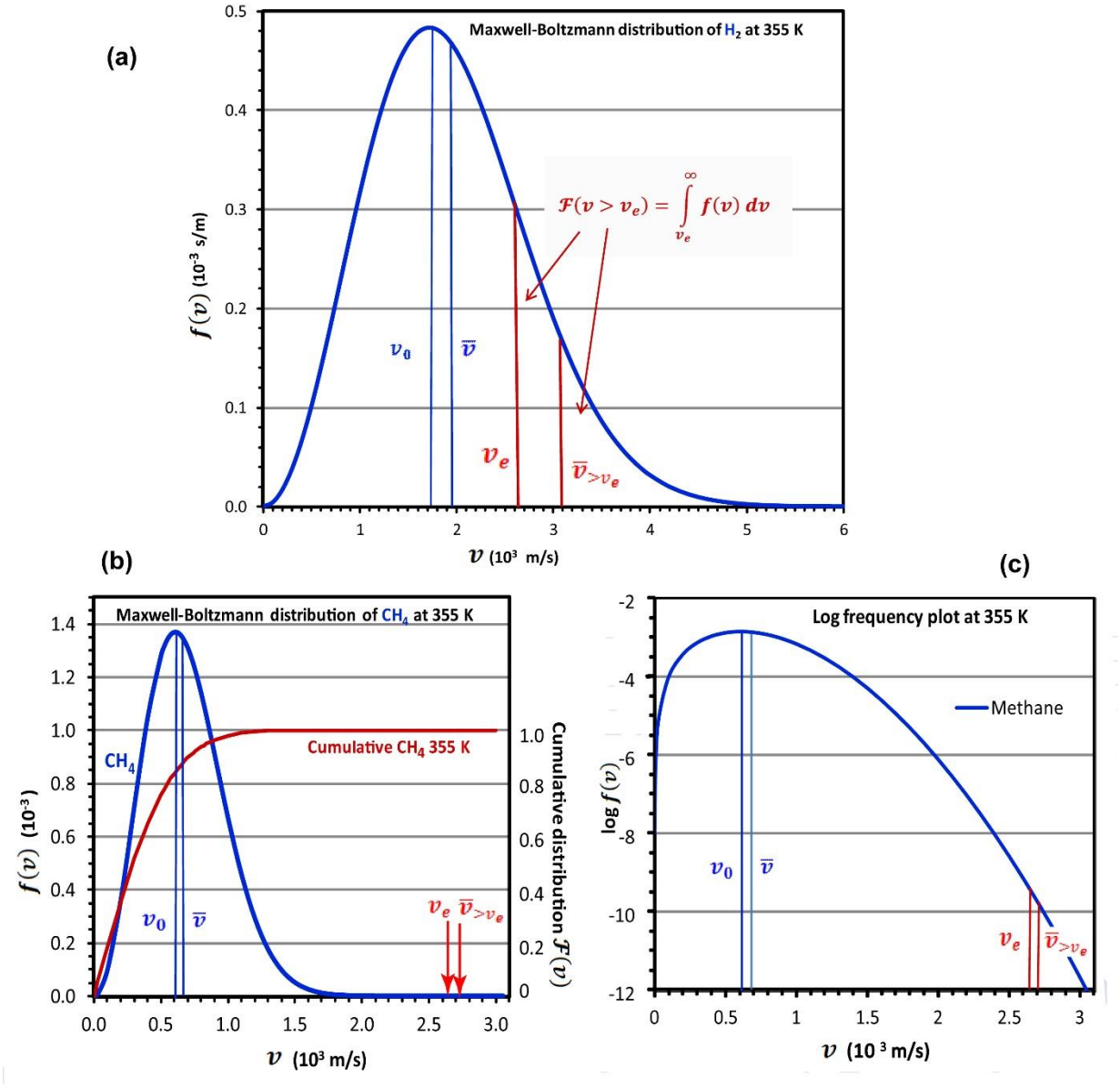

Fig. 1.3. (a) Maxwell-Boltzmann distribution of H_2 at 355 K, showing the peak velocity v_0, mean velocity $\bar{v}$, Titan escape velocity v_e, and mean velocity $\bar{v}_{>v_e}$ in the interval $v_e \leq v < \infty$. (b) Linear plot of $f(v)$ of CH_4 at 355 K. Cumulative frequency for CH_4 shown as a check of calculation. (c) Logarithmic plot of $f(v)$ of CH_4 at 355 K. Eqs. (1.13)-(1.20).

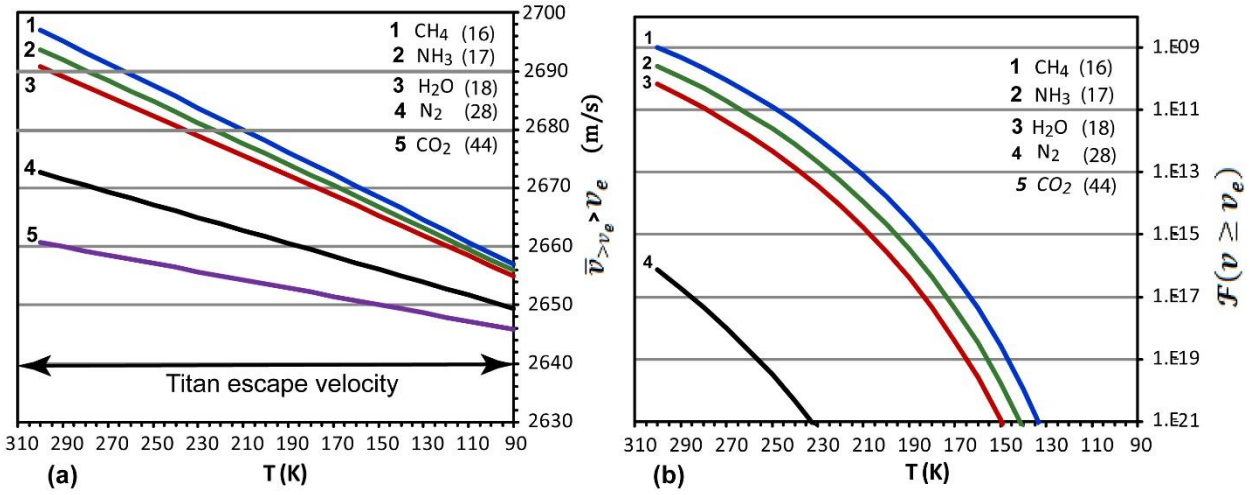

Fig. 1.4. (a) Mean escape velocity of gases $\bar{v}_{>v_e}$, above the Titan escape velocity v_e, as a function of temperature and molecular mass, Eq. (1.20). (b) Dependence of the fraction of the gas mass above the Titan escape velocity, $\mathcal{F}(v > v_e)$, on temperature and molecular mass, Eq. (1.19). CO_2 falls off the figure scale. Numbers in parentheses are molecular masses in gram/mol.

1.5.2. Gas Escape Formulation

In a gas, the directions of the gas molecules are on the average outward and inward (Maxwell, 1867, p. 50), and the fraction of the gas moving away from the planet is ½ of the fraction $\mathcal{F}(v > v_e)$ (e.g., Goody, 1976). Fig. 1.5a and Table 1.9 describe the gas escape from the atmosphere as a first-order process, $N_t = N_0\, e^{-kt}$ (kg or % of N_0), that depends on the escape rate parameter, k (s^{-1} or yr^{-1}). The latter is a function of temperature and molecular mass of the gas, through its dependence on v_0, of the Titan escape velocity, v_e, and of the quotient of the atmosphere volume to its outer surface area, V_{atm}/S_{atm}, that is effectively the atmosphere thickness h (Table 1.6 and 1.7). As the atmosphere cools over time, the fraction of gas greater than the escape velocity, $\mathcal{F}(v > v_e)$, decreases faster than the mean escape velocity $\overline{v}_{>v_e}$(Fig. 1.4). Thus, the escape rate parameter, k, decreases strongly with a decreasing temperature (Fig. 1.6).

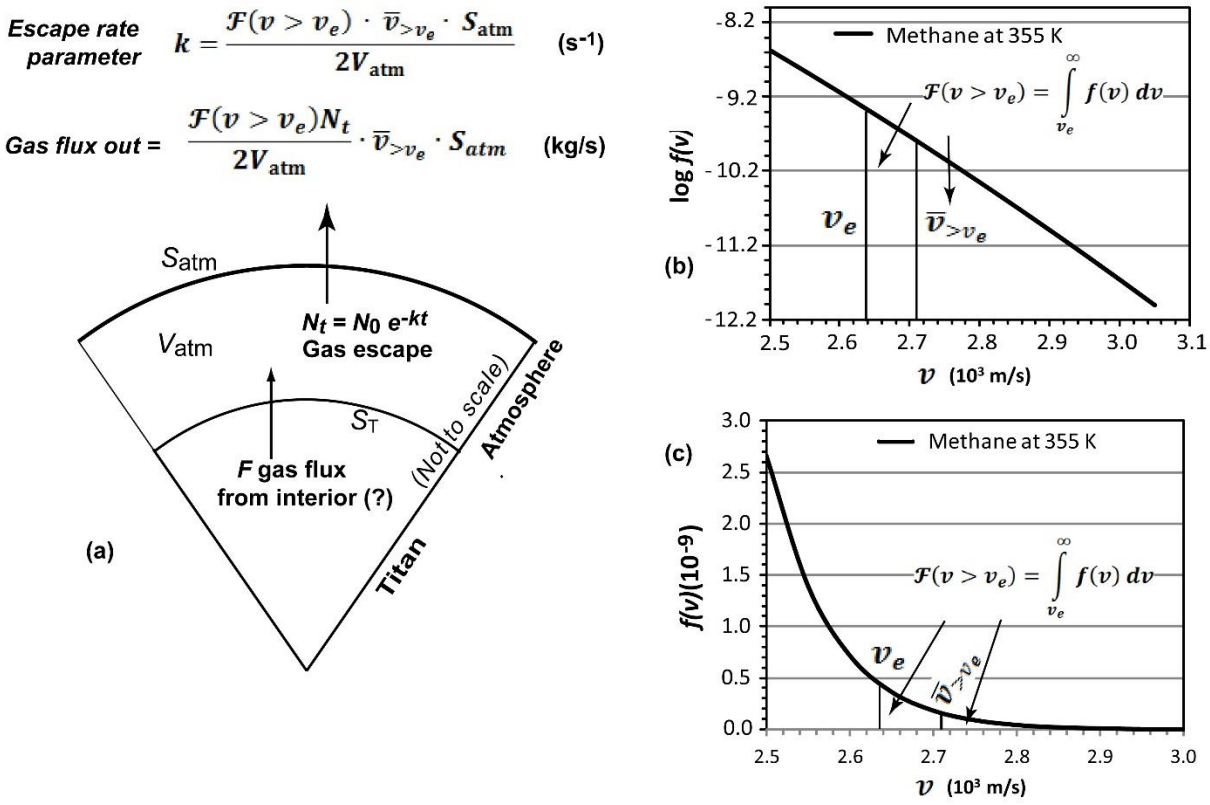

Fig. 1.5. (a) Schematic diagram of Titan and its atmosphere, gas fluxes, and main equations. (b) Logarithmic velocity frequency distribution at higher velocities. (c) Linear velocity frequency distribution at higher velocities.

Two figures (1.5b and 1.5c) show the high-tail parts of the velocity distribution (Fig. 1.3b) of methane on a logarithmic and linear scale. As these figures show, the fraction of CH_4 gas molecules that have velocities greater than the escape velocity is small. However, although $\mathcal{F}(v > v_e)$ is low for CH_4, its product with mean escape velocity above v_e assures a slow but substantial escape of CH_4 over a long period of time.

Table 1.9.
Parameters of gas escape rate.

Process or Parameter	Mathematical formulation		Explanatory comments
Gas mass remaining in the atmosphere (kg)	$N_t = N_0\, e^{-kt}$	(1.21)	N_0 initial gas mass (kg) k is escape rate parameter (s^{-1}) t is time (s)
Concentration of the escaping gas in the atmosphere (kg/m^3)	$\frac{\frac{1}{2}\mathcal{F}(v > v_e)N_t}{V_{atm}}$	(1.22)	$0.5\mathcal{F}(v > v_e)$ escaping gas fraction N_t gas mass in the atmosphere (kg) V_{atm} atmosphere volume (m^3)
Mass flux out of the atmosphere (kg/s)	$\frac{\mathcal{F}(v > v_e) \cdot \bar{v}_{>v_e} \cdot S_{atm}}{2V_{\text{atm}}} \cdot N_t = kN_t$	(1.23)	
Escape rate parameter k (s^{-1})	$k = \frac{\mathcal{F}(v > v_e)\ \cdot\ \bar{v}_{>v_e} \cdot\ S_{\text{atm}}}{2V_{\text{atm}}}$ $k = \frac{v_e}{v_0} e^{-(v_e/v_0)^2} \left[\frac{2}{\sqrt{\pi}} + \frac{1}{(v_e/v_0)^2\sqrt{\pi}}\right] \cdot \frac{2v_e[1 + (v_e/v_0)^2]}{1 + 2(v_e/v_0)^2} \cdot \frac{S_{\text{atm}}}{2V_{\text{atm}}}$	(1.24)	
Calculation of N_t	$N_{i+1} = N_i\, e^{-0.5(k_{i+1} + k_i)(t_{i+1} - t_i)}$	(1.25)	Calculated for every two consecutive time steps, $t = i$ and $t = i+1$, and a mean value of k for that period, $(k_{i+1} + k_i)/2$
Gas emission from the interior to the atmosphere and thermal loss from the latter	$N_t = \frac{F}{k}(1 - e^{-kt}) + N_0\, e^{-kt}$	(1.26)	F constant input rate (% of N_0 per yr). Other parameters as in Eq. (1.21)
Calculation of N_t, emission and escape model	$N_{i+1} = \frac{F}{0.5(k_{i+1} + k_i)}$ $\left[1 - e^{-0.5(k_{i+1} + k_i)(t_{i+1} - t)}\right] + N_0\, e^{-0.5(k_{i+1} + k_i)(t_{i+1} - t)}$	(1.27)	

1.5.3. Gas escape at 355 K

Starting at an accretion temperature of 355 K, the calculated values of k for NH_3 and CH_4 are too high and they allow the gases to escape before the atmosphere temperature drops sufficiently to prevent any further escape, which occurs below about 260 K (Fig. 1.6). The

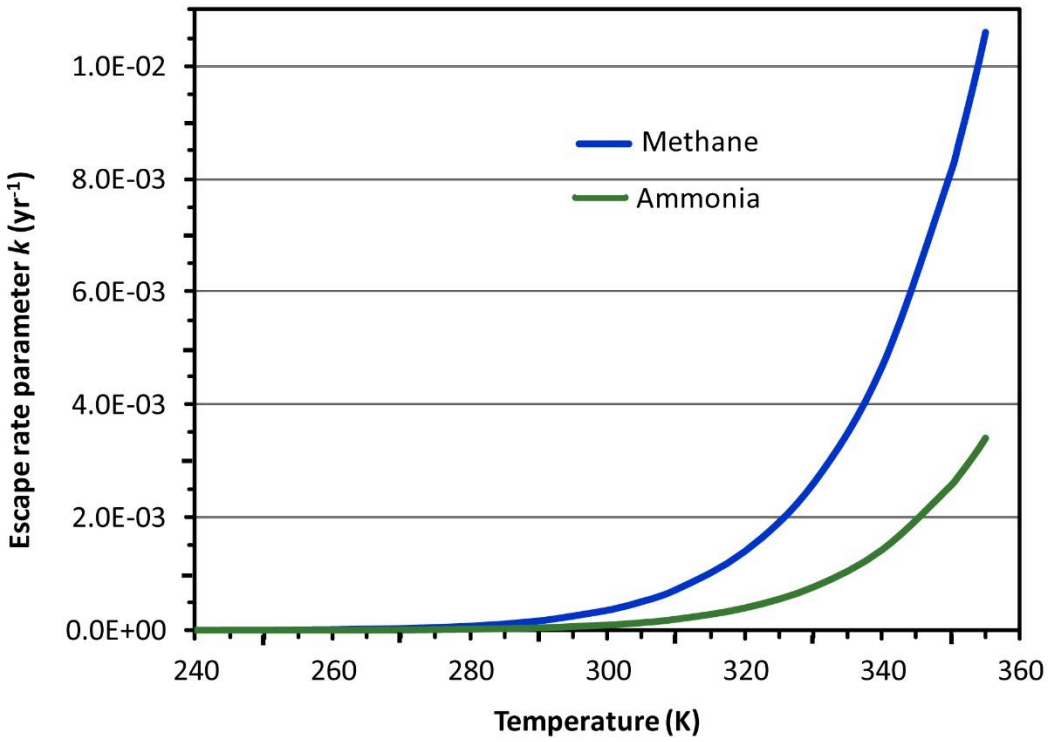

Fig. 1.6. The escape rate parameter, k, vs. temperature, T, for NH_3 and CH_4, assuming a T_{ac} = 355 K. In this model, k is not effective below $T \approx 270$ K, Eq. (1.24). Compare Fig. 1.10.

relatively high values of k for CH_4 and NH_3 near 355 K account for the fact that very little of the initial gas mass would be left in the atmosphere after a few hundred years, as shown in Fig. 1.7. Considering Titan's cooling rate (Fig. 1.2), the temperature of 150 K, as a lower limit of NH_3 to N_2 conversion (Atreya et al., 1978), is reached after about 500,000 to 600,000 years, and after such a long period of time the gas masses remaining would be vanishingly small fractions of the initial masses as given in Table 1.6, column 5.

Two hypothetical, but similarly unrealistic, explanations of slower rates of gas escape from a 355 K atmosphere may be considered:

(1) Escape rate parameter, k, as shown in Fig. 1.5 and Eq. (1.24), depends on the atmosphere outer surface area, S_{atm}. If the outer atmosphere were only partially permeable to the

escaping CH_4 and NH_3, their outgoing fluxes would have been smaller and the atmosphere might have cooled sufficiently before the two gases were exhausted. However, this requires partial permeability of the upper atmosphere to be about 5% (5.6% for CH_4 and 4.5% for NH_3) for the initial gas masses to decrease to their present-day levels.

(2) The dependence of escape rate parameter k on the quotient V_{atm}/S_{atm} and therefore on the atmosphere thickness h, could make k sufficiently smaller at a larger quotient V_{atm}/S_{atm}, to reduce the initial gas masses to their present-day levels. This, however, could be accomplished only for an unrealistic atmosphere of thickness $h \approx 4316$ km, greater than the Titan radius of 2575 km, total pressure of about 28 bar, and low density of 0.13 kg/m^3. A more realistic explanation, emissions from the interior combined with thermal escape, is given in the following section.

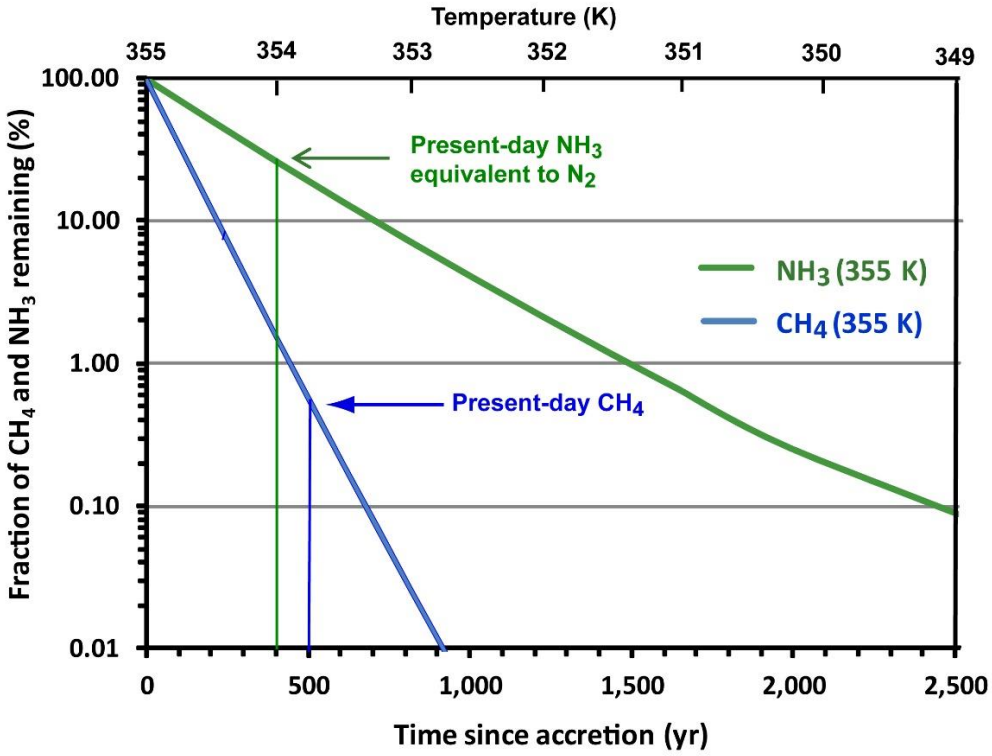

Fig. 1.7. The fraction of CH_4 and NH_3 remaining as a function of time since accretion assuming T_{ac} = 355 K, Eq. (1.25).

1.5.4. Possible Emissions from Titan's Interior

Possible cryovolcanic features on Titan's surface have been identified by the Cassini Radar Mapper, as well as other visual and infrared instruments onboard the Cassini spacecraft (Lopes et al., 2007). Cryovolcanism on Titan resembles silicate volcanism on Earth, except its eruptions consist of volatiles, such as water, ammonia, and methane, instead of molten rock. Cryovolcanism is considered by some (Atreya et al., 2006; Fortes et al., 2007; Grindrod et al., 2008) the leading mechanism for the replenishment of methane in Titan's atmosphere, where it may be irreversibly lost due to photochemical dissociation. Methane replenishment via cryovolcanism is supported by many, including Fortes et al. (2007), who estimate that a magma containing 0.5 wt% CH_4, erupted at a reasonable rate of up to ~1.0×10^{12} kg/yr, could buffer the photolytic destruction of atmospheric methane. This emission rate agrees with the lower flux in the emission-and-escape model, as shown in Table 1.10. However, a constant rate of methane input 1.0×10^{12} kg/yr would exhaust the

Table 1.10.
Summary of CH_4 and NH_3 inferred input rates to Titan's atmosphere.

Gas species and process	In solid planet (kg)	In present-day atm. 94 K		In primordial atm. 355 K	
		(kg)	(bar)	N_0 (kg) or N_0=100%	(bar)
CH_4	7.523E+20	6.163E+17	0.1	1.190E+20	19.6
NH_3 (N_2 mass equivalent in present-day atm.)	1.622E+21	1.049E+19	1.7	3.760E+19	5.8
CH_4 % of mass in solid		0.08%		15.81%	
NH_3 % of mass in solid		0.65%		2.32%	
		CH_4		NH_3	
Input to atm. F (% yr^{-1} of N_0), starting at 355 K	1.00E-06	1.00E-05	1.00E-04	8.00E-04	1.45E-03
CH_4 Input flux $FN_0/100$ (primordial) (kg/yr)	1.19E+12	1.19E+13	1.19E+14		
Time to exhaust CH_4 in the interior (yr)	6.32E+08	6.32E+07	6.32E+06		
NH_3 Input flux $FN_0/100$ (primordial) (kg/yr)				3.01E+14	5.45E+14
Time to exhaust NH_3 in the interior (yr)				5.4E+06	3.0E+06

CH_4 content of the satellite (Table 1.2) in about $(7.5\times10^{20}$ kg)/$(1.0\times10^{12}$ kg/yr) ≈ 750 Myr, a time period too short in Titan's history. Photolytic decomposition of CH_4 by UV radiation at altitudes 300 km produces ethane (C_2H_6) as one of the main stable products (Strobel, 1982; Lunine et al., 1983; Smith and Raulin, 1999; Wilson and Atreya, 2004; Atreya et al., 2006; Lunine and Atreya, 2008). Ethane accumulates on the Titan surface, but its reevaporation and reconversion to methane are not considered as realistic sources of CH_4 replenishment in the atmosphere, where its chemical lifetime is estimated from about 27,000 yr at altitude 300 km (Wilson and Atreya, 2004) to 10^7 to 10^8 yr (Atreya et al., 2006). The longer estimate of the CH_4 residence time in the atmosphere cited above, 10^7 to 10^8 yr, is much longer than our estimates of the residence time ($1/k$), increasing from 2400 yr at 300 K to 3×10^7 yr at 210 K, reached after 145,000 yr. Thus, if the longer residence time is due to photolytic destruction of CH_4, our results for the much-diminished flux out of the atmosphere do not contradict the slow rates of methane destruction and replenishment on the cooled Titan.

Among the many possible emission scenarios that may be thought of, the case we explore is gas thermal escape accompanied by emission from Titan's interior, a simple process that is a combination of a constant input rate to the atmosphere, F (% N_0/yr or kg/yr), with a first-order escape is considered here: $dN/dt = F - kN$, the solution of which is given in Eqs. (1.26)-(1.27). For CH_4, three reasonable rates of emission are shown in Fig. 1.8a and Table 1.10. If CH_4 emissions from the Titan interior were continuous, the supply would be exhausted in 6.32 to 632 Myr. To avoid complete depletion of CH_4 from the internal reservoir, and to satisfy the present-day CH_4 atmospheric level, emissions at the rates shown in Fig. 1.8a would have to stop at 57,350 (F =

1.0×10^{-4} %/yr), 117,500 ($F = 1.0\times10^{-5}$ %/yr), and 612,500 ($F = 1.0\times10^{-6}$ %/yr) years, respectively, after the start of CH_4 input to the atmosphere.

The NH_3 emissions include two reasonable rates of input: $F = 1.45\times10^{-3}$ %/yr and $F = 9.0\times10^{-4}$ %/yr (Fig. 1.8b and Table 1.10). In a continuous emission at these rates, the NH_3 reservoir would be depleted in 3 to 5.4 Myr after the emission start. A discontinuous input, with NH_3 emissions stopping at 57,360 ($F = 1.45\times10^{-3}$ %/yr) and 74,000 ($F = 9.0\times10^{-4}$ %/yr) years after the start of input to the atmosphere, would satisfy the present-day level of NH_3 (N_2 equivalent) (Table 1.6, column 3).

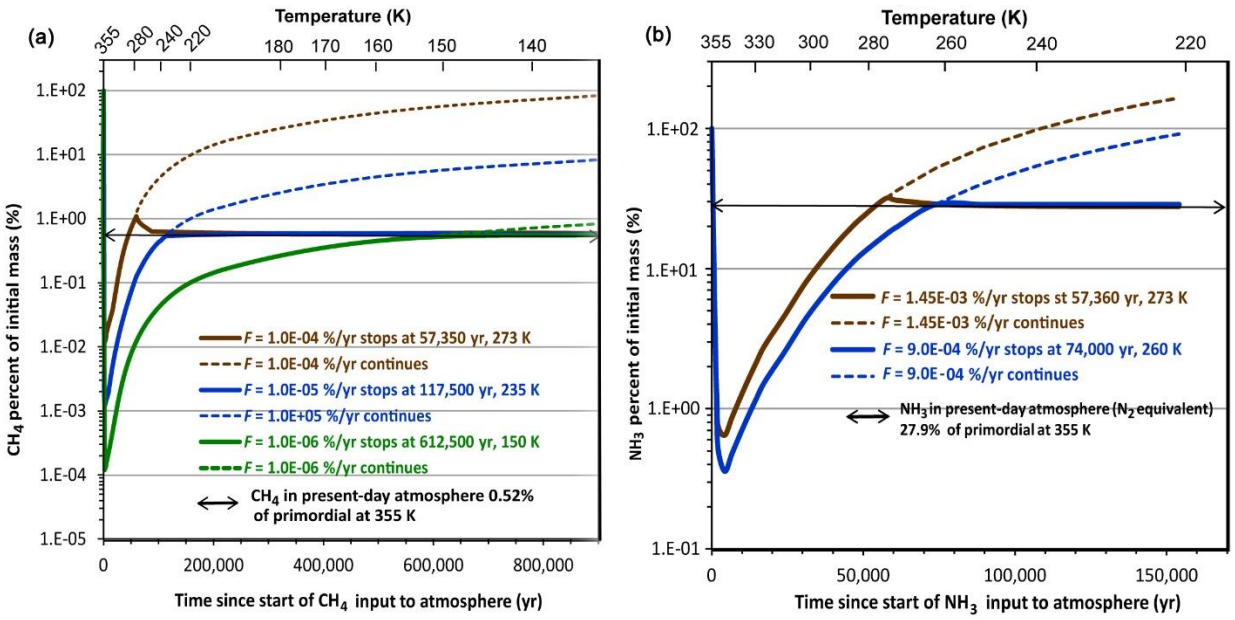

Fig. 1.8. Input of (a) CH_4 and (b) NH_3 from Titan interior to the atmosphere, added to the escaping gases. Final masses are stabilized at their present-day values (Table 1.6, column 3). Curves computed using Eq. (1.27).

It should be realized that the processes described in Fig. 1.8 and Table 1.10 assume termination of the emissions at a time that satisfies the primordial atmosphere to meet the conditions of present day. The results also show periods of variable length where the atmosphere

had very low concentrations of the two gases, until their levels were raised by emissions from the interior.

1.5.5. Gas escape at 300 K

A primordial atmosphere, initially at 300 K (Table 1.6, column 6), loses CH_4 and NH_3 by thermal escape down to their present-day levels (column 3) by the time the atmosphere has cooled to about 250 K (Fig. 1.9). As the gases are continuously lost from the atmosphere, its mass and volume decrease, making the escape rate parameter *k* slightly larger and escape rate faster. The results of this change in *k* are shown in Figs. 1.9 and 1.10, by the curves for a constant or decreasing atmosphere volume.

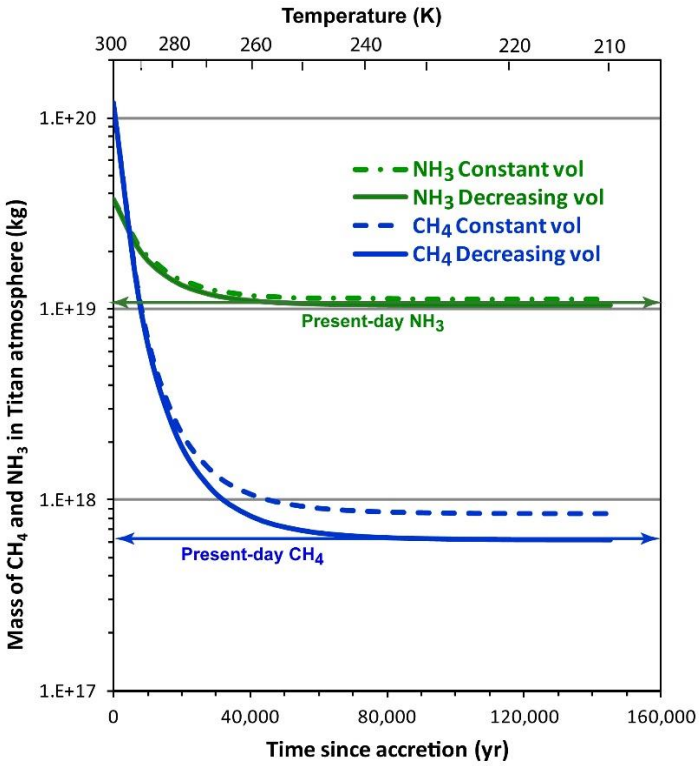

Fig. 1.9. The amount of NH_3 and CH_4 remaining in the atmosphere as a function of time since accretion assuming a T_{ac} = 300 K. Eq. (1.25).

As the value of the Titan mean heat capacity, C_p = 2232 J kg^{-1} K^{-1} at 300 K (Table 1.4), affects the time and rate of the satellite cooling (Section 1.3.2), a variation in C_p also affects the initial masses of CH_4 and NH_3 in the primordial atmosphere that are computed to make the initial masses decrease to their present-day levels (Table 1.6, columns 6 and 3). In a test of sensitivity of the results to the C_p values, a variation of ~150 J kg^{-1} K^{-1} in C_p = 2232 J kg^{-1} K^{-1} produces only very small effects on the cooling rate. At the higher C_p value, it takes slightly longer to cool from one temperature point to a lower one, and this slower cooling rate allows more gas to escape from the atmosphere. At the conditions of a higher or lower Titan C_p, 2382 or 2082 J kg^{-1} K^{-1}, the initial atmospheric mass N_0 of CH_4, would be +44% to -30% of the model value, and for NH_3 it would be ±9%. These changes are due to the greater or smaller time-interval differences, t_{i+1} - t_i, in Eq. (1.25) that affect the negative exponential term and the resulting value of the remaining gas mass fraction N_t.

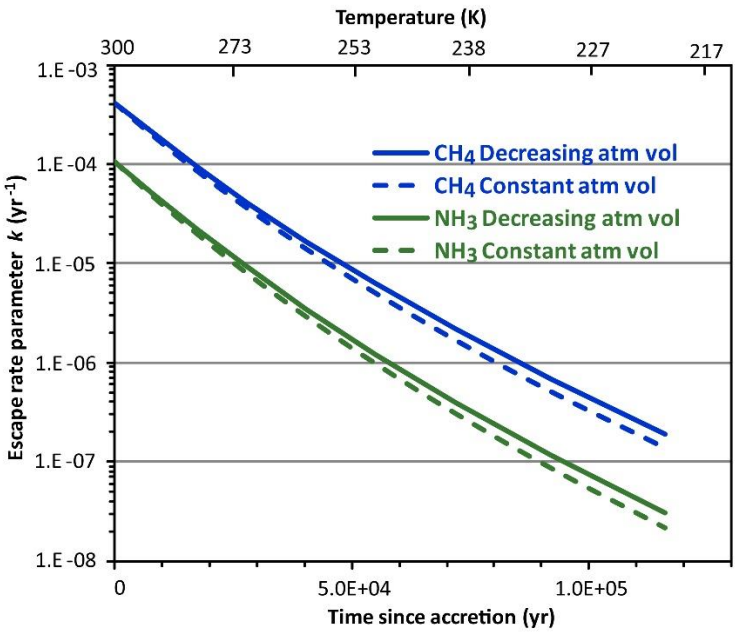

Fig. 1.10. The escape rate parameter, k, as a function of time since accretion for CH_4 and NH_3 assuming a T_{ac} = 300 K. Eq. (1.24).

In this thermal escape model, the escape of NH_3 and CH_4 ends 50,000 to 70,000 years after start, when the gas masses decline to their present-day levels. However, in the model of gas emission-and-escape (Fig. 1.8), the times of mass decline are longer: for NH_3, depending on its emission rate, it takes about 70,000 to 80,000 years. At the different emission rates of CH_4, it takes 100,000 to 600,000 years to attain a steady-state value.

1.6. Conclusions

This paper presents a new model of the NH_3 and CH_4 sinks, the two main gases, in Titan's primordial atmosphere. If NH_3 and CH_4 were removed from the atmosphere, initially at 300 K, by thermal escape as the only sink, the final result are the present-day gas masses in the atmosphere, attained after 50,000 to 70,000 yr.

An alternative model combines the two mechanisms of gas emission from Titan's interior with thermal escape. At the different estimated emission rates from the interior, the times of mass decline from the primordial, at 355 K, to present-day levels are longer: for NH_3, the decline is about 70,000 to 80,000 years; for CH_4, it takes 100,000 to 600,000 years to attain a steady-state value. We place less trust in the emission-with-escape model because of (a) arbitrary assumptions of the period lengths of the emissions and (b) significantly, the discrepancies between the reported rates of CH_4 emissions and our estimates of the available CH_4 inventory in the Titan interior.

The models of gas thermal escape and emission-with-escape are based on the estimates of Titan's post-accretional composition, as made of a solid core of antigorite ($Mg_3Si_2O_5(OH)_4$) and brucite ($Mg(OH)_2$), and an outer fluid shell made of the volatile components (H_2O, NH_3, $(NH_4)_2SO_4$, and CH_4) that account for 40.54% of Titan's mass. The accretion temperature is

estimated in the range from 300 to 355 K, based on the gravitational energy of accretion, without additional heat production or storage, and radiational emission cooling of an ideal black body. For the post-accretional cooling rate, we estimated mean heat capacity, C_p, of Titan at the two temperatures, from compilations of the C_p data for the individual components.

An analysis of the thermal escape mechanism as a Maxwell-Boltzmann gas indicates a strong dependence of the gas escape rate on temperature, molecular mass of the gas species, the escape velocity at the satellite surface, and the atmosphere thickness or the quotient of its volume to outer surface area. Titan's cooling controls the gas escape from the atmosphere, resulting in the computed primordial masses decreasing to their present-day values by the time the temperature has declined to below 250 K.

APPENDIX 1-B

B.1. Pressure, mass, volume, and thickness of the atmosphere

The equations in this Appendix are used in the calculation of the parameters in Table 1.5.

At a given total pressure P (Pa), g at the Titan surface (m/s^2) and the surface area S_T (m^2), atmospheric mass m (kg) is:

$$m = \frac{PS_T}{g} \tag{B.1}$$

In an atmosphere made of two gases — 1 CH_4 and 2 NH_3, of molar mass M_1 and M_2 (kg/mol), respectively — their partial pressures are p_1 and p_2, and $P = p_1 + p_2$. Thus the individual gas masses, from their partial pressures, are:

$$m_1 = p_1 S_T/g \quad \text{and} \quad m_2 = p_2 S_T/g \tag{B.2}$$

In an ideal-gas isothermal atmosphere, the number of mols of each gas is $n_1 = p_1 V_{atm}/(RT)$ and $n_2 = p_2 V_{atm}/(RT)$, where V_{atm} is the atmosphere volume (m^3), R is the gas constant (8.3145 J mol^{-1} K^{-1}), and T is temperature (K). The atmosphere mass m is the sum of the mols of the two gases:

$$m = n_1 M_1 + n_2 M_2 = \frac{(p_1 M_1 + p_2 M_1) V_{atm}}{RT} \tag{B.3}$$

and its volume V_{atm} is computed from the preceding equation:

$$V_{\text{atm}} = \frac{mRT}{p_1 M_1 + p_2 M_1} \tag{B.4}$$

The atmosphere thickness or scale height is determined from its volume as a spherical shell:

$$V_{\text{atm}} = \frac{4\pi}{3}[(r+h)^3 - r^3] \tag{B.5}$$

where r (m) is the Titan radius and h (m) is the atmosphere thickness.

From (B.5), the atmosphere thickness h is:

$$h = \left(\frac{3V_{\text{atm}}}{4\pi} + r^3\right)^{1/3} - r \tag{B.6}$$

The outer surface of the atmosphere, S_{atm}, is, from the preceding:

$$S_{\text{atm}} = 4\pi(r+h)^2 \tag{B.7}$$

Alternatively, scale height of the atmosphere h can also be determined from the quotient of the atmosphere volume to its outer surface area, $V_{\text{atm}}/S_{\text{atm}}$, that is used in Appendix 1-D:

$$\frac{V_{\text{atm}}}{S_{\text{atm}}} = \frac{(4\pi/3)[(r+h)^3 - r^3]}{4\pi r^2} \tag{B.8}$$

From (B.7), *h* is:

$$h^3 + \left(3r - \frac{3V_{\text{atm}}}{S_{\text{atm}}}\right)h^2 + \left(3r^2 - \frac{6rV_{\text{atm}}}{S_{\text{atm}}}\right)h - \frac{3r^2V_{\text{atm}}}{S_{\text{atm}}} = 0 \qquad \text{(B.9)}$$

The results for *h* are identical when computed by both equations (B.6) and (B.9)

APPENDIX 1-C

The table below lists the values of the heat capacity of Titan's primordial components as given in Table 1.4.

Table C.1.
Summary of C_p data at different temperatures and pressures

Heat capacities C_p (J kg^{-1} K^{-1}) [a]								
	300 K, 1 bar	5-10 bar	1 kb	2 kb	1-5 kb	5kb	47-85 kb	
Methane gas	2226				**2956**			Setzmann and Wagner (1991), Table 39, p. 1119 et seq.
Ammonia-Water ~3 wt%	4136							Calculated from Conde (2006, p. 10), mass fract. NH_3 = 0.0326
	4150							Conde (2013), from Fig. 8 in 2006 edition
H_2SO_4, mol fraction x = 4.266E-03 (C_p/R)	***763.02***							Zeleznik (1991), Table 7, p. 1189 et seq.
H_2O	4180.60		3979.8	***3882.8***		3793.8		Wagner and Pruss (2002), pp. 496, 533
x H_2SO_4+(1- x)H_2O				***3869.49***				From the C_p of mol fractions of H_2SO_4 and H_2O
NH_3-H_2SO_4-H_2O solution				**4031.21**				Mean of the NH_3-H_2O and H_2SO_4-H_2O solutions
Magnesium hydroxide	**1348.79**							Horita et al. (2002), Table 4 (mean of calc. and experim. values)
Antigorite	1985.75							Grindrod et al. (2008)
							1000	Osako et al. (2010), Fig. 3
	350 K, 1 bar	5-10 bar	1 kb	2 kb	1-5 kb	5kb	47-85 kb	
Methane gas	2365				**3020**			Setzmann and Wagner (1991), Table 39, p. 1119 et seq.
Ammonia-Water ~3 wt%	4188							Calculated from Conde (2006, p. 10), mass fract. NH_3 = 0.0326
		4400						Conde (2013), from Fig. 8 in 2006 edition
H_2SO_4, mol fraction x = 4.266E-03 (C_p/R)	***767.25***							Zeleznik (1991), Table 7, p. 1189 et seq.
H_2O	4194.5		4025.3	***3921.4***		3785.8		Wagner and Pruss (2002), pp. 496, 533
x H_2SO_4+(1- x)H_2O				***3907.94***				From the C_p of mol fractions of H_2SO_4 and H_2O
NH_3-H_2SO_4-H_2O solution				**4191.62**				Mean of the NH_3-H_2O and H_2SO_4-H_2O solutions
Magnesium hydroxide	**1472.68**							Horita et al. (2002), Table 4 (mean of calc. and experim. values)
Antigorite	1986.72							Grindrod et al. (2008)
							1100	Osako et al. (2010), Fig. 3

[a] Values in **boldface roman** are used in the calculation of mean C_p in Table 1.4, those in ***boldface italics*** are for intermediate calculations of C_p of the NH_3-H_2SO_4-H_2O solution at 300 and 350 K.

APPENDIX 1-D

D.1. Titan accretion temperature and cooling rate

D.1.1. Accretion temperature

Accretion energy of a planet or satellite, as measured by the gravitational energy released in erg s^{-1} cm^{-2} or W m^{-2} (Hanks and Anderson, 1969), is:

$$\frac{GM(r)}{r}\rho\frac{dr}{dt} \tag{D.1}$$

The term $\rho dr/dt$ is the rate of mass accretion per unit of area of the Titan surface (kg m^{-2} s^{-1}).

If the rise in accretion energy is balanced by its loss as emission by an ideal black body (Hanks and Anderson, 1969) then:

$$\frac{GM(r)}{r}\rho\frac{dr}{dt} = \sigma\left(T^4 - {T_{eq}}^4\right) \tag{D.2}$$

where the Stefan-Boltzmann constant σ = 5.67×10^{-8} W m^{-2} K^{-4}, and T_{eq} is the black body equilibrium temperature of Titan at its mean distance from the Sun. At present, with no albedo and no greenhouse, the temperature is T_{eq} = 90 K. About 4.5 billion years ago, if the solar luminosity and Sun's energy emission was about 75% of the present-day value, then the Titan $T_{eq} \approx 0.75^{1/4}\times90$ K = 84 K. (We use the value of 85 K, as representative of an early accretion stage). The accretion temperature, T_{ac}, from the preceding equation and using the parameter values as explained in Section 1.3.1, is:

$$T_{ac} = \left({T_{eq}}^4 + \frac{GM(r)}{\sigma r}\frac{\rho\, dr}{dt}\right)^{1/4} = 353 \text{ to } 355 \text{ K} \qquad \text{(D.3)}$$

D.1.2. Cooling rate

The heat content of Titan after its accretion, without any additional internal heat production, would have been dissipated by heat loss to its surrounding space that was at a temperature of 84 to 90 K. If heat dissipation occurred by means of radiation emission from an ideal black body, then the temperature of the cooling satellite as a function of time can be determined from the heat flow balance, as shown below.

The heat content of Titan after it accretion, per unit of its surface area, can be given as:

$$\frac{\frac{4}{3}\pi r^3 \rho C_p T}{4\pi r^2} = \frac{r\rho C_p T}{3} \qquad \text{J m}^{-2} \qquad \text{(D.4)}$$

where the Titan temperature is T (K), its radius r = 2575 km, its mean density ρ = 1881 kg/m^3, and its mean heat capacity C_p is 2357 J kg^{-1} K^{-1} at 350 K, and 2237 J kg^{-1} K^{-1} at 300 K. The rate of heat loss is equal to the rate of its emission by the Titan surface as a black body into the medium at T_{eq} = 85 K:

$$-\frac{r\rho C_p}{3}\cdot\frac{dT}{dt} = \sigma\left(T^4 - {T_{eq}}^4\right) \qquad \text{J s}^{-1}\text{ m}^{-2} \qquad \text{(D.5)}$$

Rearranging the terms in the preceding equation, the variables *T* and *t* are separated:

$$-\frac{r\rho C_p}{3\sigma}\cdot\frac{dT}{T^4-{T_{eq}}^4} = dt \tag{D.6}$$

To obtain *T* as a function of *t*, integration of the left-hand side can be done by use of the partial fractions or by using *Wolfram Mathematica Online Integrator* for an indefinite integral at http://integrals.wolfram.com/index.jsp:

$$-\frac{r\rho C_p}{3\sigma}\int_{T_{ac}}^{T}\frac{dT}{T^4-{T_{eq}}^4} = \int_0^t dt \tag{D.7}$$

The result is:

$$\frac{r\rho C_p}{6\sigma {T_{eq}}^3}\left[\frac{1}{2}\ln\frac{T+T_{eq}}{T-T_{eq}}\cdot\frac{T_{ac}-T_{eq}}{T_{ac}+T_{eq}} + \tan^{-1}\frac{T-T_{ac}}{T_{eq}+TT_{ac}/T_{eq}}\right] = t \tag{D.9}$$

The preceding equation relates the temperature of the cooling planet, *T*, to time *t* since the cooling began. The results for the accretion temperatures of 355 K and 300 K are shown in Figure 1.2.

D.2. The Maxwell-Boltzmann velocity distribution of gas molecules

The parameters in this section are shown in Figures 1.3 and 1.4.

$$f(v) = 4\pi \left(\frac{m}{2\pi kT}\right)^{3/2} v^2 e^{-mv^2/(2kT)}$$

$$f(v) = 4\pi \left(\frac{M}{2\pi RT}\right)^{3/2} v^2 e^{-Mv^2/(2RT)} \quad \text{(D.9)}$$

where k is the Boltzmann constant, m is the molecule mass, R (= 8.314 J mol^{-1} K^{-1}) is the gas constant, M is the molecular mass of the gas (kg mol^{-1}), and v is velocity (m/s). A historical note on notation of this equation is in footnote [1], Section 1.5.1.

The most probable velocity, v_0, at the velocity distribution peak, is found by differentiating eq. (1.1) with respect to v and equating the result to 0: $\mathrm{df(v)/dv} = 0$. This gives:

$$v_0 = \sqrt{\frac{2RT}{M}} \quad \text{(D.10)}$$

Mean velocity $\bar{v}$ of the distribution is found by integration of (D.9):

$$\bar{v} = \int_0^\infty v f(v) dv = \sqrt{\frac{8RT}{\pi M}} = \frac{2}{\sqrt{\pi}} v_0 \quad \text{(D.11)}$$

The Maxwell-Boltzmann velocity distribution in (D.9) can be rewritten as a function of $\boldsymbol{v_0}$ (e. g., Goody, 1976):

$$f(v) = \frac{4}{v_0^3\sqrt{\pi}}\, v^2 e^{-(v/v_0)^2} \tag{D.12}$$

Eqs. (D.9) and (D.12) are probability density functions and their integral from 0 to ∞ is 1. In the notation of (D.12), the cumulative distribution of gas velocities is:

$$\mathcal{F}(v) = \int_0^v f(v)dv = \text{erf}(v/v_0) - \frac{8}{v_0^3\sqrt{\pi}} e^{-(v/v_0)^2} \tag{D.13}$$

where $\text{F(v)} \rightarrow 1, \text{as v} \rightarrow \infty$ (Figure 3b).

The fraction of the gas molecules that have velocities $\boldsymbol{v}$ greater than the escape velocity of the planet, v_e = $(2gr)^{1/2}$ (Table 1.1), is found by integration of (D.12) from v_e to ∞:

$$\mathcal{F}(v \geq v_e) = \frac{4}{v_0^3\sqrt{\pi}} \int_{v_e}^{\infty} v^2 e^{-(v/v_0)^2} dv \tag{D.14}$$

The result of (D.14) is:

$$\mathcal{F}(v \geq v_e) = \frac{2v_e}{v_0\sqrt{\pi}} e^{-(v_e/v_0)^2} + \text{erfc}(v_e/v_0) \tag{D.15}$$

where erfc(x) is the error function complement of x. The error function, erf(x), is the integral of the Gaussian normal distribution and erfc(x) = 1- erf(x). The extreme values are: erfc(0) = 1 and erfc(∞) = 0. Thus the fraction of molecules of velocities $v \geq v_e$ is a function of the velocity ratio, v_e/v_0. The error function complement, erfc(v_e/v_0), for v_e/v_0 > 2 or 2.5, can be approximated to

$$\text{erfc}(v_e/v_0) = \frac{e^{-(v_e/v_0)^2}}{\sqrt{\pi}\, v_e/v_0} \tag{D.16}$$

Substitution of (D.16) into (D.15) gives:

$$\mathcal{F}(v > v_e) = \frac{2}{\sqrt{\pi}} \frac{v_e}{v_0} e^{-(v_e/v_0)^2} + \frac{e^{-(v_e/v_0)^2}}{\sqrt{\pi}\, v_e/v_0} \tag{D.17}$$

Goody (1976) gives the following approximation for $\mathcal{F}(v > v_e)$, for the same conditions of $\mathrm{v_e/v_0} > 2$:

$$\mathcal{F}(v > v_e) = \frac{4}{\pi} \frac{v_e}{v_0} e^{-(v_e/v_0)^2} \tag{D.18}$$

Goody's result in (D.18) is greater than ours in (D.17) by a factor of $2/\sqrt{\pi} = 1.13$ or about 13%.

Mean velocity $\bar{\mathrm{v}}_{>\mathrm{v_e}}$ in the interval $\mathrm{v_e} \leq \mathrm{v} < \infty$, where the Maxwell-Boltzmann distribution $f(v)$ is *not* a probability density function, can be written as:

$$\bar{v}_{>v_e} = \frac{\int_{v_e}^{\infty} v f(v) dv}{\int_{v_e}^{\infty} f(v) dv} \tag{D.19}$$

where f(v) is defined in (D.9). The result of (D.19) is:

$$\bar{v}_{>v_e} = \frac{2v_e[1+(v_e/v_0)^2]}{1+2(v_e/v_0)^2} \tag{D.20}$$

The ratio of the high-velocity mean to the escape velocity, $\bar{v}_{>v_e}/v_e$, is always greater than 1.

For a number of gases, from the lighter CH_4 to the heavier CO_2, the mean escape velocities $\bar{v}_{>v_e}$ are shown in Fig. D.1a.

D.3 Gas escape rate

D.3.1. Escape rate parameter *k*

As discussed in Section 1.5.2, the fraction of the gas escaping is ½ of the fraction $F(v > v_e)$:

$$\frac{1}{2} F(v > v_e) \tag{D.21}$$

Concentration of the escaping gas in the atmosphere is its mass, N_t, divided by the atmosphere volume, V_{atm}:

$$\frac{\frac{1}{2}F(v>v_e)N_t}{V_{atm}} \tag{D.22}$$

The escaping volume flow is a product of mean velocity, $\bar{\mathrm{v}}_{>\mathrm{v_e}}$, and the atmosphere outer surface area, S_{atm}:

$$\bar{\mathrm{v}}_{>\mathrm{v_e}} \times \mathrm{S_{atm}} \tag{D.23}$$

and the mass flux out is:

$$\frac{\mathcal{F}(v>v_e)N_t}{2V_{\mathrm{atm}}} \cdot \bar{v}_{>v_e} \cdot S_{atm} \tag{D.24}$$

Division (D.24) by the gas mass in the atmosphere, N_t, gives an escape rate parameter k:

$$k = \frac{\mathcal{F}(v>v_e) \cdot \bar{v}_{>v_e} \cdot S_{\mathrm{atm}}}{2V_{\mathrm{atm}}} \tag{D.25}$$

Substitution in (D.25) for $\mathrm{F(v > v_e)}$ from (D.17) and for $\bar{v}_{>v_e}$ from (D.20), gives and explicit form of k:

$$k = \frac{v_e}{v_0} e^{-(v_e/v_0)^2} \left[\frac{2}{\sqrt{\pi}} + \frac{1}{\sqrt{\pi}(v_e/v_0)^2}\right] \cdot \frac{2v_e[1+(v_e/v_0)^2]}{1+2(v_e/v_0)^2} \cdot \frac{S_{\mathrm{atm}}}{2V_{\mathrm{atm}}} \tag{D.26}$$

To reiterate, *k* is a function of *T* and molecular mass of the gas *M*, through its dependence on the most frequent velocity $v_0 = (2RT/M)^{1/2}$, Titan escape velocity v_e, atmosphere volume, and its outer surface area, or on the atmosphere thickness *h* that depends on the quotient V_{atm}/S_{atm}.

The *k* values at different temperatures for CH_4 and NH_3 are shown in Figs. 1.5 and 1.9. The reason for a strong decrease in *k* with decreasing *T*, is not only its direct dependence on *T* via the peak velocity v_0, but primarily a stronger decrease in the term $F(v > v_e)$ in Eq. (D.25) than in the mean velocity term $\bar{v}_{>v_e}$. As shown in Fig. 1.4a, mean velocities $\bar{v}_{>v_e}$ decrease with decreasing *T*, but the fraction of the gas mass above the Titan escape velocity, $F(v > v_e)$, decreases much faster (Fig. 1.4b) with increasing molecular mass of the gas and the heaviest CO_2 falls off the scale of the figure.

D.3.2. Calculation of the escaping gas mass in the atmosphere

The gas escape from the atmosphere is taken as a first-order process, $-dN/dt = kN$, the solution of which is:

$$N_t = N_0 \, e^{-kt} \tag{D.27}$$

where N_0 is the initial gas mass at time $t = 0$, denoted $N_0 = 100\%$. Using (D.8) that relates the temperature of Titan *T* to the cooling time *t* (Figure 1.2), successive values of *t* were calculated for temperatures decreasing from T_{ac} = 355 or 300 K, in steps of 1 to 10 K. These values of *T* and *t* were used to calculate *k* for CH_4 and NH_3 from (D.26).

The values of the remaining gas mass, N_t, were calculated for every two consecutive time steps, $t = i$ and $t = i+1$, and a mean value of k for that period, $(k_{i+1} + k_i)/2$:

$$N_{i+1} = N_i \, e^{-0.5(k_{i+1}+ k_i)(t_{i+1}- t_i)} \tag{D.28}$$

where the initial gas mass at $i = 0$ is taken as $N_0 = 100\%$. N_0 was converted to gas mass in kg that satisfies its reduction by thermal escape to the present-day value (Table 1.5, column 3). The results of N_t for CH_4 and NH_3 are shown in Figure 1.8.

D.3.3. Calculation of the escaping gas mass with input from the interior

For gas escape accompanied by emission from Titan interior, one of such processes may be described as a combination of a constant input rate, F (%/yr), with a first-order escape:

$dN/dt = F - kN$, the solution of which, similar to (D.27), is:

$$N_t = \frac{F}{k}(1 - e^{-kt}) + N_0 \, e^{-kt} \tag{D.29}$$

For incremental values of T, t, and k, a form similar to (D.28) is:

$$N_{i+1} = \frac{F}{0.5(k_{i+1}+ k_i)}\left[1 - e^{-0.5(k_{i+1}+ k_i)(t_{i+1}- t)}\right] + N_0 \, e^{-0.5(k_{i+1}+ k_i)(t_{i+1}- t)} \tag{D.30}$$

The results of (D.30) with varying input rates F (%/yr) for CH_4 and NH_3 are shown in Figure 1.7 and Table 1.6.

CHAPTER 2

Titan's Missing Ethane: From the Atmosphere to the Subsurface

2.1. Introduction

Titan, the largest moon of Saturn, is unique in the solar system. Whereas satellites in general are not known for having atmospheres, Titan not only possesses an atmosphere, it has a massive and complex one, harboring a suite of hydrocarbons that display a meteorological cycle similar to the hydrological cycle on Earth. The main components of Titan's atmosphere at present are nitrogen (N_2, 1.4 bar) and methane (CH_4, 0.1 bar). In Titan's atmosphere hydrocarbons are produced by the photodissociation of methane. In the stratosphere, which extends from the tropopause (approx. 40 km) to the stratopause (approx. 320 km), UV photolysis is responsible for ~1/3 of the total methane destruction (Atreya et al., 2009), 75% of which occurs at the Lyman α wavelength (121.6 nm) (Wilson and Atreya, 2009). At Lyman α, the photodissociation of methane produces other hydrocarbons, such as methyl radicals (CH_3). These hydrocarbons recombine to form heavier molecules (e.g. C_2H_6) that condense as liquids or solids in the lower stratosphere and vicinity of Titan's cold troposphere (Fig. 2.1) to form a haze layer and eventually precipitate from the atmosphere. In Titan's atmosphere, ethane (C_2H_6) is the main photolysis product of methane (Yung et al., 1984), with a mean production rate of 1.3×10^{8} molecules cm^{-2} s^{-1} (2.16×10^{-16} moles cm^{-2} s^{-1}) from solely the photolytic conversion of methane to ethane (Wilson and Atreya, 2009), nearly tenfold the production of the other hydrocarbons combined (Toublanc et al., 1995). Higher production rates of ethane (Cornet et al., 2015), 1.2 to 15×10^{9} molecules cm^{-2} s^{-1}, are either similar or higher than the photochemical removal rate of CH_4, 2.5×10^{9} molecules cm^{-2} s^{-1} (Wilson and Atreya, 2009). A simplified sequence of direct forward reactions from CH_4 to C_2H_6 that short-circuit the complex intermediate paths can be represented by the following (Gilliam et al., 2015):

$CH_4 \rightarrow CH_3 + H$ first-order rate parameter k_{12} (s^{-1}), $d[CH_4]/dt = F - k_{12}[CH_4]$ (2.1)

$d[CH_3]/dt = k_{12}[CH_4]$ (2.2)

$CH_3 + CH_3 \rightarrow C_2H_6$ 2nd-order rate parameter k_{23} ($cm^3\ mol^{-1}\ s^{-1}$), $d[C_2H_6]/dt = k_{23}[CH_3]^2$ (2.3)

$C_2H_6 \rightarrow$ other products first-order rate parameter k_3 (s^{-1}), $d[C_2H_6]/dt = -k_3[C_2H_6]$ (2.4)

where [ ] are atmospheric concentrations in kg, mol or molecules vol^{-1}, k_{ij} are the reaction rate parameters, and $F \geq 0$ (mass vol^{-1} $time^{-1}$) is the rate of CH_4 emission from the interior to the atmosphere. The resulting ethane is largely shielded from UV radiation by methane and acetylene (C_2H_2), making it stable against photolysis. The principal loss mechanism for ethane is condensation at the tropopause, followed by its accumulation as a liquid on the surface (Yung and DeMore, 1999).

Another mechanism of methane loss in the Titan atmosphere is hydrodynamic escape. First observed by the Voyager spacecraft and confirmed by the Cassini Ion Neutral Mass Spectrometer (INMS), the methane distribution in Titan's upper atmosphere remains uniformly mixed to the altitude of ~1100 km, where it begins to exhibit diffusive separation. Further evidence from the Cassini INMS suggested that methane is not well mixed to high altitudes (>1000 km) because of a large escape rate, 2.9×10^9 molecules $cm^{-2}\ s^{-1}$ (4.8×10^{-15} moles $cm^{-2}\ s^{-1}$) (Yelle et al., 2008). The most likely mechanism is hydrodynamic escape – a high density, slow outward expansion driven mainly by solar UV heating due to CH_4 absorption (Strobel, 2009) – as evident from heating rates gathered from the Huygens Atmospheric Structure Instrument (HASI). This loss rate is responsible for 22% of the total methane loss rate (Wilson and Atreya, 2009).

The third mechanism of methane loss is thermal escape, where the outgoing methane flux is proportional to the methane mass in the atmosphere and it depends on temperature, gas molecular mass, atmosphere thickness, and Titan's escape velocity (Gilliam and Lerman, 2014a; Gilliam et al., 2015).

Consideration of these processes suggests that Titan should have produced a substantial amount of ethane since accretion. Such an idea was first proposed by Lunine et al. (1983), who used photochemical models to predict that Titan would be covered by an ethane ocean one to several kilometers deep, and was later supported by others' models, albeit with a smaller net volume of ethane produced. Further, Mousis and Schmitt (2008) proposed a geological process that resolves "the ethane deficiency issue in a manner which is in agreement with our current knowledge of Titan: the incorporation of liquid hydrocarbons in the porous cryovolcanic subsurface". However, Cassini-Huygens observations have not shown evidence of widespread surface ethane reservoirs.

This paper addresses three issues: (1) the mass and volume of ethane that was produced on Titan since accretion, based on the production-rate estimates of other investigators; (2) the occurrence of liquid ethane in the surface depressions (craters and lakes) and in the crustal subsurface; and (3) the physical characteristics of liquid ethane as a potential medium for emerging life. To address the first issue, we present a straightforward photochemical model using primordial conditions presented in Gilliam and Lerman (2014a, b) and compare our results to the latest observations from the Cassini mission.

2.2. CH_4 Depletion and C_2H_6 Production through Time

The condensation temperature of ethane is lower than that of methane, as shown by the two liquidus curves in Fig. 2.1. Thus liquefaction and "raining" of C_2H_6 in Titan's atmosphere is expected to begin before that of CH_4 (Sagan and Thompson, 1984; Barth and Toon, 2003; Rannou et al., 2006; Lunine and Atreya, 2008). The cooling time of Titan's surface, calculated assuming heat dissipation by radiation emission from an ideal black body, from the initial accretion temperature of 300 K to 100 K is about 3×10^6 years (Gilliam and Lerman, 2014a).

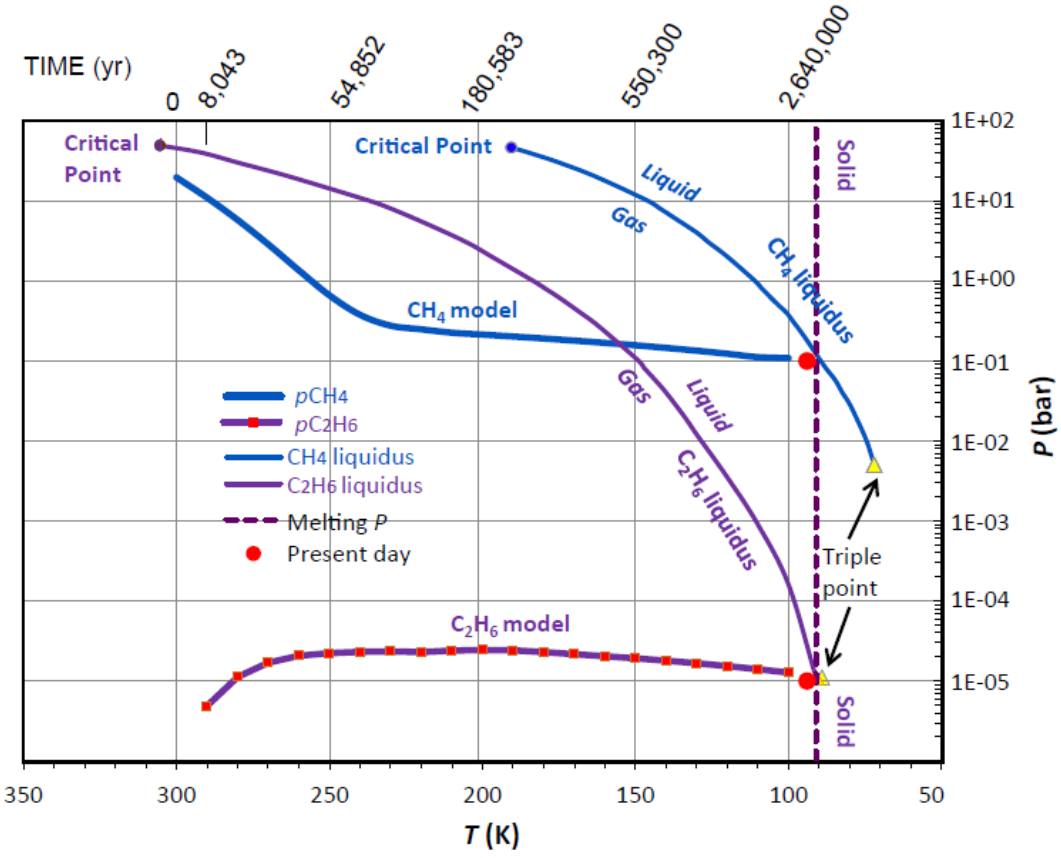

Fig. 2.1. One of the important points in the history of methane and ethane in Titan's atmosphere is that C_2H_6 condenses at a higher temperature than CH_4. The figure above shows: (a) Saturation vapor pressure or liquidus curves of each gas (CRC Handbook of Chemistry and Physics, 2016). Note that as Titan's atmosphere cools from about 300 K down, C_2H_6 liquefies before CH_4 and it also forms a solid phase at the triple point before CH_4. Thus liquefaction and "raining" of C_2H_6 in Titan's atmosphere is expected to begin before that of CH_4. (b) Calculated partial pressures of methane and ethane in the theoretical reactions sequence (2.1)-(2.4), as explained in the text. Present-day partial pressures are shown as red dots.

Atmospheric observations and numerous other works have shown that ethane does condense at higher altitudes than methane. However, there are two other possible compositions of the rain on Titan. Graves et al. (2008) considered condensation of N_2–CH_4–C_2H_6, based on N_2 being the main component of Titan's atmosphere at present. Mousis and Schmitt (2008) have also discussed the possibility of CH_4-C_2H_6-N_2 liquid condensing on the Titan surface. Atreya et al (2006) concluded that C_2H_6 condenses at altitudes above the tropopause where the temperature is near 70 K. Croft et al. (1988) have reported that water-ammonia solutions remain liquid down to 190-170 K, which suggests that if NH_3 was a component of the atmosphere in the past, an H_2O-NH_3 rain main have carried dissolved CH_4 and C_2H_6 to the surface.

With regard to liquid N_2 in Titan's atmosphere, its condensation temperature at the pressure of 1 to 2 bar is 77 to 82 K, below the 90 K of the present-day Titan surface (CRC, 2016). However, N_2 dissolves in methane-ethane mixtures (Farnsworth et al., 2016) and it forms hydrous clathrates in the temperature range from 215 K to 375 K (van Hinsberg and Schouten, 1994). If precipitation of a liquid mixture of C_2H_6-CH_4-N_2 was taking place on Titan, the total mass condensed over the lifetime of the satellite would have been greater than that of C_2H_6 alone. However, the solubility of N_2 in C_2H_6 is very low (Chevrier et al, 2015; Farnsworth et al., 2016), and it is the presence of CH_4 in the CH_4-C_2H_6 liquid mixture that promotes dissolution of N_2.

The two model curves for the evolution of CH_4 and C_2H_6 in Fig. 2.1 are a theoretical example of a model of the four simultaneous reactions (2.1)-(2.4). The model includes input of CH_4 from the interior to the atmosphere, at the rate of $F = 4.13\times10^{13}$ kg/yr or 5.46×10^{14} molecules cm^{-3} yr^{-1}. This rate of input was used to calculate the history of thermal escape of CH_4 from Titan's atmosphere in a model of input with escape (Gilliam and Lerman, 2014a). Among other estimates

of the CH_4 emission rate from the interior, the input cited operated for 57,350 yr; if it continued indefinitely, it would have exhausted the CH_4 reservoir in Titan's interior in about 6×10^6 yr. This is longer than the 3×10^6 yr for the surface temperature to cool to 100 K. The model results were also based on emission rates lower by a factor of 100, with a correspondingly longer time to exhaustion of the CH_4 reservoir.

The rate constants of reactions (2.1)-(2.4) are from the ranges given by Yung and DeMore, 1999, p. 219; Wilson and Atreya, 2004, Fig. 13; Atreya et al., 2009; and compilation in Gilliam et al., 2015): $k_{12} = 6.7\times10^{-5}$ yr^{-1}; $k_{23} = 1.5\times10^{-21}$ cm^3 molecule^{-1} yr^{-1}; $k_3 = 1\times10^{0}$ yr^{-1}. These representative figures are used at their face values, to demonstrate schematically the net results of the reaction mechanisms (2.1)-(2.4), without considering the effects of changing temperature and gas pressure. The end results agree closely with the present-day concentrations of CH_4 and C_2H_6 in Titan's atmosphere, as shown by the red dots in Fig. 2.1.

In a better model of Titan's atmosphere, where the two major pathways of CH_4 loss are direct UV photolysis and methane escape, we calculate the amount of methane remaining as a function of time since accretion, and the subsequent production of ethane through photodissociation of the methane molecules. Such calculations require an understanding of the primordial conditions of Titan, discussed in detail in Gilliam and Lerman (2014a) and summarized briefly below.

At present, with no albedo and no greenhouse effect, the radiation equilibrium temperature of Titan at its mean distance from the Sun is $T_{eq} = 90$ K. About 4.5 billion years ago, when the Sun was approximately 75% as luminous as today (Gough, 1981), Titan's $T_{eq} \cong 85$ K. The value of Titan's accretion rate and duration, as estimated from Barr et al. (2010) is 2.22 m/yr and about

1.16 Myr, respectively. This accretion rate gives in combination with T_{eq} = 85 K and other basic parameters, an accretion temperature T_{ac} = 300 K. The calculated composition of a primordial atmosphere at 300 K is given in Gilliam and Lerman (2014a, Table 6), where the initial mass of CH_4 satisfies the conditions of gas thermal escape or emission-with-escape to the present-day levels. A primordial atmospheric CH_4 mass of 1.19×10^{20} kg (7.42×10^{21} moles) is calculated from the ideal gas law and a range of early CH_4 partial pressures, as suggested by the $^{14}N/^{15}N$ ratio measured by the Cassini Huygens Gas Chromatograph Mass Spectrometer (Niemann et al., 2005; Atreya et al., 2009). Lastly, an atmosphere top surface area is calculated as 9.18×10^{13} m^2, corresponding to a scale height of 109 km.

We examine two different values for the rate of CH_4 escape from the atmosphere: (*esc*$_1$) the frequently cited 2.9×10^9 molecules cm^{-2} s^{-1} (Yelle et al., 2008) and (*esc*$_2$) a range of CH_4 escape values that vary with temperature, starting at 6.84×10^{16} molecules cm^{-2} s^{-1} just after accretion, and ending with 1.30×10^{-8} molecules cm^{-2} s^{-1} at present-day, calculated using the escape rate parameters in Gilliam and Lerman (2014a).

Using *esc*$_1$ = 2.9×10^9 molecules cm^{-2} s^{-1} and photodissociation rate of CH_4 2.5×10^9 molecules cm^{-2} s^{-1} or total of 3.8×10^9 kg/yr, and assuming that it does not vary with temperature, we calculate that 8.46×10^{17} kg of C_2H_6 should have been produced since accretion (~ 4.5 Ga) (Fig. 2.2). However, there is a problem with the latter value of methane escape rate *esc*$_1$. In Fig. 2.2, the constant rate *esc*$_1$ neither lowers sufficiently the initial methane mass to the present-day level, nor results in the initial concentration in a backwards calculation from the present-day mass. Only a rate of methane escape and photodissociation about ten-fold higher, 3.76×10^{10} molecules cm^{-2} s^{-1}

or 2.63×10^{10} kg/yr, would lower the initial mass to the present-day level, but the shape of this curve is very different from the CH_4 curves Figs. 2.3b, c.

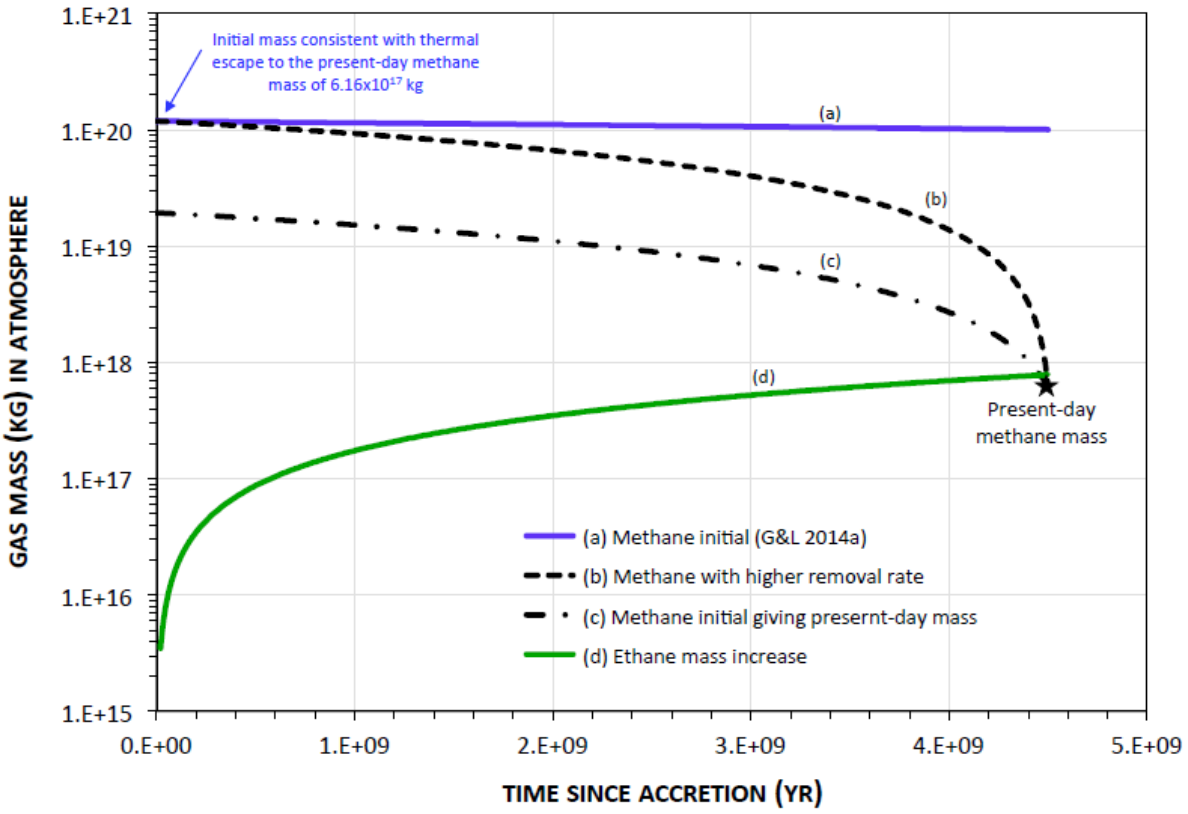

Fig. 2.2. Methane depletion and ethane production in Titan's atmosphere since accretion, using a simple model that includes direct methane photolysis and hydrodynamic escape. (a) CH_4 remaining in the atmosphere at the combined escape rate of esc_1 = 2.9×10^9 molecules cm^2 s^{-1} and photodissociation of 2.5×10^9 molecules cm^2 s^{-1} (Wilson and Atreya, 2009; Yelle et al., 2008) or a total of 3.8×10^9 kg/yr, and starting at the initial mass of 1.2×10^{20} kg (Gilliam and Lerman, 2014a). (b) Methane mass decreasing from the initial to the present-day value, using a constant escape rate higher than esc_1, 3.76×10^{10} molecules cm^2 s^{-1} or 2.63×10^{10} kg/yr. (c) Initial mass of CH_4 derived from the present-day mass of 6.16×10^{17} kg and the same escape rate esc_1. (d) C_2H_6 production from CH_4 photodissociation at 1.3×10^8 molecules cm^{-2} s^{-1}.

Using esc_2, the rate of CH_4 escape would begin to level off approximately 100,000 years after accretion (Fig. 2.3b, c), and produce 8.46×10^{17} kg of C_2H_6 (Fig. 2.3c). The initial and present-day masses are explained by the thermal escape model based on parameter *k* that depends on temperature, Titan's escape velocity, molecular mass of the gas, and atmosphere volume (Fig.

2.3a). The annual production rate of C_2H_6 in the atmosphere is 1.9×10^8 kg/yr or 9 orders of magnitude smaller than the total mass of CH_4. The total produced is about 10^4 times larger than the present-day atmospheric ethane mass of 9.24×10^{13} kg, suggesting that almost all of Titan's total ethane content is currently residing in liquid form on the surface and/or in the subsurface.

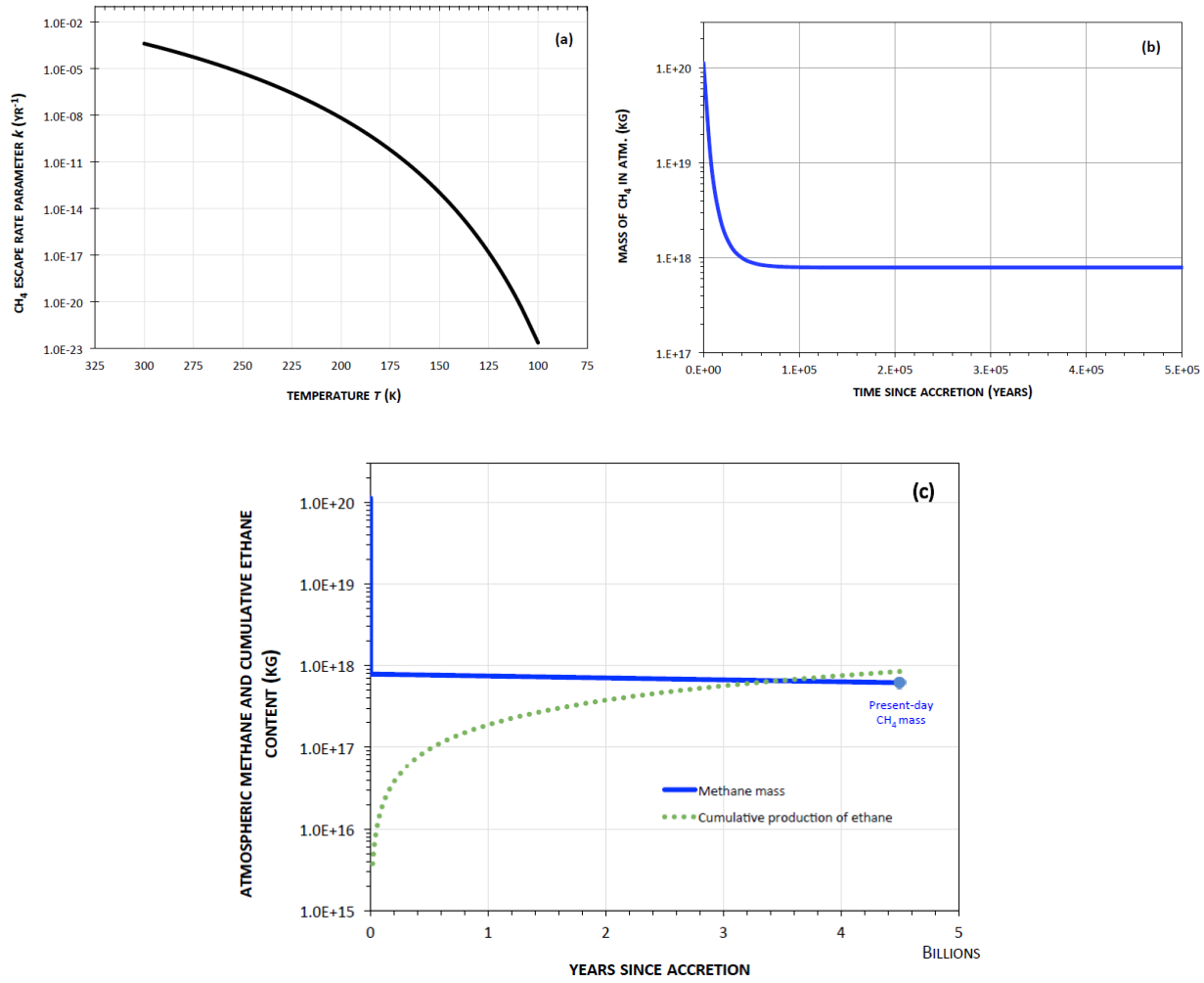

Fig. 2.3. Methane depletion and ethane production in Titan's atmosphere since accretion, using a model where the rate of methane escape varies with temperature. (a) The escape rate parameter, *k*, vs. temperature, *T*, for CH_4 assuming an accretion temperature of 300 K, from data of Gilliam and Lerman (2014a, Fig. 10). *k* depends on temperature, gas molecular mass, atmosphere thickness, and Titan's escape velocity. (b) The mass of CH_4 in Titan's atmosphere as a function of time, during the first 0.5 Myr after accretion, using the escape rate parameter, *k*, and decreasing atmosphere thickness. (c) The mass of CH_4 in Titan's atmosphere, calculated using the variable *k* (Gilliam and Lerman, 2014a), and cumulative production of C_2H_6 as a function of time during the last 4.5 Ga, with a C_2H_6 production rate of 1.3×10^8 molecules cm^{-2} s^{-1}.

2.3. Surface Reservoirs of Ethane

The lakes and seas of Titan: Prior to the arrival of Cassini in 2004, speculation that Titan had extensive hydrocarbon seas was based on the detection of methane by the earlier Voyager mission coupled with surface conditions that allow for the stability of liquid methane and ethane. Confirmation of liquid on the Titan surface finally came in July 2004, when Cassini ISS observations of the South Pole revealed multiple dark features, tens to hundreds of kilometers long. Since then, hundreds of lakes and seas have been discovered, most of them in the polar regions due to a high relative methane humidity allowing for the stability of standing bodies of liquid without the need for constant replenishment. If these bodies also contain dissolved methane, its escape to the atmosphere could be at least in part balanced by the emission of CH_4 from the interior, as discussed in Section 2.2. These lakes range in size from <10 km^2 to Kraken Mare, the area of which exceeds 400,000 km^2 (Lopes et al., 2007; Hayes et al., 2008) and is almost twice the surface area of the Laurentian Great Lakes, 244,100 km^2.

In this study, we estimate a total hydrocarbon liquid volume of all of Titan's lakes of 50,000 km^3, based on an average of the work of Lorenz et al. (2008) and Lorenz et al. (2014). As an interesting comparison, the total volume of Earth's freshwater lakes is 125,000 km^3 (Herdendorf, 1982) to 91,000 km^3 (Shiklomanov, 1993), meaning that Titan has 6 to 8.3 times more lake liquid per cubic kilometer than Earth. Assuming a reasonable liquid composition of 50% ethane, this corresponds to an ethane mass of 1.36×10^{16} kg in Titan's lakes, roughly 1.6% of the total ethane produced as calculated.

Liquid capacity in Titan's craters: Although there are only a couple of observations of hydrocarbon liquids present in Titan's 60+ craters, it is interesting to theorize the maximum

potential volume available for liquid ethane on Titan's surface. To date, 62 possible craters have been observed on the surface of Titan (Neish and Lorenz, 2012; Neish et al., 2013; Buratti et al., 2012; Wood et al., 2010), ranging in diameter from 3 to 425 km. Assuming a spherical cap for crater volume, we calculate a total crater volume of roughly 61,000 km^3, covering a total area of 238,000 km^2, with the crater surface areas following a power law distribution with a slope of -1 (Fig. 2.4). If these craters were fed by 100% ethane rainfall, their total storage capacity of ethane would be 3.8×10^{16} kg, roughly 4.5% of the total cumulative ethane production. Even after adding the total crater liquid capacity to the lake capacity, total ethane surface storage would be 6.9×10^{16} kg, still only 8.2% of the total possible ethane production. This suggests that there must be a large quantity of liquid ethane present elsewhere on Titan, perhaps sequestered in Titan's subsurface.

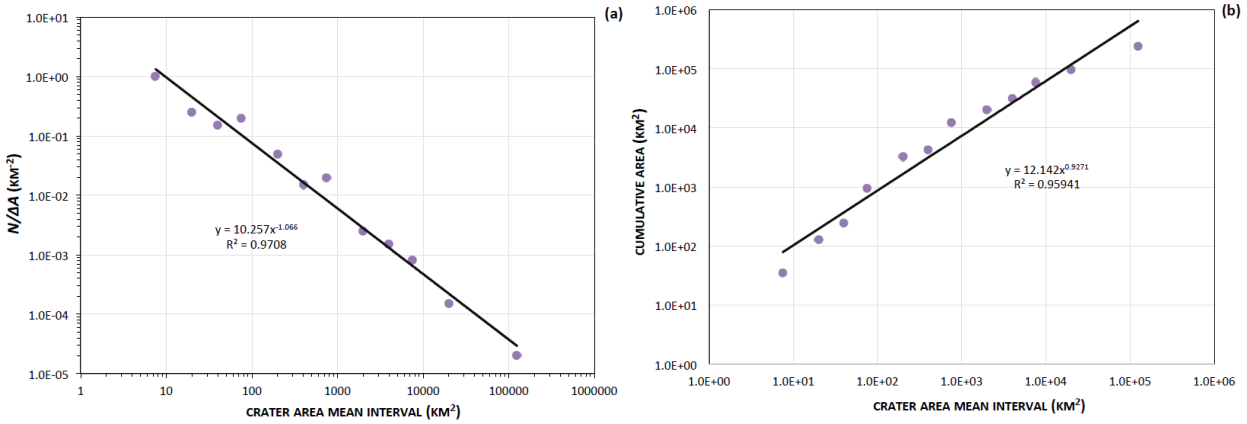

Fig. 2.4. Size distribution of Titan's 62 craters following a power-law distribution, slope -1. Crater areas calculated using Cassini measurements of crater diameters (Wood et al., 2010; Neish and Lorenz, 2012; Buratti et al., 2012; Neish et al., 2013). (a) Crater area-size distribution. (b) Cumulative crater area distribution.

2.4. Porosity and the Subsurface Reservoir of Ethane

Previous work (Fortes et al., 2007; and references in Gilliam and Lerman, 2014a, b) has suggested that Titan has a complex internal structure overlain by a 100+ km crust composed primarily of water ice (Fig. 2.5). Observations of fluvial channels on Titan's surface suggest that

the water-ice particles in Titan's crust are not cohesive, due to the difficulty of eroding coherent icy bedrock, and instead must have been ubiquitously fractured prior to erosion. Such a fractured icy crust would be highly permeable to liquid ethane and methane (Sotin et al., 2009). Possible formation mechanisms for a surface porous layer include the ascent of liquid from the subsurface ocean (Mitri et al., 2008) or from the destabilization of clathrates in Titan's ice shell (Tobie et al., 2006). In both cases, a highly porous icy material in contact with the atmosphere would have been generated (Artemieva and Lunine, 2003; Mousis and Schmitt, 2008).

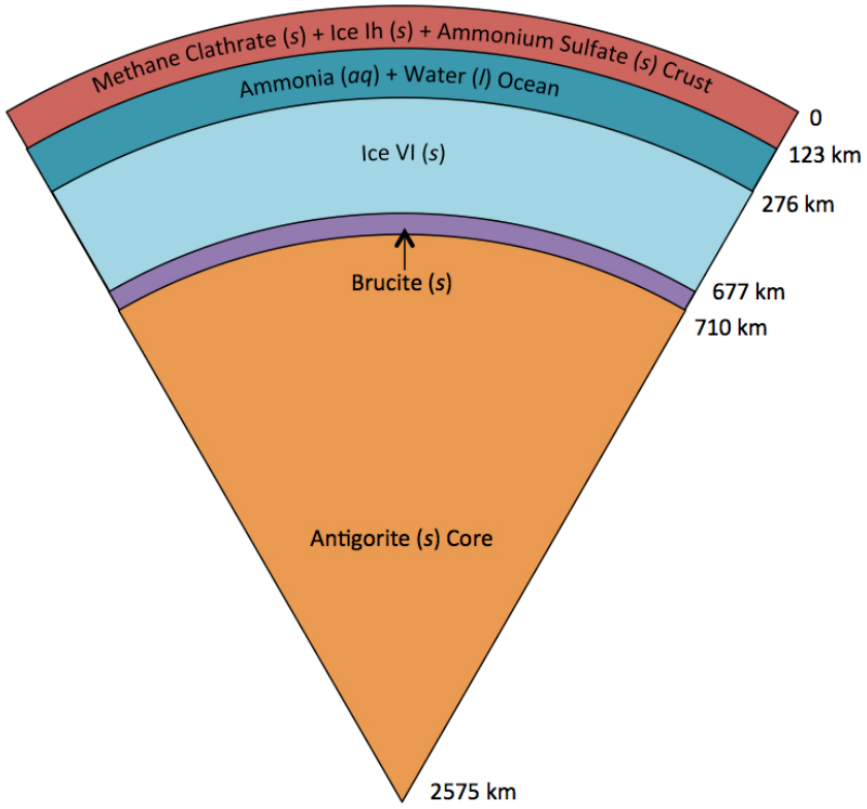

Fig. 2.5. Present-day internal structure of Titan consisting of an antigorite core overlain by a thin layer of brucite, a layer of ice VI, an ammonia-rich ocean, and a crust made of methane clathrate, ice Ih, and solid ammonium sulfate (Fortes et al., 2007; Gilliam and Lerman, 2014a).

Porosity of ice on Earth is a measure of the ice volume fraction taken up by air or other gases. It is created on a small scale by intercrystalline spaces, gas bubbles, and on a larger scale by cracks and crevasses. In ice sheets, crevasses are rarely more than 45 m deep but in some cases can be 300 m or even deeper. Beneath this point, the plasticity of the ice is too great for cracks to form (Hambrey, 1994). A general diagram of different kinds of snow and ice (Menzies and Hughes, 2002) gives a porosity of 10% for new ice and about 1% for old ice. Porosity, measured as the gas-bubble volume in Central Antarctic ice, was reported as 8 to 9% (Lipenkov et al., 1997). Other sources give the porosity of solid ice-sheet and solid sea-ice between 0.1 and 5% (Vasil'chuk, 2005). In the absence of *in situ* measurements of porosity of the upper crust of Titan, we use the ice-sheet data from Earth and allow for a higher mean porosity of 20% due to cracks and fissures.

The mass of ethane produced, 8.46×10^{17} kg, would occupy an average volume of 1.37×10^{15} m^3 (mean of densities at 150 K, 585.8 kg/m^3, and at 93 K, 651.9 kg/m^3; Younglove and Ely, 1987, p. 642). If it can be contained within the pore space of the uppermost 2 km of Titan's crust, 1.67×10^{8} km^3, then the crust would require a minimum porosity of 0.9%. This estimate is in line with the porosity of old ice sheets on Earth and the sequestration potential of Titan's crust for the liquid ethane may in fact be considerably higher.

Alternatively, using a higher yet reasonable crustal porosity of 20% – inferred from Huygens probe observations and consistent with what we know about the behavior of impact gardened icy surfaces (Artemieva and Lunine, 2003) – we estimate that the maximum porous volume of the upper 2 km of the crust is 3.33×10^{7} km^3, or 3.32×10^{7} km^3 if we do not include the volume of lakes and craters (0.01×10^{7} km^3). If the total porous volume is filled with a 100% ethane

solution, then its maximum ethane storage potential is ~2.06×10^{19} kg, which is well above the previous calculated total ethane production of 8.46×10^{17} kg. This suggests that Titan's entire liquid ethane budget could be stored in its porous crust, or it could certainly serve as additional subsurface storage.

2.5. Conclusions and Ruminations

A simple photolysis model, where the methane molecule can either escape the atmosphere or produce ethane, gives up to 8.46×10^{17} kg of liquid ethane that might have been produced since Titan's accretion. This amount is 10^4 times larger than the present-day atmospheric ethane mass of 9.24×10^{13} kg, suggesting that most of the remaining ethane resides in liquid form on or within Titan. Ethane liquefies at a temperature higher than methane and, as Titan's surface cooled in the course of time, ethane might have started to rain early in Titan's history. Indeed, our estimate for the amount of liquid ethane storage potential on Titan's surface is 1.36×10^{16} kg in lakes and seas and additional 3.34×10^{16} kg in craters, both numbers much smaller that the mass calculated. The calculated total mass of ethane produced at an estimated production rate, 8.5×10^{17} kg (mean density 619 ± 33 kg m^{-3} at 93.3 to 150 K), corresponds to a volume of 1.4×10^{15} m^3. This volume represents only a small porosity fraction of the upper 2 km of Titan's crust (1.67×10^{17} m^3): 0.9%. This is the minimum porosity needed to store in the subsurface excess of ethane produced that is greater than the volume of lakes and craters (see also Mousis and Schmitt, 2008). A higher porosity of 20% of the upper 2 km of the crust, 3.33×10^{16} m^3, is much greater that the estimated volumes of ethane produced, suggesting that Titan's entire liquid ethane budget could be stored in its porous crust.

The existence of liquid on Titan's surface and in the subsurface may be very important as a potentially suitable habitat for life. Life created in liquid hydrocarbons, such as ethane and methane, would certainly not resemble anything on Earth, but, if discovered, would be clear evidence of a "Second Coming of Life" in our Solar System. Previous studies have shown that the photochemical processes responsible for Titan's liquid hydrocarbons could be a potential source of chemical energy (on Earth, life uses only two types of energy for primary production: chemical energy and sunlight) at levels shown to be favorable for methanogenic bacteria on Earth (McKay and Smith, 2005; Schulze-Makuch and Grinspoon, 2005).

We conclude by comparing some of the characteristics of liquid ethane with those of water, as a medium of life. On Earth, the idea that life originated in water and an anoxic atmosphere, where organic molecules could aggregate and replicate themselves, is the "primordial soup" theory of Oparin (1924, 1941, 1953) and Haldane (1929, also cited in Tirard, 2011). Bernal (1951) called the origin of life "biopoesis", and Miller (1953) and Miller and Urey (1959) demonstrated the formation of organic molecules in an anoxic gas mixture by electrical discharge. The presence of methane and ethane in Titan's atmosphere has led to a long series of hypotheses that life might exist on Titan, despite its present surface temperature near 90 K. Some of the recent studies of this subject are those of Neish et al. (2010), Norman (2011), and Stevenson et al. (2015) who studied the formation of N-C-H compounds, called azotosomes, as a possible source of life in the liquid hydrocarbons on Titan's surface. Lunine and McKay (1995) have extensively discussed the parallels between the conditions on Titan's surface and in the subsurface in comparison to those on primordial Earth.

The liquid medium of a "primordial soup" is a solvent in which organic molecules can move toward each other and aggregate. The movement, similar to Brownian motion, in a liquid medium is in part controlled by diffusion of particles that further depends on the solubility of the substance, particle size, temperature, and viscosity of the medium.

Solubilities of short polyethers, organic compounds of the type R_1-O-R_2, in propane (C_3H_8) have been studied by McLendon et al. (2015). Polyethers are components of the more complex life-building molecules and they were reported as reasonably soluble in liquid propane down to about 200 K. At lower temperatures approaching 170 K, their solubilities drop almost to nil. If the same solubility relationships hold in liquid ethane, then the diffusivity of the organic molecules in solution will be controlled by the factors mentioned above.

The "primordial soup" in itself may be a fairly thick concoction and have a higher bulk viscosity than the liquid medium or solvent. Eventually, the "soup" may thicken to a slurry or close to becoming a gel. Water or seawater has a viscosity in a range from about 1×10^{-3} Pa s (25°C) to 1.8×10^{-3} Pa s (0°C) (Sharqawy et al., 2010). More viscous natural liquids, such as petroleum, have viscosities in the range from 10 to 100 Pa s below 40°C (Speight, 1998). The viscosity of liquid ethane, from 90 to 150 K, is comparable to that of water or seawater on Earth, 1.26 to 0.25×10^{-3} Pa s (Younglove and Ely, 1987, p. 642). However, two other factors exert a big effect on molecular diffusivity and the slowing down of molecular velocities in liquid ethane: particle size and temperature. The effects of temperature, particle size, and viscosity of the medium on the diffusion coefficient (D, $m^2\ s^{-1}$) follow from the equations of Einstein (1905, 1956), as given below, and Smoluchowski (1906), with the additional coefficient of $(4/3)^3 = 2.37$:

$$D = \frac{RT}{6\pi\eta r N} \tag{2.5}$$

where D is the diffusion coefficient of a particle in solution ($m^2\ s^{-1}$), T is temperature (K), η is viscosity (Pa s), r is particle radius (m), N is Avogadro's number, and R is the gas constant ($J\ mol^{-1}\ K^{-1}$).

From (2.5), denoting the parameters in ethane by subscript 2, and those in water by subscript 1, the following quotients obtain:

$$\frac{D_2}{D_1} = \left(\frac{T_2}{\eta_2 r_2}\right) / \left(\frac{T_1}{\eta_1 r_1}\right) \tag{2.6}$$

Diffusion coefficients of sugars and amino acids in dilute solutions, molecules of effective radius 4.5 ± 2 Å or of an order of 10^{-10} m and molecular mass 75 to 204 g/mol, fall in the range of 5 to 10×10^{-6} $cm^2\ s^{-1}$ at 25°C, but the D values decrease by a factor of 2 to 5 for diffusion in gels (Nakanishi et al., 1977). D values in the range from 4.5 to 9.5×10^{-6} $cm^2\ s^{-1}$ of similar substances were reported by Polson (1937). These values would be by a factor of 0.5 lower at 273 K, as follows from eq. (2.6).

For a life made of C, N, H, and O atoms to exist on Titan, polymerization of small organic molecules has been considered by a number of investigators. Polymers are heavier and bigger molecules, with the mass of medium-large polymers of 1,000 to 30,000 g/mol and linear dimensions 10^{-8} to 10^{-7} m (Cowie, 1966; Akcasu and Han, 1979).

To estimate the diffusion coefficients of organic molecules in ethane, D_2 in eq. (2.6), we use the viscosity values of water at 273 K (1.791×10^{-3} Pa s) (Sharqawy et al., 2010), liquid ethane

viscosity at 90.4 K (1.260×10^{-3} Pa s) and 150 K (0.252×10^{-3} Pa s) (Younglove and Ely, 1987, p. 642), and particle radius approximating polymers of 10^{0}-10^{3} Å or 10^{-10}-10^{-7} m. Combinations of different tiplets of temperature, corresponding viscosity, and particle size give the following diffusion coefficients of organic molecules in ethane: fractions between 0.26 and 0.47 when only the temperatures and viscosities are compared with those of water; the reduction of the diffusion coefficient in ethane is much greater, 4.7×10^{-4} to 4×10^{-3}, when larger-size polymer particles are considered.

Apart from the molecular mobility, there remains a question of the rates of chemical reactions in the cryogenic environment of Titan. A very crude estimate that can be made here is based on some values of the polymerization rate constant k_p (Ling et al., 2001; Luo et al., 2006) and the activation energy of polymerization ΔE_a (Skene et al., 1998). The estimate is based on Arrhenius reaction rate dependence on temperature:

$$ln\left(\frac{k_{\text{low}}}{k_{273}}\right) = -\frac{E_a}{R}\left(\frac{1}{T_{\text{low}}} - \frac{1}{273}\right) \tag{2.7}$$

A mean of several activation energy values for different polymerization reactions is about 130 kJ/mol at 337 K, and the rate constants vary from 0.7 to 1900 $cm^3\ mol^{-1}\ s^{-1}$ at 323 K. Using T_{low} in (2.7) as 150 K and 100 K, the rate constant at 273 K would be reduced by a very large factor of 4×10^{-21} and 9×10^{-44}, respectively.

The reduction in mobility of organic molecules in diffusion and the possibly strong lowering of the rate constants for polymerization may be less advantageous to aggregation of molecules in liquid ethane by comparison with a “primordial soup” based on water.

APPENDIX 2-E

Table E.1.
Properties of Titan's currently known impact craters.

Certainty[a]	Diameter (km)	Area (km^2)	Name
1	80	5026.55	Selk
1	115 ± 5	10386.89	Afekan
1	39 ± 2	1194.59	Ksa
1	82 ± 2	5281.02	Sinlap
1	425 ± 25	141862.54	Menerva
1	78 ± 2	4778.36	Soi
1	139	15174.68	
1	120	11309.73	Paxsi
1	40 ± 1	1256.64	Momoy
2	100 ± 5	7853.98	Hano
2	18	254.47	
2	22	380.13	
2	30	706.86	
2	33	855.30	
2	3	7.07	
2	3	7.07	
2	4	12.57	
2	4	12.57	
2	5	19.63	
2	5	19.63	
2	7	38.48	
2	7	38.48	
2	7	38.48	
2	8	50.27	
2	10	78.54	
2	14	153.94	
2	16	201.06	
2	17	226.98	
2	17	226.98	
2	20	314.16	
2	26	530.93	
2	33	855.30	
2	35	962.11	
2	45	1590.43	
2	63	3117.25	
2	68	3631.68	
2	110	9503.32	
3	3	7.07	
3	3	7.07	
3	3	7.07	
3	6	28.27	
3	8	50.27	
3	8	50.27	
3	8	50.27	
3	9	63.62	
3	10	78.54	
3	10	78.54	

3	14	153.94
3	18	254.47
3	18	254.47
3	21	346.36
3	26	530.93
3	31	754.77
3	34	907.92
3	34	907.92
3	35	962.11
3	37	1075.21
3	60	2827.43
3	11	95.03
3	11	95.03
3	18	254.47
3	19	283.53

[a] Certainty: 1 = certain, 2 = nearly certain, 3 = probable.

Table E.2.
Number of Titan craters per unit area.

ΔA Interval limits (km^2)	*ΔA* Interval (km^2)	Mean *A* interval (km^2)	*N/ΔA* (km^2)	*N* craters	Cumulative area *A* (km^2)
5-10	5	7.5	1.00	5	35.34
10-30	20	20	0.25	3	128.02
30-50	20	40	0.15	3	243.47
50-100	50	75	0.20	10	933.84
100-300	200	200	0.05	10	3198.14
300-500	200	400	0.015	3	4238.79
500-1000	500	750	0.02	10	12212.94
1000-3000	2000	2000	0.0025	5	20157.24
3000-5000	2000	4000	0.0015	3	31684.53
5000-10000	5000	7500	0.0008	4	59349.40
10000-30000	20000	20000	0.00015	3	96220.70
100000-150000	50000	125000	0.00002	1	238083.24

CHAPTER 3

Formation Mechanisms of Channels on Titan through Dissolution by Ammonium Sulfate and Erosion by Liquid Ammonia and Ethane

3.1. Introduction

Titan, the largest moon of Saturn, is the only satellite in the solar system with a significant atmosphere, harboring a suite of hydrocarbons that display a meteorological cycle similar to the hydrological cycle on Earth. Dendritic networks of sinuous valleys on the surface of Titan were first observed by the Cassini-Huygens mission, where Synthetic Aperture Radar (SAR) images revealed drainage networks with branching morphologies on the order of 100 km in length (Elachi et al., 2005). These observations were supported in greater detail by the Huygens Probe Descent Imager and Spectral Radiometer (DISR) (Tomasko et al., 2005; Soderblom et al., 2007b; Jaumann et al., 2009), and suggested formation by fluvial erosion into the water-ice bedrock. Additional support that the valleys were formed by flowing liquid is the paucity of impact craters on Titan's surface (Porco et al., 2005; Elachi et al., 2005; Jaumann et al., 2009; Wood et al., 2010), indicative of rapid burial or removal of surface topography. Additionally, at the landing site, the DISR imaged Earth-like rounded cobbles 0.3-15 cm in diameter (Tomasko et al., 2005) composed of water ice, indicating that they had undergone abrasion during fluvial transport. Further evidence of widespread fluvial processes on the surface of Titan has been revealed by the Cassini Imaging Science Subsystem (ISS) (Porco et al., 2005) and the Visual and Infrared Mapping Spectrometer (VIMS) (Barnes et al., 2007b; Jaumann et al., 2008).

Unlike on Earth, where liquid H_2O is the major agent of erosion, Titan's liquid erosion likely has multiple contributors. One possible contributor, that arguably garners the most attention, is liquid CH_4. Methane, which forms several percent of Titan's atmosphere, is a likely candidate for liquid erosion due to its stability as a liquid on the surface, its ability to participate in Titan's hydrological cycle, and direct observations of cloud-top altitudes consistent with the condensation

altitudes expected for methane (Lorenz et al., 2008). Further support for liquid methane being a primary contributor to Titan's erosion is shown in the works of, for example, Burr et al. (2006), Perron et al. (2006), Jaumann et al. (2008), Lorenz et al. (2008), Burr et al. (2009), Cartwright et al. (2011), Langhans et al. (2012), Black et al. (2012), and Burr et al. (2013), whose studies suggest that it could plausibly move enough material under conditions present on Titan to account for most of the observed fluvial features, even suggesting that mechanical erosion by liquid methane surface runoff would not require unreasonably high precipitation rates. Works similar to those cited above are numerous, but here we consider other liquids, which are also present on Titan, that could be responsible for the formation of the channels seen on the surface.

In this paper we address two different fluvial erosion processes on Titan. Specifically, we examine the possibilities of channel formation by dissolution of ice by a concentrated solution of ammonium sulfate, and by mechanical erosion by flow of liquid ammonia and liquid ethane. Each of these processes might have functioned over a certain range of temperatures during the cooling history of Titan.

That liquid ethane in Titan's atmosphere is not a pure liquid, but a solution containing CH_4 and N_2, has been shown by Tan et al. (2013, 2015). For surface liquids on Titan, such as in Ontario Lacus, the liquid was given as 15–30% CH_4, 50–80% C_2H_6, and 5-10% N_2 (Luspay-Kuri et al., 2015; Mitri et al., 2007), and a similar composition of liquid C_2H_6 solution on Titan's equator is given by Tan et al. (2015). The physical properties of a C_2H_6-CH_4-N_2 are not a weighted mean of the properties of three liquids, each of a very different liquefaction temperature. The properties are likely to be those of a solution of gaseous CH_4 and N_2 in liquid C_2H_6, similar to the properties of a solution of such gases as CO_2, N_2, and O_2 in liquid H_2O. The more soluble gas CO_2 affects the

density and viscosity of pure H_2O very little, by less than 3% (Garcia, 2001). The density of ethane solutions on the equator and the poles of Titan, as given by Tan et al. (2015) is 601 to 547 kg m^{-3}. These values are close to those of pure C_2H_6, 652 kg m^{-3} at 90.4 K and 586 kg m^{-3} at 150 K. We further assume that viscosity, like density, of pure liquid C_2H_6 does not differ much from an ethane solution of methane and nitrogen gases.

3.2. Observations of Streams on Titan

Valley-like features on the surface of Titan are known from the Huygens landing site and by three different imaging instruments onboard the Cassini spacecraft: the Visual and Infrared Mapping Spectrometer (VIMS), operating at 0.35 to 5.2 μm (Brown et al., 2004), the Imaging Science Subsystem (ISS), operating at 0.2 to 1.1 μm (Porco et al., 2005), and the Cassini Titan Radar Mapper (RADAR), emitting at 2.2 cm (Elachi et al., 2005). The resolution of VIMS and ISS images, which are hindered by atmospheric scattering and absorption, varies with both the distance of the spacecraft and emission angle. VIMS spatial resolution averages a few km/pixel but for small areas can be as high as 250 m/pixel (Jaumann et al., 2009). ISS resolution ranges from 1-10 km, with relatively small areas imaged at 1 km/pixel (Porco et al., 2004, 2005). The synthetic aperture radar (SAR) data from the RADAR are collected in swaths and are of the highest resolution (~350 m/pixel) available from the Cassini spacecraft (Lopes et al., 2010). Although RADAR coverage of the Titan surface is ~50% to date, compared to near-global coverage by the VIMS and ISS data, the SAR data provide the best resolution for mapping the fluvial networks.

In this study we examine 27 different fluvial features as identified in VIMS, ISS, and RADAR data, chosen based on their geographic diversity and resolution – or our confidence in

their classification as a fluvial feature. The locations and dimensions of these features on Titan are indicated in Figs. 3.1 and 3.2, and summarized in Table 3.1. These valleys represent an array of morphologic features and range in size from tens of kilometers to over a thousand kilometers long, and up to ten kilometers wide. The majority of these features are dendritic in nature, forming tree-shaped networks with many contributing branches that converge into larger receiving streams, up to seventh in channel order, indicative of an origin from rainfall (Tomasko et al., 2005; Perron et al., 2006; Lorenz et al., 2008; Jaumann et al., 2009).

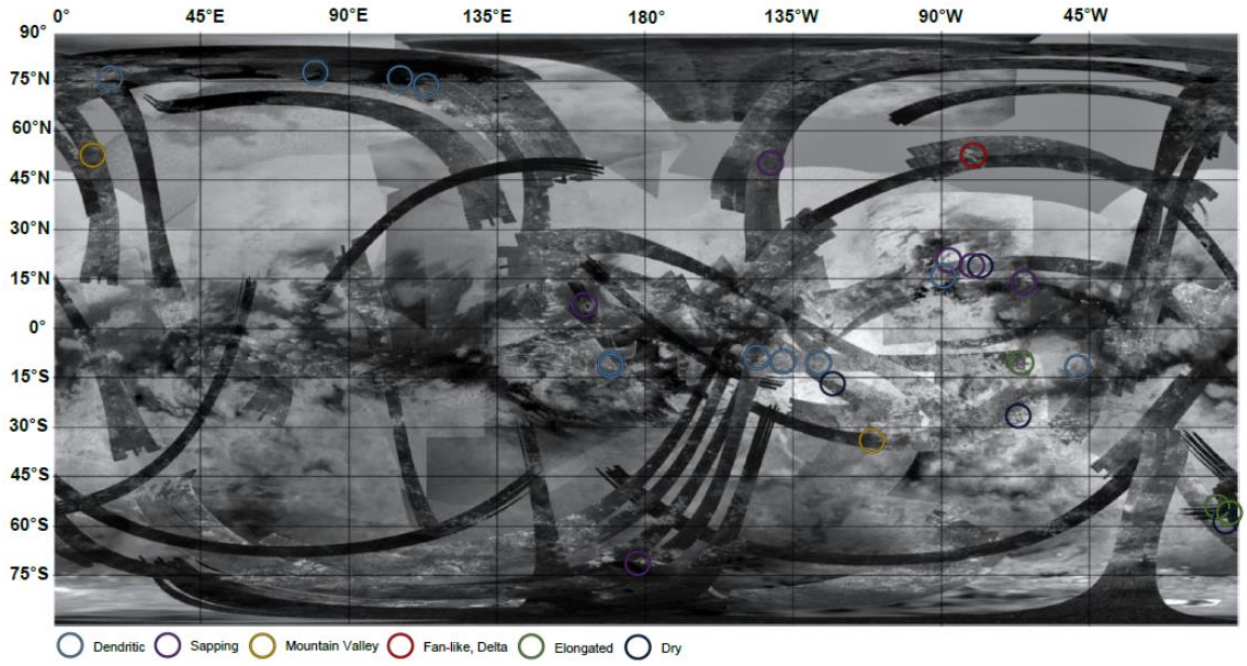

Fig. 3.1. Geographic distribution of fluvial features examined in this study, on SAR and ISS data up through T71, color-coded by network classification (see legend).

In contrast to these complex channels, there are also several fluvial features that seldom exhibit meanders, possess a low channel order, and a large channel width of up to 10 km. These features are inferred to be dry valleys, created as a result of rapid runoff events followed by prolonged droughts (Lorenz et al., 2008).

Table 3.1.
Location and physical characteristics of Titan channels. The parameters shown depend on the channel dimensions and the force of gravity on Titan, but not on the characteristics of the fluid (equations in Table 3.5).

Location	[Max] Length (km), *l*	[Max] Width (km), *w*	[Max] Order	[Max] Depth (km), *h*/300	[Max] Depth (km), *h*	[Max] Vol (km^3)	[Max] Mass of bedrock eroded from channel (kg)	Slope, *S*	Hydraulic Radius (m), R_r	Flow Velocity (m/s), *U*	Discharge (m^3/s), Q_r	Frictional Shear Velocity (m/s), *u**
11°S, 192°W	15	0.25	4	0.0013	0.38	1.44	1.34E+12	0.002	1.27	0.234	7.49E+01	0.059
54°N, 347°W	70	3	2	0.0071	2.13	448	4.17E+14	0.002	7.08	0.553	1.18E+04	0.139
10°S, 66°W	100	2	1	0.0054	1.61	323	3.00E+14	0.002	5.35	0.481	5.17E+03	0.120
36°S, 107°W	100	1	1	0.0033	1.00	100	9.30E+13	0.002	3.31	0.378	1.26E+03	0.095
54°N, 80°W	100	1	1	0.0033	1.00	100	9.30E+13	0.004	3.31	0.535	1.78E+03	0.134
56°S, 12°W	100	3	2	0.0071	2.13	640	5.95E+14	0.004	7.08	0.782	1.67E+04	0.196
58°S, 6°W	100	3	3	0.0071	2.13	640	5.95E+14	0.004	7.08	0.782	1.67E+04	0.196
72°S, 185°W	100	3	1	0.0071	2.13	640	5.95E+14	0.002	7.08	0.553	1.18E+04	0.139
75°N, 345°W	100	1	3	0.0033	1.00	100	9.30E+13	0.002	3.31	0.378	1.26E+03	0.095
7°N, 198°W	100	5	2	0.0101	3.04	1518	1.41E+15	0.001	10.1	0.467	2.36E+04	0.117
14°N, 65.4°W	125	5	1	0.0101	3.04	1897	1.77E+15	0.001	10.1	0.467	2.36E+04	0.117
8°S, 140°W	140	1.4	2	0.0042	1.26	247	2.30E+14	0.002	4.18	0.425	2.50E+03	0.107
59°S, 7°W	150	2	1	0.0054	1.61	484	4.50E+14	0.004	5.35	0.680	7.31E+03	0.170
19.6°N, 87°W	175	5	2	0.0101	3.04	2656	2.47E+15	0.002	10.1	0.660	3.34E+04	0.165
17°S, 120°W	180	8	1	0.0140	4.20	6046	5.62E+15	0.002	13.9	0.776	8.69E+04	0.194
12°S, 50°W	200	2	3	0.0054	1.61	645	6.00E+14	0.001	5.35	0.340	3.66E+03	0.085
16°N, 90°W	200	3	3	0.0071	2.13	1280	1.19E+15	0.004	7.08	0.782	1.67E+04	0.196
19°N, 77°W	200	10	3	0.0163	4.90	9796	9.11E+15	0.002	16.3	0.838	1.37E+05	0.210
50°N, 143°W	200	5	2	0.0101	3.04	3036	2.82E+15	0.002	10.1	0.660	3.34E+04	0.165
78°N, 280°W	200	5	5	0.0101	3.04	3036	2.82E+15	0.004	10.1	0.933	4.72E+04	0.234
19°N, 79°W	210	10	3	0.0163	4.90	10285	9.57E+15	0.002	16.3	0.838	1.37E+05	0.210
10°S, 125°W	300	1	3	0.0033	1.00	300	2.79E+14	0.002	3.31	0.378	1.26E+03	0.095
27°S, 67°W	350	3	2	0.0071	2.13	2241	2.08E+15	0.004	7.08	0.782	1.67E+04	0.196
73°N, 242W	400	3	2	0.0071	2.13	2561	2.38E+15	0.002	7.08	0.553	1.18E+04	0.139
10°S, 138°W	450	3	7	0.0071	2.13	2881	2.68E+15	0.004	7.08	0.782	1.67E+04	0.196
75°N, 255°W	1200	3	5	0.0071	2.13	7683	7.15E+15	0.004	7.08	0.782	1.67E+04	0.196
10°S, 192°W	1200	3	3	0.0071	2.13	7683	7.15E+15	0.004	7.08	0.782	1.67E+04	0.196
				Total channel volume, V_c		***67,269***						
Average (arithmetic mean)	**251**	**4**	**3**	**0.0075**	**2.26**	**2491**	**2.320E+15**	**0.0026**	**7.50**	**0.653**	**1.72E+04**	**0.164**

Another group of fluvial valleys recorded are believed to be the result of erosion by liquid seepage from the subsurface. These sapping channels are classified as being generally shorter and broader than those created by rainfall, and possess a low channel-order (Tomasko et al., 2005;

Jaumann et al., 2009). If correct, the presence of sapping channels indicates that Titan has a subsurface aquifer, which will be discussed in a later section.

Also notable are three features inferred as elongated valleys due to their straight course and their relatively small size, two fluvial features that exist within mountain chains and support an origin from rainfall (Langhans et al., 2012), and one system of valleys associated with alluvial fans.

In order to calculate the relative rates of stream incision into the water-ice bedrock on Titan, the channel dimensions used are as shown in Table 3.1. Measurements of channel slope were made directly from Cassini RADAR SARtopo and altimetry data, and depth from an empirical relationship between channel depth and width as outlined in William (1988). Size-distribution of the channels are shown in Fig. 3.2.

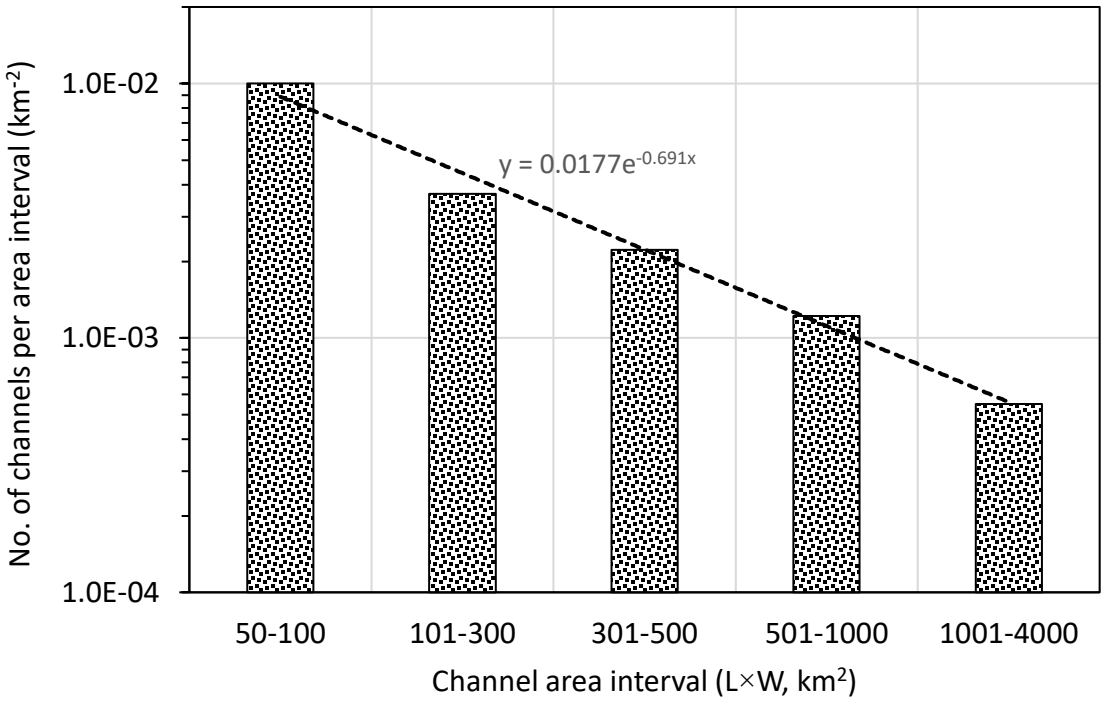

Fig. 3.2. Frequency distribution of channels by channel area interval (Table 3.1).

3.3. Crustal Composition and Structure

Previous work (Fortes et al., 2007; and references in Gilliam and Lerman, 2014a, b) has suggested that the interior of Titan is composed of a complex assemblage of silicate minerals, organic matter, liquid water in a subsurface NH_3-H_2O ocean, and ices, overlain by a crust composed primarily of low-pressure water ice, methane clathrate and ammonium sulfate. The exact thickness of the crust is mainly determined by the amount of heat available in the interior as well as the percentage of anti-freezing agents in the subsurface ocean, but is generally thought to be >100 km at present-day (Fortes et al., 2007; Gilliam and Lerman, 2014a).

The formation of the crust is a result of the interaction between Titan's primitive atmosphere and its liquid layer, which were in direct contact immediately after accretion and up until sufficient cooling of the atmosphere resulted in the crystallization of a solid shell composed of ice and methane clathrates (Tobie et al., 2006). After further cooling and thickening, macroporous clathrate grains are thought to have transported pockets of ammonium sulfate solution upwards, incorporating them into the outer shell, where they ultimately solidified to water ice and ammonium sulfate (Fortes et al., 2007). At present-day, a cross-section of the upper part of Titan's interior would reveal a top layer of ice Ih, methane clathrate, and solid ammonium sulfate, of densities 941, 988.5, and 1769 kg/m^3, respectively (Fig. 3.3, Table 3.2). On Earth, ammonium sulfate occurs as mineral mascagnite in fumaroles and volcanic vents.

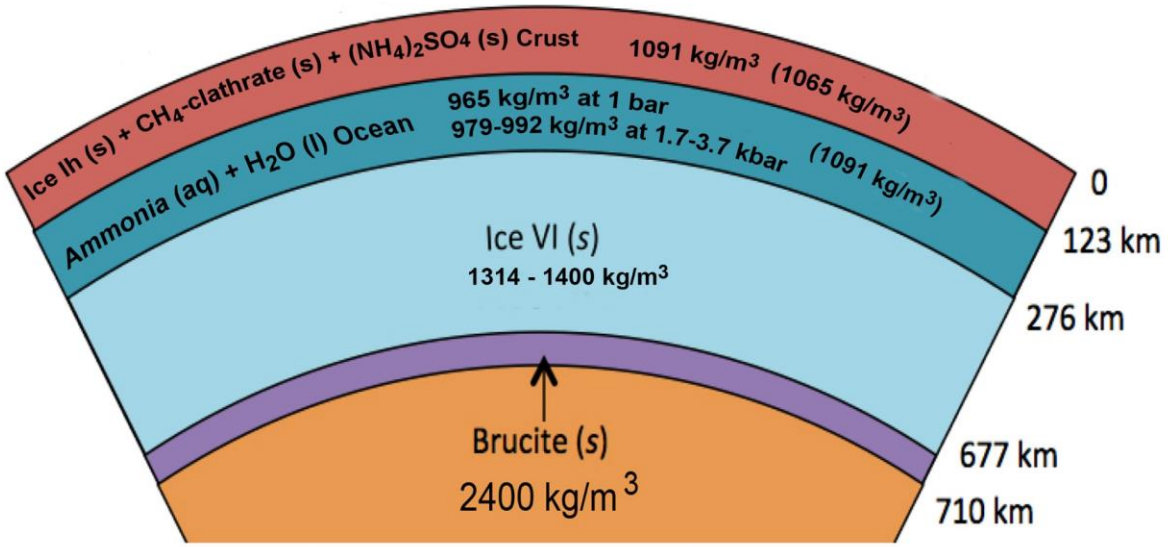

Fig. 3.3. Crustal Structure of Titan. Data in Table 3.2. Density values in parentheses from Gilliam and Lerman (2014a).

Table 3.2.
Structure and main components of Titan's upper crust (references cited in the text).

Component	Mass (kg)	Depth (km)	Thickness of layer (km)	Layer vol (m^3)	Mass from density & vol. (kg)	Density (kg/m^3)		*Density (kg/m^3) P corrected*	Pressure at layer base P (bar)	*T*(K)
						G&L (2014)	This paper			
Layer 1: Crust	1.062E+22	123	123	9.77E+18	9.87E+21	1065[1)]	1091[2)]		1.4	90
Ice Ih (s)	*3.41E+21*						941[3)]			
Ammonium Sulfate (s)	*1.60E+21*						1769[4)]			
Methane Clathrate (s)	*5.61E+21*						989[5)]		1,680	
Layer 2: Ocean	1.21E+22	276	153	1.09E+19	1.07E+22	1091[1)]	965[6)]	*979*[6)]		≥ 257
Ammonia (aq)	*1.21E+21*									
Water (liq)	*1.09E+22*							*992*[6)]	3,719	
Layer 3: Ice VI (s)	3.18E+22	677	401	2.23E+19	2.93E+22	1314-1400			10,843	120-300

1) Gilliam and Lerman (2014a), based on Fortes et al. (2007).
2) Weighted mean of the three components.
3) Density Ice Ih (kg/m^3) = 917 – 0.13×T°C (Chaplin, 2016; 90 K = -183°C).
4) Density at 20°C (CRC, 2016).
5) Mean at 50 K (English and Macelroy, 2003)
6) Croft et al. (1988)

3.4. Channel Formation Mechanisms

In this section, we consider the characteristics of the valley networks and Titan's surface environment, and several possible mechanisms of channel formation. The four, as shown in Fig. 3.4 and Table 3.3, might have operated at different times during Titan's cooling history. As far as the main component of the formation of present-day Titan's atmosphere, nitrogen gas N_2, is concerned, its condensation temperature at the pressure of 1 to 2 bar is 77 to 82 K, below the 90 K of the present-day Titan atmosphere (Jacobsen and Stewart, 1973). Figure 3.4 shows the regions of existence of the fluids derived from the atmospheric gases in a *T*-*P*-time graph. The chemical and mechanical roles of the liquid components will be discussed in the following section. The cooling of Titan's atmosphere, its temperature and total pressure as a function of time are as given in Gilliam and Lerman (2014a). The domains of gaseous and liquid methane and ethane are from Gilliam and Lerman (2016). The rectangles in the figure indicate the domains of existence of the liquid species (Table 3.3). Ethane is a gas at temperature higher than about 255 K, and it is a liquid along the dash-dotted line.

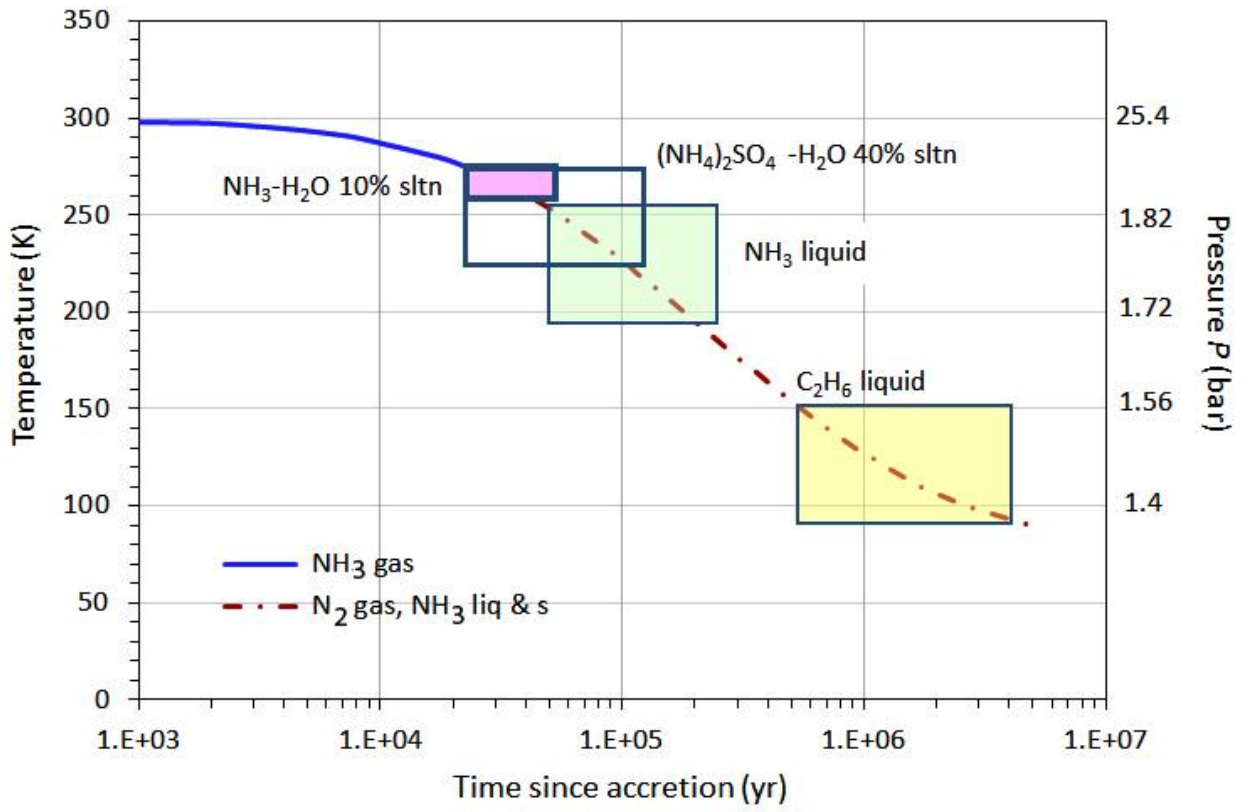

Fig. 3.4. Domains of existence of liquids on Titan's surface plotted in the *T*-*P*-time graph, from data in Table 3.2. From before T = 259 K, the temperature of NH_3 liquefaction, molecular nitrogen N_2 (0.028 kg/mol) is the main component of Titan's atmosphere that is too heavy to be lost by thermal escape. The decrease of its mass to the present-day p_{N2} = 1.3 to 1.4 bar is due to other photochemical processes (Atreya et al., 2006).

Table 3.3.
Potential liquid agents of channel formation and their characteristics in Titan's atmosphere at different times.

Liquid species	T range (K)	Time since accretion	Titan atm. P (bar)	Density kg/m^3	Viscosity Pa·s		Comments	Reference
Titan accretion	*300*	*0*	*25.4*					
Nitrogen N_2 liquid (0.02801 kg/mol)	Boiling pt. 77.36 77.36 - 63.16	------	------	808.5	(150 - 65)×10^{-6} at 80-110 K		*T* (K) range is above 1 bar total P	Littrup et al. (2004); CRC (2016). Values ≥80 K refer to P ≥ 1 bar.
Ammonia NH_3 liquid (0.017031 kg/mol)	259 - 195	40,300 -- 202,000	1.85 -- 1.71					
	251.92 at 1.8 bar			666.44				Haar and Gallagher (1978, pp. 680, 703, 709)
	195 at 1.8 bar			734.44	2.60E-04		at 0°C	CRC (2016)
	239.55 at 1.0 bar			666.44	0.33 cSt	2.199E-01	at 239 K	Seeton (2006)
	195 at 1.0 bar			734.41	0.75 cSt	2.424E-01	at 195 K	
NH_3-H_2O, 10 wt % sltn	273 - 257	20,200 -- 44,700	2.06 -- 1.84	965 979 - 992	2.00E-01		at 254 K at 1 bar at 1.8 – 3.8 kbar	G&L (2014a, Table 1), Croft et al. (1988, Fig. 1). Kargel et al. (1991, Table 1)
$(NH_4)_2SO_4$ - H_2O, 40-45 wt % solution (132.13952 g/mol)	273 - 223	20,200 – 109,000	2.06 -- 1.80	1227.7	2.530E-04		at 20°C or 293 K	Xu et al (1998), CRC (2016)
					1.223E-01		at -60°C or 213 K	Seeton (2006), 2,2-dichloro-1,1,1-trifluoroethane, R123
Ethane C_2H_6 liquid (0.03007 kg/mol)	150 - 90.5	(0.55 -- 2.7)×10^6	1.56 -- 1.4					
	90.36			651.6	1.250E-03		at 1 and 2 bar	Younglove and Ely (1987, pp. 644-647.
	100			641.2	7.980E-04			
	150			585.6	2.520E-04			

3.4.1. Chemical Erosion by Ammonium Sulfate

Given the unique combination of surface materials on Titan, the channels may be the result of dissolution features. On Earth, chemical weathering is the process of weakening and subsequent disintegration of rock by chemical reactions such as oxidation, hydrolysis, and carbonation. Physical erosion follows by the removal of dissolved material by running water and by the removal of solid particles. The dissolution of soluble bedrock such as limestone, dolomite, and gypsum

forms karst topography – an amalgamation of caves, springs, sinkholes, solution valleys, and disappearing streams (Monroe and Wicander, 2012). On Titan, the bulk crustal material, water-ice, is insufficiently soluble in methane and ethane over geologically plausible timescales to result in heavily karstic terrains (Cornet et al., 2015). As a consequence, chemical weathering was not widely predicted on Titan by theoretical models (Lorenz and Lunine, 1996; Collins 2005), and was not observed during the early stage of the Cassini-Huygens mission. However, during the T16 fly-by of Titan in 2006, the Cassini RADAR instrument revealed a multitude of complex labyrinthine terrain interpreted to be the result of dissolution and/or collapse processes (Stofan et al., 2007). Since then, additional fly-bys have revealed a large quantity of features that are karst-like in nature: clusters of nearly circular depressions in the North Polar Region and closed depressions in the South Polar Region (Mitchell et al., 2007; Malaska et al., 2010; Mitchell and Malaska, 2011). The existence of these features, combined with the knowledge that water ice is insoluble in liquid methane and ethane, prompts an investigation of the dissolution of Titan's channels by other, more unusual or less common, liquid media.

Table 3.4.
Composition of the upper layer of Titan's crust and ice dissolution.

1. *Ice Ih* (s) and liquid H_2O equivalent 18.015 g/mol (kg)	3.41E+21	**6.** Thickness of ice left after solution formed (km)	14.9
2. *Ammonium Sulfate* (s) $(NH_4)_2SO_4$ 132.14 g/mol (kg)	1.60E+21	**7.** Mass material in channels (kg) (Table 3.1)	6.26E+16
3. *Methane Clathrate* (s) $CH_4 \cdot 6H_2O$ 124.16 g/mol (kg)	5.61E+21	**8.** Volume material in channels (km^3)	6.73E+04
4. Water to make sat. solution of amm.-sulf. (41.3 wt %) at 0°C (kg H_2O) 5.3 molal	2.27E+21	**9.** Estimated time to dissolve channel mass (yr)	1100 to 280
5. Water left after ammonium-sulfate dissolution (kg)	1.14E+21		

Ammonium sulfate, $(NH_4)_2SO_4$, is an inorganic salt that is most commonly known for being a fertilizer for alkaline soils. On Earth, ammonium sulfate occurs as mineral mascagnite in fumaroles and volcanic vents. On Titan, ammonium sulfate may exist in solution in the subsurface ocean, and as a solid in the crust, probably derived from the ocean by intrusion of the original crust. The results of dissolution of all the $(NH_4)_2SO_4$ in water of the upper crustal layer of Titan are outlined in Table 3.4. The remaining water-ice would form a residual layer of 15 km in thickness where the ammonium-sulfate solution could form channels by dissolution of ice (Fig. 3.5).

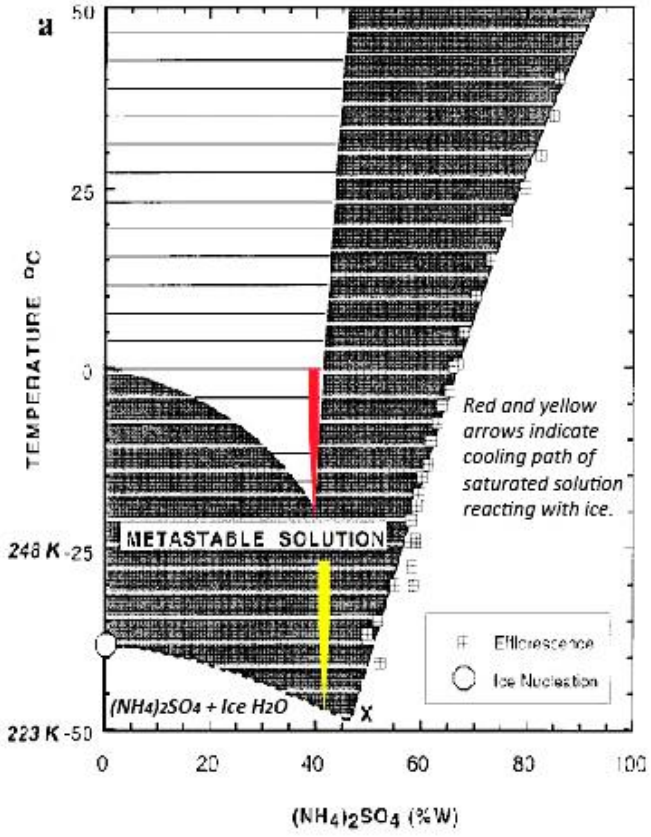

Fig. 3.5. $(NH_4)_2SO_4$-H_2O metastability phase diagram in temperature-composition domain. The pure solution equilibrium region is represented by the open striped field, whereas the metastable solution is shown as the gray striped area. Tiled squares indicate all observed efflorescence points. Homogeneous ice nucleation from pure water is labeled with the octagon. **X** marks the lowest temperature where solution microdroplets can be found. Modified from Xu et al. (1998). Reprinted with permission from *Journal of Physical Chemistry B, 102*, 7462-7469, Copyright © 1998, American Chemical Society.

The estimated time of dissolution of the ice mass in channels is based on the rates of fjord ice melting on Earth, from 0.1 to 0.4 m/day (Russell-Head, 1980; Enderlin, 2014). The volume of the channel ice (Table 3.4) would be dissolved at these rates from 280 to 1100 years. This time is much shorter than the period of about 84,000 yr that a concentrated $(NH_4)_2SO_4$-H_2O solution could exist as a liquid on the cooling Titan surface (Fig. 3.4)

3.4.2. Mechanical Erosion by Liquids

On Earth, rivers most often erode bedrock mechanically through sediment transport or by fluid discharge alone. In general, the greater the velocity of the fluid and the steeper the grade, the more sediment will be conveyed. The main processes of water erosion, as given by Hjulström (1935), Shields (1936), Sundborg (1956), Whipple et al. (2000), and Sklar and Dietrich (2001, 2004) are summarized below.

The equations of the preceding authors and of Einstein (1942), Meyer-Peter (1949, 1951), Nielsen (1992), Chanson (1999), and Finnegan et al. (2005) include a number of empirical values of the variables and they do not work with any arbitrary values of the physical and mechanical parameters. The main features of the channel-bed erosion-by-flow models are**:** (1) the channel slope *S* must be sufficiently steep to assure a strong flow; (2) the density of the particles must be greater than that of the liquid; (3) only the channel floor is being eroded; (4) erosion takes place by saltation and transport of particles (Fig. 3.6); (5) bed-shear stress (Table 3.5, No. 8) must be greater than the critical shear stress (No. 7), $\tau_b^* > \tau_c^*$; (6) and the sediment transport parameter q_s (No. 17-20) must be greater than q_t (No. 9), $q_s > q_t$. These and other parameter values are given in Table 3.5.

Fluid flow can be strong enough to suspend particles in the water column as they move downstream, or simply push them along the bottom of the channel. Sediment being transported over a bed of exposed bedrock can erode the bed significantly by the processes of abrasion, or the wearing-away of surfaces by mechanical processes such as rubbing, cutting, scratching, grinding, and polishing. This type of erosion is strongest when the river is transporting large chunks of rock or after heavy rainfall when the river's flow is turbulent. Even in the absence of a significant sediment load, a river can erode its bed and banks by tearing out large blocks along preexisting fracture using the force of the flowing water. This sort of erosion is strongest at rapids and waterfalls where the water has a high velocity. Cavitation, or the trapping and subsequent implosion of air bubbles in cracks in the river's banks, resulting in the weakening of the adjoining surface, is an additional method of erosion that is not dependent on the presence of a sediment load.

The expectation that rainfall occurs on Titan (Graves et al., 2008; Schneider et al., 2012) introduces the possibility that the valleys were carved by rivers of liquid fed by direct surface runoff, shallow underground flow, or both. In this study, we consider two different liquid medium agents responsible for mechanical erosion of the Titan channels, liquid ammonia and liquid ethane, and compare them to a case of liquid water erosion on Earth. Two other liquids – 10% NH_3-H_2O and $(NH_4)_2SO_4$ solutions in H_2O – have densities higher than the particles (Table 3.3).

Channels on Titan and Earth: On Titan, the ratio width/depth of the channels is close to 1.5 to 2 (Table 3.1). On Earth, the ratio of the river channels varies from about 60 in gravel to 5 in bedrock (Finnegan et al., 2005). The depth of the channels on Titan is measurable in kilometers, and it is much greater than river depths on Earth. The biggest rivers, thousands of km in length,

have maximum depths in the range from 10^1 to 10^2 m (Walther, 2013), but such rivers as the Missouri, the Thames and the Danube are 7-12 m deep.

The bed-slope of the channels on Titan is of the order of 10^{-3} or 1 m per 1 km (Table 3.1). On Earth, the slopes of some rivers are of the same magnitude 10^{-3} (Schaller et al., 2001) or higher in small-catchment areas 10^{-3} to 10^{-1} (Van Der Beek and Bishop, 2003). The slope of such a big river as the Mississippi is smaller, varying from 1×10^{-4} to 8×10^{-5} (Carlston, 1969). The gradient of the rivers in the Ukraine varies from 5×10^{-4} to 2×10^{-3} (Stebelsky and Teslia, 1993). We use the range of gradients from 6×10^{-4} to 1×10^{-3} for a model river channel on Earth in Table 3.6.

Liquids not suitable for erosion: Molecular nitrogen N_2 is gas at the surface conditions of Titan and it liquefies at a lower temperature than 90 K (Table 3.3). The aqueous solutions of ammonia NH_3 and ammonium sulfate $(NH_4)_2SO_4$ have densities higher than the density of the water-ice particles and cannot therefore be considered as agents of mechanical erosion.

Erosion by liquid NH_3: Present-day, the bulk of Titan's ammonia is likely to be found as a solid in its icy outer shell, or as a liquid in its subsurface ocean. However, under a warmer Titan, ammonia may have existed as a gas in the atmosphere, or even as a liquid on the surface. In fact, while the exact composition of Titan's early atmosphere is not well known, it is generally accepted that it was much more massive and denser than at present, and dominated by ammonia and methane (Gilliam and Lerman, 2014a). Based on the cooling model of Gilliam and Lerman (2014a, 2016), and assuming an accretion temperature of 300 K, we estimate that ammonia would have been in a liquid state on the surface of Titan between 40,300 and 202,000 years after accretion, or between temperatures of 259 to 195 K (Fig 3.4). Although geologically brief, this time period may have

been the first under which Titan's channels, initially formed by chemical erosion, underwent mechanical erosion by a liquid.

Erosion by C_2H_6: In Titan's atmosphere, ethane is produced as a result of UV photolysis of methane (Yung et al., 1984), with a mean production rate of 1.3×10^{8} molecules cm^{-2} s^{-1} from solely the photolytic conversion of methane to ethane (Wilson and Atreya, 2009), and subsequently condenses and precipitates from the atmosphere. Consideration of this process suggests that Titan should have produced a substantial amount of ethane since accretion. Such an idea was first proposed by Lunine et al. (1983), who used photochemical models to predict that Titan would be covered by an ethane ocean one to several kilometers deep, and was later supported by others' models, albeit with a smaller net volume of ethane produced. Further, Gilliam and Lerman (2016) estimated the mass of ethane produced since accretion as 8.46×10^{17} kg, and suggested that most of it resides in liquid form on or within Titan's porous crust. As shown in Fig. 3.4 and Table 3.3, we estimate that liquid ethane rain may have begun as early as 0.55×10^{6} years after accretion, corresponding to a Titan surface temperature of 150 K, and continues to present-day, providing ample time for Titan's channels to undergo mechanical erosion by liquid ethane.

However, there is an uncertainty in the mass balance of liquid ethane as a possible agent of channel erosion. At the ethane atmospheric production rate cited above, there would have been 9.6×10^{13} kg C_2H_6 accumulated in 550,000 years, equivalent to 1.55×10^{11} m^3 liquid C_2H_6. This volume, distributed over the total area of the channels of 23,750 km^2 (length×width, Table 3.1), would have produced a layer 6.5 m thick. But, its annual increment at the cited ethane production rate would add only 12 micrometers (1.2×10^{-5} m) to the liquid ethane layer thickness in the channels. The rate of precipitation of liquid ethane on Titan was estimate as 3.0×10^{-7} to 0.63×10^{-7}

$m^3\ m^{-2}\ yr^{-1}$ (Graves et al., 2008), equivalent to about 2.0×10^{-4} to 0.4×10^{-4} kg gaseous $C_2H_6\ m^{-2}\ yr^{-1}$. From the present-day C_2H_6 contents of Titan's atmosphere 9.24×10^{13} kg (Gilliam and Lerman, 2016), and Titan's surface area of $8.332\times10^{13}\ m^2$, the residence time of C_2H_6 with respect to precipitation from the atmosphere is 9.24×10^{13} kg/[(2.0 to 0.4)$\times10^{-4}$ kg $m^{-2}\ yr^{-1}\times8.332\times10^{13}\ m^2$] = 5500 to 27,700 yr. Despite these apparent inconsistencies in material balance of ethane, and that also appears in the balance of methane (Gilliam and Lerman, 2014a), we use liquid ethane as a potential agent of channel formation on Titan, as discussed further below.

Equations: To calculate the rates of liquid stream incision into water ice bedrock on Titan, we build on the Sklar and Dietrich (2004) model of terrestrial water erosion by saltation of bedrock particles, and analyze the effect of bed-load transport on the lowering rate using the equations of bed-load transport rate developed by Einstein (1942) and Chanson (1999). These models apply to channels of fixed width that are being deepened by erosion and abrasion of rock/ice by bed load, and assume that all bed load motion is by saltation of spherical grains of uniform size. A discussion of the fundamental equations used is as follows, and a complete list of all equations used is listed in Table 3.5 and the essentials of the process are as shown in Fig. 3.6.

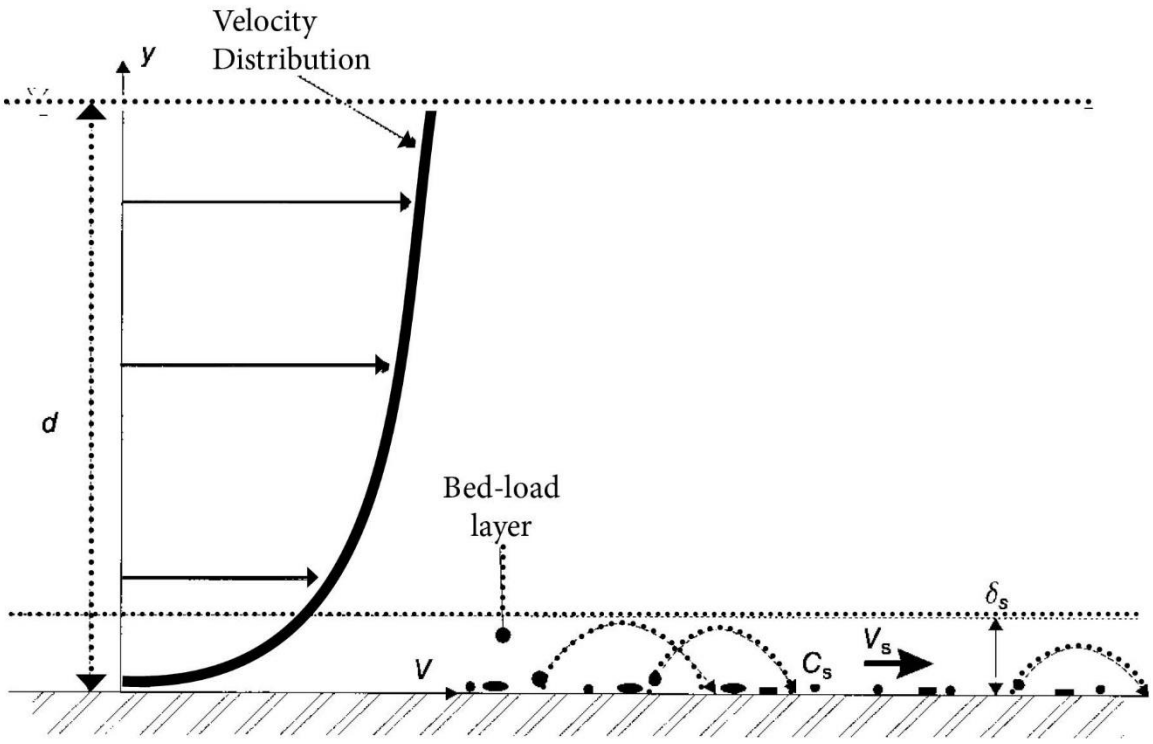

Figure 3.6. Channel erosion by flowing water. Reprinted in modified format from Chanson (1999, Fig. 10.1), by permission of Professor H. Chanson, Copywrite © Hubert Chanson 1999. Parameters listed in Tables 3.5 and 3.6.

Table 3.5.
List of the equations used in this study.

No.	Parameter description	Equation	Reference
1	Channel height (m)	$h = w^{0.69}$	William (1988); Jaumann et al. (2008)
2	Hydraulic radius for rectangular channel (m)	$R_r = wh/(w + 2h)$	Murdock (1993)
3	Flow velocity (Darcy-Weisbach equation) (m/s)	$U = \sqrt{8gR_rS/f}$	Perron et al. (2006)
4	Discharge for rectangular channel (m^3/s)	$Q_r = whU$	Perron et al. (2006)
5	Frictional shear velocity (m/s)	$u^* = (ghS)^{0.5}$	Paphitis (2001); Burr et al. (2006)
6	Boundary Reynolds number	$R_e^* = u^*D/\nu$	Paphitis (2001); Burr et al. (2006)
7	Critical shear stress	$\tau_c^* = (0.188/(1 + R_e^*)) + 0.0475\left(1 - 0.699e^{-0.015R_e^*}\right)$	Paphitis (2001); Burr et al. (2006)
8	Bed shear stress	$\tau_b^* = \rho_l ghS/\left((\rho_s - \rho_l)gD\right)$	Burr et al. (2013)
9	Sediment transport capacity (kg m^{-1} s^{-1})	$q_t = 5.7\rho_s(R_bgD^3)^{1/2}(\tau_b^* - \tau_c^*)^{3/2}$	Sklar and Dietrich (2004)
10	Total hop length (m)	$L_s = 8D\left((\tau_b^*/\tau_c^*) - 1\right)^{0.88}$	Huda and Small (2014)
11	Vertical impact velocity (m/s)	$w_{si} = 2\left(0.4(R_bgD)^{0.5}\left((\tau_b^*/\tau_c^*) - 1\right)^{0.18}\right)\left(1 - (u^*/w_f)^2\right)^{0.5}$	Sklar and Dietrich (2004)
12	Mean shear stress (kg m^{-2} s^{-1})	$\tau_0 = \rho_l gh\sin S$	Chanson (1999)
13	Volumetric particle conc. In bed-load layer	$C_s = (0.177/D)\left(\nu^2/((g_s - 1)g)\right)^{1/3}\left((\tau_b^*/\tau_c^*) - 1\right)$	Chanson (1999)
14	Average sediment velocity (m/s)	$V_s = 7(gh\sin S)^{0.5}$	Chanson (1999)
15	Thickness of the bed-load layer (m)	$\delta_s = 0.3D(D((g_s - 1)g/\nu^2)^{1/3})^{0.7}\left((\tau_b^*/\tau_c^*) - 1\right)^{0.5}$	Chanson (1999)
16	Bed load transport rate per unit width (m^2/s)	$S_T = C_sV_s\delta_s$	Chanson (1999)
17	Mass sediment flow rate per unit width (kg m^{-1} s^{-1})	$q_s = S_T\rho_s$	Chanson (1999)
18	OTHER relationships for q_s (units as above)	$q_s = 2.15\sqrt{(g_s - 1)gD^3}exp(-0.391\rho_l(g_s - 1)gD/\tau_0)\rho_s$	Einstein (1942), Chanson (1999)
19		$q_s = \left((4\tau_0/(\rho_l(g_s - 1)gD)) - 0.188\right)^{3/2}\sqrt{(g_s - 1)gD^3}\rho_s$	Meyer-Peter (1949, 1951), Chanson (1999)
20		$q_s = \sqrt{(g_s - 1)gD^3}\left((12\tau_0/(\rho_l(g_s - 1)gD)) - 0.05\right)\sqrt{\tau_0/(\rho_l(g_s - 1)gD)}\rho_s$	Nielsen (1992), Chanson (1999)
21	Erosion rate (m/s)	$E = \frac{q_sw_{si}^2Y}{L_sk_v\sigma_T^2}\left(1 - \frac{q_s}{q_t}\right)$	Sklar and Dietrich (2004)
22	Nondimensional buoyant density of sediment	$R_b = (\rho_s/\rho_l) - 1$	Huda and Small (2014)
23	Particle settling velocity (m/s)	$w_f = (\rho_s - \rho_l)gD^2/(18\mu)$ $w_f = 2.46\sqrt{(\rho_s - \rho_l)gD/(2\rho_l)}$	Caenn et al. (2011)
24	Dynamic viscosity (Pa s); ν is kinematic viscosity (m^2 s^{-1})	$\mu = \nu\rho_l$	Elson (2007)

The Sklar and Dietrich (2004) model of erosion states that

$$E = V_iI_rF_e \tag{3.1}$$

where E is erosion rate (m/s), V_i is the volume eroded per impact (m^3), I_r is impact rate per unit area (m^{-2} s^{-1}), and F_e is the fraction of the streambed that is exposed to streamflow. The value of F_e depends on the supply of sediment to the stream, and the transport stage of the stream (the ratio of the shear velocity in the flow to the critical shear velocity at the threshold of sediment motion). The value of I_r is a function of the flux of particles, and the saltation hop length. The value of V_i is dependent on the kinetic energy of each particle impact, and the resistance of the bedrock material to abrasion by small impacts. Thus, equation (3.1) can be rewritten as

$$E = \frac{q_s w_{si}^2 Y}{L_s k_v \sigma_T^2}\left(1 - \frac{q_s}{q_t}\right) \tag{3.2}$$

where the variables are as given in Table 3.5. There q_s is the mass sediment flow rate per unit width (kg m^{-1} s^{-1}), w_{si} is the vertical impact velocity (m/s), Y is the Young's Modulus (Pa), L_s is the total hop length (m), k_v is the abrasion resistance parameter, σ_T is the tensile strength (Pa), and q_t is the sediment transport capacity (kg m^{-1} s^{-1}). The value of w_{si} (No. 11) is a function of the buoyant density of the sediment, gravity, grain diameter, the critical and bed shear stresses, the frictional shear velocity, and the particle settling velocity. The value of L_s depends on the grain diameter as well as the critical and bed shear stresses. The value of q_t is a function of the sediment density and buoyant density, gravity, grain diameter, and the critical and bed shear stresses.

Mass sediment flow rate per unit width, q_s, is defined as

$$q_s = S_T \rho_s \tag{3.3}$$

where S_T is the bed load transport capacity per unit width (m^2/s), and ρ_s is the density of the sediment (kg/m^3). Numerous researchers have proposed different empirical and semi-empirical correlations of the bed load transport capacity. Other parameters are as given in Table 3.5.

Table 3.6.
Parameters used for channel calculations.

	Titan		Earth
Temperature	90 to 150	195-259	293
Surface gravity, g (m/s^2)	1.35	1.35	9.81
Fluid	Ethane (C_2H_6)	Ammonia (NH_3)	Water (H_2O)
Density, ρ_l (kg/m^3)	650	700.44	998.2
Kinematic viscosity, υ (m^2 s^{-1})	1.50E-06	3.71E-07	1.157E-06
Particle settling velocity, w_f (m/s)	1.25E+02	1.69E+02	1.435E+03
Dynamic viscosity, μ (kg m^{-1} s^{-1})	9.75E-04	2.60E-04	1.155E-03
Nondimensional buoyant density of sediment, R_b	0.43	0.33	1.51
Specific gravity, g_s	1.4308	1.328	2.505
Sediment	Water ice	Water ice	Quartz
Density, ρ_s (kg/m^3)	930	930	2500
Particle diameter, D (m)	0.033	0.033	0.033
Bedrock	Water ice	Water ice	Sandstone
Young's Modulus, Y (Pa)	9.00E+09	9.00E+09	5.00E+10
Tensile strength, σ_T (Pa)	1.00E+06	1.00E+06	2.00E+06
Abrasion resistance parameter, k_v	1.90E+04	1.90E+04	1.40E+06

3.5. Results and Conclusions

From the discussion of the modes of channel erosion in the preceding section we estimate the time (t) that it might have taken liquid ethane and ammonia on Titan and water on Earth to form a representative channel. For Titan, the dimensions and slope of a mean channel are given in Table 3.1. For Earth, a model channel is 100 km long, 100 m wide, 10 m deep, and with a slope of 0.001 and 0.0006. There are several possible formulations of the time to erosion of total volume or mass of the channels, of which we use the following two.

Time to erosion (t_1) based on total volume of the channels (V_c, in m^3, Table 3.1) and the linear erosion rate E in m/s of Sklar and Dietrich (2004), eq. (3.2):

$$t_1 = V_c^{1/3}/E \quad \text{(yr)} \tag{3.4}$$

Only the equations of Einstein (1942) and Chanson (1999) could be used for calculation of the channel-bed erosion rate E (m s^{-1}). The equations of Meyer-Peter (1949), 1951) and Nielsen (1992) do not give meaningful results of positive erosion rate $E > 0$.

And time to erosion (t_2) based on total mass of material in channels (M_c in kg, from Table 3.1) mean channel width (w in m, Table 3.1) and q_s, mean sediment flow rate per unit width (in kg m^{-1} s^{-1}, Table 3.5, Nos. 17-18), is:

$$t_2 = M_c/(q_s w) \quad \text{(yr)} \tag{3.5}$$

Using the equation of bed load transport capacity given by Chanson (1999), the rates of mass sediment flow per unit width (q_s) are 35.4 kg m^{-1} s^{-1} and 40.6 kg m^{-1} s^{-1}, corresponding to erosion rates of 3×10^{-9} m/s and 7.2×10^{-9} m/s, for liquid ethane and liquid ammonia, respectively. As a comparison, a channel of length 100 km, width 0.1 km, and slope of 0.0006-0.001, carved into sandstone on Earth by liquid water yields a mass sediment flow rate per unit width (q_s) of 0.07-0.73 kg m^{-1} s^{-1} and an erosion rate of 1.2-5.8$\times10^{-9}$ m/s.

Using the equation of bed load transport capacity given by Einstein (1942), the rate of mass sediment flow per unit width (q_s) is 7.04 kg m^{-1} s^{-1} for liquid ethane and 6.59 kg m^{-1} s^{-1} for liquid ammonia, corresponding to erosion rates of 1.3×10^{-8} m/s and 6.7×10^{-9} m/s, for liquid ethane and liquid ammonia, respectively. As a comparison, a model river channel of length 100 km, width 0.1 km, and slope of 0.0006-0.001 carved into sandstone on Earth by liquid water yields a mass sediment flow rate per unit width of 0.19-2.55 kg m^{-1} s^{-1} and an erosion rate of 2.35-8.98$\times10^{-9}$ m/s.

The results of the time to erosion t_1 and t_2 are shown in Table 3.7. The times obtained with eq. (3.4) for the Titan channels are of the order of $10^4 – 10^5$ years. For the Earth model river, the times are $10^3 – 10^4$ years. The latter estimates agree with the ages of four large European rivers of

6,000 to 42,000 yr (Schaller et al., 2001). The times from eq. (3.5) are generally lower than those from eq. (3.4), and some of the results based on Einstein's (1942) equations are higher, and some lower, than those based on Chanson (1999) and Sklar and Dietrich (2004). The models of Meyer-Peter (1949, 1951) and Nielsen (1992) are not considered here because they give negative erosion rates that are physically unrealistic in erosion models without an external source of sediment.

The erosional sequence of the channels on Titan (Fig. 3.4) might have started after the formation of water-ice on the surface by the process of chemical dissolution by $(NH_4)_2SO4$-H_2O, overlapping or followed by a period of mechanical erosion by liquid NH_3 condensed from the atmosphere. A final stage on the cooling surface of Titan might have been characterized by liquid C_2H_6 as an agent of mechanical erosion.

The periods of existence of one agent of chemical dissolution, ammonium sulfate solution, and two agents of mechanical erosion, liquid ammonia and ethane, are considerably longer that the estimated channel formation times.

Table 3.7.
Results and Conclusions

	Titan	Titan	Earth	Earth
Liquid	C_2H_6	NH_3	H_2O	H_2O
Slope	0.0026	0.0026	0.0010	0.0006
Surface grain size, D (m)	0.033	0.033	0.033	0.033
Critical shear stress, τ_{c*}	0.048	0.048	0.048	0.048
Bed shear stress, τ_{b*}	1.34	1.73	0.10	0.06
Sediment transport capacity, q_t (kg m^{-1} s^{-1})	36.8	47.7	4.02	0.48
Total hop length, L_s (m)	4.83	6.09	0.29	0.08
Vertical impact velocity, w_{si} (m/s)	0.153	0.123	0.560	0.437
Mean shear stress, τ_0 (kg m^{-1} s^{-2})	17.4	18.5	49.0	29.4
Volumetric concentration of sediment in the bed-load layer, C_s	0.015	0.008	0.00018	0.00004
Average sediment velocity, V_s (m/s)	1.14	1.14	1.55	1.20
Bed-load layer thickness, δ_s (m)	2.20	4.53	1.06	0.52
Reference	Chanson (1999)	Einstein (1942)	Chanson (1999)	Einstein (1942)	Chanson (1999)	Einstein (1942)	Chanson (1999)	Einstein (1942)
Bed-load transport rate per unit width, S_T (m^2/s)	3.76E-02	7.48E-03	4.31E-02	7.00E-03	2.93E-04	1.02E-03	2.71E-05	7.66E-05
Mass sediment flow rate per unit width, q_s (kg m^{-1} s^{-1})	35.4	7.04	40.6	6.59	0.73	2.55	0.07	0.19
Erosion rate, E (m/s)	2.95E-09	1.30E-08	7.15E-09	6.70E-09	5.77E-09	8.98E-09	1.19E-09	2.35E-09
Time to erode (yr)								
t_1, eq. (3.4)	1.35E+05	3.05E+04	5.57E+04	5.94E+04	2.55E+03	1.64E+03	1.24E+04	6.27E+03
t_2, eq. (3.5)	4.77E+02	2.40E+03	4.16E+02	2.56E+03	1.08E+02	3.11E+01	1.17E+03	4.13E+02

CHAPTER 4

CH_4-CH_3-C_2H_6 Reaction System in Titan's Atmosphere: A Geochemical Balance Model with Explicit Solutions

4.1. Introduction

The occurrence of methane and ethane in the atmosphere of Titan, the biggest satellite of Saturn, with a total atmospheric pressure of 1.5 bar, comparable to that on Earth, has been a subject of extensive research since the early 1980s, following the NASA Voyager 1 and 2 missions. The composition and evolution of Titan's atmosphere have been addressed in numerous publications summarizing the hypotheses and state of knowledge and are bracketed by, for example, those of Strobel (1982), Lunine et al. (1983), and Wilson and Atreya (2009).

A very detailed sequence of C_xH_y-species reactions in Titan's atmosphere and ionosphere has been treated by Bar-nun and Podolak (1979), Lara et al. (1995), Troublanc et al. (1995), Smith and Raulin (1999), Wilson and Atreya (2000, 2004), Romanzin et al. (2005, 2008), Atreya et al. (2006), and the authors cited in Table 4.1. This paper expands the aforementioned authors' work by presenting a simplified sequence of the chemical reactions and their mathematical solutions as a geochemical balance model of the three gases in Titan's atmosphere, which agree with the reported gas abundances. Methane (CH_4) and ethane (C_2H_6), the latter forming from the intermediary methyl (CH_3), are the two main species of the carbon cycle on Titan. A simplified sequence of direct forward reactions from CH_4 to C_2H_6 that short-circuits the complex intermediate paths may be represented by the following (Gilliam et al., 2015; Gilliam and Lerman, 2016a):

$$CH_4 \xrightarrow{k_{12}} CH_3 + H, \qquad k_{12} \text{ is first-order photolysis } [s^{-1}] \tag{4.1}$$

$$CH_3 + CH_3 \xrightarrow{k_{23}} C_2H_6, \qquad k_{23} \text{ is second-order } [cm^3 \text{ molecule}^{-1} s^{-1}] \tag{4.2}$$

$$C_2H_6 \xrightarrow{k_3} \text{Other products}, \qquad k_3 \text{ is considered as first-order } [s^{-1}] \tag{4.3}$$

Reactions (4.1)-(4.3), occurring simultaneously in Titan's atmosphere, make a geochemical reservoir balance system:

$$d[CH_4]/dt = -k_{12}[CH_4] \quad (4.4)$$

$$d[CH_3]/dt = k_{12}[CH_4] - k_{23}[CH_3]^2 \quad (4.5)$$

$$d[C_2H_6]/dt = k_{23}[CH_3]^2 - k_3[C_2H_6] \quad (4.6)$$

where t is time, [ ] are masses in kg, mol, or concentrations in molecules cm^{-3} (present-day abundances shown in Table 4.1), and k_{ij} are the reaction rate parameters. The rate of CH_3 consumption that forms from CH_4, k_{23} in eq. (4.5), does not have to be the same as the rate of CH_3 reaction that forms C_6H_6, k_{23} in eq. (4.6). For the sake of notational simplicity, only k_{23} is used in this paper, and any possible differences between the two rate parameters are noted in the text. A discussion of the different reaction rate parameters is presented in the next section, and the solutions of (4.4)-(4.6) and their relevance to the understanding of the behavior of $CH_4 - C_2H_6$ in a subsequent section.

The present-day concentrations and masses of CH_4, CH_3, and C_2H_6 are given in Table 4.1. *Scale atmosphere* is a homogeneous isothermal layer where the pressure at the surface decreases to 1/*e* at the scale height *H*. On Titan, the scale atmosphere thickness decreased from the initial 109-128 km at 300-355 K to 21 km at 94 K (e.g., Gilliam and Lerman, 2014a). It should be noted that CH_3 and C_2H_6 are several orders of magnitude less abundant than methane.

Table 4.1.
Present-day quantities of methane, methyl, and ethane in Titan's *scale atmosphere.*

Gas	Abundance		References
	molecules cm^{-3}	kg	
CH_4	1.31×10^{19}	6.16×10^{17}	Lorenz et al. (1999); Griffith et al. (2003); Jacquemart et al. (2008); Gilliam and Lerman (2014a)
CH_3	1.05×10^{12}	4.62×10^{10}	Wilson and Atreya (2004)
C_2H_6	$1.81\times10^{13} – 1.67\times10^{15}$ Mean 8.46×10^{14} Geom. Mean 1.74×10^{14}	$1.60\times10^{12} – 1.48\times10^{14}$	Gladstone et al. (1996); Yung and DeMore (1999); Wilson and Atreya (2004); Vinatier et al. (2007a)

4.2. The Kinetic Rate Constants

4.2.1. Overview of Rate Constants

Experimental and theoretical determinations of k_{ij}'s in reactions (4.1)-(4.3) are summarized in Table 4.2. The range of the reported values is very large and there are no data on the Arrhenius activation energy of the photolysis that could help relate the reaction rate constants to temperature. In this paper, we choose the rate constants of the reactions giving results consistent with the reported concentrations. The reaction rate parameter for $CH_4 \rightarrow CH_3$ ranges from 10^{-9} to 10^{-3} yr^{-1}. For the reaction from CH_3 to C_2H_6, k_{23} varies from 10^{-19} to 10^{-3} cm^3 $molecule^{-1}$ yr^{-1} and for decomposition of C_2H_6, k_3 varies from 1 to 10^{-80} yr^{-1}. Values from within these very wide ranges are used to demonstrate schematically the net results of the reaction mechanisms (4.4)-(4.6), without considering the effects of changing temperature and gas pressure, for which we are not aware of existing data.

Table 4.2.
Rate constant of direct forward reaction of the species CH_4, CH_3, C_2H_6

Reaction No.	Reaction	Rate Constant at 300 K, unless when *T* unknown	Units	Rate constants in yr^{-1}	Reaction order	Temp. range (K)	Reference
	CH_4						
R1	$CH_4 \rightarrow CH_3 + H$	2.8E-11 to 3.8E-11	s^{-1}	8.9E-04 to 1.2E-03	1	300-90	Calculated from Ly-α (Titan primord. & present)
R2	$CH_4 \rightarrow$ all branches	1.E-11	s^{-1}	3.E-04		130-180	From CH_4 chemical residence time at 300 km, 10^{12} s, and at 700 km, 10^{10} s (Wilson & Atreya, 2004, Figs. 5a, 1a)
R3	$CH_4 \rightarrow$ all branches	1.2E-12	s^{-1}	4.E-05		180	From CH_4 chemical lifetime at 300 km (Wilson & Atreya, 2004, Table 7)
R4	$CH_4 \rightarrow$ all branches	3.E-12	s^{-1}	9.E-05	1		Yung & DeMore (1999, Fig. 6.12); range 1E-15 s^{-1} at 300 km to 1E-8 s^{-1} at :750 km
R5	$CH_4 \rightarrow CH_3 + H$	3E-15 to 3E-16	s^{-1}	9.47E-08 to 9.47E-09	1		Based on CH_4 residence time (Atreya et al. 2006)
	CH_3						
R6	$CH_3 + CH_3 \rightarrow C_2H_6$	5.00E-11	cm^3/(molecule s)	1.58E-03	2	325	Fan et al. (1999)
R7	$CH_3 + CH_3 \rightarrow C_2H_6$	5.999E-11	cm^3/(molecule s)	1.89E-03	2	300	Robertson et al. (1995)
R8	$CH_3 + CH_3 \rightarrow C_2H_6$	4.65E-11	cm^3/(molecule s)	1.47E-03	2	296-577	MacPherson et al. (1983), T&H Table 16.16
R9	$CH_3 + CH_3 \rightarrow C_2H_6$	3.98E-11	cm^3/(molecule s)	1.26E-03	2	250-420	Tsang & Hampson (1986), Table 16.16
R10	$CH_3 + CH_3 \rightarrow C_2H_6$	6.82E-11	cm^3/(molecule s)	2.15E-03	2	150	Cody et al., 2003
R11	$CH_3 + CH_3 \rightarrow C_2H_6$	(5.04±1.15)E-11	cm^3/(molecule s)	1.59E-03	2	202-298	Cody et al., 2002
R12	$CH_3 + CH_3 \rightarrow C_2H_6$	1.46E-25	cm^3/(molecule s)	4.60E-18	3	300	Toublanc et al. (1995)
R13	$CH_3 + CH_3 \rightarrow C_2H_6$	3.28E-26	cm^3/(molecule s) k_0	1.03E-18	2	300	Slagle et al. (1988), cited in Wilson and Atreya (2000)
R14	$CH_3 + CH_3 \rightarrow C_2H_6$	5.98E-11	cm^3/(molecule s) k_∞	1.89E-03	2	300	Slagle et al. (1988), cited in Wilson and Atreya (2000)
R15	$CH_3 + CH_3 \rightarrow C_2H_6$	1.80E-25	cm^3/(molecule s)	5.68E-18	2		Yung and DeMore (1999, p. 70)
R16	$CH_3 + CH_3 \rightarrow C_2H_6$	1.62E-26	cm^3/(molecule s)	5.11E-19	2	296-577	MacPherson et al. (1983)
	C_2H_6						
R17	$C_2H_6 \rightarrow$ all branches	4.35E-11	s^{-1}	1.37E-03	1	180	From C_2H_6 chemical lifetime at 300 km (Wilson & Atreya, 2004, Table 7)
R18	$C_2H_6 \rightarrow$ all branches	6.7E-14 to 1.0E-07	s^{-1}	2.11E-06 to 3.15E+00	1		Gladstone et al. (1996, Table III)

R19	$C_2H_6 \rightarrow$ all branches	8.E-11	s^{-1}	2.52E-03	1		Yung & DeMore (1999, Fig. 6.12); range 6E-13 s^{-1} at 250 km to 1E-8 s^{-1} at :850 km
R20	$C_2H_6 \rightarrow C_2H_4 + 2H$	9.10E-09	s^{-1}	2.87E-01	1		
R21	$C_2H_6 \rightarrow C_2H_4 + H_2$	1.10E-08	s^{-1}	3.47E-01	1		Sources cited by Yung & DeMore (1999), Table 6.5
R22	$C_2H_6 \rightarrow C_2H_2 + 2H_2$	9.90E-09	s^{-1}	3.12E-01	1		
R23	$C_2H_6 \rightarrow CH_4 + {}^1CH_2$	6.10E-09	s^{-1}	1.92E-01	1		
R24	$C_2H_6 \rightarrow CH_3 + CH_3$	2.395E-64	cm^3/(molecule s)	7.55E-57	2	300	Baulch et al. (1994)
R25	$C_2H_6 \rightarrow CH_3 + CH_3$	3.97E-88	cm^3/(molecule s)	1.25E-80	2	300	Baulch et al. (1994)
R26	$C_2H_6 \rightarrow CH_3 + CH_3$	1.05E-48	s^{-1}	3.31E-41	1	300	Baulch et al. (1994)

NOTE: Rate constants $<5\times10^{-18}$ s^{-1} or $<1.5\times10^{-10}$ yr^{-1} correspond to reaction half-lives longer than the age of the Solar system, 4.55×10^9yr.

4.2.2. Photolysis by Lyman-α

For methane photolysis, Lyman-alpha radiation at λ_α = 121.57 nm is one of the possible energy sources cited in the literature (Atreya et al., 2006; Wilson and Atreya, 2004; Park et al, 2008; Romanzin et al., 2008). The UV Lyman-α radiation of wavelength 121.57 nm emitted by the Sun within its entire spectrum can be taken as a wavelength band of different widths: for example, it may be taken as $0 < \lambda < 121.6$ nm, $120.6 < \lambda < 121.6$ nm (bandwidth of 10 Å) or $121.5 < \lambda < 121.6$ nm at the band width of 1 Å. The fraction of the Lyman- α radiation is determined by integration of the emission intensity spectrum given by Planck's law:

$$E_{\mathrm{Ly}-\alpha} = \frac{2\pi k_B^4}{h^3 c^2} T^4 \int_{\lambda=121.6}^{u\leq\infty\ (\lambda\geq0)} \frac{u^3}{e^u - 1}\, du \tag{4.7}$$

where u is a dimensionless variable:

$$u = \frac{hc}{\lambda k_B T} \tag{4.8}$$

and other parameters are: Planck's constant h = 6.626E-34 J s, the velocity of light c = 2.9979×10^{8} m s^{-1}, wavelength λ in m, Boltzmann's constant k_B = 1.381×10^{-23} J K^{-1}, and temperature T in K. The integrand in (4.7) is evaluated by the series given in Abramowitz and Stegun (1972, p. 998, 21.1.2).

The results of the above, as shown in Table 4.3, are used to evaluate the emission flux $F(\lambda$ = Ly-α*)* in photons s^{-1} m^{-2} m^{-1} in Titan's atmosphere and compute the photolysis frequency J or the rate constant k_{12} of eqn. (4.1), given by the relationship for the 0.1 nm (1 Å) bandwidth:

$$k_{12} \equiv J = \int_{121.5\ \text{nm}}^{121.6\ \text{nm}} F(\lambda)\,\sigma(\lambda)\,\varphi(\lambda)\,d\lambda \tag{4.9}$$

where $F(\lambda)$ (is the solar energy flux on Titan, 4.87×10^{10} photons m^{-2} s^{-1} nm^{-1} primordial, about 4.55 billion years ago, and 6.94×10^{10} at present, based on the Sun the primordial Sun luminosity of 72-75% of the present (Gough, 1981) and its surface temperature of 5379 and 5780 K, respectively; $\sigma(\lambda)$ is the cross-section (2×10^{-21} m^2, Chen and Wu, 2004); and $\varphi(\lambda)$ is the quantum yield (0.291 $photon^{-1}$, Wang et al., 2000).

For a verification of our calculations of the Lyman-α flux on Titan, as given in Table 4.3, we compare them to the Lyman-α flux outside the Earth's atmosphere, as reported by Lean and Skumanich (1983) and Lean (1991): $(3.6 \pm 1.3)\times10^{15}$ photons s^{-1} m^{-2} and $(5 \pm 1)\times10^{-3}$ W m^{-2}. The bandwidths of the measured UV wavelengths cited in the preceding papers are from 0.15 to 3 nm. Our results for the Earth, using the same data as given in Table 4.3, for a 1 nm wavelength band are within a factor of two of those cited: 1.6×10^{15} photons s^{-1} m^{-2} and 2.7×10^{-3} W m^{-2}.

Table 4.3.
Lyman-α radiation and CH_4 photolysis rate parameter on Titan.

Parameter	Sun primordial (5379 K)		Sun at present (5780 K)		Titan primordial (300 K)		Titan at present (94 K)	
	W m^{-2}	Photons s^{-1} m^{-2}	W m^{-2}	Photons s^{-1} m^{-2}	W m^{-2}	Photons s^{-1} m^{-2}	W m^{-2}	Photons s^{-1} m^{-2}
Emission at Sun surface	4.75E+07	2.37E+26	6.33E+07	2.94E+26				
Fraction Ly-α [121.5 < λ < 121.6 nm] of Sun spectrum	2.83E-08		2.83E-08					
Emission Ly-α [121.5 < λ < 121.6 nm] at Sun surface	1.345	8.20E+17	1.794	1.09E+18				
Solar constant for all λ					11.27		15.03	
Solar constant/4 received over the surface					2.82		3.76	
Solar constant/4 for Ly-α [121.5 < λ < 121.6 nm]					7.99E-08	4.87E+10	1.07E-07	6.49E+10
CH_4 photolysis rate constant k_1 or $J = F(\lambda)\,\sigma(\lambda)\,\varphi(\lambda)$ (s^{-1})						2.83E-11		3.8E-11
k_1 or J as above (yr^{-1})						8.95E-04		1.19E-03

4.2.3. Rate Constants for the Model

Reasonable results from equations (4.4)-(4.6) cannot be obtained by an arbitrary choice of the rate constants. As shown in Tables 4.2 and 4.3, k_{12} by Lyman-α radiation on Titan of an order of $10^{-3} – 10^{--4}$ yr^{-1}, near the upper end of the range from 10^{-9} to 10^{-3} yr^{-1}; we use the value of the order of magnitude of 10^{-9}–10^{-8} yr^{-1}, $k_{12} = 6.7\times10^{-9}$ yr^{-1}. This value corresponds to the residence time 150 million years of CH_4 with respect to its conversion to CH_3. This residence time is considerably shorter than the age of Titan since accretion, about 4.5 billion years. If the CH_4 photolysis reaction operates from the start, it implies that CH_4 should be added from the Titan

interior to the atmosphere. If the present day mass of atmospheric CH_4, 6.163×10^{17} kg (Gilliam and Lerman, 2014a, Table 10) were depleted at the rate of $k_{12} = 6.7\times10^{-9}$ yr^{-1}, then 4.13×10^{9} kg yr^{-1} CH_4 would have to be replenished yearly. Such a rate of CH_4 emission from the satellite interior would not have depleted the internal reservoir of methane of 7.5×10^{20} kg (Gilliam and Lerman, 2014a) over the lifetime of Titan.

It should be noted that reaction (4.4) for the photolytic destruction of CH_4 at the rate of k_{12} yr^{-1} is different from the thermal escape of methane from Titan's atmosphere (Gilliam and Lerman, 2014a, b), as given by:

$$[CH_4] = [CH_4]_0 \exp(-kt) \tag{4.10}$$

where rate parameter k (yr^{-1}) is a function of the Maxwell-Boltzmann distribution of CH_4 molecules in Titan's atmosphere that also depends on temperature, on escape velocity at Titan's surface, and on the thickness of the scale atmosphere that decreases with time. k (yr^{-1}) is defined as:

$$k = \frac{\mathcal{F}(v \geq v_e) \cdot \bar{v}_{>v_e} \cdot S_{\text{atm}}}{2V_{\text{atm}}} \tag{4.11}$$

where $\mathcal{F}(v \geq v_e)$ is a fraction of the Maxwell-Boltzmann frequency distribution of the gas molecules' velocities greater than Titan's escape velocity ($v_e = \sqrt{2gr}$ m/s), $\bar{v}_{>v_e}$ (m/s) is the mean velocity in the interval $v \geq v_e$, and the quotient V_{atm}/S_{atm} (m) of the atmosphere volume to its outer surface area is effectively the atmosphere thickness, decreasing as the atmosphere loses its mass. The Maxwell-Boltzmann factor $\mathcal{F}(v \geq v_e)$ depends on temperature and molecular mass of the gas. Eqs. (4.7) and (4.8) give methane concentration in the present-day Titan atmosphere that agrees with the reported values. The escape rate parameters k decreases from 3×10^{-4} yr^{-1} at Titan's accretion temperature of 300 K to 10^{-23} yr^{-1} near 100 K (Gilliam and Lerman, 2014a, 2016a), with

a geometric mean of the two extremes at about 2×10^{-14}, a rate of escape much slower than the rate of photolytic conversion of CH_4 to CH_3.

The orders of magnitude of the two other rate constants used are $k_{23} = 5\times10^{-14}$ to 1×10^{-12} cm^3 $molecule^{-1}$ yr^{-1} and $k_3 = 1\times10^{-4}$ yr^{-1} to 1×10^{-3} yr^{-1} (cf. Table 4.2), which give results close to the reported concentration values.

The abundances of the gases in Titan's atmosphere (Table 4.1) place certain limits on the values of rate parameter k_3 in reactions (4.6) and (4.15). Concentrations of CH_3 are rising from 0 from the start – assumed to be the time of accretion – so that $d[CH_3]/dt > 0$. The following limits on the values of k_3 follow from (4.6) and gas abundance data in Table 1:

$$k_{23} < k_{12}\frac{[CH_4]}{[CH_3]^2} < (10^{-9} \text{ to } 10^{-5}) \times \frac{1.307\times10^{19}}{[1.046\times10^{12}]^2} = 10^{-14} \text{ to } 10^{-10} \qquad (4.12)$$

The values in (4.12) are within the ranges reported in Table 4.2, and the paper further shows that these values result in the computed concentrations close to the reported ones.

4.3. Results: Time-Dependent Concentrations of CH_4-CH_3-C_2H_6

4.3.1. Solution by Finite Differences

The change in methane mass or concentration with time, from eq. (4.4), when concentration tends to a steady-state value $[CH_4]_{ss}$ as $t \rightarrow \infty$, is:

$$[CH_4] = [CH_4]_{ss} + ([CH_4]_0 - [CH_4]_{ss})e^{-k_{12}t} \qquad (4.13)$$

where $[CH_4]_0$ is the initial concentration of methane in the atmosphere at time $t = 0$, $[CH_4]_{ss}$ is a steady-state concentration and other parameters are as defined under (4.4)-(4.6). The present-day atmospheric concentration of CH_4 1.31×10^{19} molecules cm^{-3} in (4.12) and Fig. 4.1, has been stable since about 5×10^5 years after accretion and it is taken as a steady-state concentration $[CH_4]_{ss}$. The

decreasing mass of CH_4 in the atmosphere and its volume and thickness give the CH_4 curve 1 in Fig. 4.1. The shape of the curve is the result of the difference between the rate of escape of CH_4 and NH_3 (Gilliam and Lerman, 2014a), assumed to be the main components of the early atmosphere, and the rate of decrease in volume of the atmosphere that cools and loses mass.

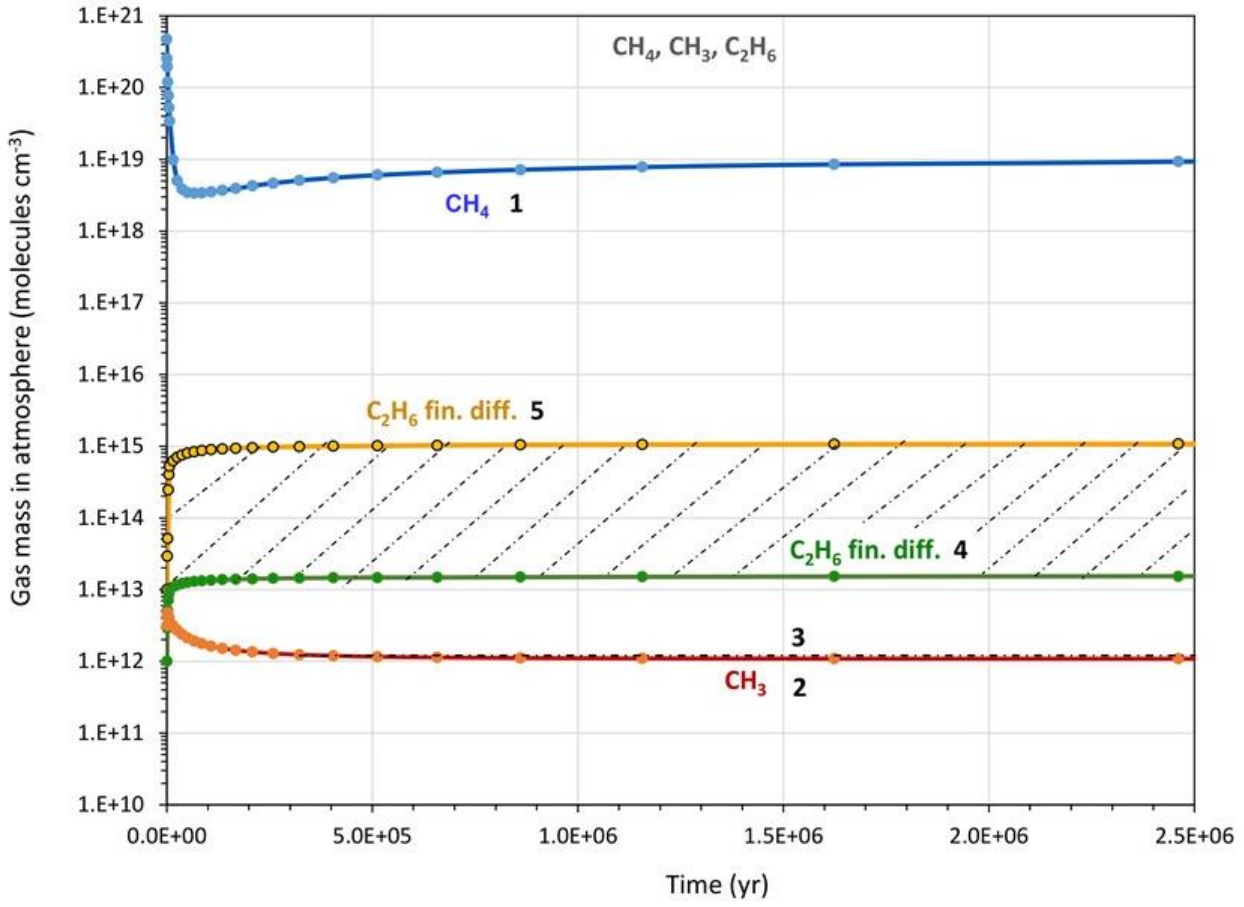

Figure 4.1. Calculated concentrations of CH_4, CH_3, and C_2H_6 in Titan's atmosphere. Additional data and information in Table 4.3. **1:** CH_4 from Gilliam and Lerman (2014a). **2:** CH_3 concentrations from the eqs. (4.11), (4.12), with $k_{12} = 6.7\times10^{-9}$ yr^{-1}, $k_{23} = 5\times10^{-14}$ cm^3 molecule^{-1} yr^{-1}. **3:** CH_3 from tanh eq. (4.20), rate parameters as in **2**. **4:** C_2H_6 from eq. (4.14), $k_{23} = 1\times10^{-13}$ cm^3 molecule^{-1} yr^{-1}, $k_3 = 1\times10^{-3}$ yr^{-1}. **5:** C_2H_6 concentration, eq. (4.14), $k_{23} = 1\times10^{-12}$ cm^3 molecule^{-1} yr^{-1}, $k_3 = 1.0\times10^{-4}$ yr^{-1}. Cross-hatched area is the domain of C_2H_6 reported concentrations.

The computation of CH_3 and C_2H_6 concentrations in Titan's atmosphere is based on the $[CH_4]$ values calculated by finite differences, as shown in Fig. 4.1, curve 1, where the rate parameters are constant, as mentioned earlier.

For $[CH_3]$, eq. (4.5) becomes:

$$\Delta[\mathrm{CH_3}]/\Delta t = k_{12}[\mathrm{CH_4}] - k_{23}[\mathrm{CH_3}]^2 \tag{4.14}$$

where $[CH_4]$ is given by eq. (4.13). The CH_3 concentration is obtained from (4.14) as:

$$[\mathrm{CH_3}]_t = [\mathrm{CH_3}]_{t-1} + \Delta[\mathrm{CH_3}]_t \tag{4.15}$$

For $[C_2H_6]$, from eq. (4.6):

$$\Delta[\mathrm{C_2H_6}]/\Delta t = k_{23}[\mathrm{CH_3}]^2 - k_3[\mathrm{C_2H_6}] \tag{4.16}$$

where $[CH_3]$ is from eq. (4.15). Finally, the concentration of ethane sought is:

$$[\mathrm{C_2H_6}]_t = [\mathrm{C_2H_6}]_{t-1} + \Delta[\mathrm{C_2H_6}]_t \tag{4.17}$$

The calculated values of CH_3, and C_2H_6 are shown in Fig. 4.1.

4.3.2. Explicit Solutions

This section gives two new explicit solutions of equations (4.5) and (4.6) for $[CH_3]$ and $[C_6H_6]$ forming sequentially from $[CH_4]$. The time-dependent explicit solutions serve the goal of deriving their asymptotic values as $t \to \infty$, in approximation to a near-steady or steady state of Titan's atmosphere.

Methyl (CH_3): Eq. (4.6) is a Riccati equation (Riccati, 1761, and references in Bagni, 1996; Watson, 1922, 1995; Bittanti et al., 1991). The first two terms include an explicit relationship for $[CH_4]$ as given in (4.12):

$$\frac{d[\mathrm{CH_3}]}{dt} = k_{12}[\mathrm{CH_4}]_{\mathrm{ss}} + (k_{12}[\mathrm{CH_4}]_0 - k_{12}[\mathrm{CH_4}]_{\mathrm{ss}})e^{-k_{12}t} - k_{23}[\mathrm{CH_3}]^2 \tag{4.18}$$

A solution of (4.18), as given in Appendix 4-F, eq. (A-9) is:

$$[\mathrm{CH_3}] = -\frac{1}{k_{23}} \frac{(pCk_{12}/2)e^{-k_{12}t/2}\, I'_{\nu}\left(Ce^{-\lambda t/2}\right)\,(qC\lambda/2)e^{-\lambda t/2}\, I'_{-\nu}\left(Ce^{-\lambda t/2}\right)}{pI_{\nu}(Ce^{-\lambda t/2}) + \, qI_{-\nu}(Ce^{-\lambda t/2})} \tag{4.19}$$

where $I_{\pm\nu}$ and $I'_{\pm\nu}$ are the modified Bessel function of the first kind and its derivative of order v, respectively (Watson, 1995; Abramowitz and Stegun, 1972; Carslaw and Jaeger, 1959; DLMF, 2015), p and q are arbitrary constants, and constants C and v are defined in Appendix 4-F, eqs. (F.6) and (F.8).

Eq. (4.19) can be simplified in the domain of CH_4 steady-state concentration (curve 1, Fig. 4.1):

$$\frac{d[\mathrm{CH_3}]}{dt} = k_{12}[\mathrm{CH_4}]_{ss} - k_{23}[\mathrm{CH_3}]^2 \tag{4.20}$$

Then the solution of (4.20) by separation of variables is:

$$[\mathrm{CH}]_3 = \sqrt{\frac{k_{12}[\mathrm{CH_4}]_{\mathrm{ss}}}{k_{23}}}\, \tanh(\sqrt{k_{12}[\mathrm{CH_4}]_{ss}k_{23}}\, t) \tag{4.21}$$

with the initial condition of $[CH_3] = 0$ at $t = 0$, and the value of the integration constant = 0 in (4.21). The steady-state value of $[CH_3]$ from (4.21) are shown in Fig. 4.1, curve 3.

Ethane (C_2H_6): The ethane formation eq. (4.6), using $[CH_3]$ from (4.21), is:

$$\frac{d[\mathrm{C_6H_6}]}{dt} = k_{12}[\mathrm{CH_4}]_{\mathrm{ss}} \tanh^2(\sqrt{k_{12}[\mathrm{CH_4}]_{ss}k_{23}}\, t) \; - k_3[\mathrm{C_6H_6}] \tag{4.22}$$

Eq. (4.22) can be integrated directly, as given in Appendix 4-G:

$$[\mathrm{C_2H_6}] = f\,(t) + \mathrm{CONST}\times\exp(-k_3 t) \tag{G.1}$$

where

$$f(t) \; = \; \frac{k_{12}[\mathrm{CH_4}]_{\mathrm{ss}}}{ac(a+2c)} \left[a^2 e^{2ct}\, \boldsymbol{F}\left(1,\, \frac{a}{2c}+1;\, \frac{a}{2c}+2;\, -e^{2ct}\right)\right.$$
$$\left. -\,(a+2c)\left(a\, \boldsymbol{F}\left(1,\, \frac{a}{2c};\, \frac{a}{2c}+1;\, -e^{2ct}\right) + a\,\tanh(ct) - c\right)\right] \tag{G.2}$$

In (G.2), constants *a* and *c* simplify the notation in terms of the reaction rate parameters k_{ij}, (defined in Appendix 4-G), and $\boldsymbol{F}$ or Gauss's function ${}_2\boldsymbol{F}_1$ is the hypergeometric series.

4.4. Steady-State Concentrations

The goal of the paper is to find the reaction rate parameters k_{12}, k_{23}, and k_3 that give atmospheric concentrations of CH_3 and C_2H_6 in agreement with their reported ranges. As mentioned earlier, a steady-state of CH_4 is effectively a result of the slowing down of thermal escape, as Titan's atmosphere cools from the initial computed 300 K to near 100 K, and the CH_4 mass in the atmosphere approaches asymptotically the present-day mass of 6.16×10^{17} kg from the initial mass of 1.19×10^{20} kg. A steady-state concentration of CH_3 from eq. (4.5) is:

$$[\mathrm{CH_3}]_{\mathrm{ss}} = \sqrt{\frac{k_{12}[\mathrm{CH_4}]_{\mathrm{ss}}}{k_{23}}} \tag{4.23}$$

The preceding is identical to the steady-state concentration of CH_3, from eq. (4.21), as $t \rightarrow\infty$ and $\tanh\ \infty \rightarrow 1$:

$$[\mathrm{CH}]_3 = \sqrt{\frac{k_{12}[\mathrm{CH_4}]_{\mathrm{ss}}}{k_{23}}} \tag{4.24}$$

From the solution of the Riccati equation (4.18) and (4.19), a steady state of $[CH_3]$, as $t \rightarrow\infty$, is given in eq. (F.15), and it is also identical to the results in (4.23) and (4.24):

$$[\mathrm{CH_3}]_{ss} = \frac{k_{12}\nu}{2k_{23}} = \sqrt{\frac{k_{12}[CH_4]_{ss}}{k_{23}}} \tag{4.25}$$

Eq. (4.25) applies to the region of steady concentration of the $[CH_4]$ in curve 1, Fig. 4.1.

For C_2H_6, steady-state concentrations are, from (4.6):

$$[C_2H_6]_{ss} = \frac{k_{23}[CH_3]_{ss}^2}{k_3} \tag{4.26}$$

and from (4.21) or (4.6) and (4.24) :

$$[C_2H_6]_{ss} = \frac{k_{12}[CH_4]_{ss}}{k_3} \tag{4.27}$$

and this relationship (4.27) is derived as given in (G.8).

In Table 4.3 are summarized the steady-state concentrations that agree within an order of magnitude with the reported concentrations of CH_4, CH_3, and C_6H_6 (Table 4.1).

Table 4.4.
Computed and reported concentrations of CH_4, CH_3, and C_2H_6 in present-day Titan's atmosphere (Table 4.1). Concentrations in units of molecules cm^{-3}. Units of the rate parameters: k and k_{12} yr^{-1}, k_{12} $[CH_4]_{ss}$ molecules cm^{-3} yr^{-1}, k_{23} cm^3 $molecule^{-1}$ yr^{-1}, k_3 yr^{-1}.

Fig. 4.1 Curve No.	Rate parameter	Value	CH_4 concentration		CH_3 concentration		C_2H_6 concentration	
			Calculated	Reported	Calculated	Reported	Calculated	Reported
1. CH_4	k	Variable [a]						
	k_{12} $\times[CH_4]_{ss}$	8.76×10^{10}	1.31×10^{19}	1.31×10^{19}				
2. CH_3 eq. (4.10)	k_{12}	6.7×10^{-9}			1.09×10^{12}	1.05×10^{12}		
	k_{23}	5.0×10^{-14}						
3. CH_3 eq. (4.19)	k_{12}	6.7×10^{-9}			1.21×10^{12}			
	k_{23}	5.0×10^{-14}						
4. C_2H_6	k_{23}	1.0×10^{-13}					1.5×10^{15}	1.81×10^{13} to 1.67×10^{15}
	k_3	1.0×10^{-3}						
5. C_2H_6	k_{23}	1.0×10^{-12}					1.5×10^{13}	
	k_3	1.0×10^{-4}						

[a] Gilliam and Lerman (2014a, 2016a)

4.5. Discussion and Conclusions

Titan is unique in the Solar System as it is the only moon that has a substantial atmosphere, reaching ten times higher in altitude than Earth's, its scale atmosphere (i.e., well-mixed atmosphere of uniform temperature) is 2.5 times thicker (21.1 km/8.4 km), and it is dominated by N_2 at 1.4 bar and CH_4 0.1 bar (e.g., Roe, 2012). In Titan's atmosphere, the carbon cycle involves the photodissociation of CH_4 that produces methyl radicals (CH_3). The CH_3 molecules recombine to form heavier molecules (e.g., C_2H_6) that condense as liquids or solids in the lower stratosphere and vicinity of Titan's cold troposphere to form a haze layer and eventually precipitate from the atmosphere at a rate of roughly 1.3×10^{8} molecules cm^{-2} s^{-1} (Atreya et al., 2006; Wilson and Atreya, 2009; Graves et al., 2008). Assuming a simple model where the methane molecules escape the atmosphere and produce ethane, up to 8.46×10^{17} kg of liquid ethane could have been produced since Titan's accretion. This amount is approximately 10^{4} times larger than the present-day atmospheric ethane mass, and indicates that most of the remaining ethane resides in liquid form on or within Titan. Titan's crust could hold all of the ethane produced (Mousis and Schmitt, 2008), and previous estimates of the amount of liquid ethane storage potential on Titan's surface are 1.36×10^{16} kg in lakes and seas, an additional 3.34×10^{16} kg in craters, and the remainder in the crust if it has a porosity of at least 0.9% (Gilliam and Lerman, 2016a).

The present-day masses of the three chemical species in Titan's atmosphere are: CH_4 6.16×10^{17} kg or 1.31×10^{19} molecules cm^{-3}; CH_3 4.62×10^{10} kg or 1.05×10^{12} molecules cm^{-3}; C_2H_6 1.60×10^{12}–1.48×10^{14} kg or 1.81×10^{13}—1.67×10^{15} molecules cm^{-3}. Taking these masses as steady-state values, and the methane input rate to the atmosphere 8.76×10^{10} molecules cm^{-3} yr^{-1} cited earlier, the present-day concentrations are obtained by using the following values of the rate

parameters in Eqs. (4.4)-(4.6), that are within the ranges of the published data: $k_{12} = 6.7\times10^{-9}$ to 6.7×10^{-7} yr^{-1}, $k_{23} = 1\times10^{-12}$ to 1×10^{-14} cm^3 molecule^{-1} yr^{-1}, and $k_3 = 1\times10^{-4}$ to 1×10^{-3} yr^{-1}.

This paper presents two new solutions of the equations of CH_3 production from CH_4, a Riccati equation, and of C_2H_6 production from CH_3. The results of these explicit solutions in the asymptotic or steady-state domain of the CH_4-CH_3-C_6H_6 system are in agreement with the reported ranges of concentrations.

The masses of the three atmospheric gases considered in this study, methane, methyl, and ethane, place certain limits on the values of rate parameters k_{23} and k_3 in reactions (4.5), (4.6), (4.9), and (4.11): k_{23} cannot exceed 8×10^{-12} cm^3 molecule^{-1} yr^{-1} and k_3 must be less than 0.05 yr^{-1}. The latter values are within the range of rate constants reported in Table 4.2, and are higher than those needed to satisfy successfully present-day concentrations.

The simplified scheme of methane-methyl-ethane reactions, represented as net one-way processes, produces concentrations of the three gases that approach present-day concentrations at a relatively short time, about 500,000 years, after the start of the processes at Titan's accretion. The suitability of liquid ethane as a potential medium for life on Titan was discussed by Gilliam and Lerman (2016a), and the approach to a steady state of each of the three gases (Fig. 4.1) is compatible with the notion of a chemically stable atmosphere and the carbon cycle on the surface of Titan cooled after its accretion.

APPENDIX 4-F

Derivation of Solution of a Riccati Equation

Beginning with eq. (4.18)

$$\frac{d[\mathrm{CH_3}]}{dt} = k_{12}[\mathrm{CH_4}]_{\mathrm{ss}} + (k_{12}[\mathrm{CH_4}]_0 - k_{12}[\mathrm{CH_4}]_{\mathrm{ss}})e^{-k_{12}t} - k_{23}[\mathrm{CH_3}]^2 \tag{F.1}$$

we then make the following substitution:

$$[\mathrm{CH_3}] = \frac{f'(t)}{k_{23}f(t).} \tag{F.2}$$

Setting

$$A = \left(k_{12}[\mathrm{CH_4}]_0 - k_{12}[\mathrm{CH_4}]_{\mathrm{ss}}\right), \tag{F.3}$$

This brings eq. (F.1) to the form

$$f''(t) = k_{23}\left(k_{12}[\mathrm{CH_4}]_{\mathrm{ss}} + Ae^{-k_{12}t}\right)f(t). \tag{F.4}$$

Now we make the change of independent variable

$$s = Ce^{-k_{12}t/2}, \tag{F.5}$$

For a constant *C* initially left undetermined, and then note that the judicious choice

$$C = \frac{2\sqrt{Ak_{23}}}{k_{12}} \tag{F.6}$$

brings our equation to modified Bessel form

$$s^2f''(s) + s\,f'(s) - \left(s^2 + \frac{4\,k_{23}k_{12}[\mathrm{CH_4}]_{\mathrm{ss}}}{{k_{12}}^2}\right)f(s) = 0. \tag{F.7}$$

A basis of solution is given by modified Bessel functions $I_{\pm\nu}(s)$ with

$$\nu = \frac{2\sqrt{k_{23}\,k_{12}[\mathrm{CH_4}]_{\mathrm{ss}}}}{k_{12}}. \tag{F.8}$$

Substituting back we arrive finally at, as given in eq. (4.19):

$$[\mathrm{CH_3}] = -\frac{1}{k_{23}} \frac{(pCk_{12}/2)e^{-k_{12}t/2}\, I'_{\nu}\left(Ce^{-\lambda t/2}\right)\,(qC\lambda/2)e^{-\lambda t/2}\, I'_{-\nu}\left(Ce^{-\lambda t/2}\right)}{pI_{\nu}(Ce^{-\lambda t/2}) + \, qI_{-\nu}(Ce^{-\lambda t/2})} \tag{F.9}$$

where $I_{\pm\nu}$ and $I'_{\pm\nu}$ are the modified Bessel function of the first kind and its derivative of order ν, respectively, and p and q are arbitrary constants, and constant C from (F.6) is

$$C = \frac{2\sqrt{k_{23}\left(k_{12}[\mathrm{CH_4}]_0 - k_{12}[\mathrm{CH_4}]_{\mathrm{ss}}\right)}}{k_{12}} \tag{F.10}$$

With the initial condition of of $[\mathrm{CH_3}]_0 = 0$ and assumed $q = 1$, the other constant p is:

$$p = \, -q\frac{I'_{-\nu}(C)}{I'_{\nu}(C)} \approx \, -1 \tag{F.11}$$

insofar as for large ν and C the quotient $I'_{-\nu}/I'_{\nu} \approx 1$.

Using the relationship between I_ν and K_ν (Watson, 1995; DLMF, 2015)

$$K_{\nu}(z) = \frac{\pi}{2}\frac{I_{-\nu}(z) - I_{\nu}(z)}{\sin(\nu\pi)} \tag{F.12}$$

and the same relationship for the derivatives, K_ν' and I_ν', eq. (4.19) simplifies to:

$$[\mathrm{CH_3}] = -\frac{Ck_{12}e^{-k_{12}t/2}}{2k_{23}}\,\frac{K'_{\nu}\left(Ce^{-\lambda t/2}\right)}{K_{\nu}(Ce^{-\lambda t/2})} \tag{F.13}$$

Since

$$K_{\nu}(z) \approx \text{constant}\cdot z^{-\nu} \tag{F.14}$$

as $z \to 0$ (Watson, 1995), the logarithmic derivative of $K_\nu(z)$ approaches $-\nu/z$ as $z \to 0$ so that as $t \to \infty$, we recover the asymptotics (which are in any event clear by inspection of stationary solutions of (4.19)):

$$[\mathrm{CH_3}]_{ss} = \frac{k_{12}\nu}{2k_{23}} = \sqrt{\frac{k_{12}[\mathrm{CH_4}]_{\mathrm{ss}}}{k_{23}}}. \tag{F.15}$$

Note that the finer analysis of (4.19) could be used to obtain rates of convergence to this equilibrium if desired.

APPENDIX 4-G

Solution of C_2H_6 Equation (4.20)

Eq. (4.22) can be integrated (Wolfram, 2016) to a form:

$$[C_2H_6] = f(t) + \text{CONST}\times\exp(-k_3 t) \tag{G.1}$$

where

$$f(t) = \frac{k_{12}[CH_4]_{ss}}{ac(a+2c)}\left[a^2 e^{2ct}\, \boldsymbol{F}\left(1,\ \frac{a}{2c}+1;\ \frac{a}{2c}+2;\ -e^{2ct}\right) - (a+2c)\left(a\, \boldsymbol{F}\left(1,\ \frac{a}{2c};\ \frac{a}{2c}+1;\ -e^{2ct}\right) + a\tanh(ct) - c\right)\right] \tag{G.2}$$

Constants a and c were introduced to simplify the notation in terms of the reaction rate parameters k_i, as defined below, and $\boldsymbol{F}$ or Gauss's function ${}_2\boldsymbol{F}_1$ is the hypergeometric series (DLMF, 2015):

$$a = k_3 \ \text{yr}^{-1}; \quad c = (k_{12}\cdot[CH_4]_{ss}\cdot k_{23})^{0.5} \ \text{yr}^{-1}. \tag{G.3}$$

The constant of integration in (G.1) is:

$$\text{CONST} = -\frac{k_{12}[CH_4]_{ss}}{ac(a+2c)}\left[a^2\boldsymbol{F}\left(1,\frac{a}{2c}+1;\ \frac{a}{2c}+2;-1\right) - (a+2c)\left(a\,\boldsymbol{F}\left(1,\frac{a}{2c};\ \frac{a}{2c}+1;\ -1\right) - c\right)\right] \tag{G.4}$$

Wolfram (2010) gives an evaluation program for function $\boldsymbol{F}$:

Start with equation (4.20), the solution of which is given in (4.22). We can drop from the asymptotics the second term involving a hypergeometric function as it is rapidly decaying (since it has no exponential factor multiplying it). Meanwhile we set:

$$z = -e^{-ct} \tag{G.5}$$

so that z tends toward 0 as $t \to \infty$ and noting that the tanh factor approaches then 1.

Per Mathematica, we get as $z \to 0$ and using the functional equation for Γ:

$$z^{-1}\boldsymbol{F}\left(1, 1+\frac{a}{2c}, 2+\frac{a}{2c}, -z^{-1}\right) \sim \frac{\Gamma\left(\frac{a}{2c}\right)\Gamma\left(2+\frac{a}{2c}\right)}{\Gamma\left(1+\frac{a}{2c}\right)^2} = \frac{a+2c}{a} \tag{G.6}$$

So overall the solution is now seen to be asymptotic to:

$$[C_2H_6]_{ss} \approx \frac{k_{12}[CH_4]_{ss}}{ac(a+2c)}\left(a^2\frac{a+2c}{a} - (a+2c)(a-c)\right) \tag{G.7}$$

This simplifies to:

$$[C_2H_6]_{ss} = \frac{k_{12}[CH_4]_{ss}}{k_3} \tag{G.8}$$

that is identical to (4.26) and (4.27).

CHAPTER 5

Formation and Retention of Methane on Titan and the Terrestrial Planets

5.1. Introduction

The interest in methane (CH_4) as a climate-modifying greenhouse gas in the atmosphere and as a possible building-block of life has received much attention since the discovery of methane as a major component of the atmosphere of Titan, the largest satellite of Saturn, at a distance of about 9.5 AU (Astronomical Units) from Earth. Much research has been done on the behavior of CH_4 in Titan's atmosphere, including its photolytic decomposition to other hydrocarbons and escape from the atmosphere (e.g., Strobel, 1974; Yung et al., 1999; Tobie et al., 1996; Atreya et al., 2006; Lunine and Atreya, 2008; Yelle et al., 2008; and Gladstone et al., 1996), but its possible origin is poorly understood on the planets and satellites other than Earth.

This chapter discusses the possibility of methane formation in a number of gas-gas and solid-gas reactions, based on chemical thermodynamic equilibria under the conditions approximating those of the atmospheres and interiors of Titan and the Terrestrial planets – Mercury, Venus, Earth, and Mars. We stress from the outset that the paths to chemical equilibrium are neither necessarily, nor always the paths of methane formation in the past and present, but they provide insight into the retention of methane in the atmosphere of different planets vs. the possibility of its escape. It is well known that the thermodynamic indication that a reaction *should* proceed in a certain direction, *does not* tell that it *would* proceed in that direction. The most common examples of this are a mixture of hydrogen and oxygen gases at room temperature that do not react to make water or the stability of graphite and diamond at Earth's atmospheric conditions that do not oxidize to CO_2. Thus in the discussion of the chemical equilibrium of methane-forming reactions in this paper, it is not implied that the reactions *in fact occur*, but they *may occur* on thermodynamic grounds.

Presently, there are two main models for the origin of methane on Titan: (1) Titan accreted CO_2 which was subsequently converted to CH_4 (e.g. by the Sabatier-Senderens reaction) or (2) Titan accreted icy planetesimals that contained some CH_4, presumably in the form of clathrate hydrate.

(1) Early Saturn generated a subnebula where temperatures and pressures were high enough to allow the conversion of CO to CH_4, which was subsequently trapped in the form of hydrate and clathrate hydrates in planetesimals which formed Titan. Prinn and Fegley (1981) argue that accreted CO_2 on Titan can be converted to CH_4 by the Sabatier reaction in the rocky-core if the geochemical conditions are conducive. A key requirement for this is a sufficiently reducing (i.e., H_2-containing) environment, which can be created by the hydrothermal oxidation, or serpentinization, of reduced iron- or sulfur-bearing minerals. Atreya et al. (2006) suggest that appropriate geological, thermal, and pressure conditions could have existed in and below Titan's ocean for lower-temperature serpentinization to occur during Titan's accretionary heating phase. Alternatively, impacts could trigger the process by raising the temperature.

(2) The model of CH_4 production by planetesimals was first proposed by Mousis et al. (2002), who argued that Titan was formed from planetesimals containing clathrate hydrates of CH_4.

5.2. Methane Forming Reactions

The five reactions, discussed below, may be responsible for the formation of methane on the Terrestrial Planets and Titan. Equilibria in the system C-H-O, where oxygen fugacities are buffered by the coexisting phases in the system Fe-FeO-Fe_3O_4-Fe_2O_3, have been extensively

studied by many authors with reference to the magmatic interior of primordial Earth (e.g., French, 1966; Holland, 1984). In this chapter, the possible production of methane is limited to the planetary atmospheres in contact with mineral solids.

Three reactions of CH_4 production:

R1 $C_{(s)} + 2H_{2(g)} \rightarrow CH_{4(g)}$

R2 $2C_{(s)} + 2H_2O_{(g\ or\ l)} = CH_{4(g)} + CO_{2(g)}$

R3 $CO_{2(g)} + 4H_{2(g)} = CH_{4(g)} + 2H_2O_{(g)}$

Two reactions of serpentinization of iron-olivine fayalite that produce CH_4 from H_2O and C in graphite or CO_2:

R4 $3Fe_2SiO_4 + 2H_2O_{(g)} + C = 2Fe_3O_4 + 3SiO_2 + CH_{4(g)}$

R5 $6Fe_2SiO_4 + 2H_2O_{(g)} + CO_{2(g)} = 4Fe_3O_4 + 6SiO_2 + CH_{4(g)}$

The graphite-hydrogen reaction R1 was reported to occur at temperatures above 1100 K (Mills and Steffgen, 1974; Vigdergauz, 2011) and R2 is known as hydrolytic disproportionation of carbon that occurs in deep coal mines in the presence of water inflow (Vigdergauz, 2014). On Earth, methane forms by diverse bacterial processes of decomposition of organic matter, known as methanogenesis (Ferry, 2012), and by thermal alteration of organic matter at higher temperatures in the subsurface and hydrothermal systems (Welhan, 1988; Stolper et al., 2014). The most commonly cited non-biogenic reaction is the production of methane by reduction of CO_2, known as the Sabatier reaction or, more correctly, Sabatier-Senderens reaction (Sabatier and

Senderens, 1902; Sabatier, 1911), shown as R3. At laboratory conditions the reaction proceeds in the temperature range from 470 to 770K (Lunde and Kester, 1973) and it has also been reported at room temperature, using photo-excitation of a mineral catalyst (Thampi et al., 1987). The abundance of H and CO_2 in the Solar System makes the Sabatier-Senderens reaction one of the likely sources of methane. In deep-ocean sediments, reduction of methane rising with the hydrothermal fluids by the sulfate-ion has been described by Mottl et al. (2003).

Serpentinization of olivine $(Mg,Fe)_2SiO_4$ can be represented as a reaction of graphite C or CO_2, water, and silica, producing either talc or antigorite (chrysotile), magnetite, and methane:

$$\underset{\text{forsterite}}{3Mg_2SiO_4} + \underset{\text{fayalite}}{3Fe_2SiO_4} + 4H_2O_{(g)} + 2SiO_2 + C = \underset{\text{talc}}{2Mg_3Si_4O_{10}(OH)_2} + \underset{\text{magnetite}}{2Fe_3O_4} + CH_{4(g)} \quad (5.1)$$

or

$$\underset{\text{forsterite}}{18Mg_2SiO_4} + \underset{\text{fayalite}}{6Fe_2SiO_4} + 26H_2O + CO_2 = \underset{\text{antigorite}}{12Mg_3Si_2O_5(OH)_4} + \underset{\text{magnetite}}{4Fe_3O_4} + CH_4 \quad (5.2)$$

Neither Mg nor Si change their oxidation state in serpentinization, so that reduction of C or CO_2 to CH_4 comes at the expense of oxidation of Fe^{II} in olivine to $Fe^{II}{\cdot}Fe^{III}$ in magnetite. Therefore the formation of methane in serpentinization can be represented by reactions R4 and R5, with either elemental carbon C in graphite or CO_2 gas as the source of carbon in methane.

On Earth, abiological production of methane under high-temperature and hydrothermal conditions is a natural source of CH_4 (French, 1966; Horita and Berndt, 1999; Stolper et al., 2014). The biological production of methane or methanogenesis is a reaction of decomposition of organic matter CH_2O or acetate CH_3COOH into CH_4 and CO_2. In Titan's atmosphere methane may be

produced by a microbial reaction utilizing acetylene (C_2H_2) and hydrogen, as proposed by McKay and Smith (2005). The biological destruction of methane by methanotrophic bacteria is a reverse process. Additionally, CH_4 is oxidized in anaerobic environments by sulfur- and nitrogen-reducing bacteria, and by reaction with the OH*-radical in the atmosphere (Mayer et al., 1982; IPCC, 2001).

5.3. Equilibrium Reactions Producing CH_4

For reactions R1-R5, the equilibrium constants as a function of temperature can be calculated from:

$$\log K = -\frac{\Delta G_r^\circ}{2.3\,RT} \tag{5.3}$$

where K is the equilibrium constant, the gas constant $R = 8.314\times10^{-3}$ kJ mol^{-1} K^{-1} (or 1.987×10^{-3} kcal mol^{-1} K^{-1}), T is temperature (K), and ΔG_r° is the Gibbs standard free energy change of the reaction (in units of kcal mol^{-1} or kJ mol^{-1}), computed from the data in Robie and Waldbaum (1970), Robie et al. (1979), and Robie and Hemingway (1995). A correction for log K at higher pressures ($1 < P < 350$ bar) is insignificant and the activities of pure solids at higher pressures in this range are only slightly greater than 1, making the contribution of log $a_{solid} \approx 0.1$. The value of log K as a function of T for reactions R1-R5 are plotted as curves in Fig. 5.1a.

The equilibrium partial pressures of CH_4 in reactions R1-R5 are obtained from the equilibrium constant, the activities of the pure solid components (a_C), and reported partial pressures of other reactant gases (p, in bar), taken as ideal gases. For example, for reaction R1,

$$K_T = \frac{p\mathrm{CH_4}}{p\mathrm{H_2^2}\,a_\mathrm{C}} \tag{5.4}$$

where for pure graphite $a_C = 1$. Thus the partial pressure of CH_4, from the calculated value of K_T and pH_2 in (5.4), is:

$$\log pCH_4 = \log K_T + 2 \log pH_2 \quad (5.5)$$

The atmospheric composition of Titan and Terrestrial planets, is shown in Table 5.1. The values of pCH_4, also shown in Fig. 5.1b, were calculated as given in the next section.

Table 5.1.
Titan and Terrestrial planets. Atmospheric composition from references in the footnotes. Calculated log *K* of reactions. R1-R5, as shown, and log pCH_4 from atmospheric composition.

Satellite or Planet	Model *T* (K)	Atmosphere *P* (bars)	Atmospheric Composition [a]	Reaction R1-R5 (see text)	log *K* [b]	log *p* CH_4 (bar)
Titan present [c]	94	1.5	93.3% N_2 or 1.4 bar 6.5% CH_4 or 0.1 bar 0.1% H_2			-1
primordial	300 (to 400)	25.4	80% CH_4 or 19.4 bar 20% NH_3 or 6 bar H_2O_{liq} a = 1	R1 R4	8.89 -2.12	1.29 $p\,H_2 \geqslant 10^{-4}$ bar 2.82
Mars	215	0.0061	95.32% CO_2 2.7% N_2 1.6% Ar 0.13% O_2 0.08% CO 0.0210% H_2O 10 ppb = 1E-06% Trace HDO, NO, Ne, Kr, Xe	R2	-10.21	-11.67
Earth present [d]	298 (real 288))	1	78% N_2 21% O_2 0.00006% O_3	 R1 R2	 8.89 -2.12	-5.74 -3.71 -1.74
Pre-man CH_4		$0.6*10^{-6}$	1.8 ppm = 0.0002% CH_4 0.9% Ar 0.038% CO_2 ~2.5% H_2O 5E-05% H_2, He, Kr			
primordial	700	342	90.6% H_2O [e] 7.4% CO_2 [e] 2% Other N_2, HCl, H_2S [e]	R1 R2 R3 R4	1.47 -1.23 2.71 -2.71	-1.34 1.94 -11.73 2.10
		0.0015	H_2 [f]	R5	-4.19	2.23
Venus	700 (735 real)	92	96.5% CO_2 3.5% N_2 0.0020% H_2O Trace SO_2, Ar, CO, He,Ne	 R2 R5	 2.59 -4.40	 -4.83 -11.82
Mercury	400 (420 to 440 real)	1E-14	42% O_2 22% H_2 6% He 29% Na, 0.5% K Trace CO_2, Ar, H_2O, N_2, Xe, Kr, Ne	R1	-5.49	-23.83

a) Jack J. Lissauer, Imke de Pater (2013)

b) Activity of pure solids taken as a = 1, except as noted for primordial Earth.

c) Lorenz et al. (1999); Griffith et al. (2003); Jacquemart et al. (2008); Gilliam and Lerman (2014a); Gladstone et al. (1966); Yung and DeMore (1999); Wilson and Atreya (2004); Vinatier et al. (2007a)

d) http://www.ux1.eiu.edu/~cfjps/1400/TBL01_0T2.JPG

e) Mackenzie and Lerman (2006)

f) Miller and Urey (1959)

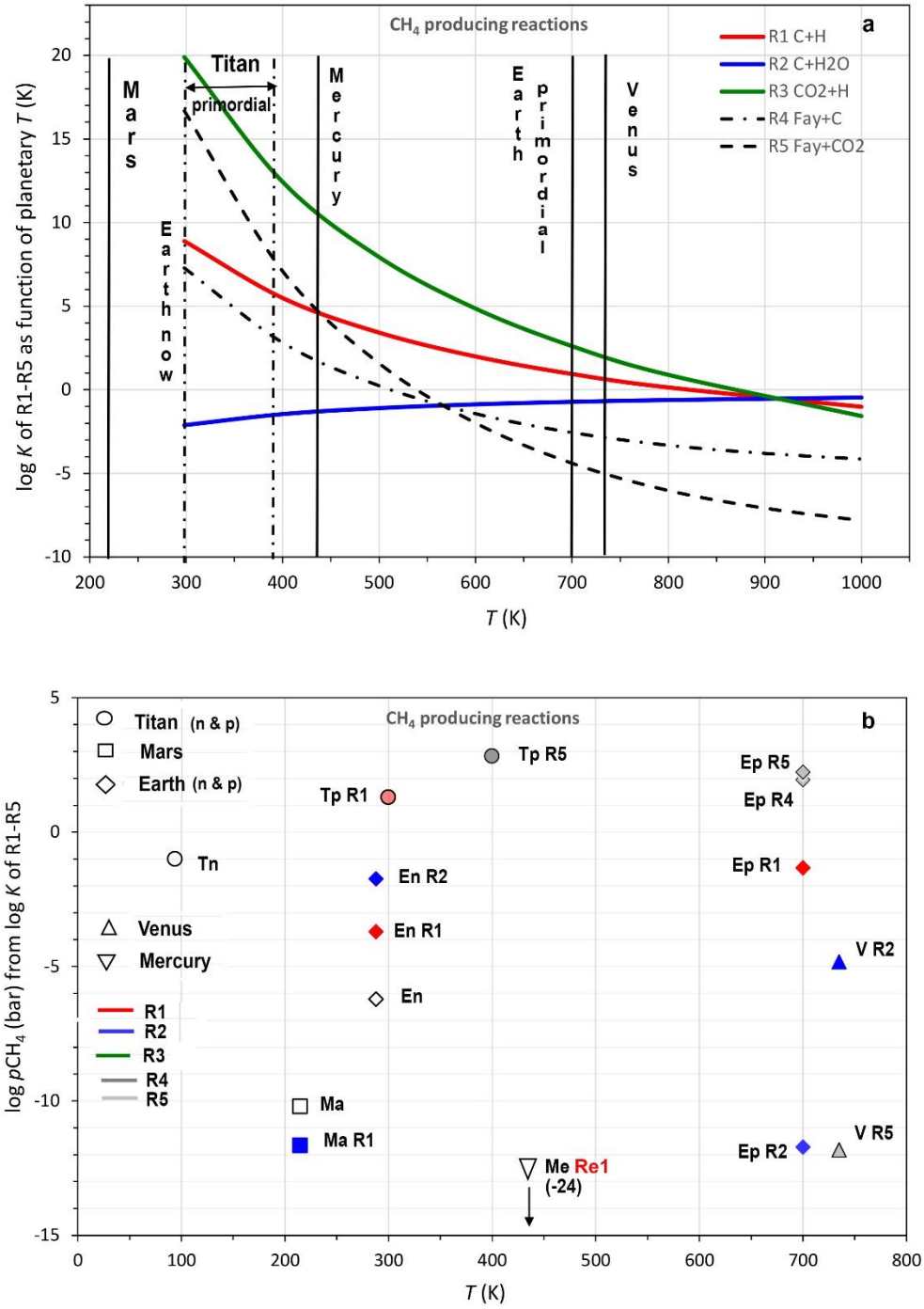

Figure 5.1. (a) Equilibrium constants log *K* for reactions R1-R5 as a function of temperature. Reactions given in the text. Vertical lines show planetary temperatures. **(b)** Equilibrium values of pCH_4 from log *K* of reactions R1-R5 and composition of planetary atmospheres as given in Table 5.1. Legend: T Titan, n = now, p = primordial (circle); Ma Mars (square); E Earth now and primordial (rhomb); V Venus (triangle); Me Mercury (inverted triangle). Filled symbols: color as in the curves of R1-R5. Open symbols: reported partial pressures of CH_4 on Titan, Earth, and Mars.

5.4. Discussion of Methane-Producing Reactions

For the aforementioned five gas-gas and solid-gas reactions, R1-R5, we estimate the amount of methane that might have been produced on Titan and the Terrestrial planets (Fig. 5.1, Table 5.1). We stress that these reactions are not necessarily and not exclusively the paths of methane formation in the past and present, but they provide insight into the source of methane and the possibility of its retention or escape in the atmosphere of different planets.

(T Titan) The assumed composition of the primordial atmosphere of Titan, shortly after its accretion about 4.5 billion yr B.P., was about 80% CH_4 or 19.4 bar, and 20% NH_3 or 6 bar, at the accretion temperature of 300 to 355 K (Gilliam and Lerman, 2014a). At present, it is 0.1 bar CH_4 and 1.4 bar N_2. The abundance of solid carbon as graphite in meteorites (Yelle et al., 2008) and of H_2 in the Universe suggests that reaction R1 might have been a likely mechanism of formation of primordial CH_4. On Titan, reaction R1 between graphite and hydrogen gas can give partial pressure of CH_4 close to the model-computed value of 19.5 bar, if $pH_2 \geq 10^{-4}$ bar.

Serpentinization reaction R4 that might have occurred on Titan (Atreya et al., 2006) gives a higher partial pressure of CH_4, about 700 bar. This would account for an internal reservoir of CH_4 in Titan's interior that is needed to replenish the photolytic conversion of CH_4 to other hydrocarbons. Estimates of the CH_4 emission rate from the interior to the atmosphere vary, and they give the residence times of CH_4 in Titan's interior from 10^5 years to longer than the age of the Solar system.

(Ma Mars) Mean surface temperature of Mars is 210 to 215 K, below the freezing point of water. However, the temperature range (diurnal and seasonal) is from 133 to 303 K (-140 to +30°C), and this lends to the possibility that reaction R2, CO_2 and atmospheric H_2O (Webster et

al., 2013) makes a likely source of CH_4. Through this reaction, log pCH_4 = -11.67, compared to observed 10 ppbv or log pCH_4 = -10.21 (Krasnopolsky et al., 2004).

The occurrence of molecular oxygen in Martian atmosphere poses a question of possible methane oxidation in a reaction:

$$CH_4 + 2O_2 = CO_2 + 2H_2O \quad (5.6)$$

The equilibrium constant of this reaction (at 298.15 K) is log K = 140, much higher than the Partial Pressure Product (*PPP*, from Table 5.1):

$$\log PPP = \log \frac{p\mathrm{H_2O}^2 \cdot p\mathrm{CO_2}}{p\mathrm{CH_4} \cdot p\mathrm{O_2^2}} \approx 6.4 \quad (5.7)$$

The quotient $PPP/K < 1$ indicates undersaturation and that the reaction would be driven to the right, toward oxidation of CH_4.

(E Earth) Earth's rich atmospheric chemistry unlocks the use of multiple CH_4 producing reactions. On present-day Earth, the production of CH_4 is primarily biogenic near the surface and inorganic at depth, as referred to in Section 2. In pre-industrial time, log pCH_4 = -6.22 (0.6×10^{-6} bar, Table 5.1) and at present it is three times higher, -5.74 or 1.8×10^{-6} bar.

The effect of the primordial atmospheric pressure of 342 bar on the equilibrium constants is small: the difference being log $K_{P>1}$ – log $K_{P=1} \leq \pm 0.5$ or smaller than |0.5|. The pressure correction is:

$$\log K_{T,P>1} = \log K_{T,P=1} - \frac{\Delta V_{r\,\mathrm{T},1}(P-1)}{2.3RT} \quad (5.8)$$

where P is total pressure (bar), T is temperature (K), R = 83.14 cm^3 bar mol^{-1} K^{-1} is the gas constant, and ΔV_r is the volume change of the reaction (cm^3 mol^{-1}), where $\Delta V_r = \Sigma V_{\mathrm{products}} - \Sigma V_{\mathrm{reactants}}$. Molar volumes of gases were taken from NIST (2016), and the molar volumes of solids at ambient

conditions (Robie et al., 1966; Robie and Hemingway, 1995) were corrected for volume expansion (Skinner, 1966) and compressibility (Birch, 1966).

If reactions R1 and R2 were active on Earth in the Recent, they would have produced reasonable values of log pCH_4 = -3.71 and -1.74, respectively, compared to observed log pCH_4 of -6.22 to -5.74. It should be borne in mind that CH_4 in the present-day Earth's atmosphere is primarily destroyed by reactions with the hydroxyl radical OH* (Mayer et al., 1982). In primordial Earth's atmosphere (Table 5.1), higher values of pCH_4 are produced in reactions R2, R4, and R5, where the high partial pressure of water vapor is one of the source species of CH_4.

It should be noted in Table 5.1 that there are large differences in the values of log pCH_4 of reactions R1-R2 on present-day Earth, where CH_4 production is at least in part biogenic, and of R1-R5 on primordial Earth. Such differences are due to the highly variable estimates of the amounts of H_2, CO_2, and H_2O in the atmosphere. It is clearly reaction R2 (Vigdergauz, 2014) that produces larger amounts of methane. If the much-cited Sabatier-Senderens reaction R3 occurred on primordial Earth, its product would have been comparable to pCH_4 produced by graphite-hydrogen reaction R1.

(V Venus) The Venusian atmosphere is hot and dense, 735 K and 92 bar. Based on the data in Table 5.1, the atmosphere of Venus is presently devoid of CH_4. However, as a geologically likely situation, we apply reaction R2 between CO_2 and H_2O to the present-day composition of Venus (96.5% CO_2; 3.5% N_2; 0.002% H_2O). Atmospheric pressure of 92 bar on Venus has practically no effect on the equilibrium constants of the reactions. The result is a low partial pressure of methane, log pCH_4 = -4.83 or 1.5×10^{-5} bar, owing to the low partial pressure of H_2O. In reaction R2, CH_4 competes with CO_2 that is present at a high partial pressure in the Venusian

atmosphere. However, in reaction R5, where fayalite (Fe_2SiO_4), H_2O, and CO_2 drive the reaction toward CH_4, the equilibrium value of log pCH_4 is much lower, -11.8, because of the low abundance of H_2O vapor in Venusian atmosphere (Table 5.1).

(Me Mercury) Measurements of the Mercurian atmosphere at about 440 K also show that it is completely bereft of CH_4, but contains H_2. In an approximation to the geologically likely occurrence of graphite in Mercury's crust, we apply reaction R1 to the known present-day composition (Table 5.1), and calculate a possible log pCH_4 of -23.8 bar, indicating that practically no CH_4 should form in its atmosphere, characterized by a very low pressure.

5.5. Potential Retention or Escape of CH_4 from Planets

If CH_4 were formed from the reactions and at partial pressures as given in the preceding section, would it have escaped or been retained in the atmospheres of the individual planets? The escape of a gas from an atmosphere depends on the fraction of the population of the gas molecules whose velocities are greater than the escape velocity of the planet (Goody, 1976; Gilliam and Lerman, 2014a). The Maxwell-Boltzmann distribution of the velocities of gas molecules is a function of the molecular mass of the gas and temperature (Fig. 5.2). The escape velocity of a planet, v_e, is a function of the gravitational acceleration on the planet (g_0) and its radius (r_0). At the planet surface, $v_e = \sqrt{2g_0r_0}$; if the reference level is at some altitude in the atmosphere $h < r_0$, then $v_e = \sqrt{2g_0r_0/(1 + h/r_0)}$ is smaller than at the surface.

Gas escape rate parameter k (yr^{-1}) is defined as (Gilliam and Lerman, 2014a):

$$k = \frac{\mathcal{F}(v \geq v_e) \cdot \bar{v}_{>v_e} \cdot S_{\text{atm}}}{2V_{\text{atm}}} \qquad (yr^{-1}) \qquad (5.9)$$

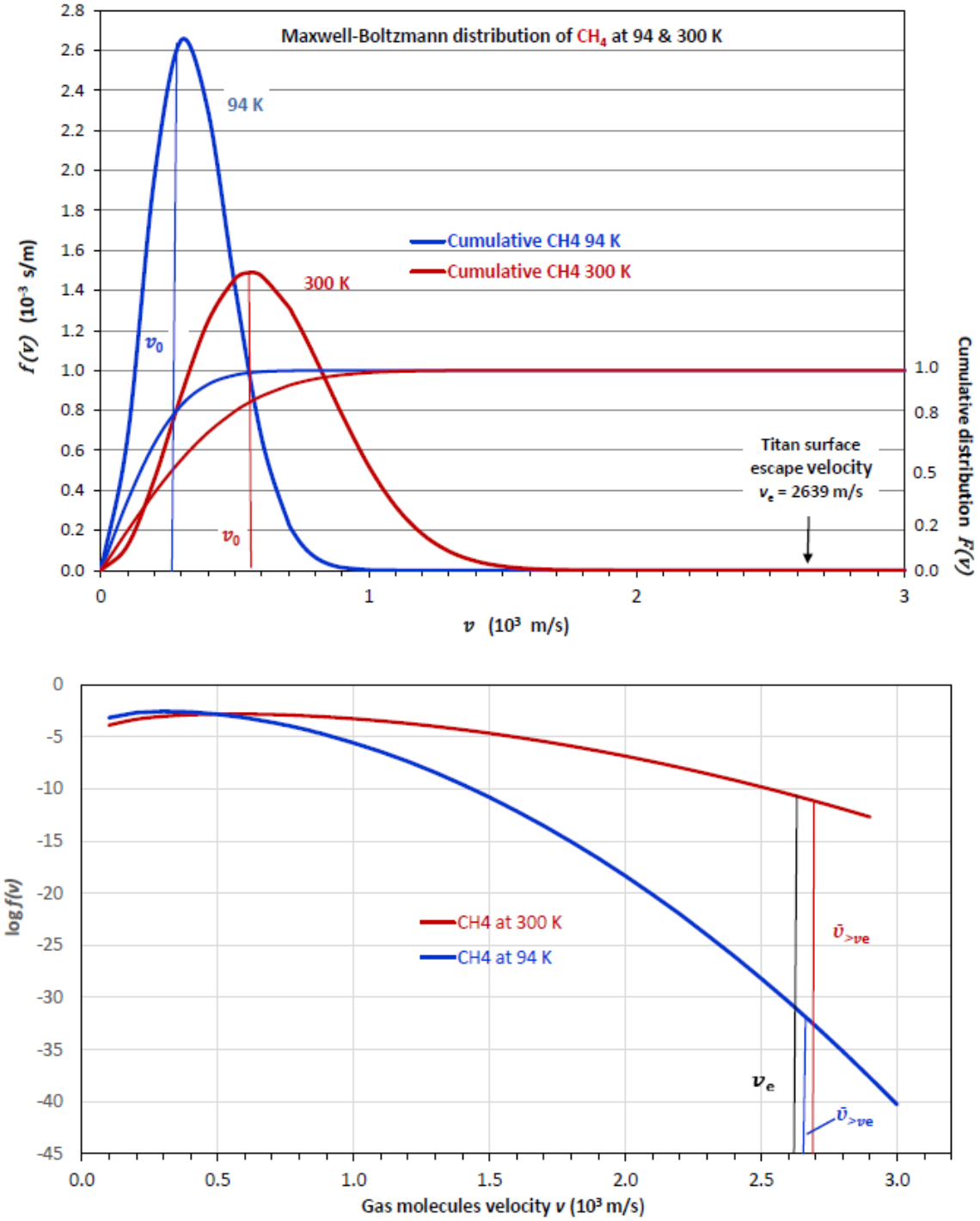

Figure 5.2. (a) Maxwell-Boltzmann distribution of CH_4 molecular velocities at 94 K and 300 K on Titan**. (b)** Same distribution shown on a logarithmic scale. Escape velocity $v_e = 2639$ m/s shown in both figures. Mean velocity of the fraction of the gas molecules above the escape velocity $\bar{v}_{>v_e}$ is also shown at both temperatures.

where $\mathcal{F}(v \geq v_e)$ is a fraction of the Maxwell-Boltzmann frequency distribution (Fig. 5.2) of the gas molecules' velocities greater than Titan's escape velocity ($v_e = \sqrt{2gr}$ m/s), $\bar{v}_{>v_e}$ (m/s) is the mean velocity in the interval $v \geq v_e$, and the quotient V_{atm}/S_{atm} (m) of the atmosphere volume to its outer surface area is effectively the scale thickness of the atmosphere.

Eq. (5.9) shows that *k*, like the Maxwell-Boltzmann distribution, depends on temperature and escape velocity of the planet. The calculated values of *k* for CH_4 are shown as functions of *T* and $\bar{v}_{>v_e}$ in Fig. 5.3. If CH_4 were produced on Mercury, the planet's high temperature of about 400 K would have made the escape of CH_4 as possible as on Titan. On Mars, Venus and on primordial Earth, retention of CH_4 would have been more likely because of the much smaller values of *k* and larger escape velocities on the latter three planets.

It should be reiterated that on present-day Earth (Figs. 5.3a, b), the short residence time of CH_4 in the atmosphere, about 8.5 yr, is shown as "escape rate", which is literally correct, but in a sense different from thermal escape.

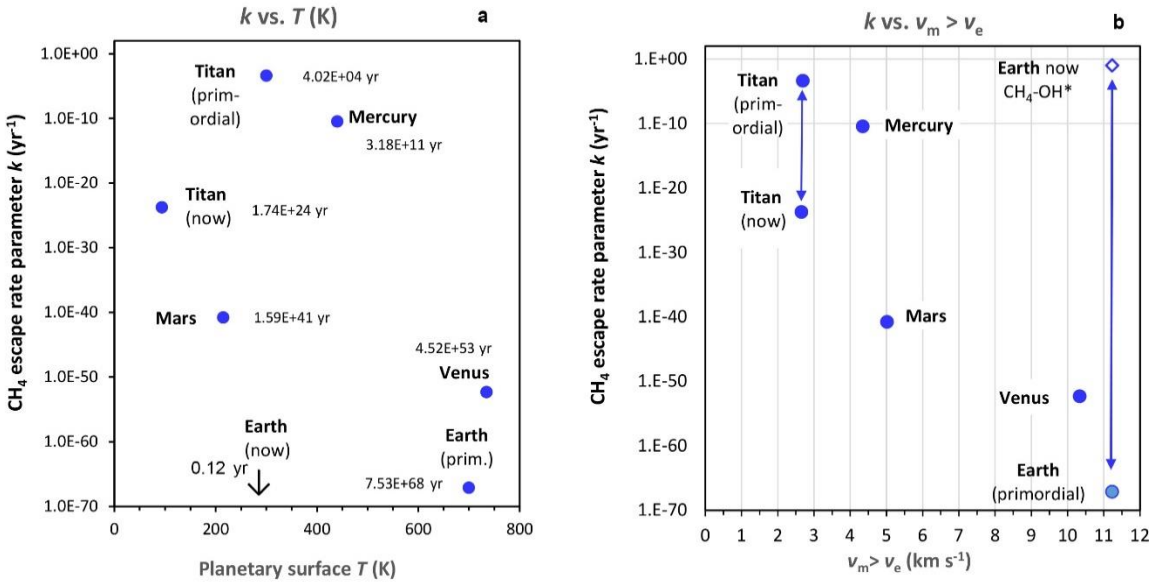

Figure 5.3. (a) CH_4 escape rate parameter *k* (yr^{-1}) *vs.* planetary temperature. Numbers in yr next to the planets' names are CH_4 residence times (1/*k*). **(b)** Plot of *k* vs. $\bar{v}_{>v_e}$, eq. (5.9).

5.6. Summary and Conclusions

Methane is known to occur on Titan, Mars and Earth. It might have also been formed on Venus and Mercury. Reactions in systems containing C graphite, H_2, H_2O, and CO_2, either as stand-alone reactions or as reactions accompanying oxidation of iron-olivine to magnetite (R1-R5), give partial pressures of CH_4 in planetary atmospheres at their reported composition, at temperatures from *29*8 to 700 K, and total pressures from <1 to 342 bar. For reasons of the composition of the atmosphere and its total pressure, pCH_4 values on Mercury and Mars would have been low. On Titan after accretion, serpentinization of the silicate core might have produced pCH_4 as high as 700 bar. On Venus and on Earth, the amount of CH_4 that might have been produced in the atmosphere depends on the reaction stoichiometry. On primordial Earth, the CH_4 partial pressure that might have been produced by reactions R1-R2 ranges from 0.05 to 86 bar, and by the two serpentinization reactions R4-R5 it is from 125 to 170 bar. Thermal escape of CH_4 from the atmosphere of a planet is controlled by the Maxwell-Boltzmann distribution of molecular velocities, temperature, and escape velocity of the planet. On the smaller bodies, such as Titan and Mercury, escape of CH_4 takes place or it might have occurred, respectively, if CH_4 formed on Mercury. On the bigger planets Mars, Earth, and Venus, the greater escape velocity would have counteracted the thermal escape of methane, despite the high temperature of about 700 K of the Venusian and primordial Terrestrial atmospheres. In the oxygen-free atmosphere of Titan, the CH_4 sinks are photolytic conversion to other hydrocarbons and thermal escape.

The similarity of the conditions on primordial Earth and on Venus, except for the low abundance of water on Venus, is demonstrated by the escape rates of CH_4 on both planets (Figs. 5.3a, b). At present, one can only speculate about the reasons of the non-detection of methane in

the Venusian atmosphere, such as perhaps the occurrence of oxidizing radicals formed from H_2O. On Earth, methane of biogenic and abiogenic origin is destroyed in the atmosphere by reactions with the OH* radical. The presence of molecular oxygen and water in the atmosphere of Mars, Venus, and Mercury would have likely resulted in stoichiometric oxidation of methane.

APPENDIX 5-H

Five CH_4-forming reactions:

R1 $C_{(s)} + 2H_{2(g)} \rightarrow CH_{4(g)}$

R2 $2C_{(s)} + 2H_2O_{(g\ or\ l)} = CH_{4(g)} + CO_{2(g)}$

R3 $CO_{2(g)} + 4H_{2(g)} = CH_{4(g)} + 2H_2O_{(g)}$

R4 $3Fe_2SiO_{4(s)} + 2H_2O(g) + C_{(s)} = 2Fe_3O_{4(s)} + 3SiO_{2(s)} + CH_{4(g)}$

R5 $6Fe_2SiO_{4(s)} + 2H_2O(g) + CO_{2(g)} = 4Fe_3O_{4(s)} + 6SiO_{2(s)} + CH_{4(g)}$

Table H.1.
Gibbs free energy of formation of species (Robie and Hemingway, 1995)

T(K)	Forsterite Mg_2SiO_4	Fayalite Fe_2SiO_4	Water steam H_2O	SiO_2 glass (amorph)	Talc $Mg_3Si_4O_{10}(OH)_2$	Antigorite -chrysotile $Mg_3Si_2O_5(OH)_4$	Magnetite Fe_3O_4	CH_4 gas	CO_2 gas
				ΔG_f^o kcal/mol					
298.15	-491.94	-329.67	-54.64	-203.3	-1324.49	-963.77	-243.09	-12.13	-94.26
400	-482.20	-321.54	-53.52	-199.00	-1293.41	-936.95	-234.88	-10.05	-94.33
500	-472.7	-313.63	-52.36	-194.78	-1262.88	-910.64	-226.99	-7.82	-94.39
600	-463.13	-305.81	-51.16	-190.58	-1232.43	-884.49	-219.3	-5.47	-94.45
700	-453.65	-298.07	-49.91	-186.39	-1202.12	-858.49	-211.82	-3.02	-94.5
800	-444.23	-290.37	-48.65	-182.22	-1171.96		-204.54	-0.51	-94.54
900	-434.83	-282.69	-47.35	-178.08	-1141.94		-197.47	2.06	-94.58
1000	-425.12	-275.02	-46.04	-173.94	-1111.58		-190.51	4.65	-94.61
1100	-415.31	-267.29	-44.71	-169.84	-1080.1		-183.45	7.28	-94.64

Table H.2.
Molar Volume
For primordial Earth (Mackenzie and Lerman, 2006), T = 700 K, P = 342 bar

T (K)	Species	Molar Vol cm^3/mol at: T = 298 K, P = 1 bar	Molar Vol cm^3/mol at: T shown, P = 1 bar	Molar Vol cm^3/mol at: T shown, P = 342 bar	a_{solid} Earth T = 700 K, P = 342 bar
625	CH_4 [a]	27,501	51,976	169.55	
700	CO_2 [a]	24,666	58,200	177.93	
700	H_2O [a]	--	58,136	68.54	
700	H_2 [a]	24,804	58,212	186.49	
700	C	5.298 [b]	5.37 [c]	5.37 [g]	1.03
700	SiO_2	27.27 [b]	27.82 [d]	27.82 [h]	1.17
700	Fe_3O_4	44.524 [b]	45.42 [e]	45.42 [i, j]	1.3
700	Fe_2SiO_4	46.39 [b]	46.95 [f]	46.95 [j, k]	1.33

[a] NIST (2016)

[b] Robie and Hemingway (1995)

[c] through [f] calculated from volume expansion coefficients of Tsang et al. (2005), AZo Materials (2016), Hancock and Finlayson (2009), Suzuki et al. (1981)

[g] through [k] calculated from compressibilities in Coleburn (1963), AZo Materials (2016), Haavik et al. (2000), Birch (1966), Plymate and Stout (1990)

REFERENCES

Abramowitz M. and Stegun I. A., 1972. Handbook of Mathematical Functions. Nat. Bureau Stand., Appl. Math. Ser. 55, xiv + 1046 p.

Adams, E.Y., 2006. Titan's thermal structure and the formation of a nitrogen atmosphere. Ph.D. Dissertation, University of Michigan.

Akcasu, A.Z. and Han, C.C., 1979. Molecular weight and temperature dependence of polymer dimensions in solution. Macromolecules 12, 276-280.

Alibert, Y., Mousis, O., 2007. Formation of Titan in Saturn's subnebula: constraints from Huygens probe measurements. Astron. Astrophys. 465, 1051-1060.

Artemieva, N. and Lunine, J., 2003. Cratering on Titan: impact melt, ejecta, and the fate of surface organics. Icarus 164, 471-480.

Atreya, S.K., Donahue, T.M., Kuhn, W.R., 1978. Evolution of a nitrogen atmosphere on Titan. Science 201, 611-613.

Atreya, S.K., Adams, E.Y., Niemann, H.B., Demick-Montelara, J.E., Owen, T.C., Fulchignoni, M., Ferri, F., Wilson, E.H., 2006. Titan's methane cycle. Planet. Space Sci. 54, 1177-1187.

Atreya, S.K., Lorenz, R.D., Waite, J.H., 2009. Volatile origin and cycles: Nitrogen and methane, in Titan from Cassini-Huygens (eds. Brown, R.H., Lebreton, J-P, Waite, J.H.). Springer, pp. 177-199.

AZo Materials, 2016. Silica — Silicon Dioxide (SiO_2). http://www.azom.com/properties.aspx?ArticleID=1114

Bagni G. T., 1996. Jacopo Riccati (1676-1754) e l'analiusi matematica nella Marca trevigiana. Cassamarca 14(X, 2), 90-94.

Barnes, J.W., et al., 2007b. Near-infrared spectral mapping of Titan's mountains and channels. Planet. 112, 11006.

Bar-nun A. and Podolak M., 1979. The photochemistry of hydrocarbons in Titan's atmosphere. Icarus 28, 115-122.

Barr, A.C., Citron, R.I., Canup, R.M., 2010. Origin of a partially differentiated Titan. Icarus 209, 858-862.

Barth, E.L., and Toon, O.B., 2003. Microphysical modeling of ethane ice clouds in Titan's atmosphere. Icarus 162, 94-113.

Baulch D. L., Cobos C. J., Cox R. A., Frank P., Hayman G., Just T., Kerr J. A., Murrells T., Pilling M. J., Troe J., Walker R.W. and Warnatz J., 1994. Evaluated kinetic data for combustion modeling. Supplement I. J. Phys. Chem. Ref. Data 23, 847-1033. doi :10.1063/1.555953.

Bernal, J. D., 1951. *The Physical Basis of Life*. London: Routledge & Kegan Paul.

Birch, F., 1966. Compressibility; elastic constants. In Clark, S.P.Jr (ed.), Handbook of Physical Constants. Geol. Soc. America Mem. 97, 97-173.

Bittani S., Laub A. and Willems J. C. (eds), 1991. The Riccati Equation. Springer-Verlag, Berlin Heidelberg.

Black, B.A., Perron, J.T., Burr, D.M., Drummond, S.A., 2012. Estimating erosional exhumation on Titan from drainage network morphology. J. Geophys. Res. 117, E08006, doi:10.1029/2012JE004085.

Boltzmann, L., 1896. Vorlesungen über Gastheorie. 1. Theil. Verlag von Johann Ambrosius Barth (Arthur Meiner), Leipzig, viii + 204 pp.

Brown, R.H., et al., 2004. The Cassini Visual and Infrared Mapping Spectrometer (VIMS) investigation. Space Sci. Rev. 115, 111-168.

Brown, R., Lebreton, J-P., Waite, J.H., eds., 2009. *Titan from Cassini-Huygens*. Springer (Dordrecht; New York). Print.

Brush, S.G., 2008. Enskog, David. Complete Dictionary of Scientific Biography, Encyclopedia.com. <http://www.encyclopedia.com/doc/1G2-2830901324.html>

Buratti, B.J., et al., 2012. A newly discovered impact crater in Titan's Senkyo: Cassini VIMS observations and comparison with other impact features. Planet. Space Sci. 60, 18-25.

Burr, D.M., et al., 2006. Sediment transport by liquid surficial flow: Application to Titan. Icarus 181, 235-242.

Burr, D.M., et al., 2009. Fluvial network analysis on Titan: Evidence for subsurface structures and west-to-east wind flow, southwestern Xanadu. Geophys. Res. Lett. 36, L22203, doi:10.1029/2009GL040909.

Burr, D.M., et al., 2013. Morphology of fluvial networks on Titan: Evidence for structural control. Icarus 226, 742-759.

Caenn, R., Darley, H.C.H., Gray, G.R., 2011. Composition and properties of drilling and completion fluids, 6th edition. Gulf Professional Publishing. 720 pp.

Carlston, C.W., 1969. Longitudinal slope characteristics of rivers of the midcontinent and the atlantic east gulf slopes. International Association of Scientific Hydrology. Bulletin, 14, 21-31.

Carslaw, H.S., Jaeger, J.C., 1959. Conduction of heat in solids, 2nd ed. Oxford University Press, x + 510 pp.

Cartwright, R., Clayton, J.A., Kirk, R.L., 2011. Channel morphometry, sediment transport, and implications for tectonic activity and surficial ages of Titan basins. Icarus 214, 561-570.

"Cassini-Huygens Mission Objectives". European Space Agency (ESA). 27 Mar. 2012. <http://sci.esa.int/science-e/www/object/index.cfm?fobjectid=2085>

Chanson, H., 1999. The hydraulics of open channel flow: an introduction. Arnold, London, UK. 495 pp.

Chaplin, M., 2016. Water structure and science. Hexagonal ice (ice Ih). www1.lsbu.ac.uk.

Chapman, S., 1916. On the law of distribution of molecular velocities, and on the theory of viscosity and thermal conduction, in a non-uniform simple monatomic gas. Phil. Trans. Roy. Soc. London A 216, 279-348.

Chapman, S., Cowling, T.G., 1970. The mathematical theory of non-uniform gases. 3rd ed. Cambridge University Press, xxiv + 423 pp.

Chen, C-T.A., Chen, J.H., Millero, F.J., 1980. Densities of NaCl, $MgCl_2$, Na_2SO_4, and $MgSO_4$ aqueous solutions at 1 atm from 0 to 50ºC and from 0.001 to 1.5 *m*. J. Chem. Eng. Data 25, 307-310.

Chen F. Z. and Wu C. Y. R., 2004. Temperature-dependent photoabsorption cross sections in the VUV-UV region. I. Methane and ethane. J. Quant. Spectrosc. Radiat. Transf. 85, 195-209.

Chevrier, V.F., Luspay-Kuti, A., Singh, S., 2015. Experimental study of nitrogen dissolution in methane-ethane mixtures under Titan surface conditions. 46th Lunar and Planetary Science Conference, 2673.

Cody R. J., Payne W. A. Jr, Thorn R. P., Nesbitt F. L., Iannone M. A., Tardy D. C. and Stief L. J., 2002. Rate constant for the recombination reaction $CH_3 + CH_3 \rightarrow C_2H_6$ at T = 298 and 202 K. J. Phys. Chem. A 106, 6060-6067.

Cody R. J., Romani P. N., Nesbitt F. L., Iannone M. A., Tardy D. C. and Stief L. J., 2003. Rate constant for the reaction $CH_3 + CH_3 \rightarrow C_2H_6$ at T = 155 K and model calculation of the CH3 abundance in the atmospheres of Saturn and Neptune. J. Geophys. Res. 108, 5119. doi:10.1029/2002JE002037.

Coleburn, N.L., 1963. The compressibility of pyrolytic graphite. US Naval Ordnance Laboratory, White Oak, Maryland, 41445, ii + 20 pp.

Collins, G.C., 2005. Relative rates of fluvial bedrock incision on Titan and Earth. Geophys. Res. Lett. 32, L22202, doi:10.1029/2005GL024551.

Conde, M., 2006. Thermophysical properties of $\{NH_3+H_2O\}$ mixtures for the industrial design of absorption refrigeration equipment. M. Conde Engineering, Zürich, 38 pp. http://www.mrc-eng.com/Downloads/NH3&H2O%20%20Props%20English.pdf

Conde, M., 2009. Aqueous solutions of lithium and calcium chlorides: property formulations for use in air conditioning equipment design. M. Conde Engineering, Zürich, 27 pp. http://www.mrc-eng.com/Downloads/Aqueous%20LiCl&CaCl2%20Solution%20Props.pdf

Conde, M., 2013. Heat capacities of ammonia-water solutions. *Personal communication*. M. Conde Engineering, Zürich.

Cornet, T., et al., 2015. Dissolution of Titan and on Earth: Towards the age of Titan's karstic landscapes. J. Geophys. Res. Planet. 120, 1044-1074.

Courtin, R.D., Sim, C., Kim, S., Gautier, D., Jennings, D.E., 2008. Latitudinal variations of tropospheric H2 on Titan from the Cassini CIRS investigation. 40th DPS meeting Abstract. 31.01, Ithaca, New York, Bull. Amer. Astron. Soc. 40(31.01): 446.

Coustenis, A., 2005. Formation and Evolution of Titan's Atmosphere. Space Sci. Rev. 116, 171-184.

Coustenis, A., et al., 2009. Earth-based perspective and pre-Cassini-Huygens knowledge of Titan. In: Brown, R.H., Lebreton, J-P., Waite, J.H. (Eds.), Titan from Cassini-Huygens. Springer, pp. 9-34.

Cowie, J.M.G., 1966. Estimation of unperturbed polymer dimensions from viscosity meqasurements in non-ideal solvents. Polymer 7, 487-495.

CRC Handbook of Chemistry and Physics, 96th ed. Haynes, W.M., Ed.. CRC Press, Boca Raton, FL, 2016.

Croft, S.K. Lunine, J.I., Kargel, J., 1988. Equation of state of ammonia-water liquid—Derivation and planetological applications. Icarus 73, 279-293.

Czechowski, L., Leliwa-Kopystyński, J., 2005. Convection driven by tidal and radiogenic heating in medium size icy satellites. Planet. Space Sci. 53, 749-769.

DLMF, 2015. Digital Library of Mathematical Functions. NIST, Washington, D.C., http://dlmf.nist.gov/

Dorofeeva, V.A., Ruskol, E.L., 2010. On the thermal history of Saturn's satellites Titan and Enceladus. Sol. Syst. Res. 44, 192-201.

Duan, Z., Mao, S., 2006. A thermodynamic model for calculating methane solubility, density and gas phase composition of methane-bearing aqueous fluids from 273 to 523 K and from 1 to 2000 bar. Geochim. Cosmochim. Acta 70, 3369-3386.

Einstein, A., 1905. Über die von der molekularkinetischen Theorie der Wärme geforderte Bewegung von in ruhenden Flüssigkeiten suspendierten Teilchen. Annalen der Physik 322, 549–560.

Einstein, H.A., 1942. Formulas for the transport of bed sediment. Trans. American Society of Civil Engineers 107, 561-574.

Einstein, A., 1956. Investigations on the Theory of the Brownian Movement. Edited with notes by R. Fürth, translated by A. D. Cowper, Dover Publications, New York.

Elachi, C., et al., 2005. Cassini radar views the surface of Titan. Science 308, 970-974.

Elson, T., 2007. Concepts of fluid flow, in Concepts of chemical engineering 4 chemists (ed. Simons, S.J.R.). The Royal Society of Chemistry, pp. 55-95.

Enderlin, E. (Univ of Maine, Orono), 2014. Just How Quickly Are Icebergs And Glaciers Melting? Polardispatches.org.

English, N.J., Macelroy, J.M.D., 2003. Structural and dynamical properties of methane clathrate hydrates. J. Comput. Chem. 24, 1569-1581.

European Space Agency (ESA), 2013. “Facts About Titan”. Web. 1 Jul. 2013. http://www.esa.int/Our_Activities/Space_Science/Cassini-Huygens/Facts_about_Titan

Fan W. Y., Knewstubb P. F., Käning M., Mechold L., Röpcke J. and Davies P. B., 1999. A diode laser and modeling study of mixed (CH_4-H_2-O_2) AC plasmas. J. Phys. Chem. A 103, 4118-4128.

Farnsworth, K., et al., 2016. Experimental study of nitrogen dissolution in methane-ethane mixtures under Titan surface conditions. 47th Lunary and Planetary Science Conference, 2380.

Ferry, J.G. (ed.), 2012. Methanogenesis: Ecology, physiology, biochemistry & genetics. Springer, 536 pp.

Finnegan, N.J., et al., 2005. Controls on the channel width of rivers: Implications for modeling fluvial incision of bedrock. Geology 33, 229-232.

Fortes, A.D., Grindrod, P.M., Trickett, S.K., Vocadlo, L., 2007. Ammonium sulfate on Titan: Possible origin and role in cryovolcanism. Icarus 188, 139-153.

Fortes, A.D., 2012. Titan's internal structure and the evolutionary consequences. Planet. Space Sci. 60, 10-17.

French, B.M., 1966. Some geological implications of equilibrium between graphite and a C-H-O gas phase at high temperatures and pressures. Rev. Geophys. 4, 223-253.

Garcia, J.E., 2001. Density of aqueous solutions of CO_2. Lawrence Berkley Nat. Lab., 1-010. https://escholarship.org/uc/item/6dn022hb

Gilliam, A.E., McKay, C.P., 2011. Titan under a red dwarf star and as a rogue planet: requirements for liquid methane. Planet. Space Sci. 59, 845-839.

Gilliam, A.E. and Lerman A., 2014a. Evolution of Titan's major atmospheric gases and cooling since accretion. Planet. Space Sci. 93-94, 41-53.

Gilliam, A.E., and Lerman, A., 2014b. Corrigendum to "Evolution of Titan's major atmospheric gases and cooling since accretion". Planet. Space Sci. 101, 210.

Gilliam, A.E., Lerman, A., Wunsch, J., 2015. Evolution of Titan's atmosphere in relation to its surface and interior. Astrobiology Science Conference 2015, 7772.

Gilliam, A.E., Lerman, A., 2016a. Titan's missing ethane: from the atmosphere to the subsurface. Icarus 275, 252-258.

Gilliam, A.E., Lerman, A., 2016b. Formation mechanisms of channels on Titan through dissolution by ammonium sulfate and erosion by liquid ammonia and ethane. Planet. Space Sci. 132, 13-22.

Gladstone G. R., Allen M. and Yung Y. L., 1996. Hydrocarbon photochemistry in the upper atmosphere of Jupiter. Icarus 119, 1-52.

Goody, R., 1976. Atmospheric evaporation, in: Tipler, P.A., Physics, pp. 241-243, Worth Publishers, New York, xxvi + 1026 pp.

Gough, O.D., 1981. Solar interior structure and luminosity variations. Solar Phys. 74, 21-34.

Grasset, O., Sotin, C., 1996. The Cooling Rate of a Liquid Shell in Titan's Interior. Icarus 123, 101-112.

Grasset, O., Sotin, C., Deschamps, F., 2000. On the internal structure and dynamics of Titan. Planet. Space Sci. 48, 617-636.

Grasset, O., Pargamin, J., 2005. The ammonia-water system at high pressures: Implications for the methane of Titan. Planet. Space Sci. 53, 371-384.

Graves, S.D.B., et al., 2008. Rain and hail can reach the surface of Titan. Planet. Space Sci. 56, 346-357.

Greenwood, N.N., Earnshaw, A., 2012. Chemistry of the elements. Elsevier, 1600 pp.

Griffith, C.A., Owen, T., Geballe, T.R., Rayner, J., Rannou, P., 2003. Evidence for the exposure of water ice on Titan's surface. Science 300, 628-630.

Grindrod, P.M., Fortes, A.D., Nimmo, F., Feltham, D.L., Brodholt, J.P., Vočadlo, L., 2008. The long-term stability of a possible aqueous ammonium sulfate ocean inside Titan. Icarus 197, 137-151.

Haar, L., Gallagher, J.S., 1978. Thermodynamic propercaruties of ammonia. J. Phys. Chem. Ref. Data 7, 635-792.

Haavik, C., Stølen, S., Fjellvåg, H., Hanfland, M., Häusermann, D., 2000. Equation of state of magnetite and its high-pressure modification: thermodynamics of the Fe-O system at high pressure. Amer. Mineralogist 85, 514-523.

Haldane, J.B.S., 1929. The origin of life: The Rationalist Annual, London (reprinted in Haldane, JBS, science and life, with an introduction by Maynard Smith, J (1968)). Pemberton Publishing Co Ltd, London.

Hambrey, M.J., 1994. Glacial Environments. CRC Press.

Hancock, Y., Finlayson, T.R., 2009. Thermal expansion of magnetite. Philosophical Magazine 89, 22-24.

Hanks, T.C., Anderson, D.L., 1969. The early thermal history of the Earth. Phys. Earth Planet. Interiors 2, 19-29.

Hayes, A., et al., 2008. Hydrocarbon lakes on Titan: Distribution and interaction with a porous regolith. Geophys. Res. Lett. 35, L09204, doi:10.1029/2008GL033409.

Herdendorf, C.E., 1982. Large lakes of the world. J. Great Lakes Res. 8, 379-412.

Hjulström, F., 1935. Studies of the morphological activity of rivers as illustrated by the river Fyris: Inaugural dissertation (Vol. 10). Almqvist & Wiksells.

Holland, H.R., 1984. The chemical evolution of the atmosphere and oceans. Princeton NJ: Princeton Univ. Press.

Horita, J., Berndt, M.E., 1999. Abiogenic methane formation and isotopic fractionation under hydrothermal conditions. Science 285, 1055-1057.

Horita, J., et al., 2002. Experimental and theoretical study of pressure effects on hydrogen isotope fractionation in the system brucite-water at elevated temperatures. Geochimica et Cosmochimica Acta 66, 3769-3788.

Huda, S.A., Small, E.E., 2014. Modeling the effects of bed topography on fluvial bedrock erosion by saltating bed load. J. Geophys. Res. Earth Surf. 119, 1222-1239.

Huygens, C., 1659. In: Systema saturnium, Hague.

IPCC, Climate Change, 2001. Third Assessment report. Ch. 4.2.1.1. Intergovernmental Panel on Climate Change, WMO, UNEP.

Jacobsen, R.T., Stewart, R.B., 1973. Thermodynamic properties of nitrogen including liquid and vapor phases from 63K to 2000K with pressures to 10,000 bar. J. Phys. Chem. Ref. Data 2, 757-922.

Jacquemart, D., Lellouch, E., Bézard, B., de Bergh, C., Coustenis, A., Lacome, N., Schmitt, B., Tomasko, M., 2008. New laboratory measurements of CH_4 in Titan's conditions and a reanalysis of the DISR near-surface spectra at the Huygens landing site. Planet. Space Sci. 56, 613-623.

Jaumann, R., et al., 2008. Fluvial erosion and post-erosional processes on Titan. Icarus 197, 526-538.

Jaumann, R., et al., 2009. Geology and surface processes on Titan. In: Brown, R.H., Lebreton, J.-P., Waite, J.H. (Eds.), Titan from Cassini-Huygens. Springer, pp. 75-140.

Jeans, J.H., 1911. Molecule. Encyclopedia Britannica, 11th ed. 18, 654-660. Cambridge University Press.

Jeans, J.H., 1916. The dynamical theory of gases, 2nd ed. Cambridge University Press, viii + 436 pp.

Jones, E.M., 2010. English Ideology, Newton & the Exploitation of Science. First Annual Catholic Conference on Geocentrism. South Bend, Ind. http://www.culturewars.com/2011/Newton.htm

Kargel, J.S., et al., 1991. Rheological properties of ammonia-water liquids and crystal-liquid slurries: Planetological applications. Icarus 89, 93-112.

Kargel, J.S., 1992. Ammonia-water volcanism on icy satellites: phase relations at 1 atmosphere. Icarus 100, 556-574.

Katz, A., 2013. Density of the Dead Sea, North Basin, brine in 2012-2013. *Personal communication*. Institute of Earth Sciences, The Hebrew University, Jerusalem.

Kaula, W.M., 1979. Thermal evolution of Earth and Moon growing by planetesimal impacts. J. Geophys. Res. 84, 999-1008.

Kelvin, Lord (Thomson, W.), 1862. On the secular cooling of the Earth. Roy. Soc. Edinburgh Trans. 23, 157-169.

Krasnopolsky, V.A., Maillard, J.P., Owen, T.C., 2004. Detection of methane in the martian atmosphere: evidence for life? Icarus 172, 537-547.

Kuramoto, K., Matsui, T., 1994. Formation of a hot proto-atmosphere on the accreting giant icy satellite: Implications for the origin and evolution of Titan, Ganymede, and Callisto. J. Geophys. Res. 99, 21,183-21, 200.

Langhans, M.H., et al., 2012. Titan's fluvial valleys: Morphology, distribution, and spectral properties. Planet. Space Sci. 60, 34-51.

Lara L.M., Lellouch E., Lopéz-Moreno J.J., Rodrigo R., 1995. Vertical distribution of Titan's atmospheric neutral constituents. J. Geophys. Res. Planets 101(E10), 23261-23283.

Lean J.L., 1991. Variations in the Sun's radiative output. Rev. Geophys. 29, 505-535.

Lean J.L. and Skumanich A., 1983. Variability of the Lyman Alpha Flux with Solar activity. J. Geophys. Res. 88(A7), 5751-5759.

Ling, J., et al., 2001. Kinetics simulation of high viscous styrene bulk polymerization system. European Polymer Jour. 37, 22407-2411.

Lipenkov, V.Ya., Salamatin, A.N., Duval, P., 1997. Bubbly-ice densification in ice sheets: II. Applications. Jour. Glaciol. 43, 397-407.

Lissauer, J.J., de Pater, I., 2013. Fundamental planetary science: physics, chemistry and habitability. Cambridge University Press.

Littrup, P., et al., 2004. Cryotherapy probe and system. Patent application WO 2004064914 AS. 5 August 2004.

Lopes, R.M.C., et al., 2007. Cryovolcanic features on Titan's surface as revealed by the Cassini Titan Radar Mapper. Icarus 186, 395-412.

Lopes, R.M.C., et al., 2007. The lakes and seas of Titan, Eos Trans. AGU 88, 569-570.

Lopes, R.M.C., et al., 2010. Distribution and interplay of geologic processes on Titan from Cassini radar data. Icarus 205, 540-558.

Lorenz, R.D., 1993. The life, death and afterlife of a raindrop on Titan. Planet. Space Sci. 41, 647-655.

Lorenz, R.D., 1994. Crater lakes on Titan: rings, horseshoes and bullseyes. Planet. Space Sci. 42, 1-4.

Lorenz, R.D., Lunine, J.I., 1996. Erosion on Titan: Past and present. Icarus 122, 79-91.

Lorenz, R.D., McKay, C.P., Lunine, J.I., 1999. Analytic investigation of climate stability on Titan: sensitivity to volatile inventory. Planet. Space Sci. 47, 1503-1515.

Lorenz, R., Mitton, J., 2002. Lifting Titan's veil : Exploring the giant moon of Saturn. Cambridge University Press. 268 pp.

Lorenz, R.D., et al., 2008. Fluvial channels on Titan : Initial Cassini Radar observations. Planet. Space Sci. 56, 1132-1144.

Lorenz, R.D., et al., 2008. Titan's inventory of organic surface materials. Geophys. Res. Lett. 35, L02206, doi :10.1029/2007GL032118.

Lorenz, R.D., et al., 2014. A radar map of Titan Seas: Tidal dissipation and ocean mixing through the throat of Kraken. Icarus, 237, 9-15.

Lunde, P.J., Kester, F.L., 1973. Rates of methane formation from carbon dioxide and hydrogen over a ruthenium catalyst. J. Catal. 30, 423-429.

Lunine, J.I., Stevenson, D.J., Yung, Y.L., 1983. Ethane ocean on Titan. Science 222 (4269), 1229-1230.

Lunine, J.I., 1985. Dissertation, California Institute of Technology Dissertation, Calif. Institute of Technology 329 pp.

Lunine, J.I., Stevenson, D.J., 1987. Clathrate and ammonia hydrates at high pressure – application to the origin of methane on Titan. Icarus 70, 61-77.

Lunine, J.I., and McKay, C. P., 1995. Surface-atmosphere interactions on Titan compared with those on the pre-biotic Earth. Adv. Space Res. 15, 303-311.

Lunine, J.I., Atreya, S.K., 2008. The methane cycle on Titan. Nature Geosci., 1, 159-164.

Luo, Z.-h., et al., 2006. Estimation of rate constants for polymerization based on Monte Carlo simulation. Jour. Shanghai Univ. 10, 274-276.

Luspay-Kuti, A., et al., 2015. Experimental constraints on the composition and dynamics of Titan's polar lakes. Earth Planet. Sci. Lett. 410, 75-83.

Lvov, S.N., Wood, R.H., 1990. Equation of state of aqueous NaCl solutions over a wide range of temperatures, pressures and concentrations. Fluid Phase Equilib. 60, 273-287.

Mackenzie, F.T., Lerman, A., 2006. Carbon in the geobiosphere: Earth's outer shell (Vol. 25). Springer Science & Business Media.

Macpherson M.T., Pilling M.J., Smith M.J.C, 1983. The pressure and temperature dependence of the rate constant for methyl radical recombination over the temperature range 296-577 K. Chem. Phys. Lett. 94, 430-433.

Malaska, M., et al., 2010. Identification of karst-like terrain on Titan from valley analysis. Lunar Planet. Inst. Sci. Conf. Abstr. 41, 1544.

Marion, G.M., 1997. A theoretical evaluation of mineral stability in Don Juan Pond, Wright Valley, Victoria Land. Antarct. Sci. 9 (01), 92-99.

Matsubaya, O., Sakai, H., Torii, T., Burton, H., Kerry, K., 1979. Antarctic saline lakes – stable isotopic ratios, chemical compositions and evolution. Geochim. Cosmochim. Acta 43, 7-25.

Maxwell, J.C., 1860. Illustrations of the dynamical theory of gases. Part I. On the motions and collisions of perfectly elastic spheres. Phil. Mag. 19, 19-32.

Maxwell, J.C., 1867. On the dynamical theory of gases. Phil. Trans. Roy. Soc. London 157, 49-88.

Maxwell, J.C., 1890. Illustrations of the dynamical theory of gases. Reprinted from Phil. Mag. 1860, 19, 19-32, and Phil Mag. 1860, 20, 21-37, in: Niven, W.D. (Ed.), 1890. The scientific papers of James Clerk Maxwell, pp. 377-409. Cambridge University Press, xxix + 609 pp. Dover, New York, edition, 1965.

Mayer, E.W., et al., 1982. Methane: Interhemispheric concentration gradient and atmospheric residence time. Proc. Nat. Acad. Sci. 79, 1366-1370.

McKay, C.P., and Smith, H.D., 2005. Possibilities for methanogenic life in liquid methane on the surface of Titan. Icarus 178, 274-276.

McLendon, C., et al., 2015. Solubility of polyethers in hydrocarbons at low temperatures. A model for potential genetic backbones on warm Titans. Astrobiology 15, 200-206.

Menzies, J., and Hughes, T.J., 2002. Glaciers and ice sheets, in Modern & Past Glacial Environments (ed. Menzies, J.) Butterworth-Heinemann, pp. 53-78.

Meyer-Peter, E., 1949. Quelques problèmes concernant le charriage des matières solides dans les rivières alpines et subalpines. La Houille Blanche, 688-706.

Meyer-Peter, E., 1951. Transport des matières solides en général et problème spéciaux. Bull. Génie Civil d'Hydraulique Fluviale, Tome 5.

Miller, S., 1953. A production of amino acids under possible primitive earth conditions. Science 17, 528–529.

Miller, S. and Urey, H., 1959. Organic compound synthesis on the primitive earth. Science 130, 245–251.

Mills, G.A., Steffgen, F.W., 1974. Catalytic Methanation. Cat. Rev. 8, 159-210 doi:10.1080/01614947408071860.

Mitchell, K.L., et al., 2007. Titan's crater lakes: Caldera vs. karst. Lunar Planet. Inst. Sci. Conf. Abstr. 38: 2064.

Mitchell, K.L., Malaska, M., 2011. Karst on Titan. In: First international planetary caves workshop: implications for astrobiology, climate, detection, and exploration. LPI Contribution No. 1640. Lunar and Planetary Institute, Houston, p. 15.

Mitri, G., et al., 2007. Hydrocarbon lakes on Titan. Icarus 186(2), 385-394.

Mitri, G., et al., 2008. Resurfacing of Titan by ammonia-water cryomagma. Icarus 196, 216-224.

Mitri, G., Showman, A.P., 2008. Thermal convection in ice-I shells of Titan and Enceladus. Icarus 193, 387-396.

Monroe, J.S., Wicander, R., 2012. The changing Earth: Exploring geology and evolution, sixth edition. Brooks/Cole, Cengage Learning, pp. 320-322.

Mosqueira, I., Estrada, P.R., 2003. Formation of the regular satellites of giant planets in an extended gaseous nebula I: subnebula model and accretion of satellites. Icarus 163, 198-231.

Mottl, M.J., et al., 2003. Deep-slab fluids fuel extremophilic Archaea on a Mariana forearc serpentinite mud volcano: Ocean Drilling Program Leg 195. Geochem. Geophys. Geosyst. 4, doi:10.1029/2003GC000588.

Mousis, O., Gautier, D., Bockelée-Morvan, D., 2002. An Evolutionary Turbulent Model of Saturn's Subnebula: Implications for the Origin of the Atmosphere of Titan. Icarus 156, 162-175.

Mousis, O., and Schmitt, B., 2008. Sequestration of Ethane in the Cryovolcanic Subsurface of Titan. Astrophys. J. Lett. 677, 67-70.

Murdock, J.W., 1993. Fundamental fluid mechanics for the practicing engineer. CRC Press. 440 pp.

Naftz, D.L., Millero, F.J., Jones, B.F., Green, W.R., 2011. An equation of state for hypersaline water in Great Salt Lake, Utah, USA. Aquat. Geochem. 17, 809-820.

Nakanishi, K., Adachi, S., Yamamoto, S., Matsuno, R., Tanaka, A., Kamikubo, T., 1977. Diffusion of saccharides and amino acids in crosslinked polymers, Agricultural and Biological Chemistry 41, 2455-2462

National Aeronautics and Space Administration (NASA), 2012. "Titan: Facts & Figures". Web. 1 Jul. 2013. http://solarsystem.nasa.gov/planets/profile.cfm?Object=Sat_Titan&Display=Facts

Neish, C. D., Somogyi, Á., Smith, M. A., 2010. Titan's Primordial Soup: Formation of Amino Acids via Low-Temperature Hydrolysis of Tholins. Astrobiology 10, 337-347.

Neish, C.D. and Lorenz, R.D., 2012. Titan's global crater population: A new assessment. Planet. Space Sci. 60, 26-33.

Neish, C.D., et al., 2013. Crater topography on Titan: Implications for landscape evolution. Icarus 223, 82-90.

Nielsen, P., 1992. Coastal bottom boundary layers and sediment transport. Vol. 4. World scientific.

Niemann, H.B., Atreya, S.K., Bauer, S.J., Carignan, G.R., Demick, J.E., Frost, R.L., Gautier, D., Haberman, J.A., Harpold, D.N., Hunten, D.M., Israel, G., Lunine, J.I., Kasprzak, W.T., Owen, T.C., Paulkovich, M., Raulin, F., Raaen, E., Way, S.H., 2005. The abundances of constituents of Titan's atmosphere from the GCMS instrument on the Huygens probe. Nature 438, 779-784.

NIST, 2016. Thermophysical Properties of Fluid Systems. http://webbook.nist.gov/chemistry/fluid/

Norman, L. H., 2011. Is there life on … Titan? Astronomy & Geophysics 52, 139-142.

Oparin, A. I. [Опарин А. И.], 1924. Происхождение жизни. М., Московский рабочий, 71 с.

Oparin, A. I., 1941. Возникновение жизни на Земле. 2-е изд., значительно дополненное. М.--Л.: Издательство Академии Наук СССР, — 267 с.

Oparin, A. I., 1953. [Originally published 1938; New York: The Macmillan Company]. The Origin of Life. Translation and new introduction by Sergius Morgulis (2nd ed.). Mineola, NY: Dover Publications.

Osako, M., Yoneda, A., Ito, E., 2010. Thermal diffusivity, thermal conductivity and heat capacity of serpentine (antigorite) under high pressure. Phys. Earth Planet. Inter. 183, 229-233.

OXY (Occidental Chemical Corporation), 2012. Calcium chloride – a guide to physical properties, 10 p. http://www.cal-chlor.com/PDF/GUIDE-physical-properties.pdf

Paphitis, D., 2001. Sediment movement under unidirectional flows: an assessment of empirical threshold curves. Coastal Engineering 43, 227-245.

Park J., Lee J., Sim K., Han J.W., Yi W., 2008. Photodissociation of methane at Lyman alpha (121.6 nm). Bull. Korean Chem. Soc. 29, 177-180.

Perron, J.T., et al., 2006. Valley formation and methane precipitation rates on Titan. J. Geophys. Res. 111, E11001, doi:10.1029/2005JE002602

"The Pioneer Missions“. NASA. 26 March 2007. <http://www.nasa.gov/centers/ames/missions/archive/pioneer.html>

Plymate, T.G., Stout, J.H., 1990. Pressure-volume-temperature behavior of fayalite based on static compression measurements at 400°C. Phys. Chem. Minerals 17, 212-219.

Polson, A., 1937. CCXXXIII. On the diffusion constants of the amino-acids. Biochem. J., 31, 1903-1912.

Porco, C.C., et al., 2004. Cassini imaging science: Instrument, characteristics and anticipated scientific investigations at Saturn. Space Sci. Rev. 115, 363-497.

Porco, C.C., et al., 2005. Imaging of Titan from the Cassini spacecraft. Nature 434, 159-168.

Prinn, R.G., Fegley, B., 1981. Kinetic Inhibition of CO and N_2 Reduction in Circumplanetary Nebulae: Implications for Satellite Composition. Astrophys. J. 249, 308-317.

Rannou, P., Montmessin, F., Hourdin, F., Lebonnois, S., 2006. The latitudinal distribution of clouds on Titan. Science 311, 201-205.

Riccati J., 1761. Opere del Conte Jacopo Riccati Nobile Trevigiano. Giusti, Lucca. 1, 433-598.

Robertson, E.C., 1988. Thermal properties of rocks. USGS Open-File Rept. 88-441, iv + 106 pp.

Robertson S.H., Pilling M.J., Baulch D.L., Green N.J.B., 1995. Fitting of pressure-dependent kinetic rate data by master equation/inverse Laplace transform analysis. J. Phys. Chem. 99, 13452-13460.

Robie, R.A., Bethke, P.M., Toulmin, M.S., Edwards, J.L., 1966. X-ray crystallographic data, densities, and molar volumes of minerals. In Clark, S.P.Jr (ed.), Handbook of Physical Constants. Geol. Soc. America Mem. 97, 27-71.

Robie, R.A., Waldbaum, D.R., 1970. Thermodynamic properties of minerals and related substances at 298.15°K (25.0°C) and one atmosphere (1.013 bars) pressure and at higher temperatures. US Geol. Surv. Bull. 1259, 1-256.

Robie, R.A., Hemingway, B.S., 1979. Thermodynamic properties of minerals and related substances at 298.15 K and 1 bar (10^5 pascals) pressure and at higher temperatures. US Geol. Surv. Bull. 2131, 1-461.

Robie, R.A., Hemingway, B.S., Fisher, J.R., 1995. Thermodynamic properties of minerals and related substances at 298.15 K and 1 bar (10^5 pascals) pressure and at higher temperatures. US Geol. Surv. Bull. 1452, 1-456.

Roe H.G., 2012. Titan's methane weather. Ann. Rev. Earth Planet. Sci. 40, 355-382.

Rogers, P.S.Z., Pitzer, K.S., 1982. Volumetric properties of aqueous sodium chloride solutions. J. Phys. Chem. Ref. Data 11, 15-81.

Romanzin C., Gazeau M.-C., Bénilan Y., Hébrard E., Jolly A., Raulin F., 2005. Methane photochemistry: A brief review in the frame of a new experimental program of Titan's atmospheric simulations. Adv. Space Res. 36, 258-267.

Romanzin C., Bénilan Y., Jolly A., Gazeau M.-C., 2008. Photolytic behaviour of methane at Lyman-a and 248 nm: Studies in the frame of a simulation program of Titan's atmosphere (S.E.T.U.P.). Adv, Space Res. 42, 2036-2044.

Russefl-Head, D.S., 1980. The melting of free-drifting icebergs. Ann. Glaciol. 1, 119-122.

Sabatier, P., Senderens, J-B., 1902. Nouvelles synthèses du méthane. Comptes Rendus Acad. Sci. Paris 134, 514-516.

Sabatier, P., 1911. Bemerkung zu meinem Vortrag vom 13. Mai 1911 über: «Hydrogénations et déshydrogénations par catalyse». Berichte der deutschen chemischen Gesellschaft 44(3), 3180, Juli–Dezember 1911.

Sagan, C., and Thompson, W.R., 1984. Production and condensation of organic gases in the atmosphere of Titan. Icarus 59, 133-161.

Samuelson, R.E., Mayo, L.A., 1997. Steady-state model for methane condensation in Titan's troposphere. Planet. Space Sci. 45 (8), 949-958.

Satsińska, G., et al., 2011. Oxygen in the Universe. EAS Publication Series, vol. 54, 2012. EDR Sciences, Les Ulis, France, xii + 370 p.

Schaller, M., et al., 2001. Large-scale erosion rates from in situ-produced cosmogenic nuclides in European river sediments. Earth Planet. Sci. Lett. 188, 441-458.

Schneider, T., et al., 2012. Polar methane accumulation and rainstorms on Titan from simulations of the methane cycle. Nature 481, 58-61.

Schubert, G., Stevenson, D.J., Ellsworth, K., 1981. Internal structures of the Galilean satellites. Icarus 47, 46-59.

Schulze-Makuch, D., and Grinspoon, D.H., 2005. Biologically enhanced energy and carbon cycling on Titan? Astrobiology 5, 560-564.

Seeds, M.A., Backman, D.E., 2016. Foundations of astronomy, enhanced. Cengage Learning, 688 pp.

Seeton, C.J., 2006. Viscosity-temperature correlation for liquids. Tribology Letters 22, 67-78.

Setzmann, U., Wagner, W., 1991. A new equation of state and tables of thermodynamic properties for methane covering the range from the melting line to 625 K at pressures up to 1000 MPa. J. Phys. Chem. Ref. Data 20, 1061-1155.

Sharqawy, M. H., Lienhard V, J. H., Zubair, S. M., 2010. Thermophysical properties of seawater: A review of existing correlations and data, Desalination and Water Treatment 16, 354-380.

Shields, A., 1936. Anwendung der Ähnlichkeitsmechanik und der Turbulenzforschung auf die Geschiebebewegung. Mitt. Preuss. Versuchsanstalt f. Wasserbau u. Schiffbau, 26, 1-26.

Shiklomanov, I.A., 1993. World fresh water resources, in Water in Crisis: A Guide to the World's Fresh Water Resources (Gleick, P.H., ed.). Oxford University Press, pp. 13-24.

Skene, W.G., et al., 1998. Decomposition kinetics, Arrhenius parameters, and bond dissociation energies for alkoxyamines of relevance in "living" free radical polymerization. Macromolecules 31, 9103-9105.

Skinner, B.J., 1966. Themral expansion. In In Clark, S.P.Jr (ed.), Handbook of Physical Constants. Geol. Soc. America Mem. 97, 75-96.

Sklar, L.S., Dietrich, W.E., 2001. Sediment and rock strength controls on river incision into bedrock. Geology 29, 1087-1090.

Sklar, L.S., Dietrich, W.E., 2004. A mechanistic model for river incision into bedrock by saltating bed load. Water Resour. Res. 40, W06301, doi:10.1029/2003WR002496.

Slagle I. R., Gutman D., Davies J.W., Pilling M.J., 1988. Study of the recombination reaction $CH_3 + CH_3 \rightarrow C_2H_6$. 1. Experiment. J. Phys. Chem. 92, 2455-2462.

Smith, N.S., Raulin, F., 1999. Modeling of methane photolysis in the reducing atmospheres of the outer solar system. J. Geophys. Res. 104 (E1), 1873-1876.

Smoluchowski, M., von, 1906. Zur kinetischen Theorie der Brownschen Molekularbewegung und der Suspensionen. Annalen der Physik 326, 756–780.

Soderblom, L.A., et al., 2007b. Topography and geomorphology of the Huygens Landing Site on Titan. Planet. Space Sci. 55, 2015-2024.

Sohl, F., Sears, W.D., Lorenz, R.D., 1995. Tidal dissipation on Titan. Icarus 115, 278-294.

Sohl, F., et al., 2003. Interior structure models and tidal Love numbers of Titan. J. Geophys. Res. 108, 5130, doi:10.1029/2003JE002044.

Sotin, C., et al., 2009. Ice – Hydrocarbon Interactions Under Titan-Like Conditions: Implications for the Carbon Cycle on Titan. Lunar and Planetary Science Conference, 40, p. 2088.

Speight, J.G., 1998. Petroleum analysis and evaluation, in Petroleum Chemistry and Refining (Speight, J.G., ed.). Taylor & Francis, pp. 39-62.

Stebelsky, I., Teslia, I., 1993. Rivers. Encyclopedia of Ukraine, Vol. 4.

Stevenson, D.J., 1991. Interior of Titan. Proceedings Symposium on Titan, Toulouse, France, 9-12 September 1991, ESA SP-338, 29-33.

Stevenson, J., Lunine, J., and Clancy, P., 2015. Membrane alternatives in worlds without oxygen: Creation of an azotosome. Sci.Adv. 1, E1400067, doi:10.1126/sciadv.1400067.

Stofan, E.R., et al., 2007. The lakes of Titan. Nature 445, 61-64.

Stolper, D.A., et al., 2014. Formation temperatures of thermogenic and biogenic methane. Science 344, 1500-1503.

Strobel, D.F., 1974. The photochemistry of hydrocarbons in the atmosphere of Titan. Icarus 21, 466-470.

Strobel, D.F., 1982. Chemistry and evolution of Titan's atmosphere. Planet. Space Sci. 30, 839-848.

Strobel, D.F., 2009. Titan's hydrodynamically escaping atmosphere: Escape rates and the structure of the exobase region. Icarus 202, 632-641.

Sundborg, Å., 1956. The river Klarälven. A study of fluvial processes. Geogr. Ann. 38, 238-316.

Suzuki, I., Seya, K., Takei, H., Sumino, Y., 1981. Thermal expansion of fayalite, Fe_2SiO_4. Phys. Chem. Minerals 7, 60-63.

Tan, S.P., Kargel, J.S., Marion, J.S., 2013. Titan's atmosphere and surface liquid: New calculation using Statistical Associating Fluid Theory. Icarus 222, 53-72.

Tan, S.P., et al., 2015. Titan's liquids: Exotic behavior and its implications on global fluid circulation. Icarus 250, 64-75.

Thampi, K.R., Kiwi, J., Grätzel, M., 1987. Methanation and photo-methanation of carbon dioxide at room temperature and atmospheric pressure. Nature 327, 506-508.

Tilling, R.I., Gottfried, D., 1969. Distribution of thorium, uranium, and potassium in igneous rocks of the Boulder Batholith region, Montana, and its bearing on radiogenic heat production and heat flow. USGA Prof. Pap. 614-E, iii + E29 pp.

Tirard, S., 2011. Haldane's Conception of Origins of Life, In: Gargaud, M. (ed.-in.ch.), Encyclopedia of Astrobiology, p. 724, Springer.

Tobie, G., et al., 2005. Titan's internal structure inferred from a coupled thermal-orbital model. Icarus 175, 496-502.

Tobie, G., Lunine, J.I., Sotin, C., 2006. Episodic outgassing as the origin of atmospheric methane on Titan. Nature 440, 61-64.

Tobie, G., Choukroun, M., Grasset, O., Le Muélic, S., Lunine, J.I., Sotin, O., Bourgeois, O., Gautier, D., Hirtzig, M., Lebonnois, S., Le Corre, L., 2009. Evolution of Titan and implication for its hydrocarbon cycle. Phil. Trans. Roy. Soc. A 367, 617-631.

Tomasko, M.G., et al., 2005. Rain, winds and haze during the Huygens probe's descent to Titan's surface. Nature 438, 765-778.

Toublanc, D., et al., 1995. Photochemical Modeling of Titan's Atmosphere. Icarus 113, 2-26.

Tsang W. and Hampson R.F., 1986. Chemical kinetic data base for combustion chemistry. Part I. Methane and related compounds. J. Phys. Chem. Ref. Data 15, 1087. doi :10.1063/1.555759.

Tsang, D.K.L., Marsden, B.J., Fok, S.L., Hall, G., 2005. Graphite thermal expansion relationship for different temperature ranges. Carbon 43, 2902-2906.

Turcotte, D.L., Schubert, G., 1982. Geodynamics. Applications of Continuum Physics to Geologcial Problems. Wiley, New York, xii + 450 p.

Van Der Beek, P., Bishop, P., 2003. Cenozoic river profile development in the Upper Lachlan catchment (SE Australia) as a test of quantitative fluvial incision models. J. Geophys. Res. 108(B6), 2309-2337.

Van Hinsberg, M.G.E., Schouten, J.A., 1994. The phase diagram of nitrogen clathrate hydrate. Am. Inst. Physics Conference Proceedings 309, 271-274.

Van Orstrand, C.E., 1940. Geothermal methods for estimating the age of the Earth. Geophysics 5, 57-79.

Van Rijn, L.C., 1993. Principles of sediment transport in rivers, estuaries and coastal seas. Amsterdam: Aqua publications.

Vasil'chuk, Yu.K., 2005. Physical properties of glacial and ground ice. In: Types and Properties of Water, Khubryanayt, M.G. (ed.), vol. II, 392 p., UNESCO, Paris.

Vigdergauz, V.E., 2011. Methane formation by the reaction of coalbed carbon with water. Geomaterials 1, 21-23.

Vigdergauz, V.E., 2014. Evidence for and thermodynamic of coal mine methane formation in catastrophic events by the hydrolytic disproportionation of carbon. Episodes 37, 14-20.

Vinatier S., et al., 2007. Vertical abundance profiles of hydrocarbons in Titan's atmosphere at 15S and 80N retrieved from Cassini/CIRS spectra. Icarus 188, 120-138.

Wagner, W., Pruss, A., 2002. The IAPWS formulation 1995 for the thermodynamic properties of ordinary water substance for general and scientific use. J. Phys. Chem. Ref. Data 31, 387-535.

Walther, J.V., 2013. Earth's natural resources. Burlington, MA: Jones & Bartlett Learning.

Wang J. –H., et al., 2000. Vacuum ultraviolet photochemistry of CH_4 and isotopomers. II. Product channel fields and absorption spectra. J. Chem. Phys. 113, 4146. doi:10.1063/1.1288145.

Watson G. N., 1995. A Treatise on the Theory of Bessel Functions. Cambridge University Press.

Webster, C.R., et al., 2013. Isotope ratios of H, C, and O in CO_2 and H_2O of the Martian atmosphere. Science 341, 260-263.

Welhan, J.A., 1988. Origins of methane in hydrothermal systems. Chem. Geol. 71, 183-198.

"Where are the Voyagers?". *Voyager: The Interstellar Mission*. Jet Propulsion Laboratory (JPL). California Institute of Technology. <http://voyager.jpl.nasa.gov/where/>.

Whipple, K.X., Hancock, G.S., Anderson, R.S., 2000. River incision into bedrock: Mechanics and relative efficacy of plucking, abrasion, and cavitation. GSA Bulletin 112, 490-503.

William, G.P., 1988. Paleofluvial estimates from dimensions of former channels and meanders. In: Baker, V.R., Kochel, R.C., Patton, P.C. (Eds.), Flood Geomorphology. Wiley, New York, pp. 321-334.

Wilson E.H. and Atreya S.K., 2000. Sensitivity studies of methane photolysis and its impact on hydrocarbon chemistry in the atmosphere of Titan. J. Geophys. Res. 105, 20,263-20,273.

Wilson, E.H., Atreya, S.K., 2004. Current state of modeling the photochemistry of Titan's mutually dependent atmosphere and ionosphere. J. Geophys. Res. Planets 109, E06002.

Wilson, E.H. and Atreya, S.K., 2009. Titan's Carbon Budget and the Case of the Missing Ethane. J. Phys. Chem. A 113, 11221-11226.

Wolfram, 2010. Hypergeometric function evaluation. http://functions.wolfram.com/webMathematica/FunctionEvaluation.jsp?name=Hypergeometric2F1

Wolfram, 2016. Mathematica online integrator. http://integrals.wolfram.com/index.jsp?expr=x^2%2F%28a+%2B+b+x%29^2&random=false

Wood C.A., et al., 2010. Impact craters on Titan. Icarus 206, 334-344.

Xu, J., et al., 1998. Ammonium sulfate: Equilibrium and metastability phase diagrams from 40 to-50C. J. Phys. Chem. B 102, 7462-7469.

Yarger, J., Lunine, J.L., Burke, M., 1993. Calorimetric studies of the ammonia-water system with application to the outer solar system. J. Geophys. Res. 98, 109-117.

Yelle, R.V., Cui, J., Müller-Wodarg, I.C.F., 2008. Methane escape from Titan's atmosphere. J. Geophys. Res. 113, E10003, doi:10.1029/2007JE003031.

Younglove, B. A., and Ely, J. F., 1987. Thermophysical Properties of Fluids. II. Methane, Ethane, Propane, lsobutane, and Normal Butane. J. Phys.Chem. Ref. Data, Vol.16, No. 4, 577-798.

Yung, Y.L., Allen, M., Pinto, J.P., 1984. Photochemistry of the Atmosphere of Titan: Comparison Between Model and Observations. Astrophys. J. Suppl. Ser. 55, 465-506.

Yung, Y.L. and DeMore, W.B., 1999. Photochemistry of Planetary Atmospheres. Oxford University Press.

Zahnle, K.J., Walker, J.C.G., 1982. The evolution of solar ultraviolet luminosity. Rev. Geophys. 20, 280-292.

Zeleznik, F.J., 1991. Thermodynamic properties of the aqueous sulfuric acid system to 350 K. J. Phys. Chem. Ref. Data 20, 1157-1200.

Ashley E. Gilliam

Department of Earth & Planetary Sciences, northwestern University
2145 Sheridan Rd – Tech F379, Evanston, IL 60208-3130
Email: ashley@earth.northwestern.edu

Education

2011 – 2016 **Northwestern University**, *Evanston, IL*
Ph.D., Earth and Planetary Sciences
Advisor: Abraham Lerman

2011 – 2013 **Northwestern University**, *Evanston, IL*
M.S., Earth and Planetary Sciences
Thesis: Evolution of Titan's major atmospheric gases and cooling since accretion.
Advisors: Abraham Lerman and Donna Jurdy

2007 – 2011 **University of California, Santa Cruz**, *Santa Cruz, CA*
B.S. with honors, Earth Sciences with a concentration in Planetary Sciences
Thesis: Titan under a red dwarf star and as a rogue planet: requirements for liquid methane.
Advisors: Christopher McKay and Adriane Steinacker

Research Interests

Planetary habitability; planetary atmospheres; geological processes and composition of planetary surfaces; surface and subsurface liquids and their implications for life; Saturn's moon Titan

Research Experience

2011 – Present **Graduate Assistant**, Northwestern University, *Evanston, IL*
Modeling the evolution of Titan's major atmospheric gases and cooling since accretion.
Advisor: Abraham Lerman.

2011 – 2014 **Graduate Assistant**, Northwestern University, *Evanston, IL*
Used Cassini RADAR, VIMS, and ISS data to examine fluvial features around some of Titan's largest impact craters, and the implications for a subsurface reservoir of liquid.
Advisor: Donna Jurdy

2010 – 2011 **Research Associate**, Space Science Division, NASA Ames Research Center, *Moffett Field, CA*
Using Cassini-Huygens data, I modeled the thermal structure of Titan's atmosphere, and determined the conditions needed to maintain liquid methane on the surface of a Titan-like world in orbit around a red dwarf star or alone as a rogue planet. My investigation was published in the journal of *Planetary and Space Science* in 2011.
Advisor: Christopher McKay.

2010 **Summer Intern**, Space Science Division, NASA Ames Research Center, *Moffett Field, CA*
NASA Undergraduate Student Research Program (USRP)

TEACHING EXPERIENCE

2013 **Guest Lecturer**, Northwestern University, *Evanston, IL*
Presented information about the discovery and exploration of Titan, focusing on its atmospheric structure and composition, including measurements of atmospheric gas escape and its antigreenhouse effect in Earth 110 – Exploration of the Solar System.

2012 **Guest Lecturer**, Northwestern University, *Evanston, IL*
Presented information about the atmospheric structure and composition of Titan, including measurements of atmospheric nitrogen, methane, and hydrogen escape in Earth 316 – Earth's Changing Climate.

2012 **Teaching Assistant**, Northwestern University, *Evanston, IL*
Earth 202 – Earth's Interior

HONORS, AWARDS, AND GRANTS

2015 **Horace A. Scott Graduate Award for Outstanding Research**, Northwestern University

2013 – 2016 **NASA Earth and Space Science Fellowship (NESSF)**

2011 **Chancellor's Undergraduate Award**, University of California, Santa Cruz

2011 **Dean's Undergraduate Award**, University of California, Santa Cruz

2011 **Honors in the major**, University of California, Santa Cruz

2011 **Thesis Honors**, University of California, Santa Cruz

2008 – 2010 **Dean's Honors**, University of California, Santa Cruz
Awarded Fall 2008, Winter 2009, Winter 2010

PUBLICATIONS

2016 **Gilliam, A.E.**, Lerman, A., 2016. Formation and retention of methane on Titan and the terrestrial planets. (under review)

2016 **Gilliam, A.E.**, Wunsch, J., Lerman, A., 2016. CH_4-CH_3-C_2H_6 reaction system in Titan's atmosphere: a geochemical balance model with explicit solutions. (under review)

2016 **Gilliam, A.E.**, Lerman, A., 2016. Formation mechanisms of channels on Titan through dissolution by ammonium sulfate and erosion by liquid ammonia and ethane. *Planetary and Space Science* 132, 13-22.

2016 **Gilliam, A.E.**, Lerman, A., 2016. Titan's missing ethane: from the atmosphere to the subsurface. *Icarus* 275, 252-258.

2014 **Gilliam, A.E.**, Lerman, A., 2014. Evolution of Titan's major atmospheric gases and cooling since accretion. *Planetary and Space Science* 93-94, 41-53.

2011 **Gilliam, A.E.**, McKay, C.P., 2011. Titan under a red dwarf star and as a rogue planet: requirements for liquid methane. *Planetary and Space Science* 59, 835-839.

ABSTRACTS

Gilliam, A., Lerman, A., 2017. Methane Formation and Retention on Titan and Terrestrial Planets. Lunar and Planetary Science Conference (to be submitted).

Gilliam, A., Wunsch, J., Lerman, A., 2017. CH_4-CH_3-C_2H_6 in Titan's Atmosphere: Explicit Solutions and Near-Steady State of a Simplified Reaction System. Lunar and Planetary Science Conference (to be submitted).

Gilliam, A., Lerman, A., 2016. Formation Mechanisms of Channels on Titan through Dissolution by Ammonium Sulfate and Erosion by Liquid Ammonia and Ethane. Enceladus and the Icy Moons of Saturn, Boulder, CO. 17 July 2016.

Gilliam, A., Lerman, A., Wunsch, J., 2015. Evolution of Titan's Atmosphere in Relation to its Surface and Interior. Astrobiology Science Conference, Chicago, IL. 17 June 2015.

Gilliam, A., Lerman, A., 2014. Methane and Ammonia in Titan's Primordial and Cooling Atmosphere. Lunar and Planetary Science Conference, The Woodlands, TX. 18 March 2014.

Gilliam, A., Jurdy, D., 2014. Titan's Impact Craters and Associated Fluvial Features: Evidence for a Subsurface Ocean? Lunar and Planetary Science Conference. The Woodlands, TX. 18 March 2014.

Gilliam, A., Lerman, A., 2013. Evolution of Titan's major atmospheric gases and cooling since accretion. American Geophysical Union Fall Meeting, San Francisco, CA. 10 December 2013.

Gilliam, A., 2010. Titan under a red dwarf star: requirements for liquid methane. NASA Ames Poster Symposium, Moffett Field, CA. 26 July 2010.

PROFESSIONAL DEVELOPMENT

2015 **Going Places with Spatial Analysis**, Environmental Systems Research Institute – A six-week online certificate course taught by Esri designed to provide students with important spatial analysis skills via hands-on exercises using ArcGIS.

2014 **Management for Scientists and Engineers Program**, Kellogg School of Management, Northwestern University, Evanston, IL – A highly competitive certificate program taught by the Kellogg School of Management designed to equip promising doctoral students in science and engineering with important business and leadership skills prior to entering academia or industry. Required courses in this eight-week program provided a fundamental understanding of business strategy, finance, risk and uncertainty, marketing, accounting, and leadership.

PUBLIC OUTREACH

2014 – 2015 **Far Horizons Project Assistant Volunteer**, Adler Planetarium, Chicago, IL – Assisting in the design, build, and launch of scientific experiments flown to heights above 100,000 feet on high altitude balloons.

2013 **Poster Judge**, Northwestern University High School Science Project Showcase, Northwestern University, Evanston, IL – Adjudicated high school student science projects as part of Northwestern University's Undergraduate Research and Arts Exposition.

2012 **Panel Member**, New Cosmic Frontiers International Science Essay Competition on the Nature of our Universe and its Habitats, University of Chicago, Chicago, IL – Assessed and ranked high school essays as part of an international competition led by the University of Chicago and funded by the John Templeton Foundation. Students' essays addressed the following question: *Are we alone in the Universe? Or, are there other life and intelligence beyond our solar system?* Submissions were judged on originality, creativity, effectiveness, and depth/breadth.

SCIENTIFIC AND UNIVERSITY SERVICE

Journal Reviewer: Planetary and Space Science

PRESS COVERAGE

"The Methane Habitable Zone." *Astrobiology Magazine*, 10 November 2011. By K. Cooper.

"Titan-like Exoplanets." *Astrobiology Magazine*, 14 April 2011. By C. Choi.

"Are There More Titans than Earths in the Milky Way?" *The Planetary Society*, 14 April 2011. By E. Lakdawalla.

Planetary and Space Science 93-94 (2014) 41–53

Contents lists available at ScienceDirect

Planetary and Space Science

journal homepage: www.elsevier.com/locate/pss

Evolution of Titan's major atmospheric gases and cooling since accretion

Ashley E. Gilliam*, Abraham Lerman

Department of Earth and Planetary Sciences, Northwestern University, 2145 Sheridan Road, Evanston, IL 60208-3130, United States

ARTICLE INFO

Article history:
Received 28 August 2013
Received in revised form
14 January 2014
Accepted 3 February 2014
Available online 12 February 2014

Keywords:
Titan
Atmosphere
Methane and ammonia
Thermal escape
Cooling
Kinetic model

ABSTRACT

This paper discusses two possible pathways of loss of the two main gases from Titan's post-accretional atmosphere, methane (CH_4) and ammonia (NH_3), by the mechanisms of thermal escape and emission from the interior coupled with thermal escape. The results give the decline of initial atmospheric gas masses to their present-day levels of 0.1 bar CH_4 and 1.4 bar N_2 (or equivalent 1.7 bar NH_3, as a precursor of N_2). From the published data on planetary and Titan's accretion rates, the accretion temperature was estimated as T_{ac}=355 to 300 K. In the first 0.5–0.6 Myr after accretion, Titan's surface cools to 150 K and it takes about 5 Myr to cool to near its present temperature of 94 K. The present-day internal composition corresponds to the accreted Titan made of two solids, antigorite and brucite, that account for 59.5 wt%, and an outer shell of an aqueous solution of $NH_3+(NH_4)_2SO_4$ accounting for 40.0 wt%, and methane for a much smaller fraction of 0.6 wt%. In thermal escape of CH_4 and NH_3, based on the Maxwell–Boltzmann distribution of gas-molecule velocities, the initial gas mass N_0 in the atmosphere is lost by a first-order flux, $N_t=N_0\exp(-kt)$, where t is time (yr) and k (yr^{-1}) is a rate parameter that depends on temperature, gas molecular mass, atmosphere thickness, and Titan's escape velocity.

The computed initial T_{ac}=355 K is too high and the two gases would be lost from the primordial atmosphere in several hundred years. However, emissions of CH_4 and NH_3 from the interior, at reasonable rates that do not deplete the Titan gas inventory and function for periods of different length of time in combination with thermal escape, may result in stable CH_4 and NH_3 atmospheric masses, as they are at the present. The periods of emissions of different magnitudes of CH_4 range from 6×10^4 to 6×10^5 yr, and those of NH_3 are 55,000–75,000 yr.

At the lower T_{ac}=300 K, thermal escape of gases alone allows their atmospheric masses to decrease from the primordial to the present-day levels in 50,000–70,000 years, when Titan's temperature has decreased to 245–255 K. Below this temperature, the NH_3 atmospheric mass is comparable to the present-day N_2 mass. Thermal escape does not contradict the existence of the photolytic sink of CH_4 in the cooled Titan atmosphere. The thermal escape mechanism does not require arbitrary assumptions about the timing of the start and duration of the gas emissions from the interior.

1. Introduction

Titan is the only known moon to have a thick atmosphere and the only world besides the Earth to have liquid on its surface. At 9.5 AU away from the Sun, Titan maintains a surface temperature of 94 K. Its atmosphere has a surface pressure of 1.5 bar – one and a half times that of our planet – and consists of approximately 95% N_2 and 5% CH_4 (mole percentage). Unlike the Galilean satellites, Titan is alone in terms of its size and mass (Table 1), comprising more than 96% of the mass in orbit around Saturn, and its diameter is larger by a factor of nearly 3.4 than the second largest Saturnian moon, Rhea. Titan is believed to have formed during the last stages of Saturn's formation (Mosqueira and Estrada, 2003) within a disk of gas and dust that was the outgrowth of the formation of Saturn itself. Within the Saturn subnebula, collisions of particles led to the formation of rock-ice planetesimals, and subsequent growth led to the formation of satellites. Titan's formation in Saturn's warm subnebula (Alibert and Mousis, 2007) allowed efficient vaporization and loss of most volatile species (CO, N_2, and noble gases) with low clathration temperatures, but left NH_3, CH_4, H_2O, and CO_2 in solid and clathrate form. Thus, Titan formed with little CO and noble gases in its atmosphere, which was dominated by NH_3 and CH_4, consistent with measurements today.

Titan's proto-atmosphere is determined by the stability of the volatile-rich solid phases, and input from comets that condensed

* Corresponding author. Tel.: +1 847 467 2467.
E-mail addresses: ashley@earth.northwestern.edu (A.E. Gilliam), alerman@northwestern.edu (A. Lerman).

http://dx.doi.org/10.1016/j.pss.2014.02.001
0032-0633

Table 1
Titan parameters[a].

Parameter	
Mean radius (km)	2575
Volume (km^3)	7.152×10^{10}
Surface area (km^2)	8.332×10^{7}
Mass (kg)	1.345×10^{23}
Mean density (kg/m^3)	1881[b]
g at the surface (m/s^2)	1.352
Escape velocity $v_e = (2gr)^{1/2}$ (m/s)	2639
Mean distance from the Sun (km)	1.427×10^{9}

[a] From ESA (2013) and NASA (2012).
[b] From Titan's present-day individual layer densities and thicknesses (Fortes et al., 2007), Titan's mean density is 2139 kg/m^3 or 14% higher than the NASA value.

outside the Saturn subnebula (Coustenis, 2005). The proto-atmosphere, once formed, might have limited the amount of radiation escaping into space, resulting in an increased surface temperature, from 300 K up to 500 K (Kuramoto and Matsui, 1994). A warm accretion is consistent with the theory that NH_3 is the primordial source of Titan's atmospheric N_2 (Atreya et al., 1978; Tobie et al., 2009).

The origin of CH_4 in Titan's atmosphere is still widely debated. Prinn and Fegley (1981) argue that the dense Saturn subnebula was rich in CO relative to CH_4 with temperatures and pressures high enough to permit the conversion of CO to CH_4 in Titan's proto-atmosphere. Another hypothesis, by Mousis et al. (2002), suggests that no conversion of CO to CH_4 occurred in the Saturn subnebula, but Titan was formed from planetesimals rich in CH_4 that migrated from the outer part of the subnebula. Regardless of methane's origin, there may be a constant source of replenishment in the atmosphere as the photolysis of methane into other hydrocarbons occurs on a relatively short timescale (~50 My) and, as our results show, its escape rate from the Titan atmosphere is too fast at an accretion temperature of 355 K. One possible source of methane addition to the atmosphere is cryovolcanism.

To date, only the Cassini–Huygens spacecraft has peered beneath Titan's thick clouds, giving an incomplete picture of its atmospheric structure and surface conditions. Even less is known about early Titan, how it formed, and how it evolved from 4.55 Ga until today. This paper, dealing primarily with the behavior of CH_4 and NH_3 in the atmosphere, is based on the available information about Titan's present-day composition and internal structure, insofar as it is germane to the atmosphere (Table 1), and it proposes two new models for the chemical and physical compositions of Titan's atmosphere post-accretion. The two models, with NH_3 and CH_4 as the only gases, define the volume, height, density, and outer surface area of the atmosphere in each case. We show how NH_3 and CH_4 could leave the atmosphere by thermal escape alone as the only sink, or by a combination of emissions from the interior and thermal escape, producing in each case the final result of the present-day gas masses in the atmosphere. For this, we calculate Titan's accretion temperature, its mean heat capacity, and subsequent cooling rate. This paper is a contribution to the story of Titan and its atmosphere, that is critically important to the understanding of the present and future of this most interesting and complex body in the solar system.

2. Internal composition and structure

Interaction between Titan's atmosphere and its subsurface, possibly through cryovolcanism, warrants a summary outline of its internal structure in addition to the atmosphere. The standard model of Titan's internal structure, as discussed by Fortes et al. (2007), consists of a large silicate core (a serpentine mineral antigorite, $Mg_3Si_2O_5(OH)_4$), overlain by a thin layer of brucite ($Mg(OH)_2$), above which are a layer of high-pressure ice VI, an aqueous ammonium sulfate ocean ($(NH_4)_2SO_4$), and a crust made of methane clathrate, ice Ih, and solid ammonium sulfate.

The presence of ammonia in the subsurface ocean is thought to be a crucial component because of its ability to lower the freezing temperature of the liquid layer, impeding complete crystallization (Grasset and Sotin, 1996). Work by Grasset et al. (2000) suggests that the liquid layer is much more complex and might contain methane and nitrogen in addition to ammonia. For an accreted Titan, this paper assumes an internal composition based on the one at present (Fortes et al., 2007): the solid core of antigorite and brucite, and an outer fluid shell of water and other volatile species in aqueous solution at the accretion temperature higher than the present (300–355 K, Section 3.1), as shown in Table 2. An ammonia–water layer is consistent with the inference that solid ammonia–water compounds condensed during or shortly after the formation of Titan (Yarger et al., 1993). A primordial ammonia composition of 5–15 wt% is often cited (Grasset and Pargamin, 2005), which can prevent complete crystallization of the liquid layer. The differences in the composition of the ocean layer, attributed by different authors (e.g., Fortes et al., 2007; Tobie et al., 2009) to the relative amounts of NH_3 and $(NH_4)_2SO_4$, do not affect the conclusions in this paper, insofar as ammonia in Titan's interior is considered only as a potential source of emissions.

At 300–355 K, all of the H_2O should be in liquid form, and NH_3 and ammonium sulfate, $(NH_4)_2SO_4$, can be dissolved in it. An aqueous solution of $NH_3+(NH_4)_2SO_4$ is stoichiometrically equivalent to a solution of $NH_3+H_2SO_4$. Methane as a gas at 300–355 K is fairly insoluble in water at 1 bar total pressure

Table 2
Primordial component masses of Titan.

Component	Mass (kg)	% Mass
Methane gas (g or aq)	7.52×10^{20}	0.56
Sulfuric acid (aq)	1.19×10^{21}	0.88
Ammonia (aq)	1.62×10^{21}	1.21
Brucite (s)	3.63×10^{21}	2.70
Water (liq)	5.10×10^{22}	37.89
Antigorite (s)	7.63×10^{22}	56.76
Total	1.345×10^{23}	100

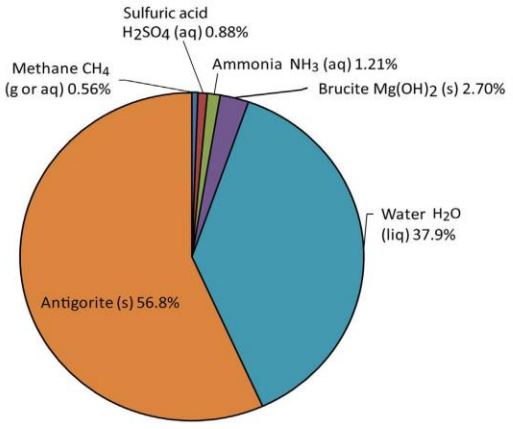

Fig. 1. Percent mass of each component in Titan's primordial internal structure.

(Duan and Mao, 2006), 2.0×10^{-5}–7.6×10^{-6} kg CH_4/kg H_2O, corresponding to only small fractions of the CH_4 mass available in Titan (7.52×10^{20} kg, Table 2), 0.14–0.05%, respectively. However, at the same temperatures and 2 kbar total pressure, the mass of CH_4 soluble in water may be 40–50% of the mass available.

A homogeneous Titan of composition as given in Table 2 and Fig. 1 is subdivided into an inner solid core of antigorite and brucite, of radius 1898 km, and an outer fluid shell of thickness h_f=677 km, containing H_2O, NH_3, H_2SO_4, and CH_4, where the fluids are separated from the solids antigorite and brucite. In this subdivision, Titan's fixed mass, volume, and mean density (Table 1) are maintained and satisfied by the densities of the inner solid core ρ=2793 kg/m^3 and the outer fluid shell ρ=1272 kg/m^3. Pressure at the base of the outer fluid shell is close to 12 kbar or 1.2 GPa, from an approximate relationship $P\approx\rho g h_f$.

The $NH_3+(NH_4)_2SO_4$ concentration in the fluid shell (Table 2) corresponds to an aqueous solution of 5.2 wt% (or 2.1 molal). Its density of 1272 kg/m^3 is comparable to that of a NaCl aqueous solution of 15 wt% (3 molal) at 25 °C and 6 kbar pressure, 1274 kg/m^3 (Lvov and Wood, 1990). The density is higher than that of pure H_2O at 300 K and 10 kbar, 1237 kg/m^3 (Wagner and Pruss, 2002), and of the 25 °C densities of such saline brines on the Earth surface as the Great Salt Lake, 1087–1140 kg/m^3 (Naftz et al., 2011), and the Dead Sea, 1242 kg/m^3 (Katz, 2013). However, it is lower than the densities of the Don Juan Pond in Antarctica, of composition variably given as $CaCl_2$–$MgCl_2$–NaCl (Marion, 1997; Matsubaya et al., 1979), 1278–1360 kg/m^3, calculated from the component-solution densities of 25 °C (OXY, 2012; Conde, 2009; Rogers and Pitzer, 1982; Chen et al., 1980).

3. Accretion temperature, primordial heat capacity, and cooling

3.1. Titan's accretion temperature

During the accretion process, part of the impact energy is converted into heat, although the details of the process are not well constrained. Grasset and Sotin (1996) assumed that the fraction of accretional energy retained as heat varies between 0.1 and 0.5 and developed an approximate accretional temperature profile for Titan. They suggested that once the growing proto-Titan reached a radius of roughly 1000–1500 km, melting and vaporization of the surface materials allowed for the development of a liquid water layer and an atmosphere. Titan's accretion temperature is an important factor in estimation of the rate of cooling and subsequent behavior of CH_4 and NH_3 in its atmosphere. Derivation of the accretion temperature T_{ac} (Hanks and Anderson, 1969), based on a balance of the release of gravitational accretion energy and cooling by ideal black body radiation emission, with no other internal heat sources or storage, is given in Eqs. (1) and (2), Table 3.

Hanks and Anderson's (1969) determination of the T_{ac} is derived from the sequence of accretion times and rates for Venus, Earth, Mars, and the Moon. If there were additional internal sources of heat production or if some of the energy was stored within Titan instead of all of it being emitted by Stefan–Boltzmann radiation (that is, if the emitting surface was not an ideal black body, but was characterized by an emissivity factor $0<\varepsilon\leq1$ before the Stefan–Boltzmann constant σ in Eq. (1)), the accretion temperature would have been higher than the calculated value in Table 3.

At present, with no albedo and no greenhouse effect, the radiation equilibruim temperature of Titan at its mean distance from the Sun (Table 1) is T_{eq}=90 K. About 4.5 billion years ago, when the Sun was approximately 75% as luminous as today (Gough, 1981), Titan's $T_{eq}\approx84$ K. The value of Titan's accretion rate and duration, as estimated from Hanks and Anderson (1969) is 4.24 ± 0.02 m/yr and about 0.6 Myr, respectively. This accretion rate gives in combination with T_{eq}=85 K and other parameters, varying slightly about their values listed in Table 1 (e.g., Turcotte and Schubert, 1982, pp. 430–431), an accretion temperature T_{ac}=353–355 K. This value agrees well with estimates of Kuramoto and Matsui (1994) that proto-Titan temperatures might have been higher than 300 K, and as high as 500 K.

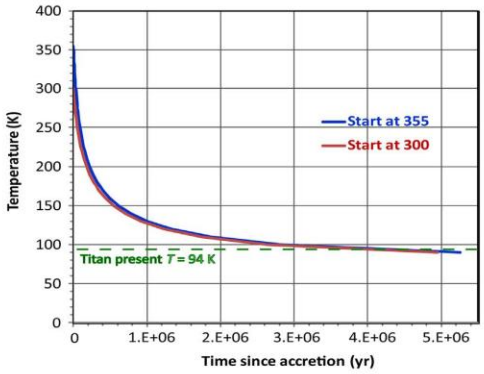

Fig. 2. Titan cooling after accretion for two different accretion temperatures, T_{ac}=355 and T_{ac}=300 K (Eq. (6)). Titan's present surface temperature (94 K) is shown for reference (dashed green line). (For interpretation of the references to color in all figure legends, the reader is referred to the web version of this article.)

Table 3
Accretion temperature models.

Process or Parameter	Mathematical formulation		Explanatory comments
Balance of gravitational energy release and Stephan–Boltzmann cooling by emission.[a] $\rho dr/dt$ is the rate of mass accretion per unit area of the Titan surface (kg m^{-2} s^{-1}). No internal heat production or storage. Emission of an ideal black body.	$\frac{GM(r)}{r}\rho\frac{dr}{dt}=\sigma(T^4-T_{eq}^4)$	(1)	$G=6.674\times10^{11}$ J m kg^{-2} $M=1.345\times10^{23}$ kg $r=2.575\times10^6$ m $\rho=1881$ kg m^{-3} $\sigma=5.670\times10^{-8}$ W m^{-2} K^{-4} T_{eq}=85 K T is accretion temperature
Accretion temperature T_{ac} from Eq. (1)	$T_{ac}=\left(T_{eq}^4+\frac{GM(r)\rho}{\sigma r}\frac{dr}{dt}\right)^{1/4}$	(2)	T_{ac}=353 to 355 K From parameter values above

[a] Hanks and Anderson (1969). Other models given by Kuramoto and Matsui (1994), Grasset and Sotin (1996) and Barr et al. (2010).

Barr et al. (2010) estimated the accretion time of Titan as ≥ 0.8 Myr to ≥ 1.3 Myr, depending on the ammonia content of the satellite. From Barr's et al. (2010) range of accretion times, 1.16 Myr gives a mean rate of accretion of 2.22 m/yr and T_{ac}=300 K from Eq. (2). The two estimates of the accretion temperature (355 and 300 K) lead to different thermal escape mechanisms of methane and ammonia, as will be shown in Section 5.

3.2. Primordial heat capacity

Heat capacity (C_p, J kg^{-1} K^{-1}) of the primordial Titan is one of the parameters needed to calculate its cooling rate (Section 3.3) and to estimate the escape velocities of the atmospheric gases during cooling (Section 5). The C_p values of Titan's components (Table 2) at 300 and 350 K are given in Table 4 as mass-weighted means of 2232 and 2357 J kg^{-1} K^{-1}. The C_p data of the individual components are listed in Table A1, Appendix A. Not all the data are available for the range of pressures up to 12 kbar in the outer fluid shell. For CH_4, the data for methane gas were used, as we are not aware of such data for aqueous CH_4 solutions at high pressures. Data at 350 K were used as an approximation for the calculated accretion $T_{ac} \approx 355$ K. The effects of uncertainty in the C_p values on the Titan cooling rate and the thermal escape rates of CH_4 and NH_3 are addressed in Sections 3.3 and 5.

3.3. Titan's cooling rate

For heat dissipation by radiation emission from an ideal black body, the time needed for the cooling satellite to reach a certain temperature can be computed from Eq. (6), Table 5. The results are shown in Fig. 2 for the starting temperatures of 355 and 300 K. The overall cooling rate is unaffected by the different accretion temperatures, and the two curves are essentially identical at $t > 1$ Myr after accretion. The initial cooling period of both curves between 0.5 and 0.6 Myr is relatively fast, where the Titan temperature decreases to 150 K. It takes about 5 Myr for it to decrease to 90 K. The cooling rate depends on the Titan heat capacity (Table 4). A higher value of C_p results in a longer cooling time and therefore in a slower cooling rate. The effects of a variation of $\sim$150 J kg^{-1} K^{-1}, comparable to the difference in the C_p values at 300 and 350 K, are very small and they would hardly be noticeable at the scale of the graph in Fig. 2. For example, the cooling time from 300 to 220 K, for the range of $C_p = 2232 \pm 150$ J kg^{-1} K^{-1} (the difference between the estimates of C_p at 350 and 300 K is 125 J kg^{-1} K^{-1}, Table 4), is 1.24×10^5, 1.16×10^5, and 1.08×10^5 years.

Table 4
Primordial heat capacity (C_p).

Component	Heat capacity (J kg^{-1} K^{-1})		% of total mass
	300 K	350 K	
Methane gas[a]	2956	3020	0.56
Ammonia–water–sulfuric acid[b]	4031	4192	39.98
Brucite[c]	1349	1473	2.70
Antigorite[d]	1000	1100	56.76
Mean C_p (J kg^{-1} K^{-1})	2232	2357	100

Heat capacity data.
[a] Setzmann and Wagner (1991).
[b] Conde (2013); Zeleznik (1991); Wagner and Pruss (2002).
[c] Horita et al. (2002).
[d] Osako et al. (2010). More details in Table (A1), Appendix A.

4. Present-day and primordial atmosphere

4.1. Composition of the present-day atmosphere

Present-day Titan's atmosphere can be divided into two main layers: the lower atmosphere (< 880 km) consisting of the troposphere, stratosphere, and mesosphere; and the upper atmosphere (> 880 km) that includes the thermosphere, ionosphere, and exosphere (Brown et al., 2009). This paper focuses on the lower atmosphere (also known as the homosphere), where the main mass of the gases resides.

Two main gases make up the bulk of Titan's atmosphere: N_2 and CH_4, which have approximate mole fractions of 0.98 and 0.014 (Niemann et al., 2005), respectively. The third most abundant molecule is hydrogen (H_2), of a mole fraction of 0.001 in the stratosphere (Courtin et al., 2008). N_2, CH_4, and H_2 are expected to be well mixed in the homosphere, although CH_4 is condensable in the troposphere (Samuelson and Mayo, 1997; Gilliam and McKay, 2011), contributing to Titan's methane hydrological cycle. Minor components in Titan's atmosphere include several hydrocarbons, nitriles, and oxygen compounds (Brown et al., 2009).

With NH_3 and CH_4 as the only gases in Titan's atmosphere, we consider two cases for the atmosphere composition in the present and three in the past. In Table 6, columns 2 and 3 give the composition and other parameters of the present-day atmosphere at 94 K, and columns 4–6 are for the primordial conditions.

In the present-day atmosphere (column 2), partial pressures of methane, as reported by Griffith et al. (2003), Jacquemart et al. (2008),

Table 5
Titan cooling rate.

Process or Parameter	Mathematical formulation	Explanatory comments
Heat content of Titan after accretion	$\frac{(4/3)\pi r^3 \rho C_p T}{4\pi r^2} = \frac{r\rho C_p T}{3}$ J m^{-2}	(3) $r = 2.575 \times 10^6$ m $\rho = 1881$ kg m^{-3} C_p = 2232 (300 K) and 2357 (350 K) J kg^{-1} K^{-1} (Table 4), assumed constant T is temperature
Loss of heat balanced by radiative emission from an ideal black body	$-\frac{r\rho C_p}{3}\frac{dT}{dt} = \sigma(T^4 - T_{eq}^4)$ J s^{-1} m^{-2}	(4) t is time (seconds) $\sigma = 5.670 \times 10^{-8}$ W m^{-2} K^{-4} T_{eq} = 85 K Other parameter values as above
Integral form of Eq. (4)	$-\frac{r\rho C_p}{3\sigma}\int_{T_{ac}}^{T}\frac{dT}{T^4 - T_{eq}^4} = \int_0^t dt$	(5) T_{ac} is accretion temperature
Integrated Eq. (5) for calculation of cooling times t at temperatures T decreasing from T_{ac} to T_{eq}.	$t = \frac{r\rho C_p}{6\sigma T_{eq}^3}\left[\frac{1}{2}\ln\frac{T+T_{eq}}{T-T_{eq}}\frac{T_{ac}-T_{eq}}{T_{ac}+T_{eq}} + \tan^{-1}\frac{T-T_{ac}}{T_{eq}+TT_{ac}/T_{eq}}\right]$	(6) Integration by parts of Eq. (5) or, identically, from an indefinite integral at *Wolfram Mathematica Online Integrator* http://integrals.wolfram.com/index.jsp.

Table 6
Present and primordial Titan atmosphere models.

1 Parameter	2 Present with N_2	3 Present with NH_3 equivalent	4 Mean of 5 models[a] [range of values]		5 Model in this paper	6 Model in this paper
T (K)	94	94	355	300	355	300
CH_4 (bar)	0.1[b]	0.1	35.9 [2.40–80]		19.58	19.58
NH_3 (bar)	1.4 (N_2)	1.70	5.7 [0.6–10]		5.82	5.82
P (bar)	1.5	1.80	41.6 [3–90]		25.40	25.40
Atm. mass (kg)	9.24×10^{18}	1.11×10^{19}	2.56×10^{20} [$(0.19–5.55)\times10^{20}$]		1.57×10^{20}	1.57×10^{20}
Mass CH_4 (kg)	6.16×10^{17} [c]	6.16×10^{17} [c]	2.21×10^{20} [$(0.15–4.93)\times10^{20}$]		1.19×10^{20}	1.19×10^{20}
Mass NH_3 (kg)	8.63×10^{18} (N_2)	1.05×10^{19} [d]	3.51×10^{19} [$(0.37–6.16)\times10^{19}$]		3.76×10^{19}	3.76×10^{19}
Atm. volume (m^3)	1.77×10^{18}	2.84×10^{18}	1.12×10^{19} [$(1.12–1.13)\times10^{19}$]	9.50×10^{18} [$(9.47–9.52)\times10^{18}$]	1.12×10^{19}	9.45×10^{18}
Scale height or thickness (km)	21.07	33.51	128.34 [127.87–128.53]	109.25 [108.85–109.42]	127.75	108.74
Atm. top surface area (m^2)	8.47×10^{13}	8.55×10^{13}	9.18×10^{13}	9.05×10^{13}	9.18×10^{13}	9.05×10^{13}
Atm. density: mass/vol. (kg/m^3)	5.22	3.91	22.80 [1.65–49.25]	26.98 [1.95–58.28]	14.0	16.57

[a] Adapted from Niemann et al. (2005) and Brown et al. (2009).
[b] References: Griffith et al. (2003), Jacquemart et al. (2008) and Lorenz et al. (1999).
[c] CH_4 mass is 0.52% of the mass in columns 5 and 6.
[d] NH_3 mass is 27.9% of the mass in columns 5 and 6.

Table 7
Relationships between atmospheric pressure, mass, volume, thickness, and outer surface area.

Process or parameter	Mathematical formulation		Explanatory comments
Atmospheric mass (m, kg) as a function of atmospheric pressure, Titan surface area, and g at the surface. m_1 and m_2 are the individual component gas masses (kg)	$m=\frac{PS_T}{g}$ $m_1=p_1S_T/g$ and $m_2=p_2S_T/g$	(7)	P is total atm. pressure (Pa) p_1 and p_2 partial pressures of gases (Pa) $S_T=8.332\times10^{13}$ m^2 (Table 1) g at the surface = 1.352 m s^{-2} (Table 1)
Relationship between the total and component gas masses, atmosphere volume, temperature and gas constant, from ideal gas law	$m=n_1M_1+n_2M_2$ $=\frac{(p_1M_1+p_2M_1)V_{atm}}{RT}$	(8)	m is atmosphere mass (kg) n_i mols of a gas component in the atm. M_i molecular mass of gas V_{atm} is atmosphere volume (m^3) R the gas constant = 8.3145 J mol^{-1} K^{-1}
Atmosphere volume from Eq. (8)	$V_{atm}=\frac{mRT}{p_1M_1+p_2M_1}$	(9)	V_{atm} in m^3
Atmosphere volume as a function of the Titan radius (r, m) and atmosphere thickness (h, m)	$V_{atm}=\frac{4\pi}{3}[(r+h)^3-r^3]$	(10)	V_{atm} in m^3 $r=2.575\times10^6$ m (Table 1)
Thickness or scale height of the atmosphere from Eq. (10)	$h=\left(\frac{3V_{atm}}{4\pi}+r^3\right)^{1/3}-r$	(11)	h in m
Atmosphere outer surface area	$S_{atm}=4\pi(r+h)^2$	(12)	S_{atm} in m^2. Other parameters as above

and Lorenz et al. (1999), are in the range from 0.05 to 0.09 bar. We round this to 0.1 bar that with the N_2 partial pressure of 1.4 bar gives total atmospheric pressure $P=1.5$ bar. From the total and individual components' partial pressures, the masses of the two gases, total atmospheric mass, and volume were calculated using Eqs. (7)–(10) in Table 7, and atmospheric scale height or thickness calculated from Eq. (11). It may be noted that the scale height is not the total height of the atmosphere, but is the thickness of an isothermal atmosphere of known mass and composition or the height from the satellite surface to where the pressure decreases to $1/e$ of its value at the surface. For N_2 in the atmosphere attributed to its precursor, NH_3 (Atreya et al., 1978), the latter's mass equivalent to the present-day mass of N_2 is shown in column 3. The mass and volume of this atmosphere are accordingly somewhat greater than those of the N_2-containing atmosphere in column 2.

4.2. Primordial atmosphere composition

The exact composition of Titan's early atmosphere is not well known, although it is generally accepted that it was much more massive and denser than at present, and dominated by ammonia and methane. The range of NH_3 and CH_4 partial pressures, shown in column 4 of Table 6, is based on the work by Niemann et al. (2005) and Brown et al. (2009). Niemann et al. (2005), from the $^{14}N/^{15}N$ ratio measured in the Titan atmosphere by the Gas Chromatograph Mass Spectrometer (GCMS) on the Huygens probe, conclude a massive early atmosphere, between two and ten times today's value. Brown et al. (2009), also from the $^{14}N/^{15}N$ ratio measured by the GCMS, estimate that early Titan should have had a N_2 pressure between 5 and 10 bar, and a CH_4 pressure between 30 and 80 bar. We use the upper and lower limits for pNH_3 and pCH_4 given by these sources and calculate their means and other parameters (column 4, Table 5), as explained in the preceding section for columns 2 and 3.

The most commonly accepted view of the origin of N_2 in Titan's atmosphere is the photodissociation of NH_3 into N_2, although Strobel (1982) believed N_2 to be primordial. Atreya et al. (1978) proposed that after cooling of Titan's surface, and once outgassing began, ammonia in the atmosphere could have been photolyzed, converting NH_3 into nitrogen-bearing compounds, including N_2. Combining all of the intermediate steps involved in their model

Table 8
Parameters of Maxwell–Boltzmann distribution and thermal gas escape.

Process or parameter	Mathematical formulation	Explanatory comments
Most probable speed at the velocity distribution peak (m/s)	$v_0 = \sqrt{2RT/M}$	(15) Solution of $df(v)/dv = 0$, where $f(v)$ is given in Eq. (13). R is the gas constant (8.3145 J mol $^{-1}$K $^{-1}$) and M is molecular mass of the gas (kg mol $^{-1}$)
Mean velocity of the distribution (m/s)	$\overline{v} = \int_0^\infty v f(v)dv = \sqrt{\frac{8RT}{\pi M}} = \frac{2}{\sqrt{\pi}} v_0$	(16) $f(v)$ is the Maxwell–Boltzmann distribution in Eq. (13)
Cumulative distribution of gas velocities (fraction)	$\mathcal{F}(v) = \int_0^v f(v)dv = \mathrm{erf}\left(\frac{v}{v_0}\right) - \frac{8}{v_0^3\sqrt{\pi}} e^{-(v/v_0)^2}$	(17) $\mathcal{F}(v) \to 1$, as $v \to \infty$
Fraction of the distribution at velocities greater than Titan's escape velocity v_e (Table 1)	$\mathcal{F}(v \geq v_e) = \frac{4}{v_0^3\sqrt{\pi}} \int_{v_e}^\infty v^2 e^{-(v/v_0)^2} dv = \frac{2v_e}{v_0\sqrt{\pi}} e^{-(v_e/v_0)^2} + \mathrm{erfc}(v_e/v_0)$	(18) Range of velocities: $v_e \leq v < \infty$
Approximation of the fraction in Eq. (19) for $v_e/v_0 > 2$ to > 2.5: $\mathrm{erfc}(v_e/v_0) = e^{-(v_e/v_0)^2}/(\sqrt{\pi}\, v_e/v_0)$	$\mathcal{F}(v > v_e) = \frac{2}{\sqrt{\pi}} \frac{v_e}{v_0} e^{-(v_e/v_0)^2} + e^{-(v_e/v_0)^2}/(\sqrt{\pi}\, v_e/v_0)$	(19) Goody (1976) gives the following approximation for $\mathcal{F}(v > v_e)$, for the same conditions of $v_e/v_0 > 2$: $\mathcal{F}(v > v_e) = \frac{4}{\pi} \frac{v_e}{v_0} e^{-(v_e/v_0)^2}$ This result is greater than that of Eq. (19) by a factor of $2/\sqrt{\pi} = 1.13$ or about 13%.
Mean velocity in the velocity interval $v_e \leq v < \infty$ (m/s)	$\overline{v}_{>v_e} = \int_{v_e}^\infty v f(v)dv \Big/ \int_{v_e}^\infty f(v)dv = \frac{2v_e\left[1+(v_e/v_0)^2\right]}{1+2(v_e/v_0)^2}$	(20) Note: in this velocity interval, the Maxwell–Boltzmann distribution is *not* a pdf. The ratio of the high-velocity mean to the escape velocity, $\overline{v}_{>v_e}/v_e$, is always > 1.

gives the overall reaction: $NH_3+NH_2 \rightarrow N_2+2H_2+H$. A crucial intermediate step of this reaction is the production of hydrazine (N_2H_4) from amidogen radicals (NH_2), created through the photolysis of NH_3, that also acts as the rate-limiting step in the production of N_2. An ideal temperature range for the production of N_2 from NH_3 on Titan is 150–250 K. NH_3 is a vapor below 150 K and whatever small amount of N_2H_4 is formed from it would condense, preventing N_2 formation. At a temperature above 250 K, water vapor pressure is sufficiently large, so that OH from its photolysis reacts with NH_2 and NH_3, producing NH whilst decreasing the amount of N_2 formed. The present atmospheric temperature on Titan should prevent NH_3 photolysis from producing N_2, and any N_2H_4 formed at the 94 K surface should sublimate prior to photolysis (Strobel, 1982). From the cooling curve in Fig. 2, Titan should have experienced these favorable temperatures between ~89,300 and 613,000 years after accretion at 355 K. This agrees with estimates of Brown et al. (2009), who report that the dissociation of NH_3 into N_2 must have occurred no later than 10 Myr after accretion.

If the Sun, in its very early history, emitted up to 10^4 times as much UV radiation than it does today (Zahnle and Walker, 1982), up to 20 bar of N_2 could be produced in less than 2 million years in Titan's primordial atmosphere (Atreya et al., 1978). This finding was confirmed by Strobel (1982), who suggested that if Titan's surface temperature was 150 K or greater for approximately 4% of its evolutionary history (or about 180 Myr), then NH_3 photolysis could account for the current levels of N_2 in its atmosphere. Our results on the cooling rate of Titan (Fig. 2) suggest that 150 K could have been reached 6×10^5 years after the start of cooling.

From the data in column 4, Table 6, the results for a primordial atmosphere at 355 K suggest an atmospheric mass of 2.56×10^{20} kg and a scale height of 128 km. At 300 K, the same atmospheric mass corresponds to a scale height of 109 km.

The calculated composition of a primordial atmosphere at 355 and 300 K is given in columns 5 and 6 in Table 6, where the initial masses of CH_4 and NH_3 satisfy the conditions of gas thermal escape or emission-with-escape to the present-day levels as given in column 3 (Section 5). In the two primordial atmosphere models, starting with the masses of CH_4 and NH_3, the other parameters were calculated from the equations in Table 7.

The two primordial atmospheric models have scale thicknesses five to six times greater than the present-day atmosphere, a total pressure of 25 bar, in comparison to 1.5 bar at present, and densities of 14–16.6 kg/m^3, compared to 5.2 kg/m^3 at present.

5. Gas escape

5.1. Maxwell-Boltzmann gas-molecular velocity distribution: H_2 and CH_4

Gases escape from the surface of a planet if their molecular or atomic velocities exceed the escape velocity of the planet $v_e = (2gr)^{1/2}$. The latter is a function of the planet's radius r and the acceleration due to the force of gravity at its surface, g (Table 1), and for Titan it is v_e=2.639 km/s. This relationship explains why some planets and moons have atmospheres and others do not: a larger fraction of the molecules on a body with a massive atmosphere and low temperature, like Titan, may have smaller fractions of the atmosphere that can escape. The distribution of molecular speeds depends strongly on (1) the mass of the molecule and (2) temperature, as represented by the Maxwell–Boltzmann distribution of gas velocities[1]

$$f(v) = 4\pi \left(\frac{M}{2\pi RT}\right)^{3/2} v^2 e^{-Mv^2/(2RT)} \tag{13}$$

[1] In modern notation, the Maxwell–Boltzmann distribution is a probability density function or pdf (e.g., Wikipedia, 2013, with references to publications in 1949–2008). The forms given by Maxwell (1860, p. 23; 1867, pp. 64, 69; 1890, p. 381) and Boltzmann (1896, p. 49) are somewhat different from a pdf, and their notation carried into the early and even later parts of the 20th century (Jeans, 1911, p. 658; 1916, p. 33; Chapman, 1916, p. 283; Chapman and Cowling, 1970, p. 69). The latter (1970, pp. 131, 407) and Brush (2008) also discussed David Enskog's earlier contributions to Maxwell's theory.

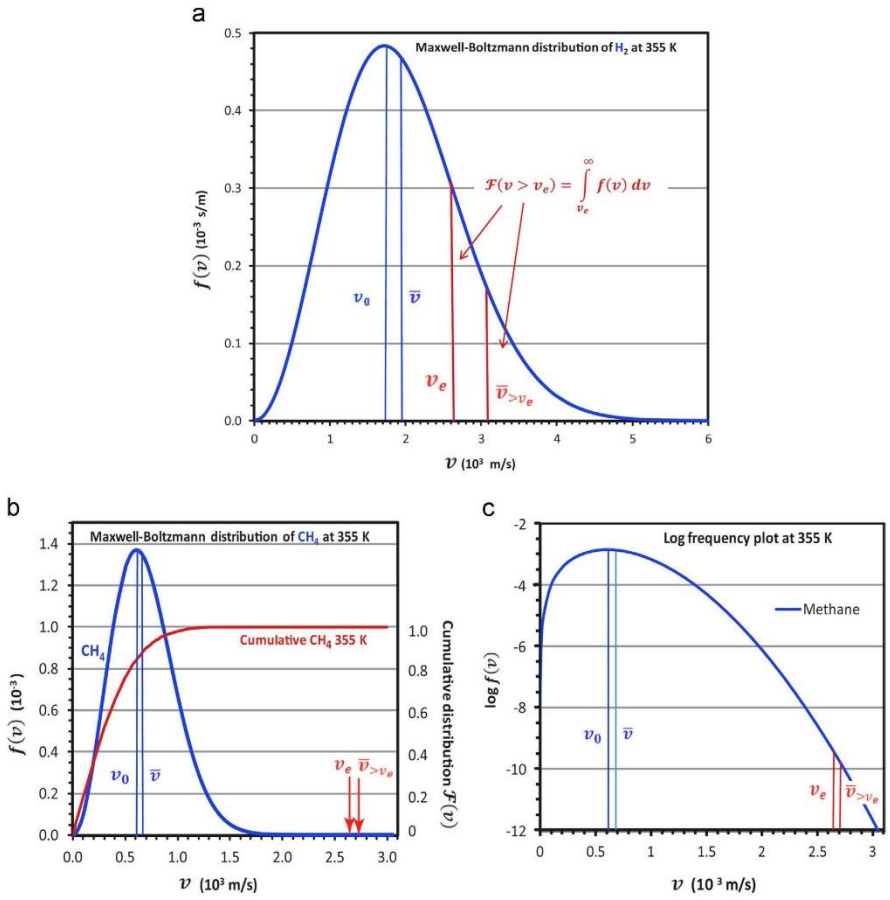

Fig. 3. (a) Maxwell–Boltzmann distribution of H_2 at 355 K, showing the peak velocity v_0, mean velocity $\overline{v}$, Titan escape velocity v_e, and mean velocity $\overline{v}_{>v_e}$ in the interval $v_e \le v < \infty$. (b) Linear plot of $f(v)$ of CH_4 at 355 K. Cumulative frequency for CH_4 shown as a check of calculation. (c) Logarithmic plot of $f(v)$ of CH_4 at 355 K. Eqs. (13)–(20).

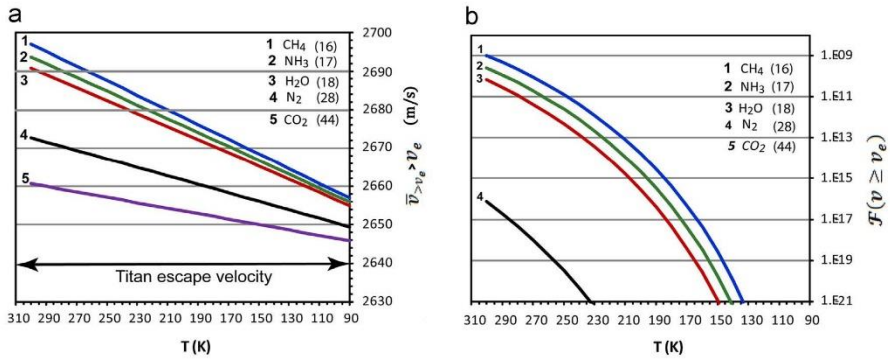

Fig. 4. (a) Mean escape velocity of gases $\overline{v}_{>v_e}$, above the Titan escape velocity v_e, as a function of temperature and molecular mass, Eq. (20). (b) Dependence of the fraction of the gas mass above the Titan escape velocity, $\mathcal{F}(v > v_e)$, on temperature and molecular mass, Eq. (19). CO_2 falls off the figure scale. Numbers in parentheses are molecular masses in gram/mol.

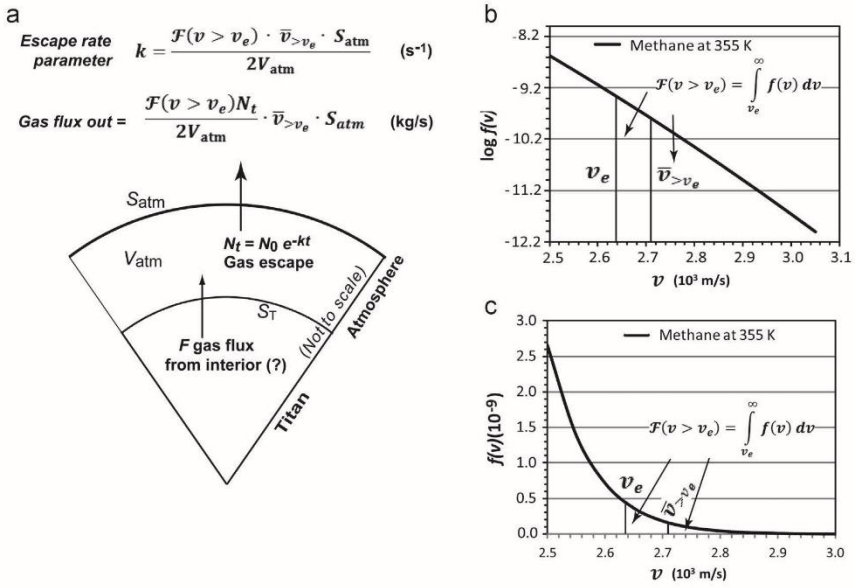

Fig. 5. (a) Schematic diagram of Titan and its atmosphere, gas fluxes, and main equations. (b) Logarithmic velocity frequency distribution at higher velocities. (c) Linear velocity frequency distribution at higher velocities.

Table 9
Parameters of gas escape rate.

Process or Parameter	Mathematical formulation		Explanatory comments
Gas mass remaining in the atmosphere (kg)	$N_t = N_0\, e^{-kt}$	(21)	N_0 initial gas mass (kg) k is escape rate parameter (s^{-1}) t is time (s)
Concentration of the escaping gas in the atmosphere (kg/m^3)	$\frac{(1/2)\mathcal{F}(v > v_e)N_t}{V_{atm}}$	(22)	$0.5\mathcal{F}(v > v_e)$ escaping gas fraction N_t gas mass in the atmosphere (kg) V_{atm} atmosphere volume (m^3)
Mass flux our of the atmosphere (kg/s)	$\frac{\mathcal{F}(v > v_e)\overline{v}_{>v_e}S_{atm}}{2V_{atm}} N_t = kN_t$	(23)	
Escape rate parameter k (s^{-1})	$k = \frac{\mathcal{F}(v > v_e)\overline{v}_{>v_e}S_{atm}}{2V_{atm}}$ $k = \frac{v_e}{v_0} e^{-(v_e/v_0)^2}\left[\frac{2}{\sqrt{\pi}} + \frac{1}{(v_e/v_0)^2\sqrt{\pi}}\right]\frac{2v_e[1+(v_e/v_0)^2]}{1+2(v_e/v_0)^2}\frac{S_{atm}}{2V_{atm}}$	(24)	
Calculation of N_t	$N_{i+1} = N_i e^{-0.5(k_{i+1}+k_i)(t_{i+1}-t_i)}$	(25)	Calculated for every two consecutive time steps, $t=i$ and $t=i+1$, and a mean value of k for that period, $(k_{i+1}+k_i)/2$
Gas emission from the interior to the atmosphere and thermal loss from the latter	$N_t = \frac{F}{k}(1-e^{-kt}) + N_0 e^{-kt}$	(26)	F constant input rate (% of N_0 per yr) Other parameters as in Eq. (21)
Calculation of N_t, emission and escape model	$N_{i+1} = \frac{F}{0.5(k_{i+1}+k_i)}[1-e^{-0.5(k_{i+1}+k_i)(t_{i+1}-t_i)}] + N_0\, e^{-0.5(k_{i+1}+k_i)(t_{i+1}-t_i)}$	(27)	

or, using Eq. (15) in Table 8,

$$f(v) = \frac{4}{v_0^3\sqrt{\pi}} v^2 e^{-(v/v_0)^2} \quad (14)$$

The Maxwell–Boltzmann distribution describes gas molecules in thermal equilibrium, moving freely without interacting with one another, except for elastic collisions. Methane and ammonia are treated as individual gases in Titan's atmosphere insofar as their molecular masses are close: CH_4, $M=0.016$ kg/mol, and for NH_3, $M=0.017$ kg/mol. Other relevant relationships and parameters are given in Table 8.

Fig. 3 shows the Maxwell–Boltzmann distribution at 355 K of H_2 gas ($M=0.002$ kg/mol), the third most abundant species in Titan's present-day atmosphere, and of the heavier CH_4 that does not lend itself to the same graphic representation as H_2 on a linear scale. Fig. 3 shows that peak velocity v_0 and mean velocity $\overline{v}_{>v_e}$ at

the high end of the distribution, where $v_e \le v < \infty$, are greater for the lighter H_2 that for the heavier CH_4 and NH_3. For these and some heavier gases, mean velocities $\overline{v}_{>v_e}$ are shown in Fig. 4.

At the starting temperature of 355 K, easy and fast escape of the much lighter H_2 is possible, but CH_4, of a higher molecular mass, has a small fraction above the escape velocity, $\mathcal{F}(v \ge v_e)$, that accounts for a slow, but significant escape over a long period of time.

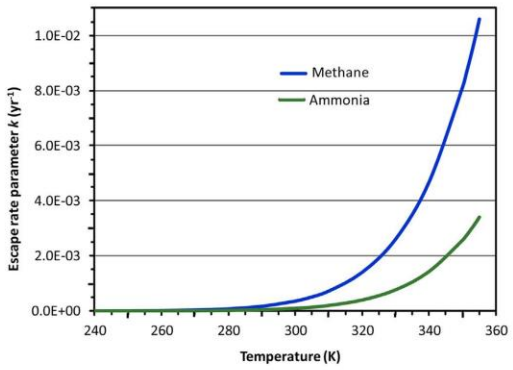

Fig. 6. The escape rate parameter, k, vs. temperature, T, for NH_3 and CH_4, assuming a T_{ac}=355 K. In this model, k is not effective below $T \approx 270$ K, Eq. (24). Compare Fig. 10.

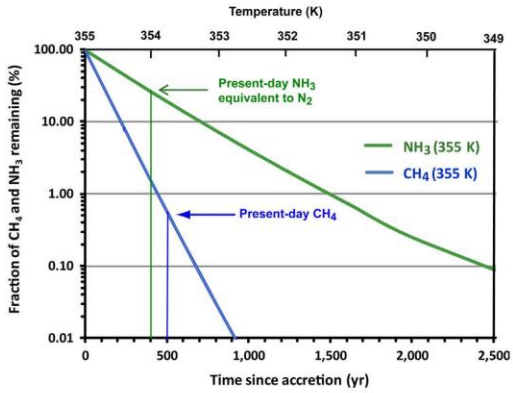

Fig. 7. The fractions of CH_4 and NH_3 remaining as a function of time since accretion assuming a T_{ac}=355 K, Eq. (25).

5.2. Gas escape formulation

In a gas, the directions of the gas molecules are on the average outward and inward (Maxwell, 1867, p. 50), and the fraction of the gas moving away from the planet is half of the fraction $\mathcal{F}(v > v_e)$ (e.g., Goody, 1976). Fig. 5a and Table 9 describe the gas escape from the atmosphere as a first-order process, $N_t = N_0\, e^{-kt}$ (kg or % of N_0), that depends on the escape rate parameter, k (s^{-1} or yr^{-1}). The latter is a function of temperature and molecular mass of the gas through its dependence on v_0, of the Titan escape velocity, v_e, and of the quotient of the atmosphere volume to its outer surface area, V_{atm}/S_{atm}, that is effectively the atmosphere thickness h (Tables 6 and 7). As the atmosphere cools over time, the fraction of gas greater than the escape velocity, $\mathcal{F}(v > v_e)$, decreases faster than the mean escape velocity $\overline{v}_{>v_e}$ (Fig. 4). Thus, the escape rate parameter, k, decreases strongly with a decreasing temperature (Fig. 6).

Fig. 5b and c shows the high-tail parts of the velocity distribution (Fig. 3b) of methane on a logarithmic and linear scale. As these figures show, the fraction of CH_4 gas molecules that have velocities greater than the escape velocity is small. However, although $\mathcal{F}(v > v_e)$ is low for CH_4, its product with mean escape velocity above v_e assures a slow but substantial escape of CH_4 over a long period of time.

5.3. Gas escape at 355 K

Starting at an accretion temperature of 355 K, the calculated values of k for NH_3 and CH_4 are too high and they allow the gases to escape before the atmosphere temperature drops sufficiently to prevent any further escape, which occurs below about 260 K (Fig. 6). The relatively high values of k for CH_4 and NH_3 near 355 K account for the fact that very little of the initial gas mass would be left in the atmosphere after a few hundred years, as shown in Fig. 7. Considering Titan's cooling rate (Fig. 2), the temperature of 150 K, as a lower limit of NH_3 to N_2 conversion (Atreya et al., 1978), is reached after about 500,000–600,000 years, and after such a long period of time the gas masses remaining would be vanishingly small fractions of the initial masses as given in Table 6, column 5.

Two hypothetical, but similarly unrealistic, explanations of slower rates of gas escape from a 355 K atmosphere may be considered:

(1) Escape rate parameter, k, as shown in Fig. 5 and Eq. (24), depends on the atmosphere outer surface area, S_{atm}. If the

Table 10
Summary of CH_4 and NH_3 inferred input rates to Titan's atmosphere.

Gas species and process	In solid planet	In present-day atm. 94 K		In primordial atm. 355 K	
	(kg)	(kg)	(bar)	N_0 (kg) or N_0=100%	(bar)
CH_4	7.523E+20	6.163E+17	0.1	1.190E+20	19.6
NH_3 (N_2 mass equivalent in present-day atm.)	1.622E+21	1.049E+19	1.7	3.760E+19	5.8
CH_4% of mass in solid		0.08%		15.81%	
NH_3% of mass in solid		0.65%		2.32%	
	CH_4			NH_3	
Input to atm. F (% yr^{-1} of N_0), starting at 355 K	1.00E−06	1.00E−05	1.00E−04	8.00E−04	1.45E−03
CH_4 Input flux $FN_0/100$ (primordial) (kg/yr)	1.19E+12	1.19E+13	1.19E+14		
Time to exhaust CH_4 in the interior (yr)	6.32E+08	6.32E+07	6.32E+06		
NH_3 input flux $FN_0/100$ (primordial) (kg/yr)				3.01E+14	5.45E+14
Time to exhaust NH_3 in the interior (yr)				5.4E+06	3.0E+06

outer atmosphere was only partially permeable to the escaping CH_4 and NH_3, their outgoing fluxes would have been smaller and the atmosphere might have cooled sufficiently before the two gases were exhausted. However, this requires partial permeability of the upper atmosphere to be about 5% (5.6% for CH_4 and 4.5% for NH_3) for the initial gas masses to decrease to their present-day levels.

(2) The dependence of escape rate parameter k on the quotient V_{atm}/S_{atm} and therefore on the atmosphere thickness h, could make k sufficiently smaller at a larger quotient V_{atm}/S_{atm}, to reduce the initial gas masses to their present-day levels. This, however, could be accomplished only for an unrealistic atmosphere of thickness $h \approx 4316$ km, greater than the Titan radius of 2575 km, total pressure of about 28 bar, and low density of 0.13 kg/m^3. A more realistic explanation, emissions from the interior combined with thermal escape, is given in the following section.

5.4. *Possible emissions from Titan's interior*

Possible cryovolcanic features on Titan's surface have been identified by the Cassini Radar Mapper, as well as other visual and infrared instruments onboard the Cassini spacecraft (Lopes et al., 2007). Cryovolcanism on Titan resembles silicate volcanism on Earth, except its eruptions consist of volatiles, such as water, ammonia, and methane, instead of molten rock. Cryovolcanism is considered by some (Atreya et al., 2006; Fortes et al., 2007; Grindrod et al., 2008) to be the leading mechanism for the replenishment of methane in Titan's atmosphere, where it may be irreversibly lost due to photochemical dissociation. Methane replenishment via cryovolcanism is supported by many, including Fortes et al. (2007), who estimate that a magma containing 0.5 wt% CH_4, erupted at a reasonable rate of up to $\sim 1.0 \times 10^{12}$ kg/yr, could buffer the photolytic destruction of atmospheric methane. This emission rate is lower than the input fluxes in the emission-and-escape model, as shown in Table 10, and it would make the methane content of the satellite practically inexhaustible, with a theoretical methane depletion time of 150 billion years. Photolytic decomposition of CH_4 by UV radiation at altitudes 300 km produces ethane (C_2H_6) as one of the main stable products (Strobel, 1982; Lunine et al., 1983; Smith and Raulin, 1999; Wilson and Atreya, 2004; Atreya et al., 2006; Lunine and Atreya, 2008). Ethane accumulates on the Titan surface, but its re-evaporation and reconversion to methane are not considered as realistic sources of CH_4 replenishment in the atmosphere, where its chemical lifetime is estimated from about 27,000 yr at altitude 300 km (Wilson and Atreya, 2004) to 10^7–10^8 yr (Atreya et al., 2006). The longer estimate of the CH_4 residence time in the atmosphere cited above, 10^7–10^8 yr, is much longer than our estimates of the residence time ($1/k$), increasing from 2400 yr at 300 K to 3×10^7 yr at 210 K, reached after 145,000 yr. Thus, if the

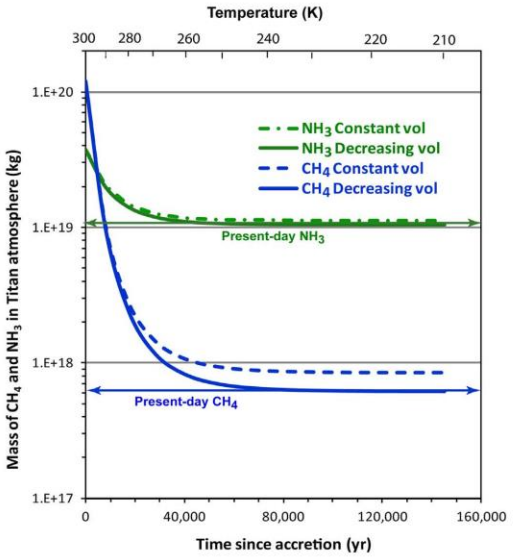

Fig. 9. The amount of NH_3 and CH_4 remaining in the atmosphere as a function of time since accretion assuming a T_{ac}=300 K. Eq. (25).

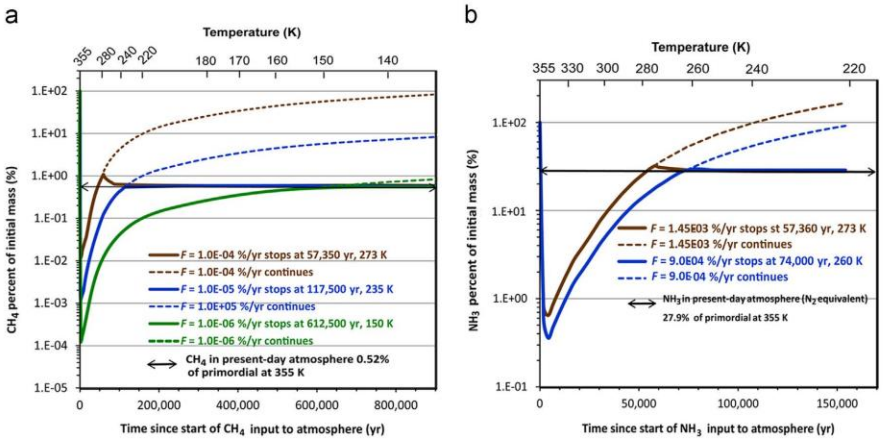

Fig. 8. Input of (a) CH_4 and (b) NH_3 from Titan's interior to the atmosphere, added to the escaping gases. Final masses are stabilized at their present-day values (Table 6, column 3). Curves computed using Eq. (27).

longer residence time is due to photolytic destruction of CH_4, our results for the much-diminished flux out of the atmosphere do not contradict the slow rates of methane destruction and replenishment on the cooled Titan.

Among the many possible emission scenarios that may be thought of, the case we explore is gas thermal escape accompanied by emission from Titan's interior, a simple process that is a combination of a constant input rate to the atmosphere, F ($\%N_0$/yr or kg/yr), with a first-order escape $dN/dt = F - kN$, the solution of which is given in Eqs. (26) and (27). For CH_4, three reasonable rates of emission are shown in Fig. 8a and Table 10. If CH_4 emissions from the Titan interior were continuous, the supply would be exhausted in 6.32–632 Myr. To avoid complete depletion of CH_4 from the internal reservoir, and to satisfy the present-day CH_4 atmospheric level, emissions at the rates shown in Fig. 8a would have to stop at 57,350 ($F = 1.0 \times 10^{-4}$%/yr), 117,500 ($F = 1.0 \times 10^{-5}$%/yr), and 612,500 ($F = 1.0 \times 10^{-6}$%/yr) years, respectively, after the start of CH_4 input to the atmosphere.

The NH_3 emissions include two reasonable rates of input: $F = 1.45 \times 10^{-3}$%/yr and $F = 9.0 \times 10^{-4}$%/yr (Fig. 8b and Table 10). In a continuous emission at these rates, the NH_3 reservoir would be depleted in 3–5.4 Myr after the emission start. A discontinuous input, with NH_3 emissions stopping at 57,360 ($F = 1.45 \times 10^{-3}$%/yr) and 74,000 ($F = 9.0 \times 10^{-4}$%/yr) years after the start of input to the atmosphere, would satisfy the present-day level of NH_3 (N_2 equivalent) (Table 6, column 3).

It should be realized that the processes described in Fig. 8 and Table 10 assume termination of the emissions at a time that satisfies the primordial atmosphere to meet the conditions of present day. The results also show periods of variable length where the atmosphere had very low concentrations of the two gases, until their levels were raised by emissions from the interior.

5.5. Gas escape at 300 K

A primordial atmosphere, initially at 300 K (Table 6, column 6), loses CH_4 and NH_3 by thermal escape down to their present-day levels (column 3) by the time the atmosphere has cooled to about 250 K (Fig. 9). As the gases are continuously lost from the atmosphere, its mass and volume decrease, making the escape rate parameter k slightly larger and escape rate faster. The results of this change in k are shown in Figs. 9 and 10, by the curves for a constant or decreasing atmosphere volume.

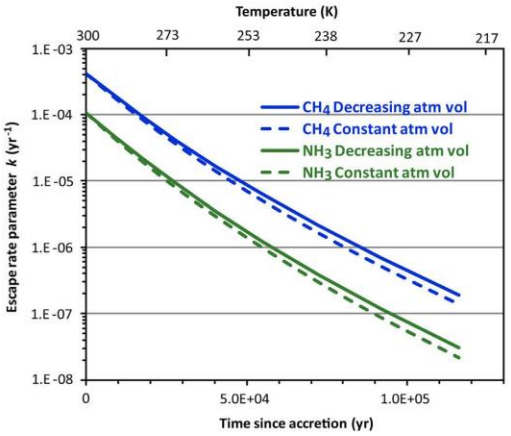

Fig. 10. The escape rate parameter, k, as a function of time since accretion for CH_4 and NH_3 assuming a $T_{ac} = 300$ K. Eq. (24).

As the value of the Titan mean heat capacity, $C_p = 2232$ J kg^{-1} K^{-1} at 300 K (Table 4), affects the time and rate of the satellite cooling (Section 3.2), a variation in C_p also affects the initial masses of CH_4 and NH_3 in the primordial atmosphere that are computed to make the initial masses decrease to their present-day levels (Table 6, columns 6 and 3). In a test of sensitivity of the results to the C_p values, a variation of ~ 150 J kg^{-1} K^{-1} in $C_p = 2232$ J kg^{-1} K^{-1} produces only very small effects on the cooling rate. At the higher C_p value, it takes slightly longer to cool from one temperature point to a lower one, and this slower cooling rate allows more gas to escape from the atmosphere. At the conditions of a higher or lower Titan C_p, 2382 or 2082 J kg^{-1} K^{-1}, the initial atmospheric mass N_0 of CH_4, would be $+44\%$ to -30% of the model value, and for NH_3 it would be $\pm 9\%$. These changes are due to the greater or smaller time-interval differences, $t_{i+1} - t_i$, in Eq. (25) that affect the negative exponential term and the resulting value of the remaining gas mass fraction N_t.

In this thermal escape model, the escape of NH_3 and CH_4 ends 50,000–70,000 years after start, when the gas masses decline to their present-day levels. However, in the model of gas emission-and-escape (Fig. 8), the times of mass decline are longer: for NH_3, depending on its emission rate, it takes about 70,00–80,000 years. At the different emission rates of CH_4, it takes 100,000–600,000 years to attain a steady-state value.

6. Conclusions

This paper presents a new model of the NH_3 and CH_4 sinks, the two main gases, in Titan's primordial atmosphere. If NH_3 and CH_4 were removed from the atmosphere, initially at 300 K, by thermal escape as the only sink, the final result is the present-day gas masses in the atmosphere, attained after 50,000–70,000 yr.

An alternative model combines the two mechanisms of gas emission from Titan's interior with thermal escape. At the different estimated emission rates from the interior, the times of mass decline from the primordial, at 355 K, to present-day levels are longer: for NH_3, the decline is about 70,000–80,000 years; for CH_4, it takes 100,000–600,000 years to attain a steady-state value. We place less trust in the emission-with-escape model because of (a) arbitrary assumptions of the period lengths of the emissions and (b) significantly, the discrepancies between the reported rates of CH_4 emissions and our estimates of the available CH_4 inventory in the Titan interior.

The models of gas thermal escape and emission-with-escape are based on the estimates of Titan's post-accretional composition, as made of a solid core of antigorite ($Mg_3Si_2O_5(OH)_4$) and brucite ($Mg(OH)_2$), and an outer fluid shell made of the volatile components (H_2O, NH_3, $(NH_4)_2SO_4$, and CH_4) that account for 40.54% of Titan's mass. The accretion temperature is estimated in the range from 300 to 355 K, based on the gravitational energy of accretion, without additional heat production or storage, and radiational emission cooling of an ideal black body. For the post-accretional cooling rate, we estimated mean heat capacity, C_p, of Titan at the two temperatures, from compilations of the C_p data for the individual components.

An analysis of the thermal escape mechanism as a Maxwell–Boltzmann gas indicates a strong dependence of the gas escape rate on temperature, molecular mass of the gas species, the escape velocity at the satellite surface, and the atmosphere thickness or the quotient of its volume to outer surface area. Titan's cooling controls the gas escape from the atmosphere, resulting in the computed primordial masses decreasing to their present-day values by the time the temperature has declined to below 250 K.

Table A1
Summary of C_p data at different temperatures and pressures.

	Heat capacities C_p (J kg^{-1} K^{-1})[a]							
	300 K, 1 bar	5–10 bar	1 kb	2 kb	1–5 kb	5 kb	47–85 kb	
Methane gas	2226				**2956**			Setzmann and Wagner (1991), Table 39, p. 1119 et seq.
Ammonia–water ~3 wt%	4136							Calculated from Conde (2006), p. 10, mass fract. NH_3=0.0326
	4150							Conde (2013), from Fig. 8 in 2006 edition
H_2SO_4, mol fraction x=4.266E−03 (C_p/R)	***763.02***							Zeleznik (1991), Table 7, p. 1189 et seq.
H_2O	4180.60		3979.8	***3882.8***		3793.8		Wagner and Pruss (2002), pp. 496, 533
$xH_2SO_4+(1-x)H_2O$				***3869.49***				From the C_p of mol fractions of H_2SO_4 and H_2O
NH_3–H_2SO_4–H_2O solution				**4031.21**				Mean of the NH_3–H_2O and H_2SO_4–H_2O solutions
Magnesium hydroxide	**1348.79**							Horita et al. (2002), Table 4 (mean of calc. and experim. values)
Antigorite	1985.75							Grindrod et al. (2008)
							1000	Osako et al. (2010), Fig. 3
	350 K, 1 bar	5–10 bar	1 kb	2 kb	1–5 kb	5 kb	47–85 kb	
Methane gas	2365				**3020**			Setzmann and Wagner (1991), Table 39, p. 1119 et seq.
Ammonia–Water ~3 wt%	4188							Calculated from Conde (2006, p. 10), mass fract. NH_3=0.0326
		4400						Conde (2013), from Fig. 8 in 2006 edition
H_2SO_4, mol fraction x=4.266E03 (C_p/R)	***767.25***							Zeleznik (1991), Table 7, p. 1189 et seq.
H_2O	4194.5		4025.3	***3921.4***		3785.8		Wagner and Pruss (2002), pp. 496, 533
$xH_2SO_4+(1-x)H_2O$				***3907.94***				From the C_p of mol fractions of H_2SO_4 and H_2O
NH_3–H_2SO_4–H_2O solution				**4191.62**				Mean of the NH_3–H_2O and H_2SO_4–H_2O solutions
Magnesium hydroxide	**1472.68**							Horita et al. (2002), Table 4 (mean of calc. and experim. values)
Antigorite	1986.72							Grindrod et al. (2008)
							1100	Osako et al. (2010), Fig. 3

[a] Values in **boldface roman** are used in the calculation of mean C_p in Table 4, those in ***boldface italics*** are for intermediate calculations of C_p of the NH_3–H_2SO_4–H_2O solution at 300 and 350 K.

Acknowledgments

We thank Professors Emile Okal and Craig Bina, Graduate Students Joshua Townsend and Michael Witek (all of this Department), and Professor John Franks (Department of Mathematics) for checking some of our mathematical derivations; Professor Emile Okal for an explanation of pressure–depth relationships in spherical, incompressible, homogeneous, and layered bodies; Professor Steven Jacobsen for a reference on NaCl solutions; Dr. Manuel Conde (M. Conde Engineering, Zürich) for his data on NH_3 solutions and release of copyrighted information; and Professor Amitai Katz (Institute of Earth Sciences, The Hebrew University, Jerusalem) for the recent density value of the Dead Sea brine. We also thank Anonymous Reviewer for insightful and helpful comments, and the Editor-in-Chief, Dr. Rita Schulz, for her efforts in having this paper reviewed. This work was supported by NASA Headquarters under the NASA Earth and Space Science Fellowship Program – Grant NNX13AO02H and by the Arthur L. Howland Fund of Northwestern University.

Appendix A

Table A1 lists the values of the heat capacity of Titan's primordial components as given in Table 4.

References

Alibert, Y., Mousis, O., 2007. Formation of Titan in Saturn's subnebula: constraints from Huygens probe measurements. Astron. Astrophys. 465, 1051–1060.

Atreya, S.K., Donahue, T.M., Kuhn, W.R., 1978. Evolution of a nitrogen atmosphere on Titan. Science 201, 611–613.

Atreya, S.K., Adams, E.Y., Niemann, H.B., Demick-Montelara, J.E., Owen, T.C., Fulchignoni, M., Ferri, F., Wilson, E.H., 2006. Titan's methane cycle. Planet. Space Sci. 54, 1177–1187.

Barr, A.C., Citron, R.I., Canup, R.M., 2010. Origin of a partially differentiated Titan. Icarus 209, 858–862.

Brown, R., Lebreton, J-P., Waite, J.H. (Eds.), 2009. Springer, Dordrecht, New York (Print).

Chen, C.-T.A., Chen, J.H., Millero, F.J., 1980. Densities of NaCl, $MgCl_2$, Na_2SO_4, and $MgSO_4$ aqueous solutions at 1 atm from 0 to 50 °C and from 0.001 to 1.5 m. J. Chem. Eng. Data 25, 307–310.

Conde, M., 2006. Thermophysical Properties of {NH_3+H_2O} Mixtures for the Industrial Design of Absorption Refrigeration Equipment. M. Conde Engineering, Zürich, 38 pp. ⟨http://www.mrc-eng.com/Downloads/NH3&H2O%20%20Props%20English.pdf⟩.

Conde, M., 2009. Aqueous Solutions of Lithium and Calcium Chlorides: Property Formulations for Use in Air Conditioning Equipment Design. M. Conde Engineering, Zürich, 27 pp. ⟨http://www.mrc-eng.com/Downloads/Aqueous%20LiCl&CaCl2%20Solution%20Props.pdf⟩.

Conde, M., 2013. Heat Capacities of Ammonia–Water Solutions. Personal Communication. M. Conde Engineering, Zürich.

Courtin, R.D., Sim, C., Kim, S., Gautier, D., Jennings, D.E., 2008. Latitudinal variations of tropospheric H2 on Titan from the Cassini CIRS investigation. 40th DPS Meeting, Abstract 31.01, Ithaca, New York, Bull. Amer. Astron. Soc. 40(31.01): 446.

Coustenis, A., 2005. Formation and evolution of Titan's atmosphere. Space Sci. Rev. 116, 171–184.

Duan, Z., Mao, S., 2006. A thermodynamic model for calculating methane solubility, density and gas phase composition of methane-bearing aqueous fluids from 273 to 523 K and from 1 to 2000 bar. Geochim. Cosmochim. Acta 70, 3369–3386.

European Space Agency (ESA), 2013. Facts about Titan. Available from: ⟨http://www.esa.int/Our_Activities/Space_Science/Cassini-Huygens/Facts_about_Titan⟩ (accessed 1.08.13.).

Fortes, A.D., Grindrod, P.M., Trickett, S.K., Vocadlo, L., 2007. Ammonium sulfate on Titan: Possible origin and role in cryovolcanism. Icarus 188, 139–153.

Gilliam, A.E., McKay, C.P., 2011. Titan under a red dwarf star and as a rogue planet: requirements for liquid methane. Planet. Space Sci. 59, 835–839.

Goody, R., 1976. Atmospheric evaporation. In: Tipler, P.A. (Ed.), Physics. Worth Publishers, New York, pp. 241–243 (xxvi+1026 pp).

Gough, O.D., 1981. Solar interior structure and luminosity variations. Solar Phys. 74, 21–34.

Grasset, O., Sotin, C., 1996. The cooling rate of a liquid shell in Titan's interior. Icarus 123, 101–112.

Grasset, O., Sotin, C., Deschamps, F., 2000. On the internal structure and dynamics of Titan. Planet. Space Sci. 48, 617–636.

Grasset, O., Pargamin, J., 2005. The ammonia–water system at high pressures: implications for the methane of Titan. Planet. Space Sci. 53, 371–384.

Griffith, C.A., Owen, T., Geballe, T.R., Rayner, J., Rannou, P., 2003. Evidence for the exposure of water ice on Titan's surface. Science 300, 628–630.

Grindrod, P.M., Fortes, A.D., Nimmo, F., Feltham, D.L., Brodholt, J.P., Vočadlo, L., 2008. The long-term stability of a possible aqueous ammonium sulfate ocean inside Titan. Icarus 197, 137–151.

Hanks, T.C., Anderson, D.L., 1969. The early thermal history of the Earth. Phys. Earth Planet. Inter. 2, 19–29.

Horita, J., Cole, D.R., Polyakov, V.B., Driesner, T., 2002. Experimental and theoretical study of pressure effects on hydrogen isotope fractionation in the system brucite-water at elevated temperatures. Geochimica et Cosmochimica Acta 66, 3769–3788.

Jacquemart, D., Lellouch, E., Bézard, B., de Bergh, C., Coustenis, A., Lacome, N., Schmitt, B., Tomasko, M., 2008. New laboratory measurements of CH_4 in Titan's conditions and a reanalysis of the DISR near-surface spectra at the Huygens landing site. Planet. Space Sci. 56, 613–623.

Katz, A., 2013. Density of the Dead Sea, North Basin, Brine in 2012–2013. Personal Communication. Institute of Earth Sciences, The Hebrew University, Jerusalem.

Kuramoto, K., Matsui, T., 1994. Formation of a hot proto-atmosphere on the accreting giant icy satellite: implications for the origin and evolution of Titan, Ganymede, and Callisto. J. Geophys. Res. 99, 21,183–21,200.

Lopes, R.M.C., et al., 2007. Cryovolcanic features on Titan's surface as revealed by the Cassini Titan Radar Mapper. Icarus 186, 395–412.

Lorenz, R.D., McKay, C.P., Lunine, J.I., 1999. Analytic investigation of climate stability on Titan: sensitivity to volatile inventory. Planet. Space Sci. 47, 1503–1515.

Lunine, J.I., Stevenson, D.J., Yung, Y.L., 1983. Ethane ocean on Titan. Science 222 (4269), 1229–1230.

Lunine, J.I., Atreya, S.K., 2008. The methane cycle on Titan. Nat. Geosci. 1, 159–164.

Lvov, S.N., Wood, R.H., 1990. Equation of state of aqueous NaCl solutions over a wide range of temperatures, pressures and concentrations. Fluid Phase Equilib. 60, 273–287.

Marion, G.M., 1997. A theoretical evaluation of mineral stability in Don Juan Pond, Wright Valley, Victoria Land. Antarct. Sci. 9 (01), 92–99.

Matsubaya, O., Sakai, H., Torii, T., Burton, H., Kerry, K., 1979. Antarctic saline lakes – stable isotopic ratios, chemical compositions and evolution. Geochim. Cosmochim. Acta 43, 7–25.

Maxwell, J.C., 1867. On the dynamical theory of gases. Philos. Trans. R. Soc. Lond. 157, 49–88.

Mosqueira, I., Estrada, P.R., 2003. Formation of the regular satellites of giant planets in an extended gaseous nebula I: subnebula model and accretion of satellites. Icarus 163, 198–231.

Mousis, O., Gautier, D., Bockelée-Morvan, D., 2002. An evolutionary turbulent model of Saturn's subnebula: implications for the origin of the atmosphere of Titan. Icarus 156, 162–175.

Naftz, D.L., Millero, F.J., Jones, B.F., Green, W.R., 2011. An equation of state for hypersaline water in Great Salt Lake, Utah, USA. Aquat. Geochem. 17, 809–820.

National Aeronautics and Space Administration (NASA), 2012. Titan: facts & figures. Available from: ⟨http://solarsystem.nasa.gov/planets/profile.cfm?Object=Sat_Titan&Display=Facts⟩ (1.08.13.).

Niemann, H.B., Atreya, S.K., Bauer, S.J., Carignan, G.R., Demick, J.E., Frost, R.L., Gautier, D., Haberman, J.A., Harpold, D.N., Hunten, D.M., Israel, G., Lunine, J.I., Kasprzak, W.T., Owen, T.C., Paulkovich, M., Raulin, F., Raaen, E., Way, S.H., 2005. The abundances of constituents of Titan's atmosphere from the GCMS instrument on the Huygens probe. Nature 438, 779–784.

Osako, M., Yoneda, A., Ito, E., 2010. Thermal diffusivity, thermal conductivity and heat capacity of serpentine (antigorite) under high pressure. Phys. Earth Planet. Inter. 183, 229–233.

OXY (Occidental Chemical Corporation), 2012. Calcium chloride – a guide to physical properties, 10 p. ⟨http://www.cal-chlor.com/PDF/GUIDE-physical-properties.pdf⟩.

Prinn, R.G., Fegley, B., 1981. Kinetic inhibition of CO and N_2 reduction in circumplanetary nebulae: implications for satellite composition. Astrophys. J. 249, 308–317.

Rogers, P.S.Z., Pitzer, K.S., 1982. Volumetric properties of aqueous sodium chloride solutions. J. Phys. Chem. Ref. Data 11, 15–81.

Samuelson, R.E., Mayo, L.A., 1997. Steady-state model for methane condensation in Titan's troposphere. Planet. Space Sci. 45 (8), 949–958.

Setzmann, U., Wagner, W., 1991. A new equation of state and tables of thermodynamic properties for methane covering the range from the melting line to 625 K at pressures up to 1000 MPa. J. Phys. Chem. Ref. Data 20, 1061–1155.

Smith, N.S., Raulin, F., 1999. Modeling of methane photolysis in the reducing atmospheres of the outer solar system. J. Geophys. Res. 104 (E1), 1873–1876.

Strobel, D.F., 1982. Chemistry and evolution of Titan's atmosphere. Planet. Space Sci. 30, 839–848.

Tobie, G., Choukroun, M., Grasset, O., Le Mouélic, S., Lunine, J.I., Sotin, O., Bourgeois, O., Gautier, D., Hirtzig, M., Lebonnois, S., Le Corre, L., 2009. Evolution of Titan and implication for its hydrocarbon cycle. Philos. Trans. R. Soc. A 367, 617–631.

Turcotte, D.L., Schubert, G., 1982. Geodynamics. Applications of Continuum Physics to Geologcial Problems. Wiley, New York (xii+450 p).

Wagner, W., Pruss, A., 2002. The IAPWS formulation 1995 for the thermodynamic properties of ordinary water substance for general and scientific use. J. Phys. Chem. Ref. Data 31, 387–535.

Wilson, E.H., Atreya, S.K., 2004. Current state of modeling the photochemistry of Titan's mutually dependent atmosphere and ionosphere. J. Geophys. Res. Planets 109 (E06002), 39.

Yarger, J., Lunine, J.L., Burke, M., 1993. Calorimetric studies of the ammonia-water system with application to the outer solar system. J. Geophys. Res. 98, 109–117.

Zahnle, K.J., Walker, J.C.G., 1982. The evolution of solar ultraviolet luminosity. Rev. Geophys. 20, 280–292.

Zeleznik, F.J., 1991. Thermodynamic properties of the aqueous sulfuric acid system to 350 K. J. Phys. Chem. Ref. Data 20, 1157–1200.

Icarus 275 (2016) 252–258

Contents lists available at ScienceDirect

Icarus

journal homepage: www.elsevier.com/locate/icarus

Titan's missing ethane: From the atmosphere to the subsurface

Ashley E. Gilliam*, Abraham Lerman

Department of Earth and Planetary Sciences, Northwestern University, 2145 Sheridan Rd – Tech F379, Evanston, IL 60208-3130, United States

ARTICLE INFO

Article history:
Received 19 October 2015
Revised 8 April 2016
Accepted 14 April 2016
Available online 26 April 2016

Keywords:
Titan, atmosphere
Titan, surface
Atmospheres, chemistry
Prebiotic chemistry

ABSTRACT

The second most abundant component of the present-day Titan atmosphere, methane (CH_4), is known to undergo photolytic conversion to ethane (C_2H_6) that accumulates as a liquid on Titan's surface. Condensation temperature of ethane is higher than that of methane, so that ethane "rain" may be expected to occur before the liquefaction of methane. At present, the partial pressure of ethane in the atmosphere is 1E−5 bar, much lower than 1E−1 bar of CH_4. Estimated 8.46E17 kg or 1.37E6 km^3 of C_2H_6 have been produced on Titan since accretion. The Titan surface reservoirs of ethane are lakes and craters, of estimated volume of 50,000 km^3 and 61,000 km^3, respectively. As these are smaller than the total volume of liquid ethane produced in the course of Titan's history, the excess may be stored in the subsurface of the crust, made primarily of water ice. The minimum porosity of the crust needed to accommodate all the liquid ethane would be only 0.9% of the uppermost 2 km of the crust. The occurrence of CH_4 and liquid C_2H_6 on Titan has led to much speculation on the possibility of life on that satellite. The aggregation of organic molecules in a "primordial soup or bullion" depends in part on the viscosity of the medium, diffusivity of organic molecules in it, and rates of polymerization reactions. The temperatures on Titan, much lower than on primordial Earth, are less favorable to the "Second Coming of life" on Titan.

1. Introduction

Titan, the largest moon of Saturn, is unique in the Solar System. Whereas satellites in general are not known for having atmospheres, Titan not only possesses an atmosphere, it has a massive and complex one, harboring a suite of hydrocarbons that display a meteorological cycle similar to the hydrological cycle on Earth. The main components of Titan's atmosphere at present are nitrogen (N_2, 1.4 bar) and methane (CH_4, 0.1 bar). In Titan's atmosphere hydrocarbons are produced by the photodissociation of methane. In the stratosphere, which extends from the tropopause (approx. 40 km) to the stratopause (approx. 320 km), UV photolysis is responsible for ~1/3 of the total methane destruction (Atreya et al., 2009), 75% of which occurs at the Lyman α wavelength (121.6 nm) (Wilson and Atreya, 2009). At Lyman α, the photodissociation of methane produces other hydrocarbons, such as methyl radicals (CH_3). These hydrocarbons recombine to form heavier molecules (e.g. C_2H_6) that condense as liquids or solids in the lower stratosphere and vicinity of Titan's cold troposphere (Fig. 1) to form a haze layer and eventually precipitate from the atmosphere. In Titan's atmosphere, ethane (C_2H_6) is the main photolysis product of methane (Yung et al., 1984), with a mean production rate of 1.3×10^8 molecules cm^{-2} s^{-1} (2.16×10^{-16} moles cm^{-2} s^{-1}) from solely the photolytic conversion of methane to ethane (Wilson and Atreya, 2009), nearly tenfold the production of the other hydrocarbons combined (Toublanc et al., 1995). Higher production rates of ethane (Cornet et al., 2015), $1.2–15 \times 10^9$ molecules cm^{-2} s^{-1}, are either similar or higher than the photochemical removal rate of CH_4, 2.5×10^9 molecules cm^{-2} s^{-1} (Wilson and Atreya, 2009). A simplified sequence of direct forward reactions from CH_4 to C_2H_6 that short-circuit the complex intermediate paths can be represented by the following (Gilliam et al., 2015):

$$CH_4 \rightarrow CH_3 + H \quad \text{first-order rate parameter } k_{12}\ (s^{-1}),\quad d[CH_4]/dt = F - k_{12}[CH_4] \tag{1}$$

$$d[CH_3]/dt = k_{12}[CH_4] \tag{2}$$

$$CH_3 + CH_3 \rightarrow C_2H_6 \quad \text{2nd-order rate parameter } k_{23}\ (cm^3\ mol^{-1}\ s^{-1}),\ d[C_2H_6]/dt = k_{23}[CH_3]^2 \tag{3}$$

$$C_2H_6 \rightarrow \text{other products first-order rate parameter } k_3\ (s^{-1}),\quad d[C_2H_6]/dt = -k_3[C_2H_6] \tag{4}$$

where [ ] are atmospheric concentrations in kg, mol or molecules vol^{-1}, k_{ij} are the reaction rate parameters, and $F \geqslant 0$ (mass vol^{-1}

* Corresponding author.
E-mail address: ashley@earth.northwestern.edu (A.E. Gilliam).

http://dx.doi.org/10.1016/j.icarus.2016.04.025
0019-1035/

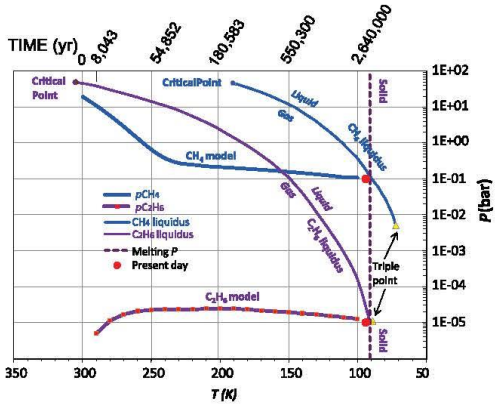

Fig. 1. One of the important points in the history of methane and ethane in Titan's atmosphere is that C_2H_6 condenses at a higher temperature than CH_4. The figure above shows: (a) saturation vapor pressure or liquidus curves of each gas (CRC Handbook of Chemistry and Physics, 2016). Note that as Titan's atmosphere cools from about 300 K down, C_2H_6 liquefies before CH_4 and it also forms a solid phase at the triple point before CH_4. Thus liquefaction and "raining" of C_2H_6 in Titan's atmosphere is expected to begin before that of CH_4. (b) Calculated partial pressures of methane and ethane in the theoretical reactions sequence (1)–(4), as explained in the text. Present-day partial pressures are shown as red dots. (For interpretation of the references to color in this figure legend, the reader is referred to the web version of this article.)

time^{-1}) is the rate of CH_4 emission from the interior to the atmosphere. The resulting ethane is largely shielded from UV radiation by methane and acetylene (C_2H_2), making it stable against photolysis. The principal loss mechanism for ethane is condensation at the tropopause, followed by its accumulation as a liquid on the surface (Yung and DeMore, 1999).

Another mechanism of methane loss in the Titan atmosphere is hydrodynamic escape. First observed by the Voyager spacecraft and confirmed by the Cassini Ion Neutral Mass Spectrometer (INMS), the methane distribution in Titan's upper atmosphere remains uniformly mixed to the altitude of ~1100 km, where it begins to exhibit diffusive separation. Further evidence from the Cassini INMS suggested that methane is not well mixed to high altitudes (>1000 km) because of a large escape rate, 2.9×10^9 molecules cm^{-2} s^{-1} (4.8×10^{-15} moles cm^{-2} s^{-1}) (Yelle et al., 2008). The most likely mechanism is hydrodynamic escape – a high density, slow outward expansion driven mainly by solar UV heating due to CH_4 absorption (Strobel, 2009) – as evident from heating rates gathered from the Huygens Atmospheric Structure Instrument (HASI). This loss rate is responsible for 22% of the total methane loss rate (Wilson and Atreya, 2009).

The third mechanism of methane loss is thermal escape, where the outgoing methane flux is proportional to the methane mass in the atmosphere and it depends on temperature, gas molecular mass, atmosphere thickness, and Titan's escape velocity (Gilliam and Lerman, 2014a; Gilliam et al., 2015).

Consideration of these processes suggests that Titan should have produced a substantial amount of ethane since accretion. Such an idea was first proposed by Lunine et al. (1983), who used photochemical models to predict that Titan would be covered by an ethane ocean one to several kilometers deep, and was later supported by others' models, albeit with a smaller net volume of ethane produced. Further, Mousis and Schmitt (2008) proposed a geological process that resolves "the ethane deficiency issue in a manner which is in agreement with our current knowledge of Titan: the incorporation of liquid hydrocarbons in the porous cryovolcanic subsurface". However, Cassini–Huygens observations have not shown evidence of widespread surface ethane reservoirs.

This paper addresses three issues: (1) the mass and volume of ethane that was produced on Titan since accretion, based on the production-rate estimates of other investigators; (2) the occurrence of liquid ethane in the surface depressions (craters and lakes) and in the crustal subsurface; and (3) the physical characteristics of liquid ethane as a potential medium for emerging life. To address the first issue, we present a straightforward photochemical model using primordial conditions presented in Gilliam and Lerman (2014a,b) and compare our results to the latest observations from the Cassini mission.

2. CH_4 depletion and C_2H_6 production through time

The condensation temperature of ethane is lower than that of methane, as shown by the two liquidus curves in Fig. 1. Thus liquefaction and "raining" of C_2H_6 in Titan's atmosphere is expected to begin before that of CH_4 (Sagan and Thompson, 1984; Barth and Toon, 2003; Rannou et al., 2006; Lunine and Atreya, 2008). The cooling time of Titan's surface, calculated assuming heat dissipation by radiation emission from an ideal black body, from the initial accretion temperature of 300 K to 100 K is about 3×10^6 years (Gilliam and Lerman, 2014a).

Atmospheric observations and numerous other works have shown that ethane does condense at higher altitudes than methane. However, there are two other possible compositions of the rain on Titan. Graves et al. (2008) considered condensation of N_2–CH_4–C_2H_6, based on N_2 being the main component of Titan's atmosphere at present. Mousis and Schmitt (2008) have also discussed the possibility of CH_4–C_2H_6–N_2 liquid condensing on the Titan surface. Atreya et al. (2006) concluded that C_2H_6 condenses at altitudes above the tropopause where the temperature is near 70 K. Croft et al. (1988) have reported that water–ammonia solutions remain liquid down to 190–170 K, which suggests that if NH_3 was a component of the atmosphere in the past, an H_2O–NH_3 rain main have carried dissolved CH_4 and C_2H_6 to the surface.

With regard to liquid N_2 in Titan's atmosphere, its condensation temperature at the pressure of 1–2 bar is 77–82 K, below the 90 K of the present-day Titan surface (CRC, 2016). However, N_2 dissolves in methane–ethane mixtures (Farnsworth et al., 2016) and it forms hydrous clathrates in the temperature range from 215 K to 375 K (van Hinsberg and Schouten, 1994). If precipitation of a liquid mixture of C_2H_6–CH_4–N_2 was taking place on Titan, the total mass condensed over the lifetime of the satellite would have been greater than that of C_2H_6 alone. However, the solubility of N_2 in C_2H_6 is very low (Chevrier et al., 2015; Farnsworth et al., 2016), and it is the presence of CH_4 in the CH_4–C_2H_6 liquid mixture that promotes dissolution of N_2.

The two model curves for the evolution of CH_4 and C_2H_6 in Fig. 1 are a theoretical example of a model of the four simultaneous reactions (1)–(4). The model includes input of CH_4 from the interior to the atmosphere, at the rate of $F = 4.13 \times 10^{13}$ kg/yr or 5.46×10^{14} molecules cm^{-3} yr^{-1}. This rate of input was used to calculate the history of thermal escape of CH_4 from Titan's atmosphere in a model of input with escape (Gilliam and Lerman, 2014a). Among other estimates of the CH_4 emission rate from the interior, the input cited operated for 57,350 yr; if it continued indefinitely, it would have exhausted the CH_4 reservoir in Titan's interior in about 6×10^6 yr. This is longer than the 3×10^6 yr for the surface temperature to cool to 100 K. The model results were also based on emission rates lower by a factor of 100, with a correspondingly longer time to exhaustion of the CH_4 reservoir.

The rate constants of reactions (1)–(4) are from the ranges given by Yung and DeMore (1999, p. 219), Wilson and Atreya (2004, Fig. 13) and Atreya et al. (2009); and compilation in

Gilliam et al. (2015)): $k_{12} = 6.7 \times 10^{-5}$ yr^{-1}; $k_{23} = 1.5 \times 10^{-21}$ cm^3 molecule^{-1} yr^{-1}; $k_3 = 1 \times 10^0$ yr^{-1}. These representative figures are used at their face values, to demonstrate schematically the net results of the reaction mechanisms (1)–(4), without considering the effects of changing temperature and gas pressure. The end results agree closely with the present-day concentrations of CH_4 and C_2H_6 in Titan's atmosphere, as shown by the red dots in Fig. 1.

In a better model of Titan's atmosphere, where the two major pathways of CH_4 loss are direct UV photolysis and methane escape, we calculate the amount of methane remaining as a function of time since accretion, and the subsequent production of ethane through photodissociation of the methane molecules. Such calculations require an understanding of the primordial conditions of Titan, discussed in detail in Gilliam and Lerman (2014a) and summarized briefly below.

At present, with no albedo and no greenhouse effect, the radiation equilibrium temperature of Titan at its mean distance from the Sun is $T_{eq} = 90$ K. About 4.5 byr ago, when the Sun was approximately 75% as luminous as today (Gough, 1981), Titan's $T_{eq} \cong 85$ K. The value of Titan's accretion rate and duration, as estimated from Barr et al. (2010) is 2.22 m/yr and about 1.16 Myr, respectively. This accretion rate gives in combination with $T_{eq} = 85$ K and other basic parameters, an accretion temperature $T_{ac} = 300$ K. The calculated composition of a primordial atmosphere at 300 K is given in Gilliam and Lerman (2014a, Table 6), where the initial mass of CH_4 satisfies the conditions of gas thermal escape or emission-with-escape to the present-day levels. A primordial atmospheric CH_4 mass of 1.19×10^{20} kg (7.42×10^{21} moles) is calculated from the ideal gas law and a range of early CH_4 partial pressures, as suggested by the $^{14}N/^{15}N$ ratio measured by the Cassini Huygens Gas Chromatograph Mass Spectrometer (Niemann et al., 2005; Atreya et al., 2009). Lastly, an atmosphere top surface area is calculated as 9.18×10^{13} m^2, corresponding to a scale height of 109 km.

We examine two different values for the rate of CH_4 escape from the atmosphere: (esc_1) the frequently cited 2.9×10^9 molecules cm^{-2} s^{-1} (Yelle et al., 2008) and (esc_2) a range of CH_4 escape values that vary with temperature, starting at 6.84×10^{16} molecules cm^{-2} s^{-1} just after accretion, and ending with 1.30×10^{-8} molecules cm^{-2} s^{-1} at present-day, calculated using the escape rate parameters in Gilliam and Lerman (2014a).

Using $esc_1 = 2.9 \times 10^9$ molecules cm^{-2} s^{-1} and photodissociation rate of CH_4 2.5×10^9 molecules cm^{-2} s^{-1} or total of 3.8×10^9 kg/yr, and assuming that it does not vary with temperature, we calculate that 8.46×10^{17} kg of C_2H_6 should have been produced since accretion (~4.5 Ga) (Fig. 2). However, there is a problem with the latter value of methane escape rate esc_1. In Fig. 2, the constant rate esc_1 neither lowers sufficiently the initial methane mass to the present-day level, nor results in the initial concentration in a backwards calculation from the present-day mass. Only a rate of methane escape and photodissociation about ten-fold higher, 3.76×10^{10} molecules cm^{-2} s^{-1} or 2.63×10^{10} kg/yr, would lower the initial mass to the present-day level, but the shape of this curve is very different from the CH_4 curves Fig. 3b and c.

Using esc_2, the rate of CH_4 escape would begin to level off approximately 100,000 years after accretion (Fig. 3b and c), and produce 8.46×10^{17} kg of C_2H_6 (Fig. 3c). The initial and present-day masses are explained by the thermal escape model based on parameter k that depends on temperature, Titan's escape velocity, molecular mass of the gas, and atmosphere volume (Fig. 3a). The annual production rate of C_2H_6 in the atmosphere is 1.9×10^8 kg/yr or 9 orders of magnitude smaller than the total mass of CH_4. The total produced is about 10^4 times larger than the present-day atmospheric ethane mass of 9.24×10^{13} kg, suggesting that almost all of Titan's total ethane content is currently residing in liquid form on the surface and/or in the subsurface.

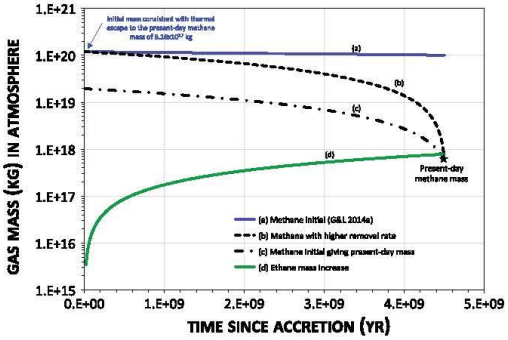

Fig. 2. Methane depletion and ethane production in Titan's atmosphere since accretion, using a simple model that includes direct methane photolysis and hydrodynamic escape. (a) CH_4 remaining in the atmosphere at the combined escape rate of $esc_1 = 2.9 \times 10^9$ molecules cm^2 s^{-1} and photodissociation of 2.5×10^9 molecules cm^2 s^{-1} (Wilson and Atreya, 2009; Yelle et al., 2008) or a total of 3.8×10^9 kg/yr, and starting at the initial mass of 1.2×10^{20} kg (Gilliam and Lerman, 2014a). (b) Methane mass decreasing from the initial to the present-day value, using a constant escape rate higher than esc_1, 3.76×10^{10} molecules cm^2 s^{-1} or 2.63×10^{10} kg/yr. (c) Initial mass of CH_4 derived from the present-day mass of 6.16×10^{17} kg and the same escape rate esc_1. (d) C_2H_6 production from CH_4 photodissociation at 1.3×10^8 molecules cm^{-2} s^{-1}.

3. Surface reservoirs of ethane

3.1. The lakes and seas of Titan

Prior to the arrival of Cassini in 2004, speculation that Titan had extensive hydrocarbon seas was based on the detection of methane by the earlier Voyager mission coupled with surface conditions that allow for the stability of liquid methane and ethane. Confirmation of liquid on the Titan surface finally came in July 2004, when Cassini ISS observations of the South Pole revealed multiple dark features, tens to hundreds of kilometers long. Since then, hundreds of lakes and seas have been discovered, most of them in the polar regions due to a high relative methane humidity allowing for the stability of standing bodies of liquid without the need for constant replenishment. If these bodies also contain dissolved methane, its escape to the atmosphere could be at least in part balanced by the emission of CH_4 from the interior, as discussed in Section 2. These lakes range in size from <10 km^2 to Kraken Mare, the area of which exceeds 400,000 km^2 (Lopes et al., 2007; Hayes et al., 2008) and is almost twice the surface area of the Laurentian Great Lakes, 244,100 km^2.

In this study, we estimate a total hydrocarbon liquid volume of all of Titan's lakes of 50,000 km^3, based on an average of the work of Lorenz et al. (2008, 2014). As an interesting comparison, the total volume of Earth's freshwater lakes is 125,000 km^3 (Herdendorf, 1982) to 91,000 km^3 (Shiklomanov, 1993), meaning that Titan has 6–8.3 times more lake liquid per cubic kilometer than Earth. Assuming a reasonable liquid composition of 50% ethane, this corresponds to an ethane mass of 1.36×10^{16} kg in Titan's lakes, roughly 1.6% of the total ethane produced as calculated.

3.2. Liquid capacity in Titan's craters

Although there are only a couple of observations of hydrocarbon liquids present in Titan's 60+ craters, it is interesting to

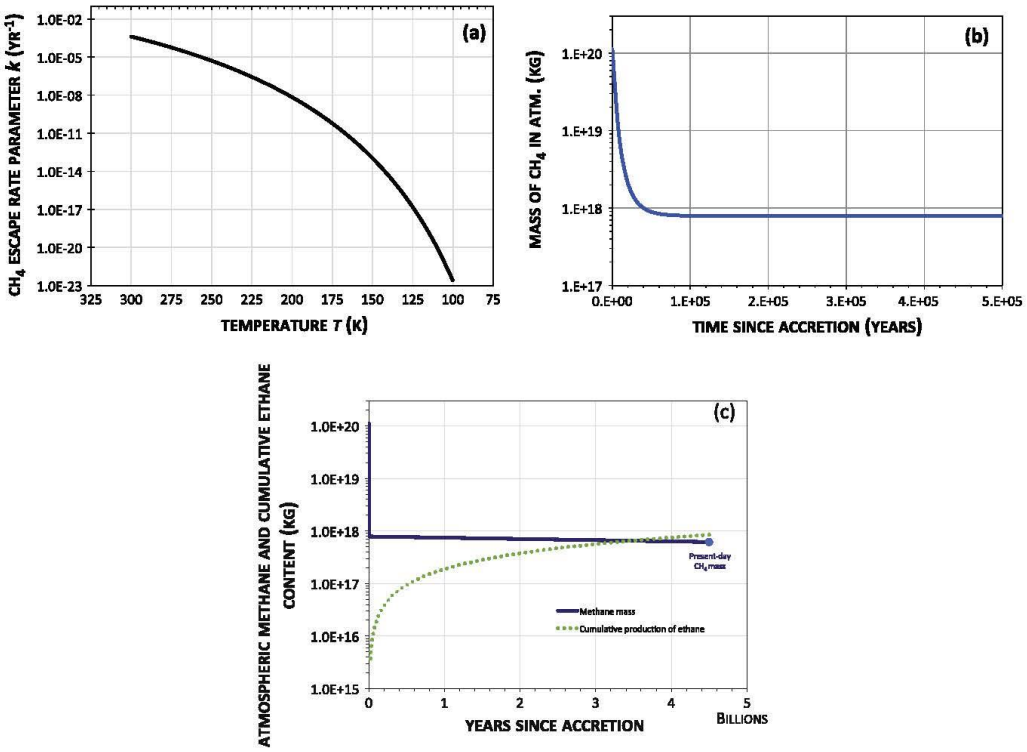

Fig. 3. Methane depletion and ethane production in Titan's atmosphere since accretion, using a model where the rate of methane escape varies with temperature. (a) The escape rate parameter, k, vs. temperature, T, for CH_4 assuming an accretion temperature of 300 K, from data of Gilliam and Lerman (2014a, Fig. 10). k depends on temperature, gas molecular mass, atmosphere thickness, and Titan's escape velocity. (b) The mass of CH_4 in Titan's atmosphere as a function of time, during the first 0.5 Myr after accretion, using the escape rate parameter, k, and decreasing atmosphere thickness. (c) The mass of CH_4 in Titan's atmosphere, calculated using the variable k (Gilliam and Lerman, 2014a), and cumulative production of C_2H_6 as a function of time during the last 4.5 Ga, with a C_2H_6 production rate of 1.3×10^8 molecules cm^{-2} s^{-1}.

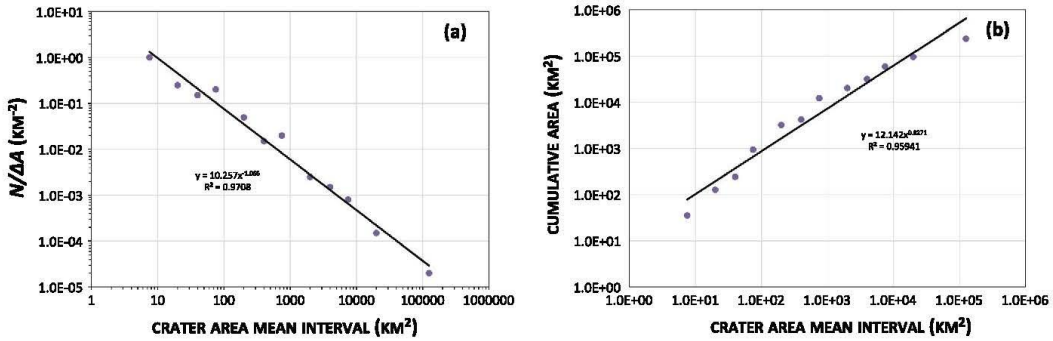

Fig. 4. Size distribution of Titan's 62 craters following a power-law distribution, slope −1. Crater areas calculated using Cassini measurements of crater diameters (Wood et al., 2010; Neish and Lorenz, 2012; Buratti et al., 2012; Neish et al., 2013). (a) Crater area-size distribution. (b) Cumulative crater area distribution.

theorize the maximum potential volume available for liquid ethane on Titan's surface. To date, 62 possible craters have been observed on the surface of Titan (Neish and Lorenz, 2012; Neish et al., 2013; Buratti et al., 2012; Wood et al., 2010), ranging in diameter from 3 to 425 km. Assuming a spherical cap for crater volume, we calculate a total crater volume of roughly 61,000 km^3, covering a total area of 238,000 km^2, with the crater surface areas following a power law distribution with a slope of −1 (Fig. 4). If these craters were fed by 100% ethane rainfall, their total storage capacity of ethane would be 3.8×10^{16} kg, roughly 4.5% of the total

cumulative ethane production. Even after adding the total crater liquid capacity to the lake capacity, total ethane surface storage would be 6.9×10^{16} kg, still only 8.2% of the total possible ethane production. This suggests that there must be a large quantity of liquid ethane present elsewhere on Titan, perhaps sequestered in Titan's subsurface.

4. Porosity and the subsurface reservoir of ethane

Previous work (Fortes et al., 2007; and references in Gilliam and Lerman, 2014a,b) has suggested that Titan has a complex internal structure overlain by a 100+ km crust composed primarily of water ice (Fig. 5). Observations of fluvial channels on Titan's surface suggest that the water–ice particles in Titan's crust are not cohesive, due to the difficulty of eroding coherent icy bedrock, and instead must have been ubiquitously fractured prior to erosion. Such a fractured icy crust would be highly permeable to liquid ethane and methane (Sotin et al., 2009). Possible formation mechanisms for a surface porous layer include the ascent of liquid from the subsurface ocean (Mitri et al., 2008) or from the destabilization of clathrates in Titan's ice shell (Tobie et al., 2006). In both cases, a highly porous icy material in contact with the atmosphere would have been generated (Artemieva and Lunine, 2003; Mousis and Schmitt, 2008).

Porosity of ice on Earth is a measure of the ice volume fraction taken up by air or other gases. It is created on a small scale by intercrystalline spaces, gas bubbles, and on a larger scale by cracks and crevasses. In ice sheets, crevasses are rarely more than 45 m deep but in some cases can be 300 m or even deeper. Beneath this point, the plasticity of the ice is too great for cracks to form (Hambrey, 1994). A general diagram of different kinds of snow and ice (Menzies and Hughes, 2002) gives a porosity of 10% for new ice and about 1% for old ice. Porosity, measured as the gas-bubble volume in Central Antarctic ice, was reported as 8–9% (Lipenkov et al., 1997). Other sources give the porosity of solid ice-sheet and solid sea-ice between 0.1% and 5% (Vasil'chuk, 2005). In the absence of *in situ* measurements of porosity of the upper crust of Titan, we use the ice-sheet data from Earth and allow for a higher mean porosity of 20% due to cracks and fissures.

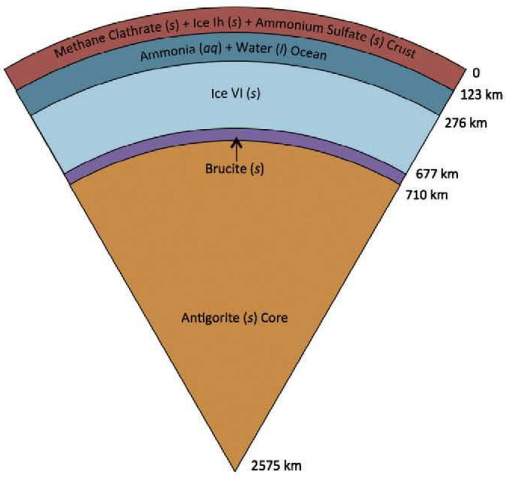

Fig. 5. Present-day internal structure of Titan consisting of an antigorite core overlain by a thin layer of brucite, a layer of ice VI, an ammonia-rich ocean, and a crust made of methane clathrate, ice Ih, and solid ammonium sulfate (Fortes et al., 2007; Gilliam and Lerman, 2014a).

The mass of ethane produced, 8.46×10^{17} kg, would occupy an average volume of 1.37×10^{15} m^3 (mean of densities at 150 K, 585.8 kg/m^3, and at 93 K, 651.9 kg/m^3; Younglove and Ely, 1987, p. 642). If it can be contained within the pore space of the uppermost 2 km of Titan's crust, 1.67×10^{8} km^3, then the crust would require a minimum porosity of 0.9%. This estimate is in line with the porosity of old ice sheets on Earth and the sequestration potential of Titan's crust for the liquid ethane may in fact be considerably higher.

Alternatively, using a higher yet reasonable crustal porosity of 20% – inferred from Huygens probe observations and consistent with what we know about the behavior of impact gardened icy surfaces (Artemieva and Lunine, 2003) – we estimate that the maximum porous volume of the upper 2 km of the crust is 3.33×10^{7} km^3, or 3.32×10^{7} km^3 if we do not include the volume of lakes and craters (0.01×10^{7} km^3). If the total porous volume is filled with a 100% ethane solution, then its maximum ethane storage potential is $\sim 2.06 \times 10^{19}$ kg, which is well above the previous calculated total ethane production of 8.46×10^{17} kg. This suggests that Titan's entire liquid ethane budget could be stored in its porous crust, or it could certainly serve as additional subsurface storage.

5. Conclusions and ruminations

A simple photolysis model, where the methane molecule can either escape the atmosphere or produce ethane, gives up to 8.46×10^{17} kg of liquid ethane that might have been produced since Titan's accretion. This amount is 10^4 times larger than the present-day atmospheric ethane mass of 9.24×10^{13} kg, suggesting that most of the remaining ethane resides in liquid form on or within Titan. Ethane liquefies at a temperature higher than methane and, as Titan's surface cooled in the course of time, ethane might have started to rain early in Titan's history. Indeed, our estimate for the amount of liquid ethane storage potential on Titan's surface is 1.36×10^{16} kg in lakes and seas and additional 3.34×10^{16} kg in craters, both numbers much smaller that the mass calculated. The calculated total mass of ethane produced at an estimated production rate, 8.5×10^{17} kg (mean density 619 ± 33 kg m^{-3} at 93.3–150 K), corresponds to a volume of 1.4×10^{15} m^3. This volume represents only a small porosity fraction of the upper 2 km of Titan's crust (1.67×10^{17} m^3): 0.9%. This is the minimum porosity needed to store in the subsurface excess of ethane produced that is greater than the volume of lakes and craters (see also Mousis and Schmitt, 2008). A higher porosity of 20% of the upper 2 km of the crust, 3.33×10^{16} m^3, is much greater that the estimated volumes of ethane produced, suggesting that Titan's entire liquid ethane budget could be stored in its porous crust.

The existence of liquid on Titan's surface and in the subsurface may be very important as a potentially suitable habitat for life. Life created in liquid hydrocarbons, such as ethane and methane, would certainly not resemble anything on Earth, but, if discovered, would be clear evidence of a "Second Coming of Life" in our Solar System. Previous studies have shown that the photochemical processes responsible for Titan's liquid hydrocarbons could be a potential source of chemical energy (on Earth, life uses only two types of energy for primary production: chemical energy and sunlight) at levels shown to be favorable for methanogenic bacteria on Earth (McKay and Smith, 2005; Schulze-Makuch and Grinspoon, 2005).

We conclude by comparing some of the characteristics of liquid ethane with those of water, as a medium of life. On Earth, the idea that life originated in water and an anoxic atmosphere, where organic molecules could aggregate and replicate themselves, is the "primordial soup" theory of Oparin (1924, 1941, 1953) and Haldane (1929, also cited in Tirard, 2011). Bernal (1951) called

the origin of life "biopoesis", and Miller (1953) and Miller and Urey (1959) demonstrated the formation of organic molecules in an anoxic gas mixture by electrical discharge. The presence of methane and ethane in Titan's atmosphere has led to a long series of hypotheses that life might exist on Titan, despite its present surface temperature near 90 K. Some of the recent studies of this subject are those of Neish et al. (2010), Norman (2011), and Stevenson et al. (2015) who studied the formation of N–C–H compounds, called azotosomes, as a possible source of life in the liquid hydrocarbons on Titan's surface. Lunine and McKay (1995) have extensively discussed the parallels between the conditions on Titan's surface and in the subsurface in comparison to those on primordial Earth.

The liquid medium of a "primordial soup" is a solvent in which organic molecules can move toward each other and aggregate. The movement, similar to Brownian motion, in a liquid medium is in part controlled by diffusion of particles that further depends on the solubility of the substance, particle size, temperature, and viscosity of the medium.

Solubilities of short polyethers, organic compounds of the type R_1–O–R_2, in propane (C_3H_8) have been studied by McLendon et al. (2015). Polyethers are components of the more complex life-building molecules and they were reported as reasonably soluble in liquid propane down to about 200 K. At lower temperatures approaching 170 K, their solubilities drop almost to nil. If the same solubility relationships hold in liquid ethane, then the diffusivity of the organic molecules in solution will be controlled by the factors mentioned above.

The "primordial soup" in itself may be a fairly thick concoction and have a higher bulk viscosity than the liquid medium or solvent. Eventually, the "soup" may thicken to a slurry or close to becoming a gel. Water or seawater has a viscosity in a range from about 1×10^{-3} Pa s (25 °C) to 1.8×10^{-3} Pa s (0 °C) (Sharqawy et al., 2010). More viscous natural liquids, such as petroleum, have viscosities in the range from 10 to 100 Pa s below 40 °C (Speight, 1998). The viscosity of liquid ethane, from 90 to 150 K, is comparable to that of water or seawater on Earth, $1.26–0.25 \times 10^{-3}$ Pa s (Younglove and Ely, 1987, p. 642). However, two other factors exert a big effect on molecular diffusivity and the slowing down of molecular velocities in liquid ethane: particle size and temperature. The effects of temperature, particle size, and viscosity of the medium on the diffusion coefficient (D, $m^2\ s^{-1}$) follow from the equations of Einstein (1905, 1956), as given below, and von Smoluchowski (1906), with the additional coefficient of $(4/3)^3 = 2.37$:

$$D = \frac{RT}{6\pi\eta r N} \tag{5}$$

where D is the diffusion coefficient of a particle in solution ($m^2\ s^{-1}$), T is temperature (K), η is viscosity (Pa s), r is particle radius (m), N is Avogadro's number, and R is the gas constant ($J\ mol^{-1}\ K^{-1}$).

From (5), denoting the parameters in ethane by subscript 2, and those in water by subscript 1, the following quotients obtain:

$$\frac{D_2}{D_1} = \left(\frac{T_2}{\eta_2 r_2}\right) \Big/ \left(\frac{T_1}{\eta_1 r_1}\right) \tag{6}$$

Diffusion coefficients of sugars and amino acids in dilute solutions, molecules of effective radius 4.5 ± 2 Å or of an order of 10^{-10} m and molecular mass 75–204 g/mol, fall in the range of $5–10 \times 10^{-6}$ $cm^2\ s^{-1}$ at 25 °C, but the D values decrease by a factor of 2–5 for diffusion in gels (Nakanishi et al., 1977). D values in the range from 4.5 to 9.5×10^{-6} $cm^2\ s^{-1}$ of similar substances were reported by Polson (1937). These values would be by a factor of 0.5 lower at 273 K, as follows from Eq. (6).

For a life made of C, N, H, and O atoms to exist on Titan, polymerization of small organic molecules has been considered by a number of investigators. Polymers are heavier and bigger molecules, with the mass of medium-large polymers of 1000–30,000 g/mol and linear dimensions 10^{-8} to 10^{-7} m (Cowie, 1966; Akcasu and Han, 1979).

To estimate the diffusion coefficients of organic molecules in ethane, D_2 in Eq. (6), we use the viscosity values of water at 273 K (1.791×10^{-3} Pa s) (Sharqawy et al., 2010), liquid ethane viscosity at 90.4 K (1.260×10^{-3} Pa s) and 150 K (0.252×10^{-3} Pa s) (Younglove and Ely, 1987, p. 642), and particle radius approximating polymers of $10^0–10^3$ Å or $10^{-10}–10^{-7}$ m. Combinations of different triplets of temperature, corresponding viscosity, and particle size give the following diffusion coefficients of organic molecules in ethane: fractions between 0.26 and 0.47 when only the temperatures and viscosities are compared with those of water; the reduction of the diffusion coefficient in ethane is much greater, 4.7×10^{-4} to 4×10^{-3}, when larger-size polymer particles are considered.

Apart from the molecular mobility, there remains a question of the rates of chemical reactions in the cryogenic environment of Titan. A very crude estimate that can be made here is based on some values of the polymerization rate constant k_p (Ling et al., 2001; Luo et al., 2006) and the activation energy of polymerization ΔE_a (Skene et al., 1998). The estimate is based on Arrhenius reaction rate dependence on temperature:

$$\ln\left(\frac{k_{low}}{k_{273}}\right) = -\frac{E_a}{R}\left(\frac{1}{T_{low}} - \frac{1}{273}\right) \tag{7}$$

A mean of several activation energy values for different polymerization reactions is about 130 kJ/mol at 337 K, and the rate constants vary from 0.7 to 1900 $cm^3\ mol^{-1}\ s^{-1}$ at 323 K. Using T_{low} in (7) as 150 K and 100 K, the rate constant at 273 K would be reduced by a very large factor of 4×10^{-21} and 9×10^{-44}, respectively.

The reduction in mobility of organic molecules in diffusion and the possibly strong lowering of the rate constants for polymerization may be less advantageous to aggregation of molecules in liquid ethane by comparison with a "primordial soup" based on water.

Acknowledgments

This work was supported by NASA Headquarters under the NASA Earth and Space Science Fellowship Program – Grant NNX13AO02H, and by the Weinberg College of Arts and Sciences at Northwestern University. We thank anonymous reviewers for their insightful suggestions and helpful criticism to the earlier version of this paper.

References

Akcasu, A.Z., Han, C.C., 1979. Molecular weight and temperature dependence of polymer dimensions in solution. Macromolecules 12, 276–280.
Artemieva, N., Lunine, J., 2003. Cratering on Titan: Impact melt, ejecta, and the fate of surface organics. Icarus 164, 471–480.
Atreya, S.K., et al., 2006. Titan's methane cycle. Planet. Space Sci. 54, 1177–1187.
Atreya, S.K., Lorenz, R.D., Waite, J.H., 2009. Volatile origin and cycles: Nitrogen and methane. In: Brown, R.H., Lebreton, J.-P., Waite, J.H. (Eds.), Titan from Cassini–Huygens. Springer, pp. 177–199.
Barr, A.C., Citron, R.I., Canup, R.M., 2010. Origin of a partially differentiated Titan. Icarus 209, 858–862.
Barth, E.L., Toon, O.B., 2003. Microphysical modeling of ethane ice clouds in Titan's atmosphere. Icarus 162, 94–113.
Bernal, J.D., 1951. The Physical Basis of Life. Routledge & Kegan Paul, London.
Buratti, B.J., et al., 2012. A newly discovered impact crater in Titan's Senkyo: Cassini VIMS observations and comparison with other impact features. Planet. Space Sci. 60, 18–25.
Chevrier, V.F., Luspay-Kuti, A., Singh, S., 2015. Experimental study of nitrogen dissolution in methane–ethane mixtures under Titan surface conditions. Lunar Planet. Sci. 46, 2673.
Cornet, T., et al., 2015. Dissolution of Titan and on Earth: Towards the age of Titan's karstic landscapes. J. Geophys. Res.: Planet. 120, 1044–1074.

Cowie, J.M.G., 1966. Estimation of unperturbed polymer dimensions from viscosity measurements in non-ideal solvents. Polymer 7, 487–495.

Croft, S.K., Lunine, J.I., Kargel, J., 1988. Equation of state of ammonia–water liquid—Derivation and planetological applications. Icarus 73, 279–293.

Einstein, A., 1905. Über die von der molekularkinetischen Theorie der Wärme geforderte Bewegung von in ruhenden Flüssigkeiten suspendierten Teilchen. Ann. Phys. 322, 549–560.

Einstein, A., 1956. Investigations on the Theory of the Brownian Movement. A.D. Cowper, Trans.. Dover Publications, New York (Edited with notes by R. Fürth).

Farnsworth, K. et al., 2016. Experimental study of nitrogen dissolution in methane–ethane mixtures under Titan surface conditions. Lunar Planet. Sci. 47, 2380.

Fortes, A.D., et al., 2007. Ammonium sulfate on Titan: Possible origin and role in cryovolcanism. Icarus 188, 139–153.

Gilliam, A.E., Lerman, A., 2014. Evolution of Titan's major atmospheric gases and cooling since accretion. Planet. Space Sci. 93–94, 41–53.

Gilliam, A.E., Lerman, A., 2014. Corrigendum to "Evolution of Titan's major atmospheric gases and cooling since accretion". Planet. Space Sci. 101, 210.

Gilliam, A.E., Lerman, A., Wunsch, J., 2015. Evolution of Titan's atmosphere in relation to its surface and interior. In: Astrobiology Science Conference 2015, 7772.

Gough, O.D., 1981. Solar interior structure and luminosity variations. Solar Phys. 74, 21–34.

Graves, S.D.B., et al., 2008. Rain and hail can reach the surface of Titan. Planet. Space Sci. 56, 346–357.

Haldane, J.B.S., 1929. The Origin of Life: The Rationalist Annual, London. Pemberton Publishing Co Ltd, London Reprinted in Haldane, JBS, science and life, with an introduction by Maynard Smith, J. (1968).

Hambrey, M.J., 1994. Glacial Environments. CRC Press.

Hayes, A., et al., 2008. Hydrocarbon lakes on Titan: Distribution and interaction with a porous regolith. Geophys. Res. Lett. 35, L09204. doi:10.1029/2008GL033409.

Haynes, W.M. (Ed.), 2016, CRC Handbook of Chemistry and Physics, 96th ed.. CRC Press, Boca Raton, FL.

Herdendorf, C.E., 1982. Large lakes of the world. J. Great Lakes Res. 8, 379–412.

Ling, J., et al., 2001. Kinetics simulation of high viscous styrene bulk polymerization system. Eur. Polym. J. 37, 22407–22411.

Lipenkov, V.Ya., Salamatin, A.N., Duval, P., 1997. Bubbly-ice densification in ice sheets: II. Applications. J. Glaciol. 43, 397–407.

Lopes, R.M.C., et al., 2007. The lakes and seas of Titan. Eos Trans. AGU 88, 569–570.

Lorenz, R.D., et al., 2008. Titan's inventory of organic surface materials. Geophys. Res. Lett. 35, 2206. doi:10.1029/2007GL032118.

Lorenz, R.D., et al., 2014. A radar map of Titan Seas: Tidal dissipation and ocean mixing through the throat of Kraken. Icarus 237, 9–15.

Lunine, J.I., Atreya, S.K., 2008. The methane cycle on Titan. Nat. Geosci. 1, 159–164.

Lunine, J.I., McKay, C.P., 1995. Surface-atmosphere interactions on Titan compared with those on the pre-biotic Earth. Adv. Space Res. 15, 303–311.

Lunine, J.I., Stevenson, D.J., Yung, Y.L., 1983. Ethane ocean on Titan. Science 222, 1229–1230.

Luo, Z.-h., et al., 2006. Estimation of rate constants for polymerization based on Monte Carlo simulation. J. Shanghai Univ. 10, 274–276.

McKay, C.P., Smith, H.D., 2005. Possibilities for methanogenic life in liquid methane on the surface of Titan. Icarus 178, 274–276.

McLendon, C., et al., 2015. Solubility of polyethers in hydrocarbons at low temperatures. A model for potential genetic backbones on warm Titans. Astrobiology 15, 200–206.

Menzies, J., Hughes, T.J., 2002. Glaciers and ice sheets. In: Menzies, J. (Ed.), Modern & Past Glacial Environments. Butterworth-Heinemann, pp. 53–78.

Miller, S., 1953. A production of amino acids under possible primitive Earth conditions. Science 17, 528–529.

Miller, S., Urey, H., 1959. Organic compound synthesis on the primitive Earth. Science 130, 245–251.

Mitri, G., et al., 2008. Resurfacing of Titan by ammonia–water cryomagma. Icarus 196, 216–224.

Mousis, O., Schmitt, B., 2008. Sequestration of ethane in the cryovolcanic subsurface of titan. Astrophys. J. 677, 67–70.

Nakanishi, K., et al., 1977. Diffusion of saccharides and amino acids in crosslinked polymers. Agric. Biol. Chem. 41, 2455–2462.

Neish, C.D., Lorenz, R.D., 2012. Titan's global crater population: A new assessment. Planet. Space Sci. 60, 26–33.

Neish, C.D., Somogyi, Á., Smith, M.A., 2010. Titan's primordial soup: Formation of amino acids via low-temperature hydrolysis of tholins. Astrobiology 10, 337–347.

Neish, C.D., et al., 2013. Crater topography on Titan: Implications for landscape evolution. Icarus 223, 82–90.

Niemann, H.B., et al., 2005. The abundances of constituents of Titan's atmosphere from the GCMS instrument on the Huygens probe. Nature 438, 779–784.

Norman, L.H., 2011. Is there life on…Titan? Astron. Geophys. 52, 139–142.

Oparin, A.I. [Опарин А. И.], 1924. Происхождение жизни. М., Московский рабочий, 71 с.

Oparin, A.I., 1941. Возникновение жизни на Земле. 2-е изд., значительно дополненное. М.-Л.: Издательство Академии Наук СССР, — 267 с.

Oparin, A.I., 1953. The Origin of Life. Translation and New Introduction by Sergius Morgulis, second ed. Dover Publications, Mineola, NY (Originally published 1938; New York: The Macmillan Company).

Polson, A., 1937. CCXXXIII. On the diffusion constants of the amino-acids. Biochem. J. 31, 1903–1912.

Rannou, P., et al., 2006. The latitudinal distribution of clouds on Titan. Science 311, 201–205.

Sagan, C., Thompson, W.R., 1984. Production and condensation of organic gases in the atmosphere of Titan. Icarus 59, 133–161.

Schulze-Makuch, D., Grinspoon, D.H., 2005. Biologically enhanced energy and carbon cycling on Titan? Astrobiology 5, 560–564.

Sharqawy, M.H., Lienhard, V.J.H., Zubair, S.M., 2010. Thermophysical properties of seawater: A review of existing correlations and data. Desalin. Water Treat. 16, 354–380.

Shiklomanov, I.A., 1993. World fresh water resources. In: Gleick, P.H. (Ed.), Water in Crisis: A Guide to the World's Fresh Water Resources. Oxford University Press, pp. 13–24.

Skene, W.G., et al., 1998. Decomposition kinetics, Arrhenius parameters, and bond dissociation energies for alkoxyamines of relevance in "living" free radical polymerization. Macromolecules 31, 9103–9105.

von Smoluchowski, M., 1906. Zur kinetischen Theorie der Brownschen Molekularbewegung und der Suspensionen. Ann. Phys. 326, 756–780.

Sotin, C. et al., 2009. Ice–hydrocarbon interactions under titan-like conditions: Implications for the carbon cycle on Titan. Lunar Planet. Sci. 40, 2088.

Speight, J.G., 1998. Petroleum analysis and evaluation. In: Speight, J.G. (Ed.), Petroleum Chemistry and Refining. Taylor & Francis, pp. 39–62.

Stevenson, J., Lunine, J., Clancy, P., 2015. Membrane alternatives in worlds without oxygen: Creation of an azotosome. Sci. Adv. 1, E1400067. doi:10.1126/sciadv.1400067.

Strobel, D.F., 2009. Titan's hydrodynamically escaping atmosphere: Escape rates and the structure of the exobase region. Icarus 202, 632–641.

Tirard, S., 2011. Haldane's conception of origins of life. In: Gargaud, M. (Ed.), Encyclopedia of Astrobiology. Springer, p. 724.

Tobie, G., Lunine, J.I., Sotin, C., 2006. Episodic outgassing as the origin of atmospheric methane on Titan. Nature 440, 61–64.

Toublanc, D., et al., 1995. Photochemical modeling of Titan's atmosphere. Icarus 113, 2–26.

Van Hinsberg, M.G.E., Schouten, J.A., 1994. The phase diagram of nitrogen clathrate hydrate. Am. Inst. Physics Conference Proceedings, vol. 309, pp. 271–274.

Vasil'chuk, Yu.K., 2005. Physical properties of glacial and ground ice. In: Khubryanayt, M.G. (Ed.). Types and Properties of Water, vol. II. UNESCO, Paris 392 p.

Wilson, E.H., Atreya, S.K., 2004. Current state of modeling the photochemistry of Titan's mutually dependent atmosphere and ionosphere. J. Geophys. Res. 109, E06002. doi:10.1029/2003JE002181.

Wilson, E.H., Atreya, S.K., 2009. Titan's carbon budget and the case of the missing ethane. J. Phys. Chem. A 113, 11221–11226.

Wood, C.A., et al., 2010. Impact craters on Titan. Icarus 206, 334–344.

Yelle, R.V., Cui, J., Müller-Wodarg, I.C.F., 2008. Methane escape from Titan's atmosphere. J. Geophys. Res. 113, E10003. doi:10.1029/2007JE003031.

Younglove, B.A., Ely, J.F., 1987. Thermophysical properties of fluids. II. Methane, ethane, propane, isobutane, and normal butane. J. Phys. Chem. Ref. Data 16 (4), 577–798.

Yung, Y.L., DeMore, W.B., 1999. Photochemistry of Planetary Atmospheres. Oxford University Press.

Yung, Y.L., Allen, M., Pinto, J.P., 1984. Photochemistry of the atmosphere of Titan: Comparison between model and observations. Astrophys. J. Suppl. Ser. 55, 465–506.

Planetary and Space Science 132 (2016) 13–22

Contents lists available at ScienceDirect

Planetary and Space Science

journal homepage: www.elsevier.com/locate/pss

Formation mechanisms of channels on Titan through dissolution by ammonium sulfate and erosion by liquid ammonia and ethane

Ashley E. Gilliam *, Abraham Lerman

Department of Earth and Planetary Sciences, Northwestern University, 2145 Sheridan Rd – Tech F379, Evanston, IL 60208-3130, United States

ARTICLE INFO

Article history:
Received 17 March 2016
Received in revised form
19 July 2016
Accepted 26 August 2016
Available online 28 August 2016

Keywords:
Titan
Channels
Dissolution
Erosion
Ammonium sulfate and ammonia
Liquid ethane

ABSTRACT

Data obtained from the Cassini Visual and Infrared Mapping Spectrometer (VIMS), Imaging Science Subsystem (ISS), and Synthetic Aperture Radar (SAR) instruments have revealed an array of fluvial channels on Titan's surface, often several hundreds of kilometers in length. The paucity of impact craters on Titan's surface suggests a formation by fluvial erosion into the water-ice bedrock. Additionally, at the landing site, the Huygens Probe Descent Imager and Spectral Radiometer (DISR) imaged Earth-like rounded cobbles 0.3–15 cm in diameter composed of water ice, reminiscent of rounded stream clasts on Earth. In this paper we examine different fluvial features on Titan, identified by the Cassini spacecraft, and evaluate the possibilities of channel formation by dissolution of ice by a concentrated solution of ammonium sulfate, and by mechanical erosion by flow of liquid ammonia and liquid ethane. We find that chemical erosion of Titan's channels could be completed in 280 to 1100 years (all units of time in this paper are Terrestrial, not Titanian), much shorter than the period of about 84,000 years that a concentrated $(NH_4)_2SO_4$-H_2O solution could exist as a liquid on the Titan surface. Mechanical erosion of Titan's channels is generally a much slower process, on the order of 10^2 to 10^5 years to completion, and is also slower than mechanical erosion of a model river on Earth, averaging 10^3 to 10^4 years. The erosional sequence of the channels on Titan may have started after the formation of water-ice on the surface by the process of chemical dissolution by $(NH_4)_2SO_4$-H_2O, overlapping, or followed by, a period of mechanical erosion by liquid NH_3. A final stage on the cooling surface of Titan might have been characterized by liquid C_2H_6 as an agent of mechanical erosion.

1. Introduction

Titan, the largest moon of Saturn, is the only satellite in the solar system with a significant atmosphere, harboring a suite of hydrocarbons that display a meteorological cycle similar to the hydrological cycle on Earth. Dendritic networks of sinuous valleys on the surface of Titan were first observed by the Cassini-Huygens mission, where Synthetic Aperture Radar (SAR) images revealed drainage networks with branching morphologies on the order of 100 km in length (Elachi et al., 2005). These observations were supported in greater detail by the Huygens Probe Descent Imager and Spectral Radiometer (DISR) (Tomasko et al., 2005; Soderblom et al., 2007b; Jaumann et al., 2009), and suggested formation by fluvial erosion into the water-ice bedrock. Additional support that the valleys were formed by flowing liquid is the paucity of impact craters on Titan's surface (Porco et al., 2005; Elachi et al., 2005; Jaumann et al., 2009; Wood et al., 2010), indicative of rapid burial or removal of surface topography. Additionally, at the landing site, the DISR imaged Earth-like rounded cobbles 0.3–15 cm in diameter (Tomasko et al., 2005) composed of water ice, indicating that they had undergone abrasion during fluvial transport. Further evidence of widespread fluvial processes on the surface of Titan has been revealed by the Cassini Imaging Science Subsystem (ISS) (Porco et al., 2005) and the Visual and Infrared Mapping Spectrometer (VIMS) (Barnes et al., 2007b; Jaumann et al., 2008).

Unlike on Earth, where liquid H_2O is the major agent of erosion, Titan's liquid erosion likely has multiple contributors. One possible contributor, that arguably garners the most attention, is liquid CH_4. Methane, which forms several percent of Titan's atmosphere, is a likely candidate for liquid erosion due to its stability as a liquid on the surface, its ability to participate in Titan's hydrological cycle, and direct observations of cloud-top altitudes consistent with the condensation altitudes expected for methane (Lorenz et al., 2008). Further support for liquid methane being a primary contributor to Titan's erosion is shown in the works of, for example, Burr et al. (2006, 2009, 2013), Perron et al. (2006), Jaumann et al. (2008), Lorenz et al. (2008), Cartwright et al. (2011), Langhans et al. (2012),

*Corresponding author.
E-mail address: ashley@earth.northwestern.edu (A.E. Gilliam).

http://dx.doi.org/10.1016/j.pss.2016.08.009
0032-0633/

Black et al. (2012), whose studies suggest that it could plausibly move enough material under conditions present on Titan to account for most of the observed fluvial features, even suggesting that mechanical erosion by liquid methane surface runoff would not require unreasonably high precipitation rates. Works similar to those cited above are numerous, but here we consider other liquids, which are also present on Titan, that could be responsible for the formation of the channels seen on the surface.

In this paper we address two different fluvial erosion processes on Titan. Specifically, we examine the possibilities of channel formation by dissolution of ice by a concentrated solution of ammonium sulfate, and by mechanical erosion by flow of liquid ammonia and liquid ethane. Each of these processes might have functioned over a certain range of temperatures during the cooling history of Titan.

That liquid ethane in Titan's atmosphere is not a pure liquid, but a solution containing CH_4 and N_2, has been shown by Tan et al. (2013, 2015). For surface liquids on Titan, such as in Ontario Lacus, the liquid was given as 15–30% CH_4, 50–80% C_2H_6, and 5–10% N_2 (Luspay-Kuti et al., 2015; Mitri et al., 2007), and a similar composition of liquid C_2H_6 solution on Titan's equator is given by Tan et al. (2015). The physical properties of a C_2H_6-CH_4-N_2 solution are not a weighted mean of the properties of three liquids, each of a very different liquefaction temperature. The properties are likely to be those of a solution of gaseous CH_4 and N_2 in liquid C_2H_6, similar to the properties of a solution of such gases as CO_2, N_2, and O_2 in liquid H_2O. The more soluble gas CO_2 affects the density and viscosity of pure H_2O very little, by less than 3% (Garcia, 2001). The density of ethane solutions on the equator and the poles of Titan, as given by Tan et al. (2015) is 601–547 kg m^{-3}. These values are close to those of pure C_2H_6, 652 kg m^{-3} at 90.4 K and 586 kg m^{-3} at 150 K. We further assume that viscosity, like density, of pure liquid C_2H_6 does not differ much from an ethane solution of methane and nitrogen gases.

2. Observations of streams on Titan

Valley-like features on the surface of Titan are known from the Huygens landing site and by three different imaging instruments onboard the Cassini spacecraft: the Visual and Infrared Mapping Spectrometer (VIMS), operating at 0.35–5.2 μm (Brown et al., 2004), the Imaging Science Subsystem (ISS), operating at 0.2–1.1 μm (Porco et al., 2005), and the Cassini Titan Radar Mapper (RADAR), emitting at 2.2 cm (Elachi et al., 2005). The resolution of VIMS and ISS images, which are hindered by atmospheric scattering and absorption, varies with both the distance of the spacecraft and emission angle. VIMS spatial resolution averages a few km/pixel but for small areas can be as high as 250 m/pixel (Jaumann et al., 2009). ISS resolution ranges from 1 to 10 km, with relatively small areas imaged at 1 km/pixel (Porco et al., 2004, 2005). The synthetic aperture radar (SAR) data from the RADAR are collected in swaths and are of the highest resolution (~350 m/pixel) available from the Cassini spacecraft (Lopes et al., 2010). Although RADAR coverage of the Titan surface is ~50% to date, compared to near-global coverage by the VIMS and ISS data, the SAR data provide the best resolution for mapping the fluvial networks.

In this study we examine 27 different fluvial features as identified in VIMS, ISS, and RADAR data, chosen based on their geographic diversity and resolution – or our confidence in their classification as a fluvial feature. The locations and dimensions of these features on Titan are indicated in Figs. 1 and 2, and summarized in Table 1. These valleys represent an array of morphologic features and range in size from tens of kilometers to over a thousand kilometers long, and up to ten kilometers wide. The majority of these features are dendritic in nature, forming tree-shaped networks with many contributing branches that converge into larger receiving streams, up to seventh in channel order, indicative of an origin from rainfall (Tomasko et al., 2005; Perron et al., 2006; Lorenz et al., 2008; Jaumann et al., 2009).

In contrast to these complex channels, there are also several fluvial features that seldom exhibit meanders, possess a low channel order, and a large channel width of up to 10 km. These features are inferred to be dry valleys, created as a result of rapid runoff events followed by prolonged droughts (Lorenz et al., 2008).

Another group of fluvial valleys recorded are believed to be the result of erosion by liquid seepage from the subsurface. These sapping channels are classified as being generally shorter and broader than those created by rainfall, and possess a low channel-order (Tomasko et al., 2005; Jaumann et al., 2009). If correct, the presence of sapping channels indicates that Titan has a subsurface aquifer, which will be discussed in a later section.

Also notable are three features inferred as elongated valleys due to their straight course and their relatively small size, two fluvial features that exist within mountain chains and support an origin from rainfall (Langhans et al., 2012), and one system of valleys associated with alluvial fans.

In order to calculate the relative rates of stream incision into the water-ice bedrock on Titan, the channel dimensions used are as shown in Table 1. Measurements of channel slope were made directly from Cassini RADAR SARtopo and altimetry data, and depth from an empirical relationship between channel depth and width as outlined in William (1988). Size-distribution of the channels are shown in Fig. 2.

3. Crustal composition and structure

Previous work (Fortes et al., 2007; and references in Gilliam and Lerman, 2014a, 2014b) has suggested that the interior of Titan is composed of a complex assemblage of silicate minerals, organic matter, liquid water in a subsurface NH_3-H_2O ocean, and ices, overlain by a crust composed primarily of low-pressure water ice, methane clathrate and ammonium sulfate. The exact thickness of the crust is mainly determined by the amount of heat available in the interior as well as the percentage of anti-freezing agents in the subsurface ocean, but is generally thought to be >100 km at present-day (Fortes et al., 2007; Gilliam and Lerman, 2014a).

The formation of the crust is a result of the interaction between Titan's primitive atmosphere and its liquid layer, which were in direct contact immediately after accretion and up until sufficient cooling of the atmosphere resulted in the crystallization of a solid shell composed of ice and methane clathrates (Tobie et al., 2006). After further cooling and thickening, macroporous clathrate grains are thought to have transported pockets of ammonium sulfate solution upwards, incorporating them into the outer shell, where they ultimately solidified to water ice and ammonium sulfate (Fortes et al., 2007). At present-day, a cross-section of the upper part of Titan's interior would reveal a top layer of ice Ih, methane clathrate, and solid ammonium sulfate, of densities 941, 988.5, and 1769 kg m^{-3}, respectively (Fig. 3, Table 2). On Earth, ammonium sulfate occurs as mineral mascagnite in fumaroles and volcanic vents.

4. Channel formation mechanisms

In this section, we consider the characteristics of the valley networks and Titan's surface environment, and several possible mechanisms of channel formation. The four, as shown in Fig. 4 and Table 3, might have operated at different times during Titan's

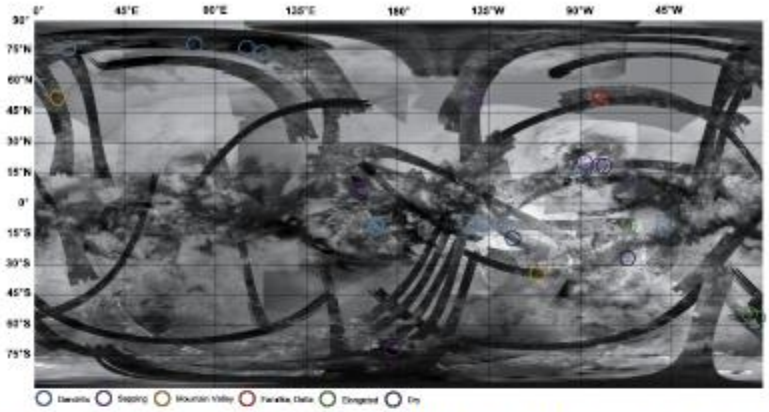

Fig. 1. Geographic distribution of fluvial features examined in this study, on SAR and ISS data up through T71, color-coded by network classification (see legend).

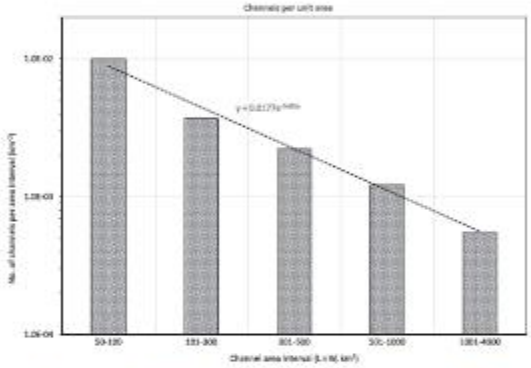

Fig. 2. Frequency distribution of channels by channel area interval (Table 1).

cooling history. As far as the main component of the formation of present-day Titan's atmosphere, nitrogen gas N_2, is concerned, its condensation temperature at the pressure of 1–2 bar is 77–82 K, below the 90 K of the present-day Titan atmosphere (Jacobsen and Stewart, 1973). Fig. 4 shows the regions of existence of the fluids derived from the atmospheric gases in a *T-P*-time graph. The chemical and mechanical roles of the liquid components will be discussed in the following section. The cooling of Titan's atmosphere, its temperature and total pressure as a function of time are as given in Gilliam and Lerman (2014a). The domains of gaseous and liquid methane and ethane are from Gilliam and Lerman (2016). The rectangles in the figure indicate the domains of existence of the liquid species (Table 3). Ethane is a gas at temperature higher than about 255 K, and it is a liquid along the dash-dotted line.

4.1. Chemical erosion by ammonium sulfate

Given the unique combination of surface materials on Titan, the channels may be the result of dissolution features. On Earth, chemical weathering is the process of weakening and subsequent disintegration of rock by chemical reactions such as oxidation, hydrolysis, and carbonation. Physical erosion follows by the removal of dissolved material by running water and by the removal of solid particles. The dissolution of soluble bedrock such as limestone, dolomite, and gypsum forms karst topography – an amalgamation of caves, springs, sinkholes, solution valleys, and disappearing streams (Monroe and Wicander, 2012). On Titan, the bulk crustal material, water-ice, is insufficiently soluble in methane and ethane over geologically plausible timescales to result in heavily karstic terrains (Cornet et al., 2015). As a consequence, chemical weathering was not widely predicted on Titan by theoretical models (Lorenz and Lunine, 1996; Collins, 2005), and was not observed during the early stage of the Cassini-Huygens mission. However, during the T16 fly-by of Titan in 2006, the Cassini RADAR instrument revealed a multitude of complex labyrinthine terrain interpreted to be the result of dissolution and/or collapse processes (Stofan et al., 2007). Since then, additional fly-bys have revealed a large quantity of features that are karst-like in nature: clusters of nearly circular depressions in the North Polar Region and closed depressions in the South Polar Region (Mitchell et al., 2007; Malaska et al., 2010; Mitchell and Malaska, 2011). The existence of these features, combined with the knowledge that water ice is insoluble in liquid methane and ethane, prompts an investigation of the dissolution of Titan's channels by other, more unusual or less common, liquid media.

Ammonium sulfate, $(NH_4)_2SO_4$, is an inorganic salt that is most commonly known for being a fertilizer for alkaline soils. On Earth, ammonium sulfate occurs as mineral mascagnite in fumaroles and volcanic vents. On Titan, ammonium sulfate may exist in solution in the subsurface ocean, and as a solid in the crust, probably derived from the ocean by intrusion of the original crust. The results of dissolution of all the $(NH_4)_2SO_4$ in water of the upper crustal layer of Titan are outlined in Table 4. The remaining water-ice would form a residual layer of 15 km in thickness where the ammonium-sulfate solution could form channels by dissolution of ice (Fig. 5).

The estimated time of dissolution of the ice mass in channels is based on the rates of fjord ice melting on Earth, from 0.1 to 0.4 m/day (Russell-Head, 1980; Enderlin, 2014). The volume of the channel ice (Table 4) would be dissolved at these rates from 280 to 1100 years. This time is much shorter than the period of about 84,000 yr that a concentrated $(NH_4)_2SO_4$-H_2O solution could exist as a liquid on the cooling Titan surface (Fig. 4).

4.2. Mechanical erosion by liquids

On Earth, rivers most often erode bedrock mechanically through sediment transport or by fluid discharge alone. In general, the greater the velocity of the fluid and the steeper the grade, the more sediment will be conveyed. The main processes of water

Table 1
Location and physical characteristics of Titan channels. The parameters shown depend on the channel dimensions and the force of gravity on Titan, but not on the characteristics of the fluid (equations in Table 5).

Location	[Max] Length (km), l	[Max] Width (km), w	[Max] Order	[Max] Depth (km), h/300	[Max] Depth (km), h	[Max] Vol (km^3)	[Max] Mass of bedrock eroded from channel (kg)	Slope, S	Hydraulic Radius (m), R_r	Flow Velocity (m/s), U	Discharge (m^3/s), Q_r	Frictional Shear Velocity (m/s), u^*
11°S, 192°W	15	0.25	4	0.0013	0.38	1.44	1.34E+12	0.002	1.27	0.234	7.49E+01	0.059
54°N, 347°W	70	3	2	0.0071	2.13	448	4.17E+14	0.002	7.08	0.553	1.18E+04	0.139
10°S, 66°W	100	2	1	0.0054	1.61	323	3.00E+14	0.002	5.35	0.481	5.17E+03	0.120
36°S, 107°W	100	1	1	0.0033	1.00	100	9.30E+13	0.002	3.31	0.378	1.26E+03	0.095
54°N, 80°W	100	1	1	0.0033	1.00	100	9.30E+13	0.004	3.31	0.535	1.78E+03	0.134
56°S, 12°W	100	3	2	0.0071	2.13	640	5.95E+14	0.004	7.08	0.782	1.67E+04	0.196
58°S, 6°W	100	3	3	0.0071	2.13	640	5.95E+14	0.004	7.08	0.782	1.67E+04	0.196
72°S, 185°W	100	3	1	0.0071	2.13	640	5.95E+14	0.002	7.08	0.553	1.18E+04	0.139
75°N, 345°W	100	1	3	0.0033	1.00	100	9.30E+13	0.002	3.31	0.378	1.26E+03	0.095
7°N, 198°W	100	5	2	0.0101	3.04	1518	1.41E+15	0.001	10.1	0.467	2.36E+04	0.117
14°N, 65.4°W	125	5	1	0.0101	3.04	1897	1.77E+15	0.001	10.1	0.467	2.36E+04	0.117
8°S, 140°W	140	1.4	2	0.0042	1.26	247	2.30E+14	0.002	4.18	0.425	2.50E+03	0.107
59°S, 7°W	150	2	1	0.0054	1.61	484	4.50E+14	0.004	5.35	0.680	7.31E+03	0.170
19.6°N, 87°W	175	5	2	0.0101	3.04	2656	2.47E+15	0.002	10.1	0.660	3.34E+04	0.165
17°S, 120°W	180	8	1	0.0140	4.20	6046	5.62E+15	0.002	13.9	0.776	8.69E+04	0.194
12°S, 50°W	200	2	3	0.0054	1.61	645	6.00E+14	0.001	5.35	0.340	3.66E+03	0.085
16°N, 90°W	200	3	3	0.0071	2.13	1280	1.19E+15	0.004	7.08	0.782	1.67E+04	0.196
19°N, 77°W	200	10	3	0.0163	4.90	9796	9.11E+15	0.002	16.3	0.838	1.37E+05	0.210
50°N, 143°W	200	5	2	0.0101	3.04	3036	2.82E+15	0.002	10.1	0.660	3.34E+04	0.165
78°N, 280°W	200	5	5	0.0101	3.04	3036	2.82E+15	0.004	10.1	0.933	4.72E+04	0.234
19°N, 79°W	210	10	3	0.0163	4.90	10,285	9.57E+15	0.002	16.3	0.838	1.37E+05	0.210
10°S, 125°W	300	1	3	0.0033	1.00	300	2.79E+14	0.002	3.31	0.378	1.26E+03	0.095
27°S, 67°W	350	3	2	0.0071	2.13	2241	2.08E+15	0.004	7.08	0.782	1.67E+04	0.196
73°N, 242°W	400	3	2	0.0071	2.13	2561	2.38E+15	0.002	7.08	0.553	1.18E+04	0.139
10°S, 138°W	450	3	7	0.0071	2.13	2881	2.68E+15	0.004	7.08	0.782	1.67E+04	0.196
75°N, 255°W	1200	3	5	0.0071	2.13	7683	7.15E+15	0.004	7.08	0.782	1.67E+04	0.196
10°S, 192°W	1200	3	3	0.0071	2.13	7683	7.15E+15	0.004	7.08	0.782	1.67E+04	0.196
Total channel volume, V_c						**67,269**						
Average (arithmetic mean)	**251**	**4**	**3**	**0.0075**	**2.26**	**2491**	**2.32E+15**	**0.0026**	**7.50**	**0.653**	**1.72E+04**	**0.164**

erosion, as given by Hjulström (1935), Shields (1936), Sundborg (1956), Whipple et al. (2000), and Sklar and Dietrich (2001, 2004) are summarized below.

The equations of the preceding authors and of Einstein (1942), Meyer-Peter (1949, 1951), Nielsen (1992), Chanson (1999), and Finnegan et al. (2005) include a number of empirical values of the variables and they do not work with any arbitrary values of the physical and mechanical parameters. The main features of the channel-bed erosion-by-flow models are: (1) the channel slope S must be sufficiently steep to assure a strong flow; (2) the density of the particles must be greater than that of the liquid; (3) only the channel floor is being eroded; (4) erosion takes place by saltation and transport of particles (Fig. 6); (5) bed-shear stress (Table 5, No. 8) must be greater than the critical shear stress (No. 7), $\tau_b^* > \tau_c^*$; (6) and the sediment transport parameter q_s (No. 17–20) must be greater than q_t (No. 9), $q_s > q_t$. These and other parameter values are given in Table 5.

Table 2
Structure and main components of Titan's upper crust (references cited in the text).

Component	Mass (kg)	Depth (km)	Thickness of layer (km)	Layer vol (m^3)	Mass from density & vol. (kg)	Density (kg/m^3)		*Density (kg/m^3) P corrected*	Pressure at layer base P (bar)	*T* (K)
						G&L (2014)	This paper			
Layer 1: Crust	1.06E+22	123	123	9.77E+18	9.87E+21	1065[a]	1091[b]		1.4	90
Ice Ih (s)	*3.41E+21*						941[c]			
Ammonium Sulfate (s)	*1.60E+21*						1769[d]			
Methane Clathrate (s)	*5.61E+21*						989[e]		1,680	
Layer 2: Ocean	1.21E+22	276	153	1.09E+19	1.07E+22	1091[a]	965[f]	979[f]		≥ 257
Ammonia (aq)	*1.21E+21*									
Water (liq)	*1.09E+22*							992[f]	3,719	
Layer 3: Ice VI (s)	3.18E+22	677	401	2.23E+19	2.93E+22	1314–1400			10,843	120–300

[a] Gilliam and Lerman (2014a), based on Fortes et al. (2007).
[b] Weighted mean of the three components.
[c] Density Ice Ih (kg/m^3) = 917–0.13 × T°C (Chaplin, 2016; 90 K ≤ −183 °C).
[d] Density at 20 °C (CRC, 2016).
[e] Mean at 50 K (English and Macelroy, 2003).
[f] Croft et al. (1988).

Table 3
Potential liquid agents of channel formation and their characteristics in Titan's atmosphere at different times.

Liquid species	T range (K)	Time since accretion	Titan atm. P (bar)	Density kg/m^3	Viscosity Pa · s	Comments	Reference
Titan accretion	300	*0*	*25.4*				
Nitrogen N_2 liquid (0.02801 kg/mol)	Boiling pt: 77.36	–	–	808.5	(150–65) × 10^{-6} at 80–110 K	T (K) range is above 1 bar total P	Lintup et al. (2004); CRC, 2016. Values ≥ 80 K refer to P ≥ 1 bar.
	77.36–63.16						
Ammonia NH_3 liquid (0.017031 kg/mol)	259–195	40,300–202,000	1.85–1.71				
	251.92 at 1.8 bar			666.44		at 0 °C	Haar and Gallagher (1978, pp. 680, 703, 709)
	195 at 1.8 bar			734.44	2.60E-04		CRC, 2016
	239.55 at 1.0 bar			666.44	0.33 cSt	2.199E-01 at 239 K	Seeton (2006)
	195 at 1.0 bar			734.41	0.75 cSt	2.424E-01 at 195 K	
NH_3–H_2O, 10 wt% NH_3	273–257	20,200–44,700	2.06–1.84	965	2.00E-01	at 254 K at 1 bar	Gill (2014a), Table 1, Croft et al. (1988), Fig. 1.
				979–992		at 1.8 – 3.8 kbar	Kargel et al. (1991), Table 1)
$(NH_4)_2SO_4$ – H_2O, 40–45 wt% solution (132.13952 g/mol)	273–223	20,200–109,000	2.06–1.80	1227.7	2.530E-04	at 20 °C or 293 K	Xu et al. (1998), CRC, 2016
					1.223E-01	at −60 °C or 213 K	Seeton (2006), 2,2-dichloro – 1,1,1-tri-fluoroethane, R123
Ethane C_2H_6 liquid (0.03007 kg/mol)	150–90.5	(0.55–2.7) × 10^9	1.56–1.4				
	90.36			651.6	1.250E-03	at 1 and 2 bar	Youngglove and Ely (1987), pp. 644-647.
	100			641.2	7.980E-04		
	150			585.6	2.520E-04		

Fluid flow can be strong enough to suspend particles in the water column as they move downstream, or simply push them along the bottom of the channel. Sediment being transported over a bed of exposed bedrock can erode the bed significantly by the processes of abrasion, or the wearing-away of surfaces by mechanical processes such as rubbing, cutting, scratching, grinding, and polishing. This type of erosion is strongest when the river is transporting large chunks of rock or after heavy rainfall when the river's flow is turbulent. Even in the absence of a significant sediment load, a river can erode its bed and banks by tearing out large blocks along preexisting fracture using the force of the flowing water. This sort of erosion is strongest at rapids and waterfalls where the water has a high velocity. Cavitation, or the trapping and subsequent implosion of air bubbles in cracks in the river's banks, resulting in the weakening of the adjoining surface, is an additional method of erosion that is not dependent on the presence of a sediment load.

The expectation that rainfall occurs on Titan (Graves et al., 2008; Schneider et al., 2012) introduces the possibility that the valleys were carved by rivers of liquid fed by direct surface runoff, shallow underground flow, or both. In this study, we consider two different liquid medium agents responsible for mechanical erosion of the Titan channels, liquid ammonia and liquid ethane, and compare them to a case of liquid water erosion on Earth. Two other liquids – 10% NH_3–H_2O and $(NH_4)_2SO_4$ solutions in H_2O – have densities higher than the particles (Table 3).

4.2.1. *Channels on Titan and Earth*

On Titan, the ratio width/depth of the channels is close to 1.5–2 (Table 1). On Earth, the ratio of the river channels varies from about 60 in gravel to 5 in bedrock (Finnegan et al., 2005). The depth of the channels on Titan is measurable in kilometers, and it is much greater than river depths on Earth. The biggest rivers, thousands of km in length, have maximum depths in the range from 10^1 to 10^2 m (Walther, 2013), but such rivers as the Missouri, the Thames and the Danube are 7–12 m deep.

The bed-slope of the channels on Titan is of the order of 10^{-3} or 1 m per 1 km (Table 1). On Earth, the slopes of some rivers are of the same magnitude 10^{-3} (Schaller et al., 2001) or higher in small-catchment areas 10^{-3} to 10^{-1} (Van Der Beek and Bishop, 2003). The slope of such a big river as the Mississippi is smaller, varying from 1×10^{-4} to 8×10^{-5} (Carlston, 1969). The gradient of the rivers in the Ukraine varies from 5×10^{-4} to 2×10^{-3} (Stebelsky and Teslia, 1993). We use the range of gradients from 6×10^{-4} to 1×10^{-3} for a model river channel on Earth in Table 6.

4.2.2. *Liquids not suitable for erosion*

Molecular nitrogen N_2 is gas at the surface conditions of Titan and it liquefies at a lower temperature than 90 K (Table 3). The aqueous solutions of ammonia NH_3 and ammonium sulfate $(NH_4)_2SO_4$ have densities higher than the density of the water-ice particles and cannot therefore be considered as agents of mechanical erosion.

4.2.3. *Erosion by liquid NH_3*

Present-day, the bulk of Titan's ammonia is likely to be found as a solid in its icy outer shell, or as a liquid in its subsurface ocean. However, under a warmer Titan, ammonia may have existed as a gas in the atmosphere, or even as a liquid on the surface. In fact, while the exact composition of Titan's early atmosphere is not well known, it is generally accepted that it was much more massive and denser than at present, and dominated by ammonia and methane (Gilliam and Lerman, 2014a). Based on the cooling model of Gilliam and Lerman (2014a, 2016), and assuming an accretion temperature of 300 K, we estimate that ammonia would have been in a liquid state on the surface of Titan between 40,300 and 202,000

Table 4
Composition of the upper layer of Titan's crust and ice dissolution.

1. *Ice Ih* (*s*) and liquid H_2O equivalent 18.015 g/mol (kg)	3.41E+21	**6.** Thickness of ice left after solution formed (km)	14.9
2. *Ammonium Sulfate* (*s*) $(NH_4)_2SO_4$ 132.14 g/mol (kg)	1.60E+21	**7.** Mass material in channels (kg) (Table 1)	6.26E+16
3. *Methane Clathrate* (*s*) $CH_4 \cdot 6H_2O$ 124.36 g/mol (kg)	5.61E+21	**8.** Volume material in channels (km^3)	6.73E+04
4. Water to make sat. solution of amm.-sulf. (41.3 wt%) at 0 °C (kg H_2O) 5.3 molal	2.27E+21	**9.** Estimated time to dis-solve channel mass (yr)	1100 to 280
5. Water left after ammonium-sulfate dissolution (kg)	1.14E+21		

years after accretion, or between temperatures of 259–195 K (Fig. 4). Although geologically brief, this time period may have been the first under which Titan's channels, initially formed by chemical erosion, underwent mechanical erosion by a liquid.

4.2.4. *Erosion by C_2H_6*

In Titan's atmosphere, ethane is produced as a result of UV photolysis of methane (Yung et al., 1984), with a mean production rate of 1.3×10^8 molecules $cm^{-2}\,s^{-1}$ from solely the photolytic conversion of methane to ethane (Wilson and Atreya, 2009), and subsequently condenses and precipitates from the atmosphere. Consideration of this process suggests that Titan should have produced a substantial amount of ethane since accretion. Such an idea was first proposed by Lunine et al. (1983), who used

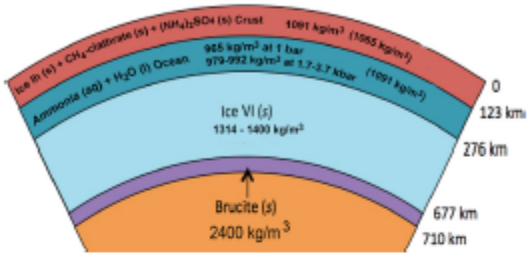

Fig. 3. Crustal Structure of Titan. Data in Table 2. Density values in parentheses from Gilliam and Lerman (2014a).

Table 5
List of the equations used in this study.

No.	Parameter description	Equation	Reference
1	Channel height (m)	$h=W^{0.69}$	William (1988); Jaumann et al. (2008)
2	Hydraulic radius for rectangular channel (m)	$R_r = wh/(w+2h)$	Murdock (1993)
3	Flow velocity (Darcy-Weisbach equation) (m/s)	$U=\sqrt{8gR_rS/f}$	Perron et al. (2006)
4	Discharge for rectangular channel (m^3/s)	$Q_r=whU$	Perron et al. (2006)
5	Frictional shear velocity (m/s)	$u^* = (gh\mathrm{S})^{0.5}$	Paphitis (2001); Burr et al. (2006)
6	Boundary Reynolds number	$R_*^* = u^*D/\nu$	Paphitis (2001); Burr et al. (2006)
7	Critical shear stress	$\tau_c^* = \left(0.188/\left(1+R_*^*\right)\right)+0.0475\left(1-0.699e^{-0.015R_*^*}\right)$	Paphitis (2001); Burr et al. (2006)
8	Bed shear stress	$\tau_b^* = \rho_f gh\mathrm{S}/\left((\rho_s-\rho_f)gD\right)$	Burr et al. (2013)
9	Sediment transport capacity (kg $m^{-1}\,s^{-1}$)	$q_s = 5.7\rho_s\left(R_g gD^3\right)^{1/2}\left(\tau_b^*-\tau_c^*\right)^{3/2}$	Sklar and Dietrich (2004)
10	Total hop length (m)	$L_s = 8D\left(\left(\tau_b^*/\tau_c^*\right)-1\right)^{0.88}$	Huda and Small (2014)
11	Vertical impact velocity (m/s)	$w_{sv} = 2\left(0.4\left(R_g gD\right)^{0.5}\left(\left(\tau_b^*/\tau_c^*\right)-1\right)^{0.18}\right)\left(1-\left(u^*/w_f\right)^2\right)^{0.5}$	Sklar and Dietrich (2004)
12	Mean shear stress (kg $m^{-2}\,s^{-1}$)	$\tau_0 = \rho_f gh\mathrm{sin}S$	Chanson (1999)
13	Volumetric particle conc. in bed-load layer	$C_s = \left(0.177/D\right)\left(\nu^2/\left(\left(g_s-1\right)g\right)\right)^{1/3}\left(\left(\tau_0^*/\tau_c^*\right)-1\right)$	Chanson (1999)
14	Average sediment velocity (m/s)	$V_s = 7\left(gh\,\mathrm{sin}S\right)^{0.5}$	Chanson (1999)
15	Thickness of the bed-load layer (m)	$\delta_b = 0.3D\left(D\left(\left(g_s-1\right)g/\nu^2\right)^{1/3}\right)^{0.7}\left(\left(\tau_0^*/\tau_c^*\right)-1\right)^{0.5}$	Chanson (1999)
16	Bed load transport rate per unit width (m^2/s)	$S_T = C_s V_s \delta_s$	Chanson (1999)
17	Mass sediment flow rate per unit width (kg $m^{-1}\,s^{-1}$)	$q_s = S_T\rho_s$	Chanson (1999)
18	OTHER relationships for q_s (units as above)	$q_s = 2.15\sqrt{\left(g_s-1\right)gD^3}\exp\left(-0.391\rho_f\left(g_s-1\right)gD/\tau_0\right)\rho_s$	Einstein (1942), Chanson (1999)
19		$q_s = \left(\left(4\tau_0/\left(\rho_f\left(g_s-1\right)gD\right)\right)-0.188\right)^{3/2}\sqrt{\left(g_s-1\right)gD^3}\rho_s$	Meyer-Peter (1948, 1951), Chanson (1999)
20		$q_s = \sqrt{\left(g_s-1\right)gD^3}\left(\left(12\tau_0/\left(\rho_f\left(g_s-1\right)gD\right)\right)-0.05\right)\sqrt{\tau_0/\left(\rho_f\left(g_s-1\right)gD\right)}\rho_s$	Nielsen (1992), Chanson (1999)
21	Erosion rate (m/s)	$E=\frac{\xi w_{si}^2 Y}{i_s k_v \sigma^2}\left(1-\frac{q_s}{q}\right)$	Sklar and Dietrich (2004)
22	Nondimensional buoyant density of sediment	$R_b = \left(\rho_s/\rho_f\right)-1$	Huda and Small (2014)
23	Particle settling velocity (m/s)	$w_f = \left(\rho_s-\rho_f\right)gD^2/(18\mu)$ $w_f = 2.46\sqrt{\left(\rho_s-\rho_f\right)gD/\left(2\rho_f\right)}$	Caenn et al. (2011)
24	Dynamic viscosity (Pa s); ν is kinematic viscosity ($m^2\,s^{-1}$)	$\mu=\nu\rho$	Elson (2007)

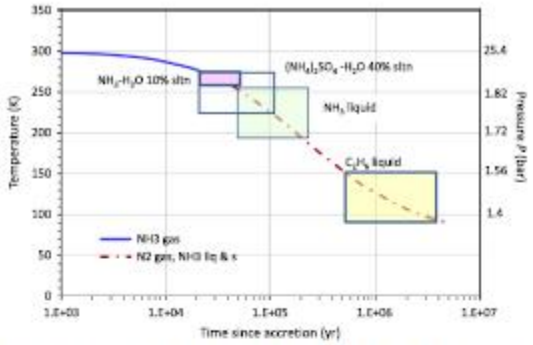

Fig 4. Domains of existence of liquids on Titan's surface plotted in the *T-P*-time graph, from data in Table 2. From before $T=259$ K, the temperature of NH_3 liquefaction, molecular nitrogen N_2 (0.028 kg/mol) is the main component of Titan's atmosphere that is too heavy to be lost by thermal escape. The decrease of its mass to the present-day $p_{N2}=1.3$–1.4 bar is due to other photochemical processes (Ameya et al., 2006).

photochemical models to predict that Titan would be covered by an ethane ocean one to several kilometers deep, and was later supported by others' models, albeit with a smaller net volume of ethane produced. Further, Gilliam and Lerman (2016) estimated the mass of ethane produced since accretion as 8.46×10^{17} kg, and suggested that most of it resides in liquid form on or within Titan's porous crust. As shown in Fig. 4 and Table 3, we estimate that liquid ethane rain may have begun as early as 0.55×10^{6} years after accretion, corresponding to a Titan surface temperature of 150 K, and continues to present-day, providing ample time for Titan's channels to undergo mechanical erosion by liquid ethane.

However, there is an uncertainty in the mass balance of liquid ethane as a possible agent of channel erosion. At the ethane atmospheric production rate cited above, there would have been 9.6×10^{13} kg C_2H_6 accumulated in 550,000 years, equivalent to 1.55×10^{11} m^3 liquid C_2H_6. This volume, distributed over the total area of the channels of 23,750 km^2 (length × width, Table 1), would have produced a layer 6.5 m thick. But, its annual increment at the cited ethane production rate would add only 12 μm (1.2×10^{-5} m) to the liquid ethane layer thickness in the channels. The rate of precipitation of liquid ethane on Titan was estimate as

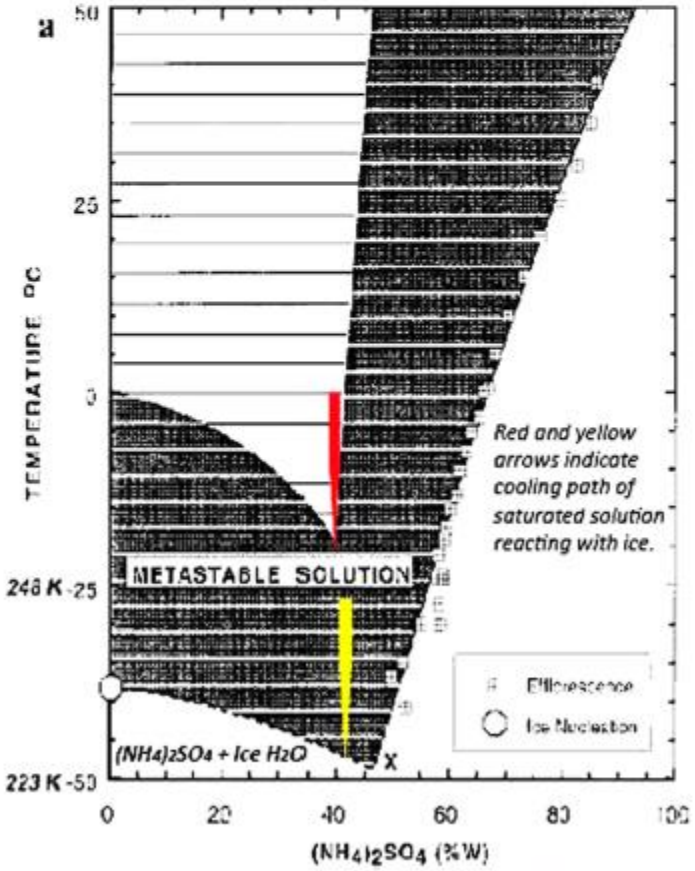

Fig 5. $(NH_4)_2SO_4$-H_2O metastability phase diagram in temperature-composition domain. The pure solution equilibrium region is represented by the open striped field, whereas the metastable solution is shown as the gray striped area. Tiled squares indicate all observed efflorescence points. Homogeneous ice nucleation from pure water is labeled with the octagon. X marks the lowest temperature where solution microdroplets can be found. Modified from Xu et al. (1998). Reprinted with permission from *Journal of Physical Chemistry B, 102*, 7462–7469, Copyright © 1998, American Chemical Society.

Table 6
Parameters used for channel calculations.

	Titan		Earth
Temperature	90 to 150	195–259	293
Surface gravity, g (m/s^2)	1.35	1.35	9.81
Fluid	Ethane (C_2H_6)	Ammonia (NH_3)	Water (H_2O)
Density, ρ_f (kg/m^3)	650	700.44	998.2
Kinematic viscosity, ν (m^2 s^{-1})	1.50E-06	3.71E-07	1.157E-06
Particle settling velocity, w_f (m/s)	1.25E+02	1.69E+02	1.435E+03
Dynamic viscosity, μ (kg m^{-1} s^{-1})	9.75E-04	2.60E-04	1.155E-03
Nondimensional buoyant density of sediment, R_b	0.43	0.33	1.51
Specific gravity, g_s	1.4308	1.328	2.505
Sediment	Water ice	Water ice	Quartz
Density, ρ_s (kg/m^3)	930	930	2500
Particle diameter, D (m)	0.033	0.033	0.033
Bedrock	Water ice	Water ice	Sandstone
Young's Modulus, Y (Pa)	9.00E+09	9.00E+09	5.00E+10
Tensile strength, σ_T (Pa)	1.00E+06	1.00E+06	2.00E+06
Abrasion resistance parameter, k_v	1.90E+04	1.90E+04	1.40E+06

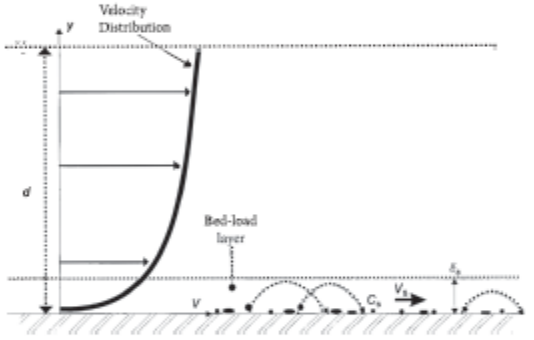

Fig. 6. Channel erosion by flowing water. Reprinted in modified format from Chanson (1999), Fig. 10.1, by permission of Professor H. Chanson, Copywrite © Hubert Chanson, 1999. Parameters listed in Tables 5 and 6.

3.0×10^{-7} to 0.63×10^{-7} m^3 m^{-2} yr^{-1} (Graves et al., 2008), equivalent to about 2.0×10^{-4} to 0.4×10^{-4} kg gaseous C_2H_6 m^{-2} yr^{-1}. From the present-day C_2H_6 contents of Titan's atmosphere 9.24×10^{13} kg (Gilliam and Lerman, 2016), and Titan's surface area of 8.332×10^{13} m^2, the residence time of C_2H_6 with respect to precipitation from the atmosphere is 9.24×10^{13} kg/[2.0-0.4) $\times$ 10^{-4} kg m^{-2} yr$^{-1}\times8.332\times10^{13}$ m^2]= 5500 to 27,700 yr. Despite these apparent inconsistencies in material balance of ethane, and that also appears in the balance of methane (Gilliam and Lerman, 2014a), we use liquid ethane as a potential agent of channel formation on Titan, as discussed further below.

4.2.5. Equations

To calculate the rates of liquid stream incision into water ice bedrock on Titan, we build on the Sklar and Dietrich (2004) model of terrestrial water erosion by saltation of bedrock particles, and analyze the effect of bed-load transport on the lowering rate using the equations of bed-load transport rate developed by Einstein (1942) and Chanson (1999). These models apply to channels of fixed width that are being deepened by erosion and abrasion of rock/ice by bed load, and assume that all bed load motion is by saltation of spherical grains of uniform size. A discussion of the fundamental equations used is as follows, and a complete list of all equations used is listed in Table 5 and the essentials of the process are as shown in Fig. 6.

The Sklar and Dietrich (2004) model of erosion states that

$$E = V_i I_r F_e \tag{1}$$

where E is erosion rate (m/s), V_i is the volume eroded per impact (m^3), I_r is impact rate per unit area (m^{-2} s^{-1}), and F_e is the fraction of the streambed that is exposed to streamflow. The value of F_e depends on the supply of sediment to the stream, and the transport stage of the stream (the ratio of the shear velocity in the flow to the critical shear velocity at the threshold of sediment motion). The value of I_r is a function of the flux of particles, and the saltation hop length. The value of V_i is dependent on the kinetic energy of each particle impact, and the resistance of the bedrock material to abrasion by small impacts. Thus, Eq. (1) can be rewritten as

$$E = \frac{q_s w_{si}^2 Y}{L_s k_v \sigma_T^2}\left(1-\frac{q_s}{q_t}\right) \tag{2}$$

where the variables are as given in Table 5. There q_s is the mass sediment flow rate per unit width (kg m^{-1} s^{-1}), w_{si} is the vertical impact velocity (m/s), Y is the Young's Modulus (Pa), L_s is the total hop length (m), k_v is the abrasion resistance parameter, σ_T is the tensile strength (Pa), and q_t is the sediment transport capacity (kg m^{-1} s^{-1}). The value of w_{si} (No. 11) is a function of the buoyant density of the sediment, gravity, grain diameter, the critical and bed shear stresses, the frictional shear velocity, and the particle settling velocity. The value of L_s depends on the grain diameter as well as the critical and bed shear stresses. The value of q_t is a function of the sediment density and buoyant density, gravity, grain diameter, and the critical and bed shear stresses.

Mass sediment flow rate per unit width, q_s, is defined as

$$q_s = S_T \rho_s \tag{3}$$

where S_T is the bed load transport capacity per unit width (m^2/s), and ρ_s is the density of the sediment (kg/m^3). Numerous researchers have proposed different empirical and semi-empirical correlations of the bed load transport capacity. Other parameters are as given in Table 5.

5. Results and conclusions

From the discussion of the modes of channel erosion in the preceding section we estimate the time (t) that it might have taken liquid ethane and ammonia on Titan and water on Earth to form a representative channel. For Titan, the dimensions and slope of a mean channel are given in Table 1. For Earth, a model channel is 100 km long, 100 m wide, 10 m deep, and with a slope of 0.001 and 0.0006. There are several possible formulations of the time to erosion of total volume or mass of the channels, of which we use the following two.

Time to erosion (t_1) based on total volume of the channels (V_c, in m^3, Table 1) and the linear erosion rate E in m/s of Sklar and Dietrich (2004), Eq. (2):

$$t_1 = V_c^{1/3}/E \quad (yr) \tag{4}$$

Only the equations of Einstein (1942) and Chanson (1999) could be used for calculation of the channel-bed erosion rate E (m s^{-1}). The equations of Meyer-Peter (1949, 1951) and Nielsen (1992) do not give meaningful results of positive erosion rate $E > 0$.

And time to erosion (t_2) based on total mass of material in channels (M_c in kg, from Table 1) mean channel width (w in m, Table 1) and q_s, mean sediment flow rate per unit width (in kg m^{-1} s^{-1}, Table 5, Nos. 17–18), is:

Table 7
Results and Conclusions.

	Titan		Titan		Earth		Earth	
Liquid	C_2H_6		NH_3		H_2O		H_2O	
Slope	0.0026		0.0026		0.0010		0.0006	
Surface grain size, D (m)	0.033		0.033		0.033		0.033	
Critical shear stress, τ_{c*}	0.048		0.048		0.048		0.048	
Bed shear stress, τ_b,	1.34		1.73		0.10		0.06	
Sediment transport capacity, q_c ($kg\,m^{-1}\,s^{-1}$)	36.8		47.7		4.02		0.48	
Total hop length, L_t (m)	4.83		6.09		0.29		0.08	
Vertical impact velocity, w_{is} (m/s)	0.153		0.123		0.560		0.437	
Mean shear stress, τ_0 ($kg\,m^{-1}\,s^{-2}$)	17.4		18.5		49.0		29.4	
Volumetric concentration of sediment in the bed-load layer, C_t	0.015		0.008		0.00018		0.00004	
Average sediment velocity, V_s (m/s)	1.14		1.14		1.55		1.20	
Bed-load layer thickness, δ_s (m)	2.20		4.53		1.06		0.52	
Reference	Chanson (1999)	Einstein (1942)	Chanson (1999)	Einstein (1942)	Chanson (1999)	Einstein (1942)	Chanson (1999)	Einstein (1942)
Bed-load transport rate per unit width, S_T (m^2/s)	3.76E-02	7.48E-03	4.31E-02	7.00E-03	2.93E-04	1.02E-03	2.71E-05	7.66E-05
Mass sediment flow rate per unit width, q_s ($kg\,m^{-1}\,s^{-1}$)	35.4	7.04	40.6	6.59	0.73	2.55	0.07	0.19
Erosion rate, E (m/s)	2.95E-09	1.30E-08	7.15E-9	6.70E-09	5.77E-09	8.98E-09	1.39E-09	2.35E-09
Time to erode (yr)								
t_1, Eq.(4)	1.35E+05	3.05E+04	5.57E+04	5.94E+04	2.55E+03	1.64E+03	1.24E+04	6.27E+03
t_2, Eq.(5)	4.77E+02	2.40E+03	4.16E+02	2.56E+03	1.08E+02	3.11E+01	1.17E+03	4.13E+02

$$t_2 = M_c/(q_s w) \quad (\mathrm{yr}) \tag{5}$$

Using the equation of bed load transport capacity given by Chanson (1999), the rates of mass sediment flow per unit width (q_s) are 35.4 $kg\,m^{-1}\,s^{-1}$ and 40.6 $kg\,m^{-1}\,s^{-1}$, corresponding to erosion rates of 3×10^{-9} m/s and 7.2×10^{-9} m/s, for liquid ethane and liquid ammonia, respectively. As a comparison, a channel of length 100 km, width 0.1 km, and slope of 0.0006–0.001, carved into sandstone on Earth by liquid water yields a mass sediment flow rate per unit width (q_s) of 0.07–0.73 $kg\,m^{-1}\,s^{-1}$ and an erosion rate of $1.2–5.8\times10^{-9}$ m/s.

Using the equation of bed load transport capacity given by Einstein (1942), the rate of mass sediment flow per unit width (q_s) is 7.04 $kg\,m^{-1}\,s^{-1}$ for liquid ethane and 6.59 $kg\,m^{-1}\,s^{-1}$ for liquid ammonia, corresponding to erosion rates of 1.3×10^{-8} m/s and 6.7×10^{-9} m/s, for liquid ethane and liquid ammonia, respectively. As a comparison, a model river channel of length 100 km, width 0.1 km, and slope of 0.0006–0.001 carved into sandstone on Earth by liquid water yields a mass sediment flow rate per unit width of 0.19–2.55 $kg\,m^{-1}\,s^{-1}$ and an erosion rate of $2.35–8.98\times10^{-9}$ m/s.

The results of the time to erosion t_1 and t_2 are shown in Table 7. The times obtained with Eq. (4) for the Titan channels are of the order of 10^4–10^5 years. For the Earth model river, the times are 10^3–10^4 years. The latter estimates agree with the ages of four large European rivers of 6,000 to 42,000 yr (Schaller et al., 2001). The times from Eq. (5) are generally lower than those from Eq. (4), and some of the results based on Einstein's (1942) equations are higher, and some lower, than those based on Chanson (1999) and Sklar and Dietrich (2004). The models of Meyer-Peter (1949, 1951) and Nielsen (1992) are not considered here because they give negative erosion rates that are physically unrealistic in erosion models without an external source of sediment.

The erosional sequence of the channels on Titan (Fig. 4) might have started after the formation of water-ice on the surface by the process of chemical dissolution by $(NH_4)_2SO_4$–H_2O, overlapping or followed by a period of mechanical erosion by liquid NH_3 condensed from the atmosphere. A final stage on the cooling surface of Titan might have been characterized by liquid C_2H_6 as an agent of mechanical erosion.

The periods of existence of one agent of chemical dissolution, ammonium sulfate solution, and two agents of mechanical erosion, liquid ammonia and ethane, are considerably longer that the estimated channel formation times.

Acknowledgements

We thank Professor Hubert Chanson, of the School of Engineering, University of Queensland, Brisbane, Australia, for permission to reproduce Fig. 6, and Ms. Kare M. Berg for its electronic redrafting. We are also grateful to anonymous Reviewer for insightful and helpful criticisms and suggestions to an earlier version of this paper, and to Professor Jared Wunsch, of the Mathematics Department of this University, for his guidance in mathematical details. This work was supported by NASA Headquarters under the NASA Earth and Space Science Fellowship Program – Grant NNX13AO02H, and by Weinberg College of Arts and Sciences, Northwestern University.

References

Atreya, S.K., et al., 2006. Titan's methane cycle. Planet. Space Sci. 54, 1177–1187.
Barnes, J.W., et al., 2007b. Near-infrared spectral mapping of Titan's mountains and channels. Planet 112, 11006.
Black, B.A., Perron, J.T., Burr, D.M., Drummond, S.A., 2012. Estimating erosional exhumation on Titan from drainage network morphology. J. Geophys. Res. 117, E08006. http://dx.doi.org/10.1029/2012JE004085.
Brown, R.H., et al., 2004. The Cassini Visual and Infrared Mapping Spectrometer (VIMS) investigation. Space Sci. Rev. 115, 111–168.
Burr, D.M., et al., 2006. Sediment transport by liquid surficial flow: application to Titan. Icarus 181, 235–242.
Burr, D.M., et al., 2009. Fluvial network analysis on Titan: evidence for subsurface structures and west-to-east wind flow, southwestern Xanadu. Geophys. Res. Lett. 36, L22203. http://dx.doi.org/10.1029/2009GL040909.
Burr, D.M., et al., 2013. Morphology of fluvial networks on Titan: Evidence for structural control. Icarus 226, 742–759.
Caenn, R., Darley, H.C.H., Gray, G.R., 2011. Composition and properties of drilling and completion fluids, 6th edition. Gulf Professional Publishing, p. 720.
Carlston, C.W., 1969. Longitudinal slope characteristics of rivers of the midcontinent and the atlantic east gulf slopes. Int. Assoc. Sci. Hydrol. Bull. 14, 21–31.
Cartwright, R., Clayton, J.A., Kirk, R.L., 2011. Channel morphometry, sediment

transport, and implications for tectonic activity and surficial ages of Titan basins. Icarus 214, 561–570.
Chanson, H., 1999. The Hydraulics of Open Channel Flow: An Introduction. Arnold, London, UK. 495 pp.
Chaplin, M., 2016. Water Structure and Science. Hexagonal ICE (ICE Ih). www1.lsbu.AC.UK.
Collins, G.C., 2005. Relative rates of fluvial bedrock incision on Titan and Earth. Geophys. Res. Lett. 32, L22202. http://dx.doi.org/10.1029/2005GL024551.
Cornet, T., et al., 2015. Dissolution on Titan and on Earth: Toward the age of Titan's karstic landscapes. J. Geophys. Res. Planet 120, 1044–1074.
CRC, 2016. Handbook of Chemistry and Physics. In: Haynes, W.M. (Ed.), 96th ed. CRC Press, Boca Raton, FL.
Croft, S.K., Lunine, J.I., Kargel, J., 1988. Equation of state of ammonia-water liquid: derivation and planetological applications. Icarus 73, 279–293.
E., Endeflin (Univ of Maine, Orono), 2014. Just How Quickly Are Icebergs And Glaciers Melting? Polardispatches.org.
Einstein, H.A., 1942. Formulas for the transport of bed sediment. Trans. Am. Soc. Civil Eng. 107, 561–574.
Elachi, C., et al., 2005. Cassini Radar views the surface of Titan. Science 308, 970–974.
Elson, T., 2007. Concepts of Fluid Flow, in Concepts of Chemical Engineering 4 Chemists. In: Simons, S.J.R. (Ed.), 2007. The Royal Society of Chemistry, pp. 55–95.
English, N.J., Macelroy, J.M.D., 2003. Structural and dynamical properties of methane clathrate hydrates. J. Comput. Chem. 24, 1569–1581.
Finnegan, N.J., et al., 2005. Controls on the channel width of rivers: Implications for modeling fluvial incision of bedrock. Geology 33, 229–232.
Fortes, A.D., Grindrod, P.M., Trickett, S.K., Vočadlo, L., 2007. Ammonium sulfate on Titan: Possible origin and role in cryovolcanism. Icarus 188, 139–153.
Garcia, J.E., 2001. Density of Aqueous Solutions of CO_2. Lawrence Berkley Nat. Lab, 1–010 (https://escholarship.org/uc/item/6dn022hb).
Gilliam, A.E., Lerman, A., 2014a. Evolution of Titan's major atmospheric gases and cooling since accretion. Planet. Space Sci. 93–94, 41–53.
Gilliam, A.E., Lerman, A., 2014b. Corrigendum to "Evolution of Titan's major atmospheric gases and cooling since accretion". Planet. Space Sci. 101, 210.
Gilliam, A.E., Lerman, A., 2016. Titan's missing ethane: from the atmosphere to the subsurface. Icarus 275, 252–258.
Graves, S.D.B., et al., 2008. Rain and hail can reach the surface of Titan. Planet. Space Sci. 56, 346–357.
Haar, L., Gallagher, J.S., 1978. Thermodynamic propercaruties of ammonia. J. Phys. Chem. Ref. Data 7, 635–792.
Hjulström, F., 1935. Studies of the morphological activity of rivers as illustrated by the river Fyris: Inaugural dissertation (Vol. 10). Almqvist & Wiksells.
Huda, S.A., Small, E.E., 2014. Modeling the effects of bed topography on fluvial bedrock erosion by saltating bed load. J. Geophys. Res. Earth Surf. 119, 1222–1239.
Jacobsen, R.T., Stewart, R.B., 1973. Thermodynamic properties of nitrogen including liquid and vapor phases from 63K to 2000K with pressures to 10,000 bar. J. Phys. Chem. Ref. Data 2, 757–822.
Jaumann, R., et al., 2008. Fluvial erosion and post-erosional processes on Titan. Icarus 197, 526–538.
Jaumann, R., et al., 2009. Geology and surface processes on Titan. In: Brown, R.H., Lebreton, J.H., Waite, J.H. (Eds.), Titan from Cassini-Huygens. Springer, pp. 75–140.
Kargel, J.S., et al., 1991. Rheological properties of ammonia-water liquids and crystal-liquid slurries: Planetological applications. Icarus 89, 93–112.
Langhans, M.H., et al., 2012. Titan's fluvial valleys: Morphology, distribution, and spectral properties. Planet. Space Sci. 60, 34–51.
Littrup, P., et al., 2004. Cryotherapy probe and system. Patent Application WO 2004064914 A3. 5 August 2004.
Lopes, R.M.C., et al., 2010. Distribution and interplay of geologic processes on Titan from Cassini radar data. Icarus 205, 540–558.
Lorenz, R.D., et al., 2008. Fluvial channels on Titan: Initial Cassini RADAR observations. Planet. Space Sci. 56, 1132–1144.
Lorenz, R.D., Lunine, J.I., 1996. Erosion on Titan: Past and present. Icarus 122, 79–91.
Lunine, J.I., Stevenson, D.J., Yung, Y.L., 1983. Ethane ocean on Titan. Science 222, 1229–1230.
Luspay-Kuti, A., et al., 2015. Experimental constraints on the composition and dynamics of Titan's polar lakes. Earth Planet. Sci. Lett. 410, 75–83.
Malaska, M., et al., 2010. Identification of karst-like terrain on Titan from valley analysis. Lunar Planet. Inst. Sci. Conf. Abstr. 41, 1544.
Meyer-Peter, E., 1949. Quelques problèmes concernant le charriage des matières solides dans les rivières alpines et subalpines. La Houille Blanche, 688–706.
Meyer-Peter, E., 1951. Transport des matières solides en général et problème spéciaux. Bull. Génie Civil d'Hydraulique Fluviale. Tome, 5.
Mitchell, K.L., et al., 2007. Titan's crater lakes: Caldera vs. karst. Lunar Planet. Inst. Sci. Conf. Abstr. 38: 2064.
Mitchell, K.L., Malaska, M., 2011. Karst on Titan. In: First international planetary caves workshop: implications for astrobiology, climate, detection, and exploration. LPI Contribution No. 1640. Lunar and Planetary Institute, Houston, p. 15.
Mitri, G., et al., 2007. Hydrocarbon lakes on Titan. Icarus 186 (2), 385–394.
Monroe, J.S., Wicander, R., 2012. The changing Earth: Exploring Geology and Evolution, sixth edition. Cengage Learning, Brooks/Cole, pp. 320–322.
Murdock, J.W., 1993. Fundamental Fluid Mechanics for the practicing Engineer. CRC Press, p. 440.
Nielsen, P., 1992. Coastal bottom boundary layers and sediment transport. World Sci. 4.
Paphitis, D., 2001. Sediment movement under unidirectional flows: an assessment of empirical threshold curves. Coast. Eng. 43, 227–245.
Perron, J.T., et al., 2006. Valley formation and methane precipitation rates on Titan. J. Geophys. Res. 111, E11001. http://dx.doi.org/10.1029/2005JE002602.
Porco, C.C., et al., 2004. Cassini imaging science: instrument, characteristics and anticipated scientific investigations at Saturn. Space Sci. Rev. 115, 363–497.
Porco, C.C., et al., 2005. Imaging of Titan from the Cassini spacecraft. Nature 434, 159–168.
Russell-Head, D.S., 1980. The melting of free-drifting icebergs. Ann. Glaciol. 1, 119–122.
Schaller, M., et al., 2001. Large-scale erosion rates from in situ-produced cosmogenic nuclides in European river sediments. Earth Planet. Sci. Lett. 188, 441–458.
Schneider, T., et al., 2012. Polar methane accumulation and rainstorms on Titan from simulations of the methane cycle. Nature 481, 58–61.
Seeton, C.J., 2006. Viscosity-temperature correlation for liquids. Tribol. Lett. 22, 67–78.
Shields, A., 1936. Anwendung der Ähnlichkeitsmechanik und der Turbulenzforschung auf die Geschiebebewegung. Mitt. Preuss. Versuchsanstalt f. Wasserbau u. Schiffbau 26, 1–26.
Sklar, L.S., Dietrich, W.E., 2001. Sediment and rock strength controls on river incision into bedrock. Geology 29, 1087–1090.
Sklar, L.S., Dietrich, W.E., 2004. A mechanistic model for river incision into bedrock by saltating bed load. Water Resour. Res. 40, W06301. http://dx.doi.org/10.1029/2003WR002496.
Soderblom, L.A., et al., 2007b. Topography and geomorphology of the Huygens Landing Site on Titan. Planet. Space Sci. 55, 2015–2024.
Stebelsky, I., Teslia, I., 1993. Rivers. Encyclopedia of Ukraine, Vol. 4.
Stofan, E.R., et al., 2007. The lakes of Titan. Nature 445, 61–64.
Sundborg, Å., 1956. The river Klarälven. A study of fluvial processes. Geogr. Ann. 38, 238–316.
Tan, S.P., et al., 2015. Titan's liquids: Exotic behavior and its implications on global fluid circulation. Icarus 250, 64–75.
Tan, S.P., Kargel, J.S., Marion, J.S., 2013. Titan's atmosphere and surface liquid: new calculation using statistical associating fluid theory. Icarus 222, 53–72.
Tobie, G., Lunine, J.I., Sotin, C., 2006. Episodic outgassing as the origin of atmospheric methane on Titan. Nature 440, 61–64.
Tomasko, M.G., et al., 2005. Rain, winds and haze during the Huygens probe's descent to Titan's surface. Nature 438, 765–778.
Van Der Beek, P., Bishop, P., 2003. Cenozoic river profile development in the Upper Lachlan catchment (SE Australia) as a test of quantitative fluvial incision models. J. Geophys. Res. 108 (B6), 2309–2337.
Walther, J.V., 2013. Earth's Natural Resources. Jones & Bartlett Learning, Burlington, MA.
Whipple, K.X., Hancock, G.S., Anderson, R.S., 2000. River incision into bedrock: Mechanics and relative efficacy of plucking, abrasion, and cavitation. GSA Bulletin 112, 490–503.
William, G.P., 1988. Paleofluvial estimates from dimensions of former channels and meanders. In: Baker, V.R., Kochel, R.C., Patton, P.C. (Eds.), Flood Geomorphology. Wiley, New York, pp. 321–334.
Wilson, E.H., Atreya, S.K., 2009. Titan's carbon budget and the case of the missing ethane. J. Phys. Chem. A 113, 11221–11226.
Wood, C.A., et al., 2010. Impact craters on Titan. Icarus 206, 334–344.
Xu, J., et al., 1998. Ammonium sulfate: Equilibrium and metastability phase diagrams from 40 to-50C. J. Phys. Chem. B 102, 7462–7469.
Younglove, B.A., Ely, J.F., 1987. Thermophysical properties of fluids. II. Methane, ethane, propane, isobutene, and normal butane. J. Phys. Chem. Ref. Data 16, 577–798.
Yung, Y.L., Allen, M., Pinto, J.P., 1984. Photochemistry of the atmosphere of Titan: comparison between models and observations. Astrophys. J. Suppl. Ser. 55, 465–506.

CONTROL ID: 1807869
TITLE: Evolution of Titan's Major Atmospheric Gases and Cooling Since Accretion
CURRENT SECTION/FOCUS GROUP: Planetary Sciences (P)
CURRENT SESSION: P019. Planetary Atmospheres and Evolution

AUTHORS (FIRST NAME, LAST NAME): Ashley Gilliam[1], Abraham Lerman[1]
INSTITUTIONS (ALL): 1. Earth and Planetary Sciences, Northwestern University, Evanston, IL, United States.

ABSTRACT BODY: Titan, the largest moon of Saturn, has been to date explored by only one spacecraft, giving us an incomplete picture of its atmospheric structure and surface conditions. Using available information about Titan's present-day atmosphere composition and internal structure, we present a new model for the chemical and physical composition of primordial Titan and its atmosphere. We propose that Titan had a nearly homogeneous structure shortly after accretion, consisting of an inner solid core of antigorite and brucite, of radius 1898 km, and an outer fluid shell containing H_2O, NH_3, $(NH_4)_2SO_4$, and CH_4, of thickness 677 km. From a balance of the release of gravitational accretion energy and cooling by an ideal black body emission, with no other internal heat sources, we calculate from a published range of accretion times an accretion temperature of 355 to 300 K. We also consider the gas dynamics in Titan's atmosphere and calculate the escape rates of the two main gases in Titan's primordial atmosphere, NH_3 and CH_4, as a function of time. At 355 K, the atmosphere would be depleted of NH_3 and CH_4 in short times, except under certain hypothetical conditions or by their supply by emissions from the interior over certain periods of time. However, a lower accretion temperature of 300 K allows the gases to escape thermally down to their present-day masses. Our results show that the Titan temperature decreases to 150 K, corresponding to the reported lower limit of NH_3 to N_2 conversion, during the relatively fast initial cooling period between 0.5 and 0.6 Myr. Furthermore, it takes about 5 Myr for the temperature to decrease to 90 K. We present two atmospheric models at 355 and 300 K, and calculate the composition of a primordial atmosphere where the initial masses of NH_3 and CH_4 satisfy the conditions of gas thermal escape to the present-day levels, including calculations of the partial and total pressures, the volume, thickness, and outer surface area of the atmosphere. The two atmospheres in our models, where the loss of NH_3 and CH_4 is by thermal escape alone (at the initial T = 300 K) or by a combination of emissions from the interior and thermal escape (at the initial T = 355 K), have scale thicknesses five to six times greater than the present-day atmosphere, a total pressure of 25 bar, in comparison to 1.5 bar at present, and densities of 14 to 16.6 kg/m^3, compared to 5.2 kg/m^3 at present. Finally, we consider possible emissions from Titan's interior through cryovolcanism, and propose that resupply of atmospheric methane and ammonia through this process can satisfy present-day conditions only if emissions were discontinuous.

INDEX TERMS: 6281 PLANETARY SCIENCES: SOLAR SYSTEM OBJECTS Titan, 5405 PLANETARY SCIENCES: SOLID SURFACE PLANETS Atmospheres, 5210 PLANETARY SCIENCES: ASTROBIOLOGY Planetary atmospheres, clouds, and hazes

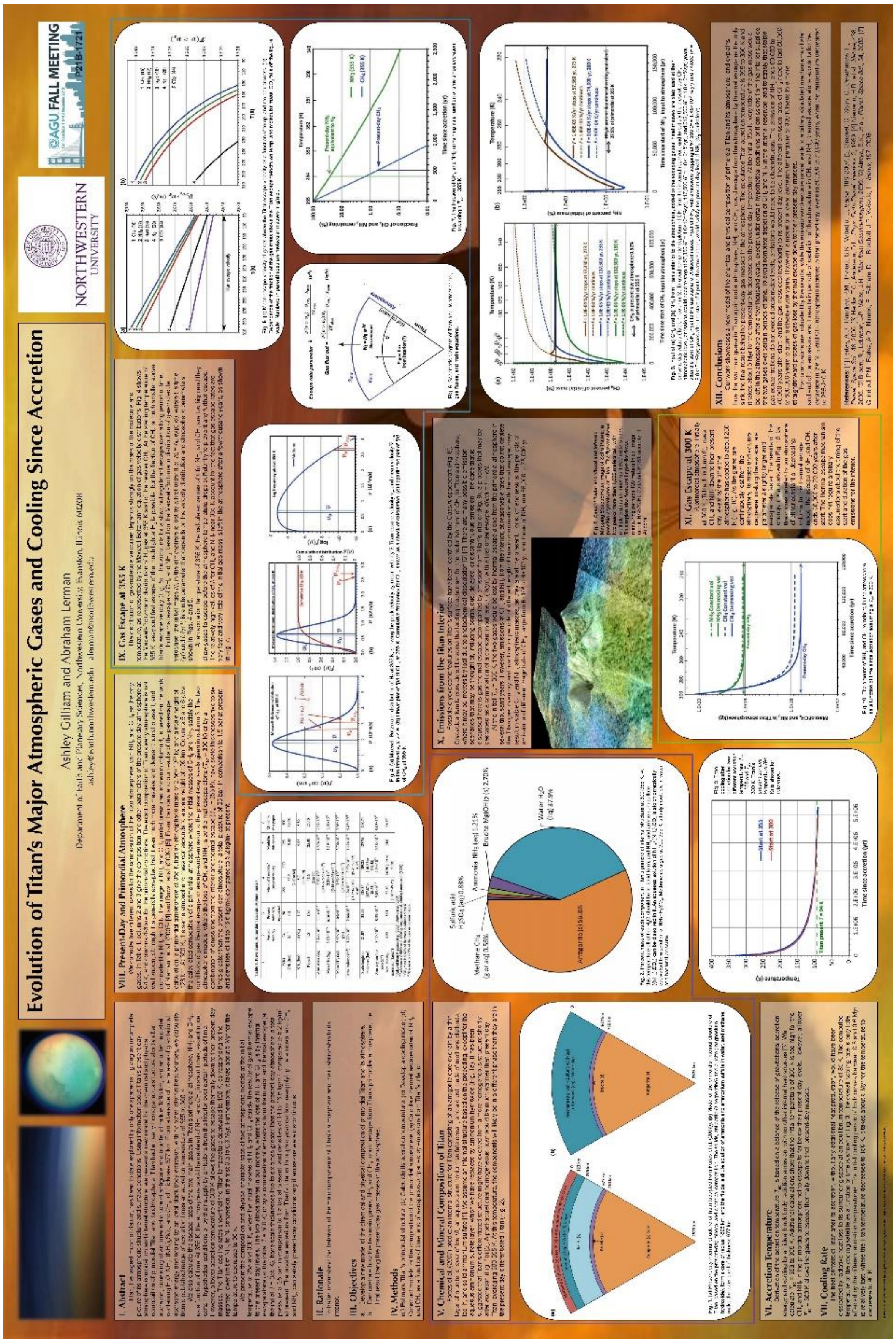

Evolution of Titan's Major Atmospheric Gases and Cooling Since Accretion
Ashley Gilliam and Abraham Lerman
NORTHWESTERN UNIVERSITY
AGU FALL MEETING
I. Abstract
II. Rationale
III. Objectives
IV. Methods
V. Chemical and Mineral Composition of Titan
VI. Accretion Temperature
VII. Cooling Rate
VIII. Present-Day and Primordial Atmosphere
IX. Gas Escape at 355 K
X. Emissions from the Titan Interior
XI. Gas Escape at 300 K
XII. Conclusions

45th Lunar and Planetary Science Conference (2014) 2435.pdf

TITAN'S IMPACT CRATERS AND ASSOCIATED FLUVIAL FEATURES: EVIDENCE FOR A SUBSURFACE OCEAN? A. E. Gilliam and D. M. Jurdy, Department of Earth and Planetary Sciences, Northwestern University, Evanston IL, 60208-3130 (ashley@earth.northwestern.edu).

Introduction: Impact craters may hold direct clues about Titan's subsurface ocean. Previous studies of Jupiter's moon Europa showed that impact craters could identify the thickness of the ice shell, and thus the proximity of its ocean to the surface. A careful investigation of Titan's surface craters could constrain the thickness of the ice layer, and give an indication of a subsurface ocean. A study of Titan's impact craters with associated fluvial features could determine the subsurface structure. Understanding the morphology of these fluvial features can give information about their origin, whether they be pluvial, created by sapping or seepage, or the result of a flood caused by a large impact. The latter may prove the most revealing, suggesting that the impactor was able to breach through the ice shell, releasing liquids from an internal reservoir or the subsurface ocean.

We take a geomorphological approach to examine craters on Titan, focusing on those that have features interpreted as fluvial in origin. Using a combination of *Cassini* RADAR, VIMS, and ISS data, we present measurements of the depth and diameter of Titan's impact craters. We also measure the stream order and length of the channels near three of Titan's confirmed impact craters to assess whether these features provide evidence for a subsurface ocean, which has implications for the distribution of environments that may support life.

Craters and Associated Fluvial Features: Although the very first *Cassini* radar image of Titan showed no impact craters, by 2012, as surface coverage increased to ~40%, 7 certain impact craters have been identified, as well as 52 nearly certain and probable craters [1, 2, 3]. From neighboring moons, Hyperion and Rhea, it was initially estimated that Titan should have 10,000 craters over its entire surface [4]. However, with only 59 detected as of 2012, an active process of burial and erosion must occur on the surface, removing a large number of craters [5].

The largest crater, Menrva, a 445 km wide double-ring impact basin, is heavily eroded and hosts a complex network of channels. On the western, more degraded side of the crater, channels cut through the outer rim. To the east of Menrva, a curious network of channels start near the rim crest and appear to have flowed away into a large catchment basin, a complex called Elivagar Flumina. Channels have also been observed near two other craters, Selk and Ksa. A halo of channels cut the outer rim of Selk, an 80 km diameter crater with a small central peak. Also, Ksa, a 30 km diameter crater with a bright central peak and radial ejecta, displays a sinuous feature resembling a channel running north-south on the eastern edge of the crater ejecta.

Crater Morphology: It is difficult to infer crater depth on Titan from the scaling relations for craters on the terrestrial bodies due to the difference in surface composition (icy vs. rocky). Thus, we examine scaling relationships of other bodies in the outer Solar System in order to find a crater scaling relationship that could be used for Titan. Craters on Ganymede, an icy moon of Jupiter, have been identified as far back as the *Voyager* mission. Because of the similar geology, and because Ganymede is of comparable size to Titan and thus has a surface gravity close to Titan's, crater morphologies on Titan and Ganymede should be similar. Using a numerical relationship between crater depth and diameter for Ganymede [6] we estimate the depth of Titan's craters with known diameters. This suggests that the depth of Titan's largest crater, Menrva, reaches ~2.8 km, agreeing with another study that proposes craters larger than 60 km in diameter on Ganymede (and Titan) have a very small depth/diameter ratio of ~0.01 [7].

Channel Order and Origin: Titan's surface may reveal a connection with its subsurface ocean. If cratering penetrated through the surface and made a connection to the subsurface ocean, then we would expect to see low-order channels flowing away from the crater rim. Examination of Menrva reveals several radar-bright river tributaries flowing toward and away from the crater rim (Fig. 1). Channels surrounding Menrva display a low order, measuring one or two, occasionally up to three. This matches observations of two other confirmed impact craters with associated fluvial features, Selk and Ksa. These differ radically from the tree-shaped dendritic channels common on Titan, generally attributed to heavy rainfall. For example, the Xanadu region exhibits a very complex and dendritic network of channels that reach up to third order, although others have reported that channels in the western Xanadu region reach up to sixth or seventh order [8].

Using the Integrated Software for Imagers and Spectrometers (ISIS), we measure the length and width of the channels surrounding Menrva, Selk, and Ksa craters, as well as those associated with Elivagar Flumina. We compare these results with a dendritic

network of channels (the Xanadu region) and a canyon system with channels created by sapping. Analysis showed the dendritic network of channels in the Xanadu region had the longest length, with some channels reaching ~450 km. This contrasts with the channels near Menrva, Ksa, and Selk, where the longest length recorded was ~175 km. The channels associated with Elivagar Flumina also display a moderate length, the shortest being ~23 km in length, and the longest nearly 210 km. Channels near Titan's craters most resemble the canyon system of channels attributed to sapping, which has a maximum length of ~200 km. Channels created by sapping are usually much shorter and often wider than those created by precipitation. The canyon system of sapping channels reported in this paper have a stream order of up to two, and a considerable width of 5 km, unlike the narrow dendritic channels which have high stream orders [8].

Discussion and Conclusions: In this study, we investigate the craters on the surface of Titan and their associated fluvial features as possible evidence of a subsurface ocean. Using a scaling relationship for craters on Ganymede, we calculate a depth of Titan's largest crater, Menrva, of ~2.8 km. If Titan's crust has remained at a constant thickness of ~123 km over the course of its history, we find that it is unlikely that the impactor that created Menrva was able to break through to the ocean layer below, however, it cannot be ruled out, especially if there exists a localized subsurface reservoir of liquid closer to the surface.

A study of Menrva, Selk, and Ksa reveals the existence of several river tributaries flowing toward and away from these craters. These low-order channels differ radically from the dendritic network of channels on Titan, as observed in the Xanadu region, where the channels can reach up to sixth or seventh order. Because dendritic channels are generally attributed to heavy rainfall, this hints that the channels near Titan's craters may have formed through another mechanism. This hypothesis is further supported by measurements of the length of these channels. The dendritic network of channels in the Xanadu region reach 450 km, in contrast to the channels associated with Menrva, Selk, and Ksa craters, with the longest length recorded only 175 km. The channels flowing into Elivagar Flumina also display a moderate length. These results are comparable to the canyon system of channels observed on the T16 swath, which are thought to have been created by sapping, further suggesting that the channels associated with Titan's largest craters may not be pluvial in origin, but instead may be the result of seepage or even record a flood.

References: [1] Wood C.A. et al. (2010) *Icarus, 206,* 334-344. [2] Soderblom J.M. et al. (2010) *Icarus, 208,* 905-912. [3] Neish C.D. and Lorenz R.D. (2012) *Planet. Space Sci., 60,* 26-33. [4] Lorenz R.D. (1994) *Planet. Space Sci., 42,* 1-4. [5] Lorenz R.D. et al. (2007) *Geophys. Res. Lett., 34,* L07204, doi:10.1029/2006GL028971. [6] McKinnon W.B. and Schenk P.M. (1995) *Geophys. Res. Lett., 22,* 1829-1832. [7] O'Brien D.P., Lorenz R.D., Lunine J.I. (2005) *Icarus, 173,* 243-253. [8] Langhans M.H. et al. (2012) *Planet. Space Sci., 60,* 34-51.

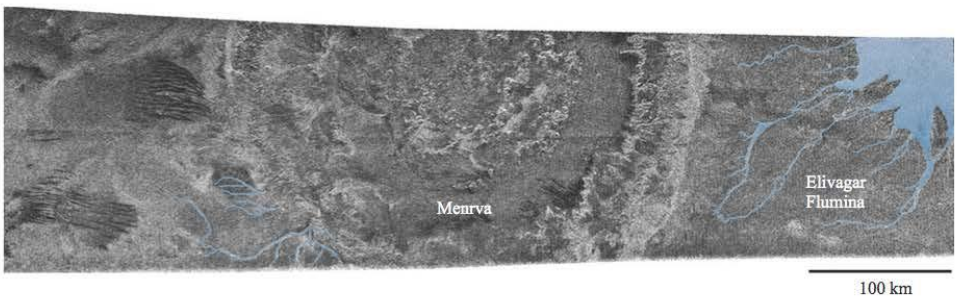

Fig. 1. *Cassini* RADAR image of Menrva and Elivagar Flumina taken during the T3 fly-by, showing the channels near Menrva and the catchment basin (highlighted in blue).

Titan's Impact Craters and Associated Fluvial Features: Evidence for a Subsurface Ocean?

Ashley Gilliam and Donna Jurdy
Department of Earth and Planetary Sciences, Northwestern University, Evanston, Illinois 60208
ashley@earth.northwestern.edu

NORTHWESTERN UNIVERSITY

45th LPSC Lunar and Planetary Science Conference 2435

1. Abstract

The Cassini spacecraft has mapped ~ 50% of Titan's surface, revealing very few impact structures. The paucity of craters implies that the surface is very dynamic and relatively young. Dynamical models of the internal structure suggest the possibility of a subsurface ocean of ammonia water, and beneath its icy shell, it's large subsurface ocean does exist, it should have measurable effects on Titan's surface and the morphology of its craters. Observations of impact craters with associated fluvial features may also provide evidence for the subsurface structure.

We investigate the morphology of the craters on the surface of Titan using Cassini data, and propose a formation mechanism for dark fluvial features. Using a scaling relationship for craters on Ganymede, we calculate a depth of Titan's largest crater, Menrva, of ~ 2.6 km. Assuming a relatively thick crust, Menrva's fluvial features may not directly sample the subsurface ocean. However, the mechanics and thermal processes of impact events must be investigated before this possibility can be eliminated.

Measurements – using the Integrated Software for Imagers and Spectrometers (ISIS) – of the morphology of Titan's fluvial network near craters contrast with those attributed to rainfall, but resemble those created by sapping. This suggests these channels are not solely pluvial in origin, but may also result from seepage or even recent flood. Known flooding events on Mars further support this hypothesis. Using MOLA topography and THEMIS daytime IR data, we present new observations of three ancient flooding events on Mars: Eberswalde, Lyot, and Jezero craters. These show evidence of ancient flooding in and around the craters, formed from groundwater release and/or increased precipitation triggered by their respective impact events. Measurements of channel length, width order, and overall morphology are akin to those on Titan. This suggests that ancient impacts on Titan may have triggered floods, creating fluvial features.

2. Crater Morphology

The morphology of Titan's impact craters may give insight into crustal strength and rheology, as well as the subsurface structure. An estimate of crater depth on Titan can be made using scaling relations for craters on other comparable bodies. We use a simplified relationship between crater depth and diameter for Ganymede [1] to estimate the depth of Titan's craters with known diameters. We find that the depth of Titan's largest crater, Menrva, a 445 km wide double ring impact basin with a complex network of channels, is ~ 2.6 km. If Titan's crust has remained at a constant thickness of ~ 123 km [2] over the course of its history, we find it unlikely that the impactor that created Menrva was able to break through to the ocean layer below. Unless there exists a localized subsurface reservoir of liquid closer to the surface, Perhaps a more plausible crater mechanism for Menrva's channels, observed on the western outer rim and near the eastern inner crest, is impact induced melting of the methane clathrate ice ammonium sulfate crust.

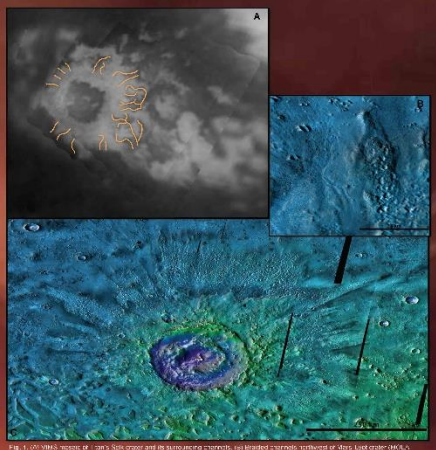

Fig. 1. (A) VIMS mosaic of Titan's Soik crater and its surrounding channels. (B) Braided channels northwest of Xanadu. Lyot crater (HiSAR topography over subframe of HiSAR swath no. 30). (C) Lyot crater and surrounding terrain. In the north, west, and east of Lyot is an extensive channel network scoured region, including braided reaches are large areas of scour. The channels, covering about 330,000 km², are attributed to sapping by sediment-laden water from the crater rather than rainfall. Evidence of shallow groundwater by breaks in slope and the rapid evaporation of standing bodies [3]. The morphology of Lyot's basin is reminiscent of the debris-aprons of the channels surrounding Soik crater as well, suggesting that impact ejecta, but debris flow may have also occurred on Titan.

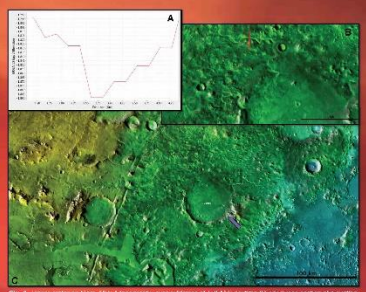

Fig. 3. Menrva crater on Titan. (A) A topography over subframe of HiSAR swath no. 30. (B) Close section of the western (or northern channel (pg. 1) valley networks (~ 150 and ~ 70 km long) enter the crater from the east and north, depositing sediments at their mouth. (C) Menrva crater and surrounding terrain. As a bi- channel of the eastern crater rim (extending over 40 km and long at an elevation above the valley deposits) suggests that influx of water from these valleys filled the crater until the eastern rim was overtopped and breached. Assuming the rate of martian drainage – a precipitation-related crater filling – 1 Earth year [4], the relatively short duration of this accumulation a comparable amount of liquid water, such as impact-induced precipitation. The morphology of this system bears striking resemblance to that of Titan's Menrva crater (pg. 7), both having channels flowing in and out of the crater.

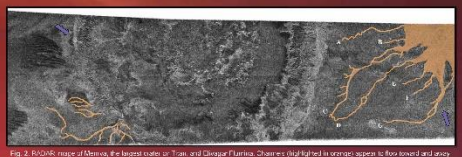

Fig. 2. RADAR image of Menrva, the largest crater on Titan, and Elivagar Flumina. Channels (highlighted in orange) appear to flow toward and away from the crater. To the north, a dendritic network of channels start near the ejecta crest and flow away into a large catchment basin, Elivagar Flumina. On the western, more degraded side of the crater, channels cut through the ejecta rim. Main channels of Elivagar Flumina are designated with letters.

3. Fluvial Network Analysis on Titan: Order

For our analysis, Cassini RADAR and VIMS data were obtained using NASA's Planetary Data System. Examination of Menrva crater reveals several "box-in-the" river tributaries flowing toward and away from the crater rim (Fig. 2). To the east of Menrva, a curious network of channels start near the rim crest and appear to have flowed away into a large catchment basin, a complex called Elivagar Flumina. Channels surrounding Menrva display a low dendritic measuring, one or two, occasionally up to three. This matches observations of two other confirmed impact craters with associated fluvial features. A halo of low-order channels encircles Soik (Fig. 1B), and Ksa has a feature that resembles a first order channel. These differ radically from the dendritic channels on Titan, generally attributed to heavy rainfall. For example, the Xanadu region exhibits a more complex and chaotic network of channels that reach up to seventh order [3]. See Table 2.

4. Fluvial Network Analysis on Titan: Length and Origin

Using the Integrated Software for Imagers and Spectrometers (ISIS), we measured the length and width of the channels surrounding Menrva, Soik, and Ksa craters, as well as those associated with Elivagar Flumina. The results were then compared to a dendritic network of channels (the Xanadu region) and a canyon system (which channels created by sapping). Analysis showed that the channels in the Xanadu region has the longest length. This contrasts with the moderate-length channels near Menrva, Ksa, and Soik craters. The channels associated with Elivagar Flumina also display a moderate length, with the shortest channel "E" at ~ 40 km in length and the longest channel "C" at ~ 210 km (Fig. 2).

Channels near Titan's craters most resemble the canyon system of channels attributed to sapping. These channels are usually much shorter and often wider than those created by precipitation. These results suggest that the channels associated with Titan's largest craters may not be solely pluvial in origin. Instead, the channels may be the result of seepage or even recent a flood, or some combination of all three processes. See Table 2.

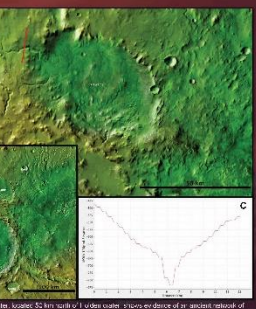

Table 1. Titan, Mars, and Earth parameters relevant for flood generation

Parameter	Titan	Mars	Earth
Surface gravity (m/s²)	1.35	3.71	9.81
Surface temperature (K)	94	210	287
Surface pressure (bar)	1.5	0.007	1.01
Atmospheric composition	95% N_2, 5% CH_4	95% CO_2, 2.7% N_2, 1.6% Ar	78% N2, 20% O2
Fluvial liquid density (kg/m³)	CH_4/N_2, 450	H_2O, 1000	H_2O, 1000
Liquid viscosity (Pa·s)	2×10^{-4}	$\sim10^{-3}$	$\sim10^{-3}$
Flood-generating mechanisms	Possible causes: cryovolcanism, basin overflow, precipitation, impact-induced precipitation and groundwater mobilization of subsurface fluids	Basin overflow, precipitation, volcanism, impact induced precipitation and groundwater release	Glaciation, volcanism, basin overflow, precipitation

Fig. 4. (A) Mars Eberswalde crater, located 30 km north of Holden crater, shows evidence of an ancient network of multi-order fluvial valleys feeding a fan deposit in the northwest margin of the crater. The fan is locally interpreted as a delta formed in a standing body of water over a period of at least ~ 100,000 years. (B) Eberswalde and Holden craters. A recent study suggests that the much larger Holden crater could have triggered flooding by fluvial seeping of pre-existing groundwater possibly in combination with stress changes [7]. (C) Measurements of this event demonstrate a dramatic network with five orders of tributary branching, a nearly constant channel width of ~ 2 km and depths reaching up to 70 m. The morphology of the fluvial valleys resemble those at Elivagar Flumina on Titan, which also display trellis-style channels lengths and orders. This suggests a possible common forming mechanism.

5. Palaeoflooding on Mars: Implications for the Origin of Titan's Fluvial Features

Fluvial channels are present on Earth, Mars, and Titan, but only Earth and Mars show definitive evidence of channelized liquid flood flow. Key parameters relevant for flood generation on those three bodies are listed in Table 1. On Earth, megaflooding is generally attributed to a large reservoir of water from glacial lakes, volcanism, or tectonic basin overflow. Similar to Earth, Mars' flooding is typically associated with basin overflow, volcanism, precipitation, or impact events [4]. The morphologies of these martian channels may provide an analog for flooding on Titan.

We present new observations of three ancient martian flooding events that exhibit channel morphologies like those on Titan, using a combination of MOLA topography and THEMIS daytime IR data (Table 2). Perhaps not surprisingly, these three flooding events, located at Eberswalde, Lyot, and Jezero craters, are all attributed to impact-induced precipitation or groundwater release.

6. Preliminary Conclusions

In this study, we investigated the morphology of the craters on the surface of Titan and formation mechanisms for their fluvial features. Using a scaling relationship for craters on Ganymede, we calculate a depth of Titan's largest crater, Menrva, of ~ 2.6 km, suggesting that its fluvial features are not evidence of a subsurface ocean. Analysis of the morphology of Titan's fluvial networks near craters reveals an apparent contrast to those attributed to rainfall, but a similarity to those created by sapping. This suggests those channels are not pluvial in origin, but instead may be the result of seepage or even recent a flood. This hypothesis is further supported by a study of known flooding events on Mars. Observations of Mars' Eberswalde, Lyot, and Jezero craters show evidence of ancient flooding in and around the craters, formed from groundwater release and/or precipitation triggered by impact events. Measurements of channel length, width order, and overall morphology are akin to those on Titan, suggesting that Titan's fluvial features may be evidence of ancient floods triggered by impacts.

Table 2. Fluvial features on Titan and Mars

Associated With	Body	Location (Lat., Lon.)	Origin	Channel Length (km)	Channel Width (km)	Maximum Channel Order
Menrva crater	Titan	-9.6, -87	?	≤ 175	≤ 5	2
Ksa crater	Titan	-14, -65.4	?	< 125	≤ 5	1
Soik crater	Titan	7, -106	?	≤ 100	≤ 5	2
Elivagar Flumina	Titan	19, -79	?	≤ 210	≤ 10	3
Xanadu Region	Titan	-13, -135	Precipitation	≤ 150	≤ 3	7
Canyon system	Titan	50, -110	Subsurface seepage	< 200	< 5	2
Eberswalde crater	Mars	-24.2, -33.5	Impact-induced groundwater release and precipitation	< 70	< 2	5
Lyot crater	Mars	50.7, 29.2	Impact-induced groundwater release	≤ 300	≤ 1	1
Jezero crater	Mars	18.3, 77.4	Impact-driven precipitation	≤ 160	≤ 2	1

References: [1] McKinnon W.B. and Schenk P.M. (1995) *Geophys. Res. Lett.* 22, 1829-1832. [2] Gilliam A.E. and Lemmon A. (2014) *Planet. Space Sci.*, http://dx.doi.org/10.1016/j.pss.2014.02.001. [3] Langhans M.H. et al. (2012) *Planet. Space Sci.*, 60, 34-51. [4] Burr D.M. (2010) *Geol. Planet. Change*, 70, 5-13. [5] Burr D.M. (2010) *Geol. Planet. Change*, 70, 5-13. [6] Harrison T.N. et al. (2010) *Geophys. Res. Lett.*, 37, L21201. [6] Fassett C.I. and Head J.W. (2008) *Geophys. Res. Lett.*, 32, L14201. [7] Mangold N. et al. (2012) *Icarus*, 220, 530-551.

45th Lunar and Planetary Science Conference (2014) 1545.pdf

METHANE AND AMMONIA IN TITAN'S PRIMORDIAL AND COOLING ATMOSPHERE. A. E. Gilliam and A. Lerman, Department of Earth and Planetary Sciences, Northwestern University, Evanston IL, 60208-3130 (ashley@earth.northwestern.edu).

Introduction: To date, only the *Cassini-Huygens* spacecraft has been able to peer beneath Titan's thick clouds. Even less is known about early Titan, how it formed, and how it evolved from 4.55 Ga until today. We use available information about Titan's present-day atmosphere composition and internal structure and propose a new model for the chemical and physical composition of Titan and its atmosphere post-accretion. We show how the two main gases in Titan's primordial atmosphere, NH_3 and CH_4, could escape from the atmosphere with thermal escape as the only sink, the final result being the present-day gas masses in the atmosphere. For this, we estimate the structure of primordial Titan based on its present-day internal composition, calculate its accretion temperature, estimate its mean heat capacity, and develop its cooling model. We also model the composition of the primordial Titan atmosphere, with NH_3 and CH_4 as the only gases, and calculate the corresponding volume, height, density, and outer surface area of the atmosphere in each case. Finally, we calculate the escape rates of NH_3 and CH_4 as a function of time by mechanisms of gas thermal escape alone and by thermal escape accompanied by emissions from Titan's interior.

Chemical and Mineral Composition of Titan: The internal structure for Titan is thought to consist of an antigorite core overlain by a thin layer of brucite, a layer of ice VI, an aqueous ammonium sulfate ocean, and a crust made of methane clathrate, ice Ih, and solid ammonium sulfate [1]. We assume an internal structure based on the preceding, with the volatiles in the outer fluid shell: aqueous solution of NH_3, $(NH_4)_2SO_4$, and CH_4 gas. It has been suggested that Titan's differentiated structure evolved from a more homogeneous structure shortly after accretion [2]. A post-accretional homogeneous Titan would be much warmer than present-day Titan, averaging 300-355 K. At this temperature, the components will likely be in a different phase than they are in the present-day differentiated Titan.

Accretion Temperature and Cooling: Accretion temperature, T_{ac}, is based on a balance of the release of gravitational accretion energy and cooling by an ideal black body radiation emission, with no other internal heat sources or heat storage [3]. The overall cooling rate (Fig. 1) is based on our estimates of Titan's composition and heat capacity and it is unaffected by the different accretion temperatures: the two curves are essentially identical at $t > 1$ Myr after accretion. The initial cooling period of both curves between 0.5 and 0.6 Myr is relatively fast, where the Titan temperature decreases to 150 K. It takes about 5 Myr for the temperature to decrease to 90 K.

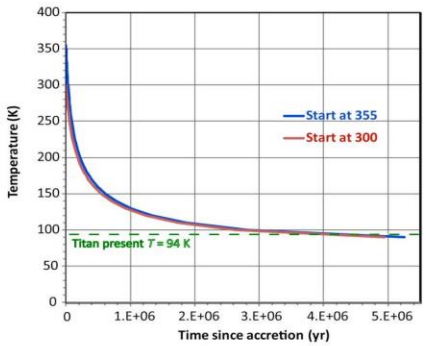

Fig. 1. Titan cooling after accretion for two different accretion temperatures, T_{ac} = 355 and T_{ac} = 300 K.

Present-Day and Primordial Atmosphere: We consider two cases for Titan's present-day atmosphere, with N_2 or NH_3 and CH_4 as the only gases, and three cases for the primordial atmosphere. It is generally accepted that Titan's primordial atmosphere was much more massive and denser than at present, and dominated by NH_3 and CH_4: two to ten times today's mass [4] or an atmosphere of a N_2 pressure 5-10 bar and a CH_4 pressure 30-80 bar [5]. From our results of the gas-escape calculation, primordial atmosphere scale thickness was five to six times greater than at present (109 to 128 km), a total pressure of 25 bar, in comparison to 1.5 bar at present, and densities of 14 to 16.6 kg/m^3, compared to 5.2 kg/m^3 at present.

Gas Escape: In a gas, the directions of the gas molecules are on average outward and inward [6], and the fraction of the gas moving away from the planet is ½ of the fraction of gas molecules that have velocities greater than the escape velocity of the planet. The gas mass remaining in the atmosphere $N_t = N_0\, e^{-kt}$ (kg or %), where N_0 is the initial gas mass at time $t = 0$, is taken as a first-order flux that is controlled by the escape rate parameter, k. The value of k depends on temperature and molecular mass of the gas, the Titan escape velocity, and on the atmosphere thickness. Fig. 2 shows the CH_4 and NH_3 escape since accretion.

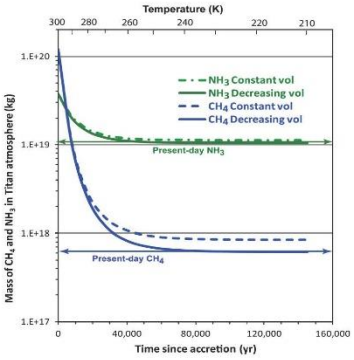

Fig. 2. The amount of NH_3 and CH_4 remaining in the atmosphere as a function of time since accretion assuming a T_{ac} = 300 K.

Possible Emissions from the Interior: Possible cryovolcanic features on Titan's surface have been identified by the *Cassini* spacecraft [7]. Cryovolcanism is considered by some the leading mechanism for the replenishment of CH_4 in Titan's atmosphere, where it may be irreversibly lost due to photochemical dissociation [8]. Among the many possible emission scenarios that may be thought of, the case we explore is gas thermal escape accompanied by emission from Titan's interior, a process that is a combination of a constant input rate to the atmosphere, F (% N_0/yr), with a first-order escape: $dN/dt = F - kN$, as shown in Fig. 3.

Discussion and Conclusions: Our work showcases a new model of the chemical and physical composition of primordial Titan and its atmosphere, and explains how the two main gases in Titan's primordial atmosphere, NH_3 and CH_4, could leave the atmosphere by thermal escape as the only sink, the final result being the present-day gas masses in the atmosphere. The calculated Titan T_{ac} = 355 to 300 K, and it takes about 5 Myr for the temperature to decrease to the present-day temperature.

At the initial 355 K, very little of the gas mass would be left in the atmosphere after a few hundred years, except under certain hypothetical conditions or if emissions from the interior supplied the two gases over certain periods of time. To avoid complete depletion of CH_4 and NH_3 in the internal reservoir, and to satisfy that stable gas concentrations do not exceed present-day levels, emissions would need to be discontinuous and stop at different times, depending on the emission rate. The emission of NH_3 ends 60,000 to 70,000 yr ($F = 1.45\times10^{-3}$ to 9.0×10^{-4} %/yr) after start, and the gas mass declines shortly to its present-day level. The different emission rates of CH_4 need to last 60,000 to 600,000 yr ($F = 1.0\times10^{-4}$ to 1.0×10^{-6} %/yr) to attain a steady-state value. However, a model of a lower accretion temperature of 300 K leads to a more straightforward process of gas loss by thermal escape down to their present-day masses.

References: [1] Fortes A.D., Grindrod P.M., Trickett S.K., Vočadlo L. (2007) *Icarus, 188,* 139-153. [2] Grasset O., Sotin C., Deschamps F. (2000) *Planet. Space Sci., 48,* 617-636. [3] Hanks T.C. and Anderson D.L. (1969) *Phys. Earth Planet. Interiors, 2,* 19-29. [4] Niemann H.B. et al. (2005) *Nature, 438,* 779-784. [5] Brown R., Lebreton J-P., Waite J.H, eds. (2009) *Titan from Cassini-Huygens*, Springer, 535 pp. [6] Maxwell J.C. (1867) *Phil. Trans. Roy. Soc. London, 157,* 49-88. [7] Lopes R.M.C. et al. (2007) *Icarus, 186,* 395-412. [8] Atreya S.K. et al. (2006) *Planet. Space Sci., 54,* 1177-1187.

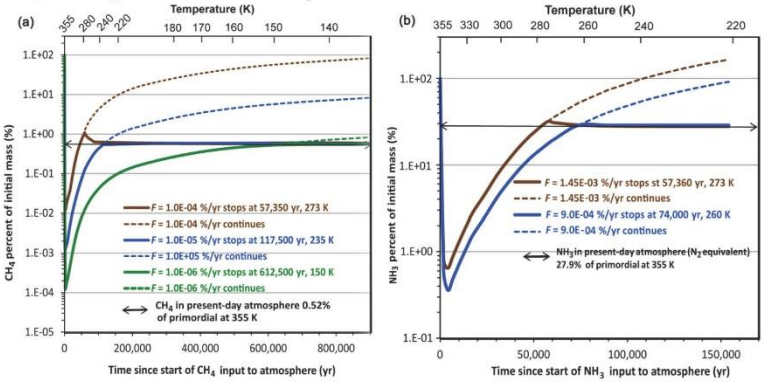

Fig. 3. Input of (a) CH_4 and (b) NH_3 from Titan's interior to the atmosphere, added to the escaping gases. Final masses are stabilized at their present-day values.

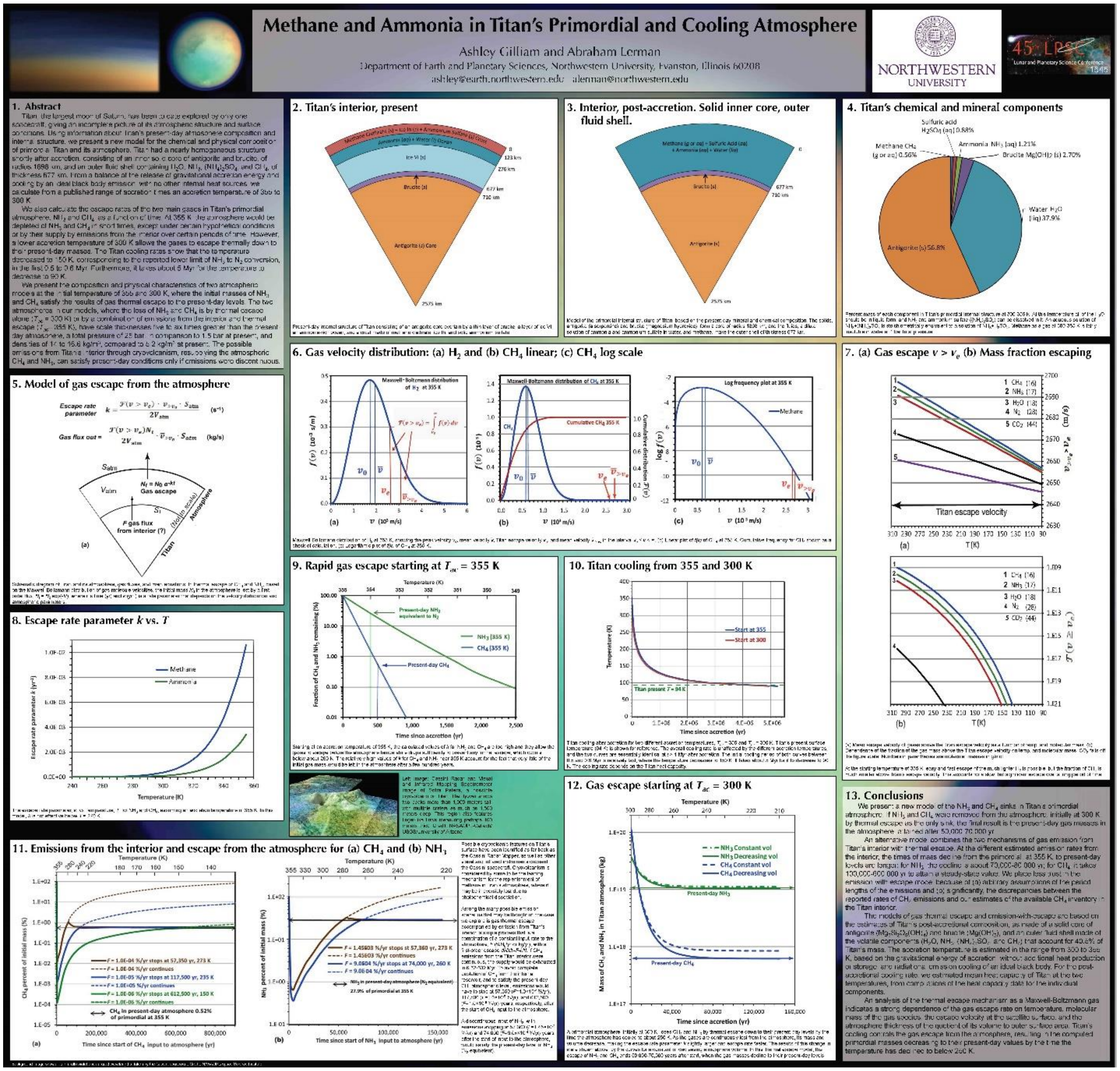
Methane and Ammonia in Titan's Primordial and Cooling Atmosphere
Ashley Gilliam and Abraham Lerman
Department of Earth and Planetary Sciences, Northwestern University, Evanston, Illinois 60208
ashley@earth.northwestern.edu alerman@northwestern.edu
NORTHWESTERN UNIVERSITY
45 LPSC
1. Abstract
2. Titan's interior, present
3. Interior, post-accretion. Solid inner core, outer fluid shell.
4. Titan's chemical and mineral components
5. Model of gas escape from the atmosphere
6. Gas velocity distribution: (a) H2 and (b) CH4 linear; (c) CH4 log scale
7. (a) Gas escape v > ve (b) Mass fraction escaping
8. Escape rate parameter k vs. T
9. Rapid gas escape starting at Tac = 355 K
10. Titan cooling from 355 and 300 K
11. Emissions from the interior and escape from the atmosphere for (a) CH4 and (b) NH3
12. Gas escape starting at Tac = 300 K
13. Conclusions

Astrobiology Science Conference 2015 (2015) **7772.pdf**

EVOLUTION OF TITAN'S ATMOSPHERE IN RELATION TO ITS SURFACE AND INTERIOR. A. E. Gilliam[1], A. Lerman[1], and J. Wunsch[2], [1]Department of Earth and Planetary Sciences, Northwestern University, Evanston IL, 60208-3130 (ashley@earth.northwestern.edu), [2]Department of Mathematics, Northwestern University, Evanston IL, 60208-2730.

Introduction: Titan is the only known moon to have a thick atmosphere and the only world besides the Earth to have a liquid on its surface. In Titan's atmosphere, photochemistry of the methane (CH_4) molecule controls the composition of the atmosphere as well as the surface. In the upper atmosphere, direct and irreversible photolysis of methane principally produces ethane (C_2H_6), which is subsequently condensed in the atmosphere and eventually accumulates on the surface. The irreversible destruction of methane by photolysis in, and its escape from, Titan's atmosphere suggest a much larger atmospheric methane budget on early Titan and a substantial surface liquid reservoir of ethane on present-day Titan. A careful investigation of the pathways of methane to ethane conversion throughout time could constrain the amount of ethane expected to be present on the surface of Titan, and give clues as to its subsurface composition.

CH_4 Depletion and C_2H_6 Production Through Time: In Titan's atmosphere, the production of all hydrocarbons commences with the photodissociation of methane. In the stratosphere, UV photolysis is responsible for ~1/3 of the total methane destruction [1], 75% of which occurs at the Lyman α wavelength (121.6 nm) [2]. At Lyman α, the photodissociation of methane is capable of producing other hydrocarbons, such as methyl radicals (CH_3). Once these hydrocarbons are formed they recombine to form heavier molecules (e.g. C_2H_6) that condense and eventually precipitate from the atmosphere. In Titan's atmosphere, ethane is the main photolysis product of methane [3], with a production rate of 1.3×10^8 molecules cm^{-2} s^{-1}.

Another mechanism responsible for methane loss in the Titan atmosphere is hydrodynamic escape. First observed by the Voyager spacecraft and confirmed by the Cassini Ion Neutral Mass Spectrometer, the methane distribution in Titan's upper atmosphere remains uniformly mixed up to ~1100 km, where it begins to exhibit diffusive separation. Further evidence from the Cassini INMS suggested that methane is not well mixed to high altitudes because of a large escape rate.

Using a simplified model of Titan's atmosphere, we can calculate the amount of methane remaining as a function of time since accretion, and the subsequent production of ethane through photodestruction of the methane molecules. Expanding on our previous primordial atmospheric model [4], we assume a primordial atmospheric temperature of 300-355 K, an atmospheric CH_4 mass of 1.19×10^{20} kg, and a scale atmosphere 128 km thick and top surface area of 9.18×10^{13} m^2. Under these conditions, we calculate that 8.46×10^{17} kg of atmospheric ethane should have been produced since accretion (~4.5 Ga). As a comparison, Ligeia Mare, the second largest lake on Titan (126,000 km^2), is thought to contain $\sim 5 \times 10^{15}$ kg of hydrocarbons [5]. Assuming a liquid solution of 40% ethane [6], this corresponds to a mass of 2×10^{15} kg of liquid ethane. Our results predict a mass of ethane roughly 400× larger than observed in the second largest surface liquid reservoir on Titan, or 150× larger than its total hydrocarbons, suggesting a large quantity of liquid ethane in Titan's lakes and perhaps in Titan's subsurface.

CH_4-C_2H_6 in Titan's Atmosphere: 1st and 2nd Order Reaction Systems, Exact and Numerical Solutions of Simultaneous Equations: Simultaneous 1st and 2nd order chemical reactions occur in such systems as the transitions from CH_4 (1st order) → CH_3 (2nd order) → C_2H_6 (1st order) → Other products, in the atmosphere of Titan. As far as we are aware, no exact mathematical solutions of the mixed 1st and 2nd order reaction systems are available in the literature. The novel exact solutions are for a case of the source species CH_4 with input from Titan's interior to its atmosphere. The exact solutions are compared to the approximations that are easier to handle in some cases. The results are based on the published and estimated values of the 1st and 2nd order reaction rate constants of the species. The rate and duration of CH_4 input to the atmosphere are uncertain because of the finite size of methane reservoir in the satellite interior, a feature often overlooked in mass balance calculations. The new exact solutions of the reactive system help to analyze evolution of Titan's atmosphere since its accretion and through subsequent cooling, and identify the rates of the different processes that are consistent with the present-day occurrences of methane and ethane in its atmosphere.

References: [1] Brown R., Lebreton J-P., Waite J.H., eds (2009) *Springer* (Print). [2] Wilson E.H. and Atreya S.K. (2009) *J. Phys. Chem. A., 113,* 11221-11226. [3] Yung Y.L., Allen M., Pinto J.P. (1984) *Astrophys. J. Suppl. S., 55,* 465-506. [4] Gilliam A.E. and Lerman A. (2014) *Planet. Space Sci., 93-94,* 41-53. [5] Mousis O., et al. (2014) *Icarus, 239,* 39-45. [6] Graves S.D.B., et al. (2008) *Planet. Space Sci., 56,* 346-357.

Evolution of Titan's Atmosphere in Relation to its Surface and Interior

Ashley Gilliam[1], Abraham Lerman[1], and Jared Wunsch[2]
[1]Department of Earth and Planetary Sciences, Northwestern University, Evanston, Illinois 60208
[2]Department of Mathematics, Northwestern University, Evanston, Illinois 60208
ashley@earth.northwestern.edu

NORTHWESTERN UNIVERSITY

AbSciCon 2015

7772

1. Abstract

Titan is the only known moon to have a thick atmosphere and the only world besides Earth to have a liquid on its surface. In Titan's atmosphere, photochemistry of the methane (CH_4) molecule and its thermal escape control the composition of the atmosphere as well as the surface. In the upper atmosphere, direct and reversible photolysis of methane or indirectly produces ethane (C_2H_6), which is subsequently condensed in the atmosphere and eventually accumulates on the surface. The irreversible destruction of methane by photolysis in Titan's atmosphere suggests a much larger atmospheric methane budget on early Titan and a substantial surface liquid reservoir of ethane on present-day Titan. A careful investigation of the pathways of methane to ethane conversion throughout time would constrain the amount of ethane expected to be present on the surface of Titan and give clues as to its subsurface state.

ATMOSPHERE

2. Photodissociation of CH_4

In Titan's atmosphere, the production of all hydrocarbons commences with the photodissociation of methane. In the stratosphere, UV photolysis is responsible for ~1/3 of the total methane destruction [1], ~8% of which occurs at the Lyman-α wavelength (121.6 nm) [2]. At Lyman-α, the photodissociation of methane is capable of producing three hydrocarbons, such as methyl radicals (CH_3). Once these hydrocarbons are formed they recombine to form heavier molecules (e.g. C_2H_6) that condense as liquids or solids in the lower stratosphere and vicinity of Titan's solid troposphere (Fig. 2) to form a haze layer and eventually precipitate from the atmosphere. In Titan's atmosphere, ethane is the main photolysis product of methane [3], with a production rate of 1.2×10^9 molecules cm^{-2} s^{-1} [2], nearly tenfold the production of the other hydrocarbons combined [4]. The resulting ethane is largely shielded from UV radiation by methane and acetylene (C_2H_2), making it stable against photolysis or by attack of polyyne radicals. The principal loss mechanism for ethane is condensation at the tropopause, followed by accumulation on the surface [5].

3. CH_4 Depletion and C_2H_6 Production Through Time

Using a simplified model of Titan's atmosphere, where the two major pathways of CH_4 loss are direct UV photolysis and methane escape, we calculate the amount of methane remaining as a function of time since accretion and the subsequent production of ethane through photo-destruction of the methane molecules (e.g. 1). Expanding on our previous primordial atmosphere model [6], we assume a primordial atmosphere temperature of 300–350 K, an atmospheric CH_4 mass of 1.19×10^{20} kg and an atmosphere top surface area of 5.15×10^{14} m^2. We assume two different values for the rate of CH_4 escape: (a) the frequently cited 2.9×10^9 molecules cm^{-2} s^{-1} and (b) 1.77×10^9 molecules cm^{-2} s^{-1} calculated using the escape rate parameters found in the primordial model of [6]. Using escape rate (a), we calculate that 8.45×10^{21} kg of atmospheric ethane should have been produced since accretion (~4.0 Ga). Using escape rate (b), CH_4 will be completely removed from the atmosphere in ~ 5.6 Myr, but not before producing 1.07×10^{21} kg of C_2H_6.

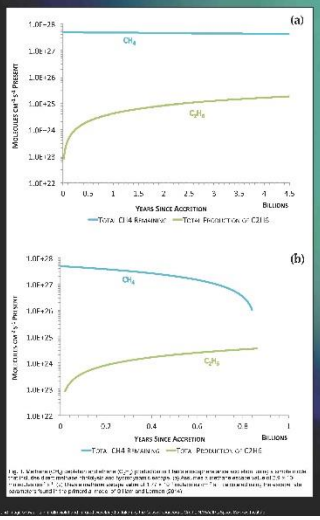

4. CH_4-C_2H_6 in Titan's Atmosphere: 1st and 2nd Order Reaction Systems

Simultaneous 1st and 2nd order chemical reactions occur in such systems as the transitions from CH_4 (1st order) → C_2H_6 (1st order) → Other products, in the atmosphere of Titan. As far as we are aware, no exact mathematical solutions of the mixed 1st and 2nd order reaction systems are available in the literature. We present most exact solutions for a case of the source gas CH_4 with input from Titan's interior or to its atmosphere. The new exact solutions of the reactive system help to analyze evolution of Titan's atmosphere since its accretion and through subsequent cooling, and identify the rates of the different processes that are consistent with the present day concentrations of methane and ethane in the atmosphere.

A simplified sequence of direct forward reactions from CH_4 to C_2H_6 that short-circuits the complex intermediate paths may be represented by the following:

$$CH_4 \xrightarrow{k_{21}} (CH_3 + H) \xrightarrow{k_{32}} C_2H_6 \xrightarrow{k_{43}} \text{Other products}$$

The reactions above, occurring simultaneously in Titan's atmosphere, make a geochemical reservoir balance system:

(1) $d[C_1]/dt = F - k_{21}[C_1]$

(2) $d[C_2]/dt = k_{21}[C_1] - k_{32}[C_2]^2$

(3) $d[C_3]/dt = k_{32}[C_2]^2 - k_3[C_3]$

where t is time, $[\ ]$ are concentrations in molecules cm^{-3} and F is input of CH_4 by emission from the satellite's interior, in molecules cm^{-3} s^{-1}. The large range of the reaction rate constants for the preceding reactions is given in Table 1.

Eqs. (1) and (2) are simultaneous nonlinear differential equations. To find their solution, we write them for a steady state, when $t \to \infty$ and $d/dt = 0$. Our results (Table 2) agree well with the observed values of CH_4 and C_2H_6 in Titan's present-day atmosphere. Parameter ranges used in this model are in Table 3.

Table 1. Rate constants of direct forward and back reactions of the species CH_4, CH_3, C_2H_6

Reaction	Rate Constant at 200 K, unless where T indicated	Units	Reaction order	Temperature range (K)
$CH_4 \rightarrow CH_3 + H$	2.05E-09 to 9.84E-06	s^{-1}	1	40-200
$CH_4 \rightarrow$ all branches	1.0e-9	s^{-1}	1	175-350
$CH_4 \rightarrow$ all branches	1.42E-9	s^{-1}	1	180
$CH_3 \rightarrow$ all branches	2.8E-12	s^{-1}	1	
$CH_3 \rightarrow CH_4 + H$	3.0e-5 to 1.4e-4	s^{-1}	1	
$CH_3 \cdot + CH_3 \cdot \rightarrow C_2H_6$	5.00E-11	cm^3/(molecule·s)	2	225
$CH_3 \cdot + CH_3 \cdot \rightarrow C_2H_6$	5.0e-11	cm^3/(molecule·s)	2	300
$CH_3 \cdot + CH_3 \cdot \rightarrow C_2H_6$	5.97E-11	cm^3/(molecule·s)	2	296-377
$CH_3 \cdot + CH_3 \cdot \rightarrow C_2H_6$	2.40E-11	cm^3/(molecule·s)	2	250-320
$CH_3 \cdot + CH_3 \cdot \rightarrow C_2H_6$	6.8E-11	cm^3/(molecule·s)	2	150
$CH_3 \cdot + CH_3 \cdot \rightarrow C_2H_6$	5.38E-11	cm^3/(molecule·s)	2	300
$C_2H_6 \rightarrow$ all branches	4.5E-11	s^{-1}		150
$C_2H_6 \rightarrow$ all branches	5.70e-10 to 1.0e-07			
$C_2H_6 \rightarrow$ all branches	8.0e-11	s^{-1}	1	

Table 2. Solution of simultaneous 1st and 2nd order chemical reactions

CH_4, now, (molecule cm^{-3})	CH_4 (molecules cm^{-3})	C_2H_6 (molecules cm^{-3})	C_2H_6 now (molecule cm^{-3})
6.81E-18	3.36E-09	1.61E-01	3.23E-17	1.62E-01
Value from the literature	Calculated from published data (section 1)		Value from the literature (Section 4) provided Titan's atmosphere

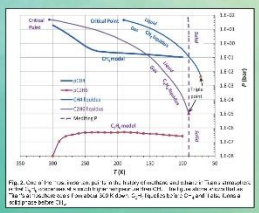

Fig. 2. One of the most recent models of the history of methane and ethane in Titan's atmosphere, as the CH_4 concentration in each time step per one liter CH_4 is plotted as a function of time. The "main methane zone" is located between 600 Kelvin, C_2H_6 liquefies to form C_2H_6 and falls, forming a solid phase before CH_4.

5. Surface Reservoirs of Ethane

In this study, we assume a hydrocarbon liquid lake volume of 50,000 km^3, based on an average of the work of [7] & [8]. Assuming a reasonable liquid composition of 50% ethane, this corresponds to an ethane mass of 1.26×10^{18} kg in Titan's lakes, roughly 1/62 the amount of total ethane predicted in Section 3 for 1/12 if assuming Section 3, Model (b). This suggests that there must be a large quantity of liquid ethane existing elsewhere on Titan, perhaps in the subsurface.

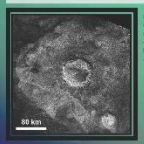

(L) Cassini RADAR image of Sinlap, one of Titan's largest craters. Image credit: NASA/JPL/Caltech/ ASI/GBFC

(L) Ligeia Mare, the second largest lake on Titan, displayed in false color (R) Earth's Lake Superior, shown for size comparison. Image Credit: NASA/JPL/ Asterbot

6. Liquid Capacity in Titan's Craters

Although there are only a couple of observations of hydrocarbon liquids present in Titan's sub-craters, it is interesting to theorize the maximum liquid storage potential of these craters to determine whether they could have in the past, been a suitable site for the excess ethane (as calculated in Section 5).

To date, 62 possible craters have been observed on the surface of Titan [9] [10] [11] [12], ranging in diameter from 3 to 425 km. Assuming a spherical cap for crater volume, we calculate a total crater volume of roughly 91,000 km^3, covering a total area of 236,000 km^2, that follow a power law distribution (Fig. 3). Assuming that these craters would be fed by 100% ethane rainfall, their total storage capacity of ethane would be 3.34×10^{19} kg, roughly 1/25 of the total ethane production in Model (a) or 1/5 of Model (b), even after accounting the total crater liquid capacity to the dune capacity, we get a total ethane surface storage of 4.2×10^{19} kg, still only 1/2 (a) or 1/5 (b) of the total ethane production, suggesting that there must be liquid ethane storage elsewhere, perhaps in the subsurface.

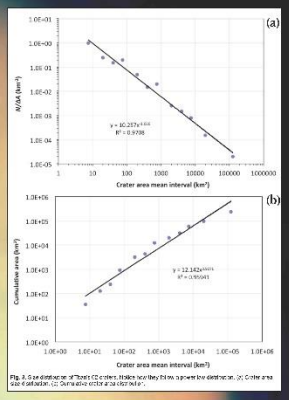

Fig. 3. (a) Distribution of Titan's 62 craters. Plotted on the y-axis is the cumulative distribution, (b) Crater area size distribution. (c) Cumulative crater area distribution.

SUBSURFACE

7. Porosity and the Subsurface Reservoir of Ethane

Previous work [6] [13] has suggested that Titan has a complex crustal structure overlain by a 100+ km crust composed primarily of water ice. Observations of fluvial channels on Titan's surface suggest that the water ice particles in Titan's crust are not cohesive, due to the difficulty of eroding coherent ice bedrock, and instead must have been ubiquitously fractured prior to fluvial erosion. Such a fractured icy crust would be extremely permeable to liquid ethane and methane [14].

Using a reasonable crustal porosity of 20%, and assuming that the porosity extends to 1 km beneath Titan's surface, we estimate that the total porous crust volume is 1.66×10^7 km^3, or 1.64×10^7 km^3 if we do not include the crustal area already occupied by lakes and craters.

If we assume that the total porous volume is filled with a 100% ethane solution, then its maximum ethane storage potential is ~ 9.0×10^{21} kg, which is well above our previous calculated total ethane production of 5.48×10^{21} kg. This suggests that Titan's entire liquid ethane budget could be stored in its porous crust, or it could also only serve as additional subsurface storage.

8. Conclusions

Using a simple photolysis model where the methane molecule can either escape the atmosphere or go on to produce ethane, up to 5.48×10^{21} kg of liquid ethane might have been produced. This amount is greater than the total liquid ethane storage as well as in Titan's present day lakes and craters, suggesting that there is a sizeable subsurface reservoir of liquid ethane beneath Titan's icy crust (Table 3). The estimated time of ethane residence by rain-out in Titan's atmosphere is 8 to 20 Earth days.

Table 3. Summary of our investigation and key results.

CH_4 Depletion and C_2H_6 Production Through Time	
CH_4 escape rate (Model (a))	2.9×10^9 molecules cm^{-2} s^{-1}
CH_4 escape rate (Model (b))	1.77×10^9 molecules cm^{-2} s^{-1}
C_2H_6 produced since accretion (a)	8.46E21 kg
C_2H_6 produced since accretion (b)	1.2 E21 kg
Surface Reservoir of Ethane	
Mass of Liquid C_2H_6 in lakes	1.26E18 kg
Liquid Capacity in Titan's Craters	
Total crater volume	91000 km^3
Amount of liquid C_2H_6 crater can hold	3.34E19 kg
Porosity and the Subsurface Reservoir of Ethane	
Total porous crust volume (porosity = 20%)	1.66E7 km^3
Amount of liquid C_2H_6 crust can hold	9.0E21 kg

References: [1] Raven, R. J. Atkinson, J.-P. Pirolle, J.M. Cadle, J. Geophys. Res. 92, 2085–2097 (1987). [2] Wilson, E.H. and Atreya, S.K. (2009) J. Phys. Chem. A. 113, 1221–1226. [3] Yung, Y.L., Allen, M., Pinto, J. P. (1984) Astrophys. J. Suppl. S. 55, 465–506. [4] Toublanc, D., et al. (1995) Icarus, 113, 2-26. [5] Yung, Y.L. and DeMore, W.B. (1999) Oxford University Press (NY). [6] Gilliam, A.E. and Lerman, A. (2014) Planet. Space Sci., 93-94, 41-53. [7] Lorenz, R.D., et al. (2008) Geophys. Res. Lett., 35, L02206. [8] Lorenz, R.D., et al. (2013) Icarus, 237, 9-15. [9] Neish, C.D. and Lorenz, R.D. (2012) Planet. Space Sci., 60, 26-33. [10] Neish, C.D., et al. (2013) Icarus, 223, 82-90. [11] Neish, C.D., et al. (2010) Astrobiology, 10, 3-19. [12] Wood, C.A., et al. (2010) Icarus, 206, 334-344. [13] Yoder, A.D., et al. (2007) Icarus, 188, 139–153. [14] Barr, C., et al. (2009) Lunar and Planetary Science Conference, Vol. p. 2288.

FORMATION MECHANISMS OF CHANNELS ON TITAN. A. E. Gilliam[1] and A. Lerman[1], [1]Department of Earth and Planetary Sciences, Northwestern University, Evanston IL, 60208-3130 (ashley@earth.northwestern.edu).

Introduction: Titan, the largest moon of Saturn, is the only satellite in the solar system with a significant atmosphere, harboring a suite of hydrocarbons that display a meteorological cycle similar to the hydrological cycle on Earth. Dendritic networks of sinuous valleys on the surface of Titan were first observed by the Cassini-Huygens mission, where Synthetic Aperture Radar (SAR) images revealed drainage networks with branching morphologies on the order of 100 km in length [1]. These observations were supported in greater detail by the Huygens Probe Descent Imager and Spectral Radiometer (DISR) [2][3][4], and suggested formation by fluvial erosion into the water-ice bedrock. Additional support that the valleys were formed by flowing liquid is the paucity of impact craters on Titan's surface [4][5][6][7], indicative of rapid burial or removal of surface topography. Additionally, at the landing site, the DISR imaged Earth-like rounded cobbles 0.3-15 cm in diameter [2] composed of water ice, indicating that they had undergone abrasion during fluvial transport.

In this study we address fluvial erosion processes on Titan. Specifically, we examine the possibilities of channel formation by dissolution of ice by a concentrated solution of ammonium sulfate, and by mechanical erosion by flow of liquid ammonia and liquid ethane. Each of these processes might have functioned over a certain range of temperatures during the cooling history of Titan.

Observations of Streams on Titan: In this study we examine 27 different fluvial features as identified in VIMS, ISS, and RADAR data, chosen based on their geographic diversity and resolution – or our confidence in their classification as a fluvial feature. These valleys represent an array of morphologic features and range in size from tens of kilometers to over a thousand kilometers long, and up to ten kilometers wide. The majority of these features are dendritic in nature, forming tree-shaped networks with many contributing branches that converge into larger receiving streams, up to seventh in channel order, indicative of an origin from rainfall [2][4][8][9].

In order to calculate the relative rates of stream incision into the water-ice bedrock on Titan, the channel dimensions must be known. Measurements of channel slope were made directly from Cassini RADAR SAR-topo and altimetry data, and depth from an empirical relationship between channel depth and width as outlined in [10].

Mechanical Erosion: To calculate the rates of liquid stream incision into water ice bedrock on Titan, we build on a previous model of terrestrial water erosion by saltation of bedrock particles [11], and analyze the effect of bed-load transport on the lowering rate using the equations of bed-load transport rate developed by Einstein (1942) [12] and Chanson (1999) [13]. These models apply to channels of fixed width that are being deepened by erosion and abrasion of rock/ice by bed load, and assume that all bed load motion is by saltation of spherical grains of uniform size.

Results: We find that chemical erosion of Titan's channels could be completed in 280 to 1100 years, much shorter than the period of about 84,000 years that a concentrated $(NH_4)_2SO_4$-H_2O solution could exist as a liquid on the Titan surface. Mechanical erosion of Titan's channels is generally a much slower process, on the order of 10^2 to 10^5 years to completion, and is also slower than mechanical erosion of a model river on Earth, averaging 10^3 to 10^4 years. The erosional sequence of the channels on Titan may have started after the formation of water-ice on the surface by the process of chemical dissolution by $(NH_4)_2SO4$-H_2O, overlapping, or followed by, a period of mechanical erosion by liquid NH_3. A final stage on the cooling surface of Titan might have been characterized by liquid C_2H_6 as an agent of mechanical erosion.

References: [1] Elachi C. et al. (2004) *Space Sci. Rev. 115,* 71-110. [2] Tomasko M. G. et al. (2005) *Nature 438,* 765-778. [3] Soderblom L. A. et al. (2007) *Planet. Space Sci. 55,* 2015-2024. [4] Jaumann R. et al. (2009) *Titan from Cassini-Huygens,* 75-140. [5] Porco C. C. et al. (2005) *Nature 434,* 159-168. [6] Elachi C. et al. (2005) *Science 308,* 970-974. [7] Wood C. A. et al. (2010) *Icarus 206,* 334-344. [8] Lorenz R. D. et al. (2008) *Planet. Space Sci. 56,* 1132-1144. [9] Perron J. T. et al. (2006) *J. Geophys. Res. 111,* E11001. [10] William G. P. (1988) *Flood Geomorphology,* 321-334. [11] Sklar L. S. and Dietrich W. E. (2004) *Water Resour. Res. 40,* W06301. [12] Einstein H. A. (1942) *American Society of Civil Engineers 107,* 561-574. [13] Chanson H. (1999) *The Hydraulics of Open Channel Flow: An Introduction.*

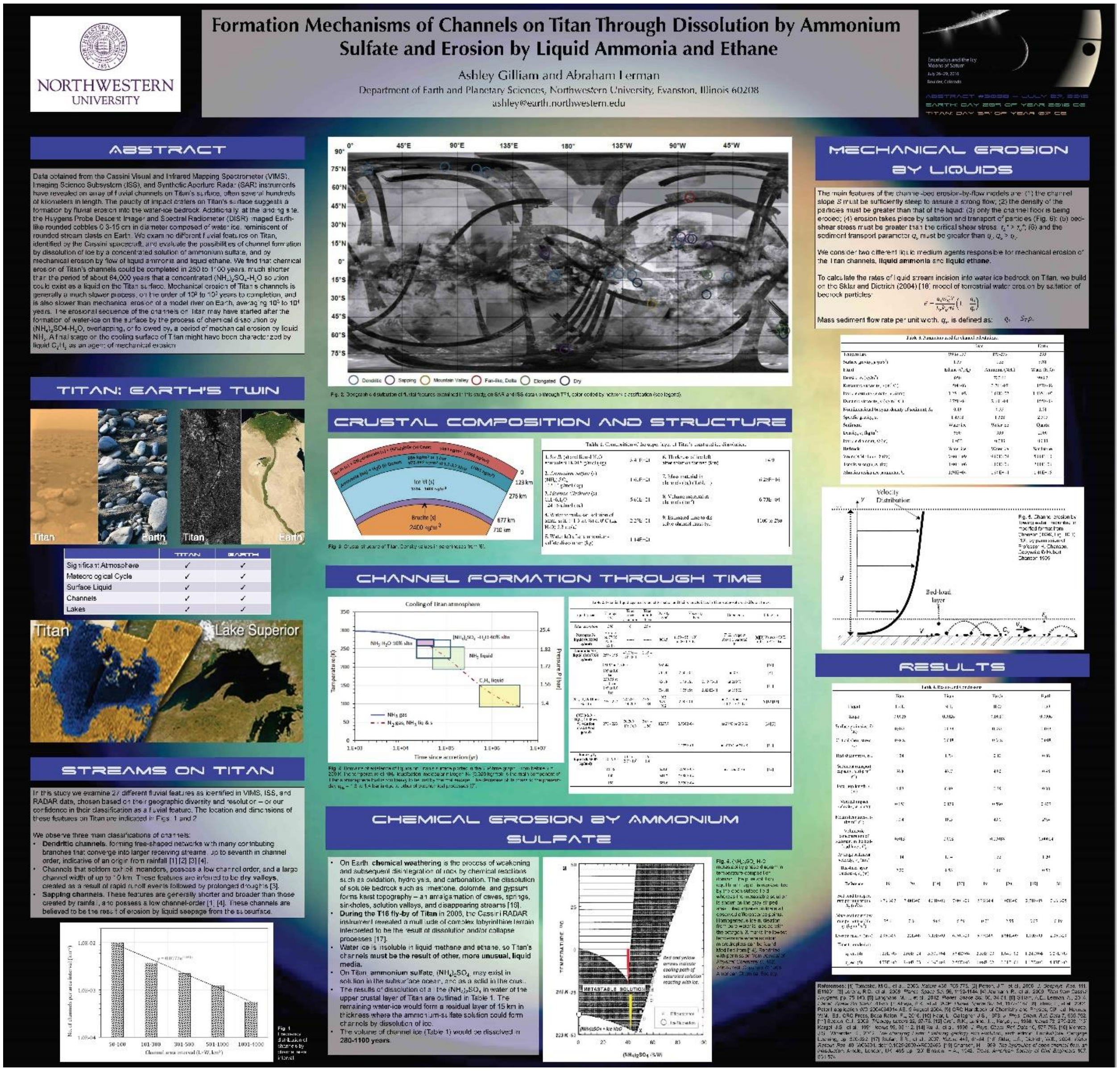
NORTHWESTERN UNIVERSITY
Formation Mechanisms of Channels on Titan Through Dissolution by Ammonium Sulfate and Erosion by Liquid Ammonia and Ethane
Ashley Gilliam and Abraham Lerman
Department of Earth and Planetary Sciences, Northwestern University, Evanston, Illinois 60208
ashley@earth.northwestern.edu
ABSTRACT
Data obtained from the Cassini Visual and Infrared Mapping Spectrometer (VIMS), Imaging Science Subsystem (ISS), and Synthetic Aperture Radar (SAR) instruments have revealed an array of fluvial channels on Titan's surface, often several hundreds of kilometers in length. The paucity of impact craters on Titan's surface suggests a formation by fluvial erosion into the water-ice bedrock. Additionally, at the landing site, the Huygens Probe Descent Imager and Spectral Radiometer (DISR) imaged Earth-like rounded cobbles 0.3-15 cm in diameter composed of water ice, reminiscent of rounded stream clasts on Earth. We examine different fluvial features on Titan, identified by the Cassini spacecraft, and evaluate the possibilities of channel formation by dissolution of ice by a concentrated solution of ammonium sulfate, and by mechanical erosion by flow of liquid ammonia and liquid ethane. We find that chemical erosion of Titan's channels could be completed in 280 to 1100 years, much shorter than the period of about 84,000 years that a concentrated $(NH_4)_2SO_4$-H_2O solution could exist as a liquid on the Titan surface. Mechanical erosion of Titan's channels is generally a much slower process, on the order of 10^2 to 10^3 years to completion, and is also slower than mechanical erosion of a model river on Earth, averaging 10^3 to 10^4 years. The erosional sequence of the channels on Titan may have started after the formation of water-ice on the surface by the process of chemical dissolution by $(NH_4)_2SO_4$-H_2O, overlapping, or followed by, a period of mechanical erosion by liquid NH_3. A final stage on the cooling surface of Titan might have been characterized by liquid C_2H_6 as an agent of mechanical erosion.
TITAN: EARTH'S TWIN
Titan
Earth
Titan
Earth
TITAN EARTH
Significant Atmosphere ✓ ✓
Meteorological Cycle ✓ ✓
Surface Liquid ✓ ✓
Channels ✓ ✓
Lakes ✓ ✓
Titan
Lake Superior
STREAMS ON TITAN
CRUSTAL COMPOSITION AND STRUCTURE
CHANNEL FORMATION THROUGH TIME
CHEMICAL EROSION BY AMMONIUM SULFATE
MECHANICAL EROSION BY LIQUIDS
RESULTS

To be submitted in December 2016 to 47th Lunar and Planetary Science Conference, March 21-25, 2017

CH_4-CH_3-C_2H_6 IN TITAN'S ATMOSPHERE: EXPLICIT SOLUTIONS AND NEAR-STEADY STATE OF A SIMPLIFIED REACTION SYSTEM.

A. E. Gilliam[1], J. Wunsch[2], and A. Lerman[1]. [1]Department of Earth and Planetary Sciences, Technological Institute F-379, 2145 Sheridan Road, Northwestern University, Evanston IL 60208-3130, ashley@earth.northwestern.edu, [2]Department of Mathematics, 2033 Sheridan Road, Northwestern University, Evanston IL 60208, jwunsch@northwestern.edu

Introduction: Methane gas (CH_4) is one of the main components of the atmosphere of Titan, the largest satellite of Saturn. At present, $pCH_4 = 0.1$ bar, and the remainder made of N_2 at the total $P = 1.5$ bar. Methane undergoes thermal escape from Titan's atmosphere and photolytic dissociation to other hydrocarbons [1, 2]. The very detailed sequence of reactions leading from CH_4 to CH_3 to ethane C_2H6 accumulating on Titan's surface and other products may be replaced by a simplified system of three reactions:

(1) $d[CH_4]/dt = - k_{12}[CH_4]$ k_{12} (yr^{-1})

(2) $d[CH_3]/dt = k_{12}[CH_4]$ $k_{23}[CH_3]^2$ k_{23} (cm^3 $molec^{-1}$ yr^{-1})

(3) $d[C_2H_6]/dt = k_{23}[CH_3]^2 - k_3[C_2H_6]$ k_3 (yr^{-1})

where brackets [ ] denote concentrations in molecules/cm^3.

Eqs. (1) and (3) are first-order ordinary differential equations (ODE), and (2) is a Riccati equation. Eqs. (1)-(3) can be solved numerically for known values of the reaction rate parameters k_i, but no explicit solution, as far as we are aware, has been published for the entire reaction system.

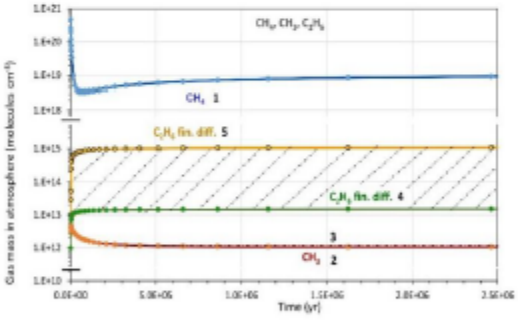

Fig. 1. Calculated concentrations of CH_4, CH_3, and C_2H_6 in Titan's atmosphere. **1:** CH_4 [1]. **2:** CH_3 concentration from $k_{12} = 6.7\times10^{-9}$ yr^{-1}, $k_{23} = 5\times10^{-14}$ cm^3 $molecule^{-1}$ yr^{-1}. **3:** CH_3 from eq. (2b), rate parameters as in 2. **4:** C_2H_6 from eq. (5), $k_{23} = 1\times10^{12}$ cm^3 $molecule^{-1}$ yr^{-1}, $k_3 = 1\times10^{-3}$ yr^{-1}. **5:** C_2H_6 from eq. (5), $k_{23} = 1\times10^{-12}$ cm^3 $molecule^{-1}$ yr^{-1}, $k_3 = 1.0\times10^{4}$ yr^{-1}. Cross-hatched area is the domain of C_2H_6 reported concentrations.

Reaction Rate Parameters k_i: From the very extensive data base of experimentally and theoretically determined values of k_{12}, k_{23}, and k_3, their ranges are: k_{12} from 9.5E-09 to 3E-04 yr^{-1}; k_{23} from 5.1E-19 to 1.3E-03 cm^3 $molecule^{-1}$ yr^{-1}; k_3 from 1.3E-80 to 3E+0 yr^{-1}. The ranges are very large and values $<1.5\times10^{-10}$ yr^{-1} correspond to reaction half-lives longer than the age of the Solar system, 4.55×10^{9}yr. The rate constants cannot be chosen arbitrarily to make the equations produce present-day concentrations of CH4, CH3, and C2H6 in Titan's atmosphere. The value that agree with the present day concentrations (Fig. 1) are $k_{12} = 6.7$E-09 yr^{-1}, $k_{23} =$ 5E-14 to 1E-12 cm^3 $molecule^{-1}$ yr^{-1}, and $k3 =$ 1E-04 to 1E-03 yr^{-1}.

Present-Day Abundance: Present day abundances of CH_4, CH_3, and C_2H_6 in Titan's atmosphere are given in Table 1.

Table 1.

Gas	Abundance		References
	molecules cm^{-3}	kg	
CH_4	1.31×10^{19}	6.16×10^{17}	[3], [4], [5], [1]
CH_3	1.05×10^{12}	4.62×10^{10}	[6]
C_2H_6	1.81×10^{13}–1.67×10^{15}	1.60×10^{12}–1.48×10^{14}	[7], [8], [6]. [9]
Mean	8.46×10^{14}		
Geom.	1.74×10^{14}		

Near-Steady-State Concentrations: In the course of Titan's cooling since accretion, thermal escape of CH_4 slowed down, approaching the present-day atmospheric mass [1]. This suggests that at the present temperature of about 94 K, Titan's atmosphere has attained a near-steady state. The steady state or asymptotic solutions of eqs. (1)-(3) and (2a)-(3a) give the same results [10]:

From (2), (2a), (2b), $[CH_3]_{ss} = \sqrt{\frac{k_{12}[CH_4]_{ss}}{k_{23}}}$ (4)

From (3), (3a) $[C_2H_6]_{ss} = \frac{k_{23}[CH_3]^2_{ss}}{k_3} = \frac{k_{12}[CH_4]_{ss}}{k_3}$ (5)

The computed concentrations from the preceding two equations and k_i values cited above are given in Table 2.

Solution of (1):

(1a) $[CH_4] = [CH_4]_{ss} + ([CH_4]_0 - [CH_4]_{ss})e^{-k_{12}t}$

where $[CH_4]_0$ is the initial and $[CH_4]_{ss}$ steady-state concentration (Fig. 1)

Solution of (2) [10]:

$$\frac{d[CH_3]}{dt} = k_{12}[CH_4]_{ss} + (k_{12}[CH_4]_0 - k_{12}[CH_4]_{ss})e^{-k_{12}t} - k_{23}[CH_3]^2$$

(2a) $$[CH_3] = -\frac{1}{k_{23}}\frac{(pCk_{12}/2)e^{-k_{12}t/2}\, I'_{\nu}(Ce^{-\lambda t/2})\,(qC\lambda/2)e^{-\lambda t/2}\, I'_{-\nu}(Ce^{-\lambda t/2})}{pI_{\nu}(Ce^{-\lambda t/2}) + qI_{-\nu}(Ce^{-\lambda t/2})}$$

where C and ν are constants defined in terms of k_i, $[CH_4]_0$, $[CH_4]_{ss}$, and constants $q = 1$, $p = -1$.

Alternatively, in the regime where the CH4 concentration is near steady-state (Fig. 1),

$$\frac{d[CH_3]}{dt} = k_{12}[CH_4]_{ss} - k_{23}[CH_3]^2$$

(2b) $$[CH]_3 = \sqrt{\frac{k_{12}[CH_4]_{ss}}{k_{23}}}\tanh(\sqrt{k_{12}[CH_4]_{ss}k_{23}}\,t)$$

$$\frac{d[C_6H_6]}{dt} = k_{12}[CH_4]_{ss}\tanh^2(\sqrt{k_{12}[CH_4]_{ss}k_{23}}\,t) - k_3[C_6H_6]$$

(3a) And finally, $[C_2H_6] = f(t) + \mathrm{CONST}\times\exp(-k_3 t)$

$$f(t) = \frac{k_{12}[CH_4]_{ss}}{ac(a+2c)}\left[a^2e^{2ct}F\left(1,\frac{a}{2c}+1;\frac{a}{2c}+2;-e^{2ct}\right) - (a+2c)\left(aF\left(1,\frac{a}{2c};\frac{a}{2c}+1;-e^{2ct}\right) + a\tanh(ct) - c\right)\right]$$

where $a = k_3$ yr^{-1}; and $c = (k_{12}\cdot[CH_4]_{ss}\cdot k_{23})^{0.5}$ yr^{-1}, and F or Gauss's function ${}_2F_1$ is the hypergeometric series.

CONST = $-f(t = 0)$

Table 2. Calculated and reported CH_4, CH_3, and C_2H_6 concentrations in present-day Titan's atmosphere.

Fig. 1	Rate parameter	Value	CH_4 (molec./cm^3)		CH_3 (molec./cm^3)		C_2H_6 (molec./cm^3)	
			Calc.	Rep.	Calc.	Rep	Calc.	Rep.
1. CH_4	k escape $k_{12}\times[CH_4]_{ss}$	Variable [1] 8.76×10^{10}	1.31×10^{19}	1.31×10^{19}				
2. CH_3 eq. (10)	k_{12} k_{23}	6.7×10^{-9} 5.0×10^{-14}			1.09×10^{12}	1.05×10^{12}		
3. CH_3 eq. (19)	k_{12} k_{23}	6.7×10^{-9} 5.0×10^{-14}			1.21×10^{12}			
4. C_2H_6	k_{23} k_3	1.0×10^{-13} 1.0×10^{-3}					1.5×10^{15}	1.81×10^{13} to 1.67×10^{15}
5. C_2H_6	k_{23} k_3	1.0×10^{-12} 1.0×10^{-4}					1.5×10^{13}	

References: [1] Gilliam A.E. and Lerman A. (2014) *Planet. Space Sci., 93-94,* 41-53. [2] Atreya S.K. et al. (2006) *Planet. Space Sci., 54,* 1177-1187. [3] Lorenz A.D. et al. (1999) *Planet. Space Sci., 47,* 1503-1515. [4] Griffith C.A. et al. (2003) *Science, 300,* 628-630. [5] Jacquemart D. et al. (2008) *Planet. Space Sci., 56,* 613-623. [6] Wilson E.H. and Atreya S.K. (2004) *J. Geophys. Res., 109,* E06002, doi :10.1029/2003JE002181. [7] Gladstone G.R. et al. (1996) *Icarus, 119,* 1-52. [8] Yung Y.L. and DeMore W.B. (1999) *Photochemistry of Planetary Atmospheres.* Oxford Univ. Press. [9] Vinatier S. et al. (2007) *Icarus, 188,* 120-138. [10] DLMF (2015) NIST http://dlmf.nist.gov/

To be submitted in December 2016 to 47th Lunar and Planetary Science Conference, March 21-25, 2017

METHANE FORMATION AND RETENTION ON TITAN AND TERRESTRIAL PLANETS. A. E. Gilliam[1] and A. Lerman[1], [1]Department of Earth and Planetary Sciences, Technological Institute F-379, 2145 Sheridan Road, Northwestern University, Evanston IL 60208-3130, ashley@earth.northwestern.edu

Introduction: Much research has been done on the behavior of CH_4 in Titan's atmosphere, including its photolytic decomposition to other hydrocarbons and escape from the atmosphere (e.g., [1][2][3][4][5]), but its possible origin is poorly understood on the planets and satellites other than Earth.

We examine the possibility of methane formation in a number of gas-gas and solid-gas reactions, based on chemical thermodynamic equilibria under the conditions approximating the reported atmospheric composition of Titan and the Terrestrial planets – Mercury, Venus, Earth, and Mars. The paths to chemical equilibrium provide insight into the retention of methane in the atmosphere of different planets vs. the possibility of its escape. This study does not imply that the equilibrium reactions *in fact occur*, but they *may occur* on thermodynamic grounds.

Methane Forming Reactions: The five reactions below may be responsible for the formation of methane on the Terrestrial planets and Titan. Equilibria in the system C-H-O, where oxygen fugacities are buffered by the coexisting phases in the system Fe-FeO-Fe_3O_4-Fe_2O_3 have been extensively studied by many authors with reference to the magmatic interior of primordial Earth (e.g., [6][7]). In this study, the possible production of methane is limited to the planetary atmospheres in contact with mineral solids.

Three reactions of CH_4 production:

R1 $C_{(s)} + 2H_{2(g)} \rightarrow CH_{4(g)}$

R2 $2C_{(s)} + 2H_2O_{(g\ or\ l)} = CH_{4(g)} + CO_{2(g)}$

R3 $CO_{2(g)} + 4H_{2(g)} = CH_{4(g)} + 2H_2O_{(g)}$

Two reactions of serpentinization of iron-olivine fayalite that produce CH_4 from H_2O and C in graphite or CO_2:

R4 $3Fe_2SiO_4 + 2H_2O_{(g)} + C = 2Fe_3O_4 + 3SiO_2 + CH_{4(g)}$

R5 $6Fe_2SiO_4 + 2H_2O_{(g)} + CO_{2(g)} = 4Fe_3O_4 + 6SiO_2 + CH_{4(g)}$

Equilibrium Reactions Producing CH_4: For reactions R1-R5, the equilibrium constants as a function of temperature can be calculated from:

$$\log K = -\Delta G_r^\circ/(2.3RT)$$

where K is the equilibrium constant, R is the gas constant (kJ mol^{-1} K^{-1}), T is temperature (K), and ΔG_r° is the Gibbs standard free energy change of the reaction (kJ mol^{-1}) at temperature T, computed from the data in [8]. The value of log K as a function of T for reactions R1-R5 are plotted as curves in Fig. 1. The equilibrium partial pressures of CH_4 in reactions R1-R5 are computed from log K, the activities of the pure solid components ($a_{mineral}$), and reported partial pressures of other reactant gases (p, in bar), taken as ideal gases, and are shown in Fig. 2. For primordial Earth [11] at 700 K and 342 bar atm. pressure, a small correction to log K is

$$\log K_{P>1} = \log K_{P=1} - \Delta\bar{V}_r(P-1)/(2.3RT)$$

where $\bar{V}_r$ is the reaction volume change (cm^3/mol).

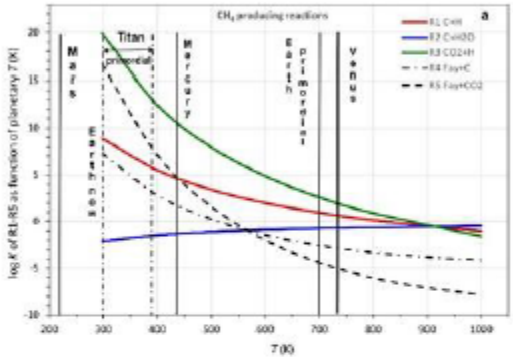

Fig. 1. Equilibrium constants log K for reactions R1-R5 as a function of temperature. Vertical lines show planetary temperatures.

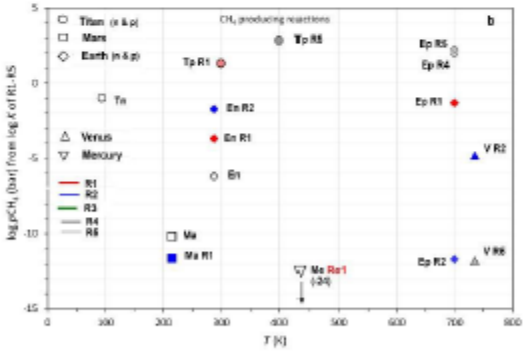

Fig. 2. Calculated CH_4 partial pressures from planetary atmosphere data.

Discussion of Methane-Producing Reactions: For the aforementioned five gas-gas and solid-gas reactions, R1-R5, we estimate the amount of methane that might have been produced on Titan and the Terrestrial planets.

(T, Titan) The assumed composition of the primordial atmosphere of Titan, shortly after its accretion about 4.5 Ga, was about 80% CH_4 or 19.4 bar, and 20% NH_3 or 6 bar, at the accretion temperature of 300 to 355 K [9]. At present, it is 0.1 bar CH_4 and 1.4 bar N_2. The

abundance of solid carbon as graphite in meteorites [4] and of H_2 in the Universe suggests that reaction R1 might have been a likely mechanism of formation of primordial CH_4. On Titan, reaction R1 between graphite and hydrogen gas can give partial pressures of CH_4 close to the model-computed value of 19.5 bar, if $pH_2 \geq 10^{-4}$ bar. Serpentinization reaction R4 that might have occurred on Titan [2] gives a higher partial pressure of CH_4, about 700 bar. This would account for an internal reservoir of CH_4 in Titan's interior that is needed to replenish the photolytic conversion of CH_4 to other hydrocarbons.

(Ma, Mars) Mean surface temperature of Mars is 210 to 215 K, below the freezing point of water. However, the temperature range (diurnal and seasonal) is from 133 to 303 K, and this lends to the possibility that reaction R2, CO_2 and atmospheric H_2O [10] makes a likely source of CH_4.

(E, Earth) Earth's rich atmospheric chemistry unlocks the use of multiple CH_4 producing reactions. On present-day Earth, the production of CH_4 is primarily biogenic near the surface and inorganic at depth. If reactions R1 and R2 were active on Earth in the recent, they would have produced reasonable values of log pCH_4 = -3.71 and -1.74, respectively, compared to observed log pCH_4 of -6.22 to -5.74.

(V, Venus) The Venusian atmosphere is hot and dense, and is presently devoid of CH_4. However, as a geologically likely situation, we apply reaction R2 between CO_2 and H_2O to the present-day composition of Venus. The result is a low partial pressure of methane, log pCH_4 = -4.83 or 1.5×10^{-5} bar, owing to the low partial pressure of H_2O. In reaction R2, CH_4 competes with CO_2 that is present at a high partial pressure in the Venusian atmosphere. However, in reaction R5, where fayalite, H_2O, and CO_2 drive the reaction towards CH_4, the equilibrium value of log pCH_4 is much lower, -11.8 because of the low abundance of H_2O vapor in Venus' atmosphere.

(Me, Mercury) Measurements of the Mercurian atmosphere at about 440 K also show that it is completely bereft of CH_4, but contains H_2. In an approximation to the geologically likely occurrence of graphite in Mercury's crust, we apply reaction R1 to the known present-day composition, and calculate a possible log pCH_4 of -23.8 bar, indicating that practically no CH_4 should form in its atmosphere.

Potential Retention or Escape of CH_4 from Planets: If CH_4 were formed from the aforementioned reactions, would it have escaped or been retained in the atmospheres of the individual planets? The escape of a gas from an atmosphere depends on the fraction of the population of the gas molecules whose velocities are greater than the escape velocity of the planet. Gas escape rate parameter k (yr^{-1}) is defined as [9, with references]:

$$k = \frac{\mathcal{F}(v \geq v_e) \cdot \bar{v}_{>v_e} \cdot S_{atm}}{2V_{atm}}$$

where $\mathcal{F}(v \geq v_e)$ is a fraction of the Maxwell-Boltzmann frequency distribution of the gas molecules' velocities greater than Titan's escape velocity, $\bar{v}_{>v_e}$ (m/s) is the mean velocity in the interval $v \geq v_e$, and the quotient V_{atm}/S_{atm} (m) of the atmosphere volume to its outer surface area is effectively the scale thickness of the atmosphere. The calculated values of k for CH_4 are shown as a function of planetary T in Fig. 3. If CH_4 were produced on Mercury, the planet's high temperature would have made the escape of CH_4 as possible as on Titan. On Mars, Venus, and on primordial Earth, retention of CH_4 would have been more likely because of the much smaller values of k and larger escape velocities on the latter three planets.

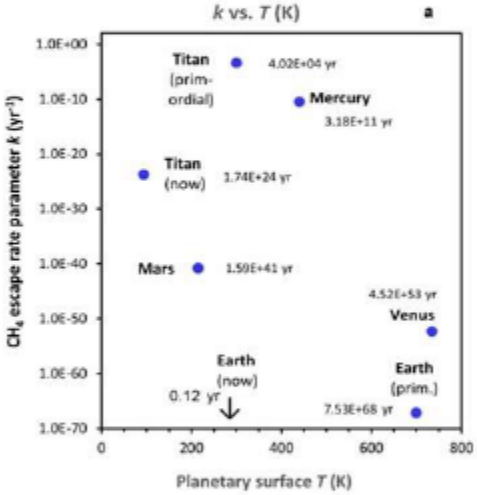

Fig. 3. CH_4 escape rate parameter k (yr^{-1}) vs. planetary temperature. Numbers in yr next to the planets' names are CH_4 residence times ($1/k$).

References: [1] Strobel D.F. et al. (1974) *Icarus, 21,* 466-470. [2] Atreya S.K. et al. (2006) *Planet. Space Sci., 54,* 1177-1187. [3] Lunine J.I. and Atreya S.K. (2008) *Nat. Geosci., 1,* 159-164. [4] Yelle R.V. et al. (2008) *J. Geophys. Res. Planets, 113.* [5] Gladstone G.R. et al. (1996) *Icarus, 119,* 1-52. [6] French B.M. (1966) *Rev. Geophys., 4,* 223-253. [7] Holland H.R. (1984) *Princeton Univ. Press.* [8] Robie R.A. and Hemingway B.S. (1995) *US Geol. Surv. Bull., 1452,* 1-456. [9] Gilliam A.E. and Lerman A. (2014) *Planet. Space Sci., 93-94,* 41-53. [10] Webster C.R. et al. (2013) *Science, 341,* 260-263. [11] Mackenize F.T. and Lerman A. (2006) *Springer,* Dordrecht.